Study of the immunomodulatory effects of radiation therapy in solid cancers

Joseph Ikin Sia

ORCID 0000-0002-9056-0903

Submitted in total fulfilment for the degree of

Doctor of Philosophy

April 2020

Sir Peter MacCallum Department of Oncology

Faculty of Medicine, Dentistry, and Health Sciences

The University of Melbourne

Thesis Abstract

Radiation therapy (RT) has evolved over more than a century into a well-established, highly sophisticated and major cancer treatment modality today. A paradigm shift that has occurred within the last two decades is the growing understanding that RT can induce host immune responses that contribute to tumour control, beyond direct radiation-induced cytotoxicity. Contemporaneously, the advent of modern cancer immunotherapy such as immune checkpoint inhibitors has revolutionised the field of oncology and highlighted the potential of harnessing the immune system to suppress and eradicate tumours. Inevitably, resistance to cancer immunotherapy has also brought into focus immunological barriers that preclude cancer immunity. In this context, an increasing body of pre-clinical and clinical studies substantiate the use of RT as a unique candidate to complement cancer immunotherapy in non-overlapping mechanisms to overcome such barriers.

However, instruction on the optimal integration of RT and cancer immunotherapy is scarce. For the radiation oncologist, an outstanding gap in knowledge is how radiation dose-fractionation influences the immunomodulatory effects of RT and its synergy with cancer immunotherapy. In this PhD project, mouse models of solid cancer were used to systematically interrogate this question by employing a series of rationally selected radiation dose-fractionation regimens to dissect the immunological impact of dose per fraction (DPF) from that of total dose, as represented by biological effective dose (BED). In orthotopic AT3-OVA mammary carcinomas, radiation-induced $CD8^+$ T cell responses were found to be regulated by radiation DPF, rather than BED. By contrast, radiation-induced natural killer (NK) cell responses in the same tumours were independent of radiation DPF but required a sufficient BED. Mechanistic investigations examining the cellular and transcriptional changes in AT3-OVA tumours evoked by radiation demonstrated that the differential regulation of anti-tumour immune responses by radiation DPF and BED was not primarily dictated by differences in tumour cell-intrinsic immunogenicity, but rather by the effector and suppressor dynamics in the tumour immune microenvironment, of which regulatory T cells played a central role. Furthermore, cross-examination of subcutaneously implanted MC38 colon carcinomas and publicly available transcriptomic data of human cancers pre- and post-RT suggested that radiation-induced immune responses are also significantly shaped by the tumour type. Lastly, the impact of radiation dose-fractionation on the anti-tumour activity of immune checkpoint inhibitors targeting the adaptive and innate immune arms was examined in AT3-OVA tumours, confirming the corollary that RT and immune checkpoint inhibitors do not universally synergise, but require selection of radiation regimens and checkpoint targets that are predicated on biological rationale.

Overall, this PhD project represents a comprehensive side-by-side pre-clinical study of the effects of radiation dose-fractionation on host anti-tumour immune responses. Results presented herein contribute towards a clearer understanding of this complex and clinically urgent question. More broadly, insights from this project will help guide the refashioning of RT into an exciting key adjunct in the immuno-oncology era.

Declaration

This declaration is to certify that:

i. This thesis comprises only my original work towards the PhD except where indicated in the Preface,

ii. Due acknowledgement has been made in the text to all other material used,

iii. The thesis is fewer than 100,000 words in length, exclusive of tables, maps, bibliographies and appendices

Joseph Ikin Sia

Sir Peter MacCallum Department of Oncology
Faculty of Medicine, Dentistry, and Health Sciences
The University of Melbourne
Melbourne, Victoria, Australia

20th April, 2020

Preface

This PhD candidature has been supported by the Australian Government Research Training Program Scholarship and the Royal Australian New Zealand College of Radiologists (RANZCR) Withers and Peters Grant.

Acknowledgements

Diving deep into the laboratory from the clinic has been a journey of wonder, learning and meeting many people who have greatly helped me along the way.

Nicole, thank you for this project, for patiently training me when I first started, for guiding me, and for being so approachable through the years. I have learnt much more than science from you.

Ricky, your commitment to students despite your heavy schedule speaks loudly of your leadership. Thank you for being a solid support during my candidature.

Trevor, my PhD pursuit began because of your foresight to bridge the gap between radiation oncology and the cancer research laboratories. Thank you for believing in me.

Ioana, it is no understatement that your faithful help in the laboratory has made my PhD journey infinitely more bearable. I owe much of this PhD project to you.

Jim, you have sacrificed so much, without even a grumble, in coming to Parkville to operate the linacs late in the evenings for us to irradiate mice.

To the Peter Mac Department of Radiation Oncology and the RANZCR Faculty of Radiation Oncology, I am immensely grateful for the professional, collegial, and financial support you have shown me over the previous years. I am so privileged.

I would also like to acknowledge the specific help I have received in the experimental work for this PhD project: Nicole, for the many mouse injections and harvests (and much more); Ioana, for essentially being a second pair of hands in nearly everything I did; Maria Doyle, Niko Thio, Stephin Vervoot and Anna Trigos for clearing up much of my befuddlement around gene expression analysis; and Keefe Chan and Ben Blyth for brainstorming with me on the senescence work.

Finally, my wife Emily, thank you for being so gracious with an absent-minded and energy-drained husband for the most part of our marriage so far. In the many decades to come, the work done and the words written for this PhD project will no longer matter, but you will still, so much.

Table of Contents

List of Abbreviations

ADCC	Antibody-dependent cellular cytotoxicity
AMP	Adenosine monophosphate
APC	Antigen presenting cell
ATM	Ataxia-telangiectasia mutated
ATP	Adenosine triphosphate
ATR	Ataxia-telangiectasia and Rad3-related protein
BED	Biological effective dose
CAF	Cancer-associated fibroblast
cGAMP	2',3'-cyclic GMP-AMP
cGAS	Cyclic GMP-AMP synthase
cIg	Control immunoglobulin
CPM	Counts per million
Cr	Chromium
CTLA-4	Cytotoxic T-lymphocyte-associated protein 4
DAMP	Danger-associated molecular pattern
DAPI	4',6-diamidino-2-phenylindole
DC	Dendritic cell
DDAOG	9H-(1,3-dichloro-9,9-dimethylacridin-2-one-7-yl) β-D-galactopyranoside
DNA	Deoxyribonucleic acid
DPF	Dose per fraction
dsDNA	double-stranded DNA
ES	Enrichment score
FACS	Fluorescence activated cell sorting
FBS	Foetal bovine serum
Fc	Fragment, crystallisable
FDR	False discovery rate
Foxp3	Forkhead box P3
GEO	Gene Expression Omnibuss
GFP	Green fluorescent protein
GMP	Guanosine monophosphate
GO-BP	Gene Ontology-Biological Process
GSEA	Gene Set Enrichment Analysis

HMGB-1	High mobility group box 1
ICD	Immunogenic cell death
IFN	Interferon
IFNAR1	Interferon alpha and beta receptor subunit 1
Ig	Immunoglobulin
IL	Interleukin
KEGG	Kyoto Encyclopaedia of Genes and Genomes
KIR	Killer immunoglobulin-like receptor
LAG-3	Lymphocyte-activation gene 3
m.f.p.	Mammary fat pad
MDSC	Myeloid-derived suppressive cell
MDS	Multi-dimensional scaling
MFI	Mean fluorescence intensity
MHC	Major histocompatibility complex
mRNA	Messenger RNA
mTOR	Mammalian target of rapamycin
NK	Natural killer
NMS	Normal mouse serum
Nrp1	Neuropilin-1
OS	Overall survival
OVA	Ovalbumin
PBS	Phosphate-buffered saline
PD-1	Programmed cell death protein 1
PD-L1/2	Programmed death-ligand 1/2
PDAC	Pancreatic ductal adenocarcinoma
PFS	Progression free survival
RNA	Ribonucleic acid
ROAST	Rotational Gene Set Test
RT	Radiation therapy
RT-qPCR	Quantitative reverse transcription polymerase chain reaction
s.c.	Subcutaneous
SA-β-gal	Senescence-associated β-galactosidase
SABR	Stereotactic ablative body radiotherapy
SASP	Senescence-associated secretory phenotype
SEM	Standard error of the mean
SF	Surviving fraction

STING	Stimulator of interferon genes
TCR	T cell receptor
TGF-β	Transforming growth factor beta
TIGIT	T cell immunoreceptor with Ig and ITIM domains
TIM-3	T-cell immunoglobulin and mucin domain-3
TNF	Tumour necrosis factor
TRAIL	TNF-related apoptosis-inducing ligand
Treg	Regulatory T cell
TREX1	Three prime repair exonuclease 1

List of Figures

List of Tables

Chapter 1: Literature review

1. Cancer in the context of the host immune system

1.1 The cancer immunoediting model

Because cancer has largely been viewed as fundamentally a disease of dysregulated proliferation, paradigms for understanding cancer have focused on its cell-autonomous effects. The concept of the host immune system influencing the initiation and progression of cancers has nonetheless been debated for over a century. In the late 1990's, advances in animal models and in our knowledge of immunology made possible the unequivocal demonstration of the immune system as an important extrinsic tumour suppressor (Dunn *et al.*, 2002). It is now understood that the immune system not only controls tumour initiation but also shapes tumour immunogenicity, a concept referred to as the cancer immunoediting model (reviewed in Schreiber *et al.*, 2011). According to this model, immune cells and effector molecules recognise and destroy tumour cells, but in the same process paradoxically favours growth of variants that are more capable of surviving immune pressure. Three distinct and sequential phases are described in cancer immunoediting: elimination, equilibrium, and escape. The directionality of these phases is affected by a confluence of external factors such as environmental stress, therapeutic intervention and the increasingly appreciated gut microbiome, resulting in the heterogeneous outcomes of tumour-immune system interactions (Vesely *et al.*, 2011; Dart, 2018).

Beyond the robust and growing body of animal studies elucidating the mechanisms involved in each phase, the relevance of the immunoediting model in humans is substantiated by three key threads of evidence: 1) the correlation between intra-tumoural immune responses and the prognosis of the cancer patient, 2) the higher relative rates of cancer incidence in immunosuppressed individuals, and 3) the development of spontaneous immune responses associated with cancer, including that of paraneoplastic syndromes (Schreiber *et al.*, 2011). An important implication of this model is that all clinically apparent tumours in the immunocompetent patient have been shaped by the host immune system and enriched for pathways for immune evasion. This critical yet relatively recent shift towards the recognition of the pervasive influence of the host immune system on tumour evolution was reflected in its inclusion in Hanahan and Weinberg's update on the hallmarks of cancer (Hanahan and Weinberg, 2011). Significantly, this framework of understanding has undergirded the development of modern immunotherapeutic strategies to address points of failure in the immune control of cancer. Cancer immunotherapy therefore represents a treatment modality of distinct mechanism of action compared to the major conventional modalities of surgery, radiation therapy (RT), and chemotherapy.

1.2 The major immune cell subsets in cancer control

The immune system consists of the innate and adaptive arms, most notably distinguished by their response characteristics and antigen specificity. Collectively, these two arms form a highly complex network of cellular and molecular subsets with multiple layers of regulation both within and between the arms. Natural killer (NK) and $CD8^+$ T cells are the primary cytotoxic subsets of the innate and adaptive arms respectively, and regulatory T cells (Tregs) represent a unique suppressive subset of $CD4^+$ T cells that are critical for immune homeostasis. The importance of these cells in tumour immunology is well-established by experimental animal work and further corroborated by their significance as prognostic markers in various human cancers (Galon and Bruni, 2020). A brief review of these cells, focusing on their regulation as is most pertinent for this PhD project, is provided below. Many other immune subsets also play important roles in cancer control but fall outside the primary scope of this PhD project.

1.2.1 $CD8^+$ T cells and DCs

Cytotoxic ($CD8^+$) T cells, alongside helper (CD4+) T cells, make up the two major subsets of T cells that express the αβ T cell receptor (TCR) complex. Naïve $CD8^+$ T cells do not survey peripheral tissues, but circulate between lymphoid organs, where they continuously scan antigens acquired and presented by migratory dendritic cells (DCs) and other antigen presenting cells (APCs) (Paul, 2013). The activation, or priming, of T cells requires three signals, which are provided by DCs in most circumstances: 1) major histocompatibility complex (MHC)-restricted recognition of peptide antigen by the TCR, 2) CD28 co-stimulatory receptor engagement, and 3) inflammatory cytokines such as interleukin (IL)-2, IL-12, and type I interferon (IFN) (*Figure 1.1*) (Curtsinger and Mescher, 2010). The degree of requirement for each signal is influenced by the strength of the TCR-peptide-MHC interaction, and insufficient signalling may lead to suboptimal activation or T cell anergy. When activated, $CD8^+$ T cells undergo rapid clonal expansion and change their expression pattern of chemokine receptors, such as the downregulation of CCR7 and upregulation of CXCR3, which permits their exit from secondary lymphoid organs and migration to sites of inflammation (Paul, 2013). There, they exert two major effector functions: cytotoxicity via the granzyme/perforin pathway and secretion of death receptor molecules such as Fas ligand and tumour necrosis factor (TNF) related apoptosis-inducing ligand (TRAIL); as well as secretion of immunomodulatory cytokines including IFN-γ and TNF-α. In a normal setting, the contraction phase takes place following clearance of the source of inflammation, in which the majority of the expanded pool of activated $CD8^+$ T cells undergo apoptosis. A small subset (approximately 5-10%) of activated $CD8^+$ T cells escape death to differentiate into long-lived memory T cells.

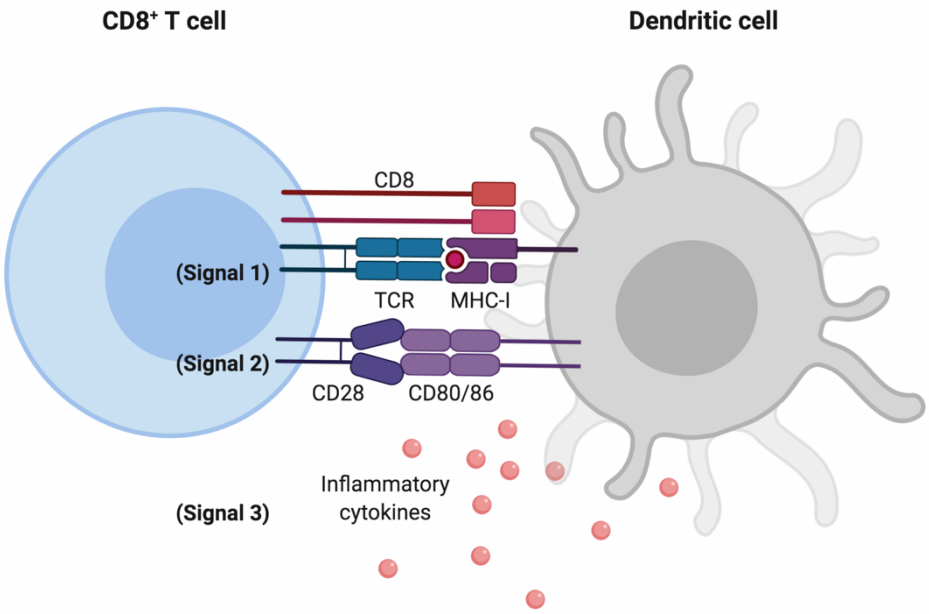

Figure 1.1. Priming of naïve CD8$^+$ T cells. Three signals are required for the efficient activation, or priming, of naïve CD8$^+$ T cells. These signals are generally provided by dendritic cells (DCs), which are professional antigen presenting cells (APCs). The synapse between the T cell receptor (TCR) and major histocompatibility complex class I (MHC I)-peptide complex provides the first signal. The second signal is mediated through binding of the positive co-stimulatory receptor CD28 with its cognate ligands CD80 and CD86. Soluble inflammatory cytokines, such as IL-2, IL-12 and type 1 interferon (IFN), serve as the third signal. Insufficient engagement of T cells may lead to suboptimal activation or T cell hyporesponsiveness, or anergy.

APCs, among which DCs are an important subset, constantly sample peripheral tissues for antigens. Upon detection of pathogen-associated or danger-associated molecular patterns (PAMPs or DAMPs) and capture of foreign material, DCs undergo a process of maturation and migrate to secondary lymphoid organs where they engage and activate T cells (Paul, 2013). Secretion of inflammatory cytokines and expression of the co-stimulatory ligands CD80 and CD86 are tightly regulated and limited to mature DCs. The cross-presentation of antigens to CD8$^+$ T cells is dependent on a subset of DCs called type 1 conventional DCs (cDC1s), which predominantly reside in lymphoid organs but also in tumours (reviewed in Bottcher and Reis, 2018). cDC1s can be identified by expression of the transcription factors BATF3, IRF8, and ID2, and selective expression of the chemokine receptor XCR1 and C-type lectin receptor CLEC9A, and integrins CD103 in mice and BDCA3 in humans. Mice deficient for cDC1s lose the ability to mount CD8$^+$ T cell-mediated rejection of tumours, highlighting that this subset is non-redundant. Additionally, the efficient cross-presentation function by this subset is reported to selectively require type I IFN (Diamond *et al.*, 2011; Fuertes *et al.*, 2011). Although cDC1-CD8$^+$ T cell priming interactions predominantly occur

in lymphoid organs, the importance of tumour-associated cDC1s is increasingly recognised, with their frequency being correlated with response to anti-PD-1 therapy (discussed below) and improved cancer patient survival (Broz *et al.*, 2014; Barry *et al.*, 2018; Bottcher *et al.*, 2018). Migration of cDC1s into tumours is promoted by the secretion of chemoattractants such as CXCL1, CCL2, CCL5 and XCL1 by tumour cells and tumour-associated NK cells (Barry *et al.*, 2018; Bottcher *et al.*, 2018; Li *et al.*, 2018a). The roles of tumour-associated cDC1s are currently unclear, but may be linked to further recruitment, repositioning and restimulation of T cells (Broz *et al.*, 2014; Bottcher and Reis, 2018; Chow *et al.*, 2019).

T cell activation is tightly regulated by several distinct mechanisms of immune tolerance. Central tolerance refers to clonal deletion of high-affinity self-reactive clones during T cell development in the thymus. Beyond the thymus, peripheral tolerance is regulated via cell-intrinsic and cell-extrinsic mechanisms. A key cell-intrinsic mechanism of peripheral tolerance is the expression of negative co-stimulatory receptors on effector T cells, also known as immune checkpoint receptors (*Figure 1.2*). Two well-characterised immune checkpoint receptors are cytotoxic T-lymphocyte-associated protein 4 (CTLA-4) and programmed cell death protein 1 (PD-1), the expression of which are tightly linked with TCR engagement (reviewed in Wei *et al.*, 2018). CTLA-4 restricts T cell activation primarily by competing with the co-stimulatory receptor CD28 for binding to CD80 and CD86 on APCs. Therefore, the CTLA-4 axis is thought to be most relevant in secondary lymphoid organs, where T cell priming predominantly occurs. Reflecting the central role of CTLA-4 in regulating T cell activation and expansion, *Ctla4*$^{-/-}$ mice develop uncontrolled lymphoproliferation and do not survive beyond 3-4 weeks of age (Waterhouse *et al.*, 1995). By contrast, PD-1 binds to programmed death-ligand 1 (PD-L1) and programmed death-ligand 2 (PD-L2), which are highly expressed on a range of immune and non-immune cells at sites of inflammation, such as on macrophages and tumour cells. Upon engagement, PD-1 recruits the tyrosine phosphatase SHP2 to attenuate upstream TCR signalling elements. *Pdcd1*$^{-/-}$ (PD-1-deficient) mice demonstrate autoimmune pathologies upon ageing, consistent with the role of PD-1 in maintaining peripheral tolerance (Nishimura *et al.*, 1999). Thus, there are general distinctions in tissue location and molecular mechanism of regulation by CTLA-4 and PD-1. Nonetheless, recent data has suggested that PD-1 also attenuates CD28 co-stimulation, which could indicate a common mechanism of action between CTLA-4 and PD-1 (Hui *et al.*, 2017; Kamphorst *et al.*, 2017). "Non-canonical" facets of PD-1 and CTLA-4 biology are progressively being uncovered and are further discussed in Section 1.4.2.

Other T cell checkpoint receptors that have increasingly attracted attention include lymphocyte-activation gene 3 (LAG-3), T-cell immunoglobulin and mucin domain-3 (TIM-3), T cell immunoreceptor with Ig and ITIM domains (TIGIT), and CD96 (Anderson *et al.*, 2016; Dougall *et al.*, 2017). LAG-3 is expressed on activated CD4^{+} and CD8^{+} T cells and a subset of NK cells, and

its only known ligand at present is the peptide-MHC-II complex. Even though $CD8^+$ T and NK cells do not typically interact with the MHC-II molecule, LAG-3 can intriguingly bind to non-cognate peptide-MHC-II complexes on APCs (Maruhashi *et al.*, 2018). TIM-3 is expressed on T cells and innate immune cells including DCs, NK cells and monocytes. Its primary ligand is galectin 9, although other ligands have been identified, including high mobility group box 1 (HMGB1). Thus, TIM-3 can interfere with the inflammatory role of extracellular HMGB1 (reviewed in Section 2.4.3) (Anderson *et al.*, 2016). Importantly, co-expression of PD-1 with LAG-3 and/or TIM-3 more reliably identifies "exhausted" or dysfunctional $CD8^+$ T cells than PD-1 expression alone (Sakuishi *et al.*, 2010; Anderson *et al.*, 2016). TIGIT is expressed on Tregs, activated effector T cells, and NK cells, while CD96 is expressed primarily on NK cells but also on activated T cells. TIGIT and CD96 compete with the positive co-stimulatory receptor DNAM-1 (also known as CD226) for binding to CD155 and CD112, which are stress-induced ligands. Therefore, TIGIT and CD96 are analogous to CTLA-4 in that they share the same ligands as a positive co-stimulatory receptor for competitive inhibition (Dougall *et al.*, 2017).

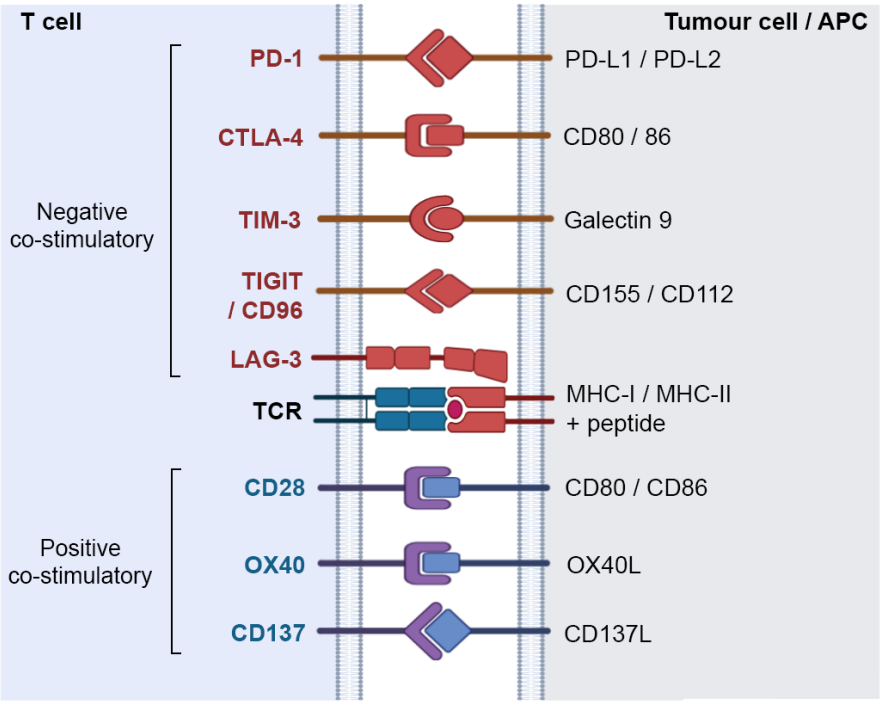

Figure 1.2. Positive and negative co-stimulatory receptors regulate T cell activation. The optimal activation of $CD8^+$ T cells requires engagement of positive co-stimulatory receptors with their cognate ligands. In general, negative co-stimulatory receptors, also known as immune checkpoints, are upregulated upon T cell activation as a homeostatic mechanism to regulate the activation status of T cells. Listed are some of the best characterised receptors and their ligands. These receptors each have distinct signalling pathways and are not all expressed on the same cell. *APC: antigen presenting cell, CTLA-4: cytotoxic T-lymphocyte-associated antigen 4, Gal-9: galectin 9, LAG-3: lymphocyte activation gene 3, MHC: major histocompatibility complex,*

PD-1: programmed cell death protein 1, PD-L1/2: programmed death-ligand 1/2, TCR: T cell receptor, TIGIT: T cell immunoglobulin and ITIM domain, TIM-3: T cell membrane protein 3.

1.2.2 NK cells

NK cells were originally identified by their spontaneous ability to kill tumour and virus-infected cells *in vitro* without prior activation (Herberman *et al.*, 1975; Kiessling *et al.*, 1975). They arise from the same lymphoid lineage as T and B cells, but lack receptors encoded by rearranged genes. Rather, NK cells rely on an array of germline-encoded, invariant activating and inhibitory receptors, the sum of signals from which determine their reactivity (*Table. 1.1*). In general, NK cell-activating receptors recognise stress-induced ligands and viral molecules while NK cell-inhibitory receptors recognise self MHC-I. This pattern of activation is called the "missing-self" and "altered-self" hypotheses, whereby NK cells survey tissues for cells that have downregulated MHC-I expression to escape recognition by the adaptive immune arm, and/or express signs of transformation, damage, or viral infection (Paul, 2013). Additionally, NK cells express Fcγ receptors (although not uniformly in human NK cells), which bind to the Fc portion of class-G immunoglobulins (IgGs) to transmit an activating signal, thus mediating antibody-dependent cellular cytotoxicity (ADCC). NK cells are also modulated by a variety of cytokines. IL-15 is a major cytokine that regulates the entire spectrum of NK cell differentiation, proliferation, maintenance and activation *in vivo* (Guillerey *et al.*, 2016). Other key NK cell-regulating cytokines are IL-12, IL-18, and IL-21, which have been shown to significantly influence NK cell effector function, by promoting cytotoxicity and IFN-γ production (Brady *et al.*, 2010).

Receptor	**Species***	**Ligand(s)***
Activating receptors		
KIR2DL4	H	HLA-G
KIR2DS1-5	H	HLA-class I
KIR3DS1	H	HLA-Bw4
CD16 (FcγRIII)	H, M	Immune complexes
CD27	H, M	CD70
DNAM1 (CD226)	H, M	CD112, CD155
NKG2C, NKG2E	H, M	H: HLA-E

		M: Qa-1
NKG2D	H, M	H: MICA/B; M: H60, MULT1, RAE1
NKp46	H, M	Viral haemagglutinin, HSPG
Ly49D	M	H-2D^{d}
Ly49H	M	MCMV m157
Ly49P	M	H-2D^{k} / MCMV m04
Activating/inhibitory receptors		
CD244	H, M	CD48
NKR-P1A, B, C, E, F	M	Clr family
PILRα/PILRβ	M	O-glycosylated CD99
Inhibitory receptors		
KIR2DL1, 2, 3	H	HLA-C
KIR2DL5	H	Unknown
KIR3DL1	H	HLA-Bw4
KIR3DL2	H	HLA-A3, A11
NKR-P1A	H	CLEC2D
KLRG1	H, M	E-, R-, N-cadherins
NKG2A	H, M	H: HLA-E; M: Qa-1
LILRB1	H, M	HLA-class I
Ly49A-C, E-G, I-O	M	MHC-I
NKR-P1B, D	M	Clr-b, Clr-g

** H: human; M: mouse*

Table 1.1. NK cell-activating and inhibitory receptors. NK cells recognise targets by a balance of signals conveyed through the binding of germline encoded receptors on NK cells to cognate ligands expressed on target cells. These receptors are classified as either activating or inhibitory. In general, activating receptors recognise stress-induced ligands and viral molecules, while inhibitory receptors recognise MHC-I. The killer immunoglobulin-like receptor

(KIR) and Ly49 families of receptors are analogous but have independently evolved in humans and mice, respectively. Table adapted from (Paul, 2013).

NK cells are early responders to sites of infection and inflammation. In contrast to T cells, this rapid response is facilitated by the ability of an individual NK cell to respond to a multitude of activating ligands (compared to the specificity of a T cell for only one antigen) and its constitutive expression of cytokine receptors (Paul, 2013). Significantly, as early responders, NK cells can shape subsequent adaptive immune responses (reviewed in Pallmer and Oxenius, 2016). For example, production of IFN-γ by NK cells promotes DC maturation and polarises Th1 responses (Martin-Fontecha *et al.*, 2004). NK cells also selectively kill immature DCs, enriching for mature DCs with sufficient cross-presentation capabilities (Chijioke and Munz, 2013). Recently, it was shown that NK cell-derived CCL5 and XCL1 were essential for the recruitment of DCs into the tumour microenvironment for priming of $CD8^+$ T cell responses (Bottcher *et al.*, 2018).

Testament to their role in cancer control, tumour infiltration of NK cells is prognostic in a wide range of human cancers, including melanoma, non-small cell lung cancers, gastric, colorectal, renal and prostate carcinomas (Ishigami *et al.*, 2000; Donskov and von der Maase, 2006; Gannon *et al.*, 2009; Coppola *et al.*, 2015; Soo *et al.*, 2018; Cursons *et al.*, 2019). The involvement of NK cells in suppressing the growth of primary tumours is demonstrated in pre-clinical models of solid cancers, although the extent of this in the human setting is unclear (Lopez-Soto *et al.*, 2017). NK cells very likely play a prominent role in the control of metastases, as tumour cells modify their surface ligand expression when undergoing epithelial-to-mesenchymal transition (Krasnova *et al.*, 2017). It has become apparent too that NK cells can work alongside conventional cancer therapies in mediating anti-tumour activity. For example, targeted therapies such as anti-EGFR and anti-HER2 antibodies achieve their full therapeutic potential in part via engaging NK cells for ADCC (Ferris *et al.*, 2018). Cytotoxic modalities, such as chemotherapy and RT, induce the expression of stress ligands and death receptors which theoretically support elimination by NK cells (Zingoni *et al.*, 2017).

1.2.3 Tregs

Tregs play a critical role in mediating cell-extrinsic peripheral immune tolerance. They have two distinct ontologies *in vivo*: derived either from the thymus (natural or thymic Tregs) or from differentiation of naïve $CD4^+$ T cells in the periphery (induced or peripheral Tregs) (Shevach and Thornton, 2014). Forkhead box P3 (Foxp3) is the master regulator of Tregs, orchestrating the development and function of Tregs through regulation of approximately 700 genes (Lu *et al.*, 2017). Treg molecular programmes notably include repression of IL-2 production and expression of CD25 and CTLA-4. Lack of IL-2 expression coupled with the high expression of CD25, which is a member of the IL-2 receptor, renders Tregs highly dependent on exogenous IL-2 for maintenance. This establishes a negative feedback control mechanism,

whereby IL-2 secreted by activated T cells for immunostimulatory functions also expands and activates Tregs for immunosuppression (Sakaguchi *et al.*, 2008). Tregs are identified by concurrent expression of the surface protein CD4 and transcription factor Foxp3, but there are currently no widely accepted markers to differentiate between natural and induced Tregs. The transcription factor Helios and the surface protein neuropilin-1 (Nrp1) have been proposed as candidate markers for natural Tregs, but neither perfectly delineate the Treg subsets in all circumstances tested (Shevach, 2018).

Tregs express TCRs and homing receptors that are similar to effector T cells, and are found in a variety of tissues, including lymph nodes, mucosal barriers, sites of inflammation, and tumours (Sakaguchi *et al.*, 2008). Tregs suppress the proliferation, differentiation, and effector functions of a range of immune subsets, such as non-regulatory T cells, DCs, and NK cells, via indirect and direct mechanisms (reviewed in von Boehmer, 2005). Indirect mechanisms include generation of immunosuppressive molecules such as IL-10, IL-35, TGF-β, and adenosine, as well as competitive consumption of IL-2. Direct cell contact-dependent pathways include granzyme/perforin-mediated killing of effector T cells and CTLA-4-mediated regulation of T cell activation. CTLA-4 on Tregs not only competitively binds to the co-stimulatory ligands CD80 and CD86 to restrict access by other T cells, but also captures those molecules from the surface of migratory DCs for degradation via transendocytosis (Qureshi *et al.*, 2011; Ovcinnikovs *et al.*, 2019). Indeed, the CTLA-4 pathway is critical for the suppressive function of Tregs, and *Ctla4* was recently confirmed to be a core member of a gene signature shared by all Tregs (Sakaguchi *et al.*, 2008; Zemmour *et al.*, 2018).

1.3 Mechanisms of immune evasion by cancer

Because tumours are continuously sculpted by immune selection pressure, suppressive and tolerance mechanisms of the immune system are often co-opted by tumour cells for survival. Any point in the immune cascade could potentially be hijacked, but broadly, these mechanisms can be categorised as alterations in the tumour cell (tumour cell-intrinsic), or generation of an immunosuppressive tumour microenvironment (tumour cell-extrinsic). These mechanisms have been reviewed extensively in (Drake *et al.*, 2006; Vesely *et al.*, 2011).

A major tumour cell-intrinsic mechanism of immune evasion involves deficiencies in antigen processing and presentation pathways to avoid adaptive immune recognition. These include positive selection of antigen loss variants and alterations in the MHC-I peptide-loading machinery and IFN response pathways (Zaretsky *et al.*, 2016; Burr *et al.*, 2019; Fares *et al.*, 2019). Tumour cells also suppress expression of stress ligands or production of danger signals to impair recognition by NK cells and activation of DCs, respectively (Wang *et al.*, 2004). Besides suppressing expression, surface-bound NK cell-activating ligands can be proteolytically shed (Ferrari de Andrade *et al.*, 2018). A more active role in resisting immune cell-mediated killing can also be adopted by tumour cells through upregulation of immune

checkpoint ligands such as PD-L1, expression of mutated non-functional forms of death receptors, and increase in intracellular anti-apoptotic factors (Vesely *et al.*, 2011).

Tumour cells also secrete molecules that favour the development of an immunosuppressive microenvironment. For example, release of TGF-β by tumour cells inhibits DC and T cell function, and induces peripheral conversion of $CD4^+$ T cells into Tregs. Factors such as CSF1, IL-1β and IL-4 are also expressed by tumour cells, leading to recruitment or expansion of myeloid-derived suppressive cells (MDSCs) and macrophages in the tumour microenvironment (Vesely *et al.*, 2011). More recently, it was uncovered that one of the pro-tumourigenic actions of tumour-derived prostaglandin E2 (PGE_2) is the inhibition of XCR1 and CCR5 production by NK cells, which are required for migration of cDC1s into the tumour microenvironment (Bottcher *et al.*, 2018). Tumour secretion of indoleamine 2,3-dioxygenase (IDO) metabolises the essential amino acid tryptophan into kynurenines in the microenvironment, which exerts a dual immunosuppressive function of starving T cells of tryptophan and inducing kynurenine-mediated toxicity (Lob *et al.*, 2009). Tumour-derived factors not only affect immune cells directly, but also indirectly through the tumour stroma (reviewed in Joyce and Fearon, 2015). For example, tumour-derived PGE_2 and VEGF induce the expression of Fas ligand in the tumour vasculature, evoking selective apoptosis of $CD8^+$ T cells but sparing Tregs that have relatively higher levels of the anti-apoptotic protein c-FLIP. T cells can also be excluded from the tumour microenvironment by stimulation of cancer-associated fibroblasts (CAFs) to produce highly dense extracellular matrix as a physical barrier to chemotaxis. The role of the microenvironment and stroma in promoting tumour development is a complex and evolving field as new processes are continually being elucidated (Joyce and Fearon, 2015).

1.4 Cancer immunotherapy

1.4.1 The cancer-immunity cycle

Understanding tumour cell-intrinsic and -extrinsic mechanisms of immune evasion allows strategies for re-establishing cancer immunity to be devised. In an optimal anti-tumour immune response, a sequence of events occurs in a self-propagating cyclic process, which persists until all tumour cells have been destroyed (*Figure 1.3*). These steps are referred to as the cancer-immunity cycle, in which seven major steps have been described (Chen and Mellman, 2013): 1) release of tumour-associated antigens in a suitable inflammatory milieu, 2) capture and presentation of antigens by DCs to T cells in secondary lymphoid organs, 3) priming and activation of tumour antigen-specific T cell responses, 4) trafficking of activated T cells through the blood vessels, 5) infiltration of T cells into the tumour, 6) recognition of tumour cells by T cells, and 7) T cell-mediated killing of tumour cells. Tumour cell death releases further tumour-associated antigens, which restarts the cycle, resulting in an iterative expansion of both the repertoire and amplitude of T cell responses. Each step of the cycle is regulated by stimulatory and inhibitory factors and can be subverted by the tumour for immune evasion. Importantly, points of failure can potentially be reversed, such as with immunotherapy, to allow the immune system to regain control of the tumour.

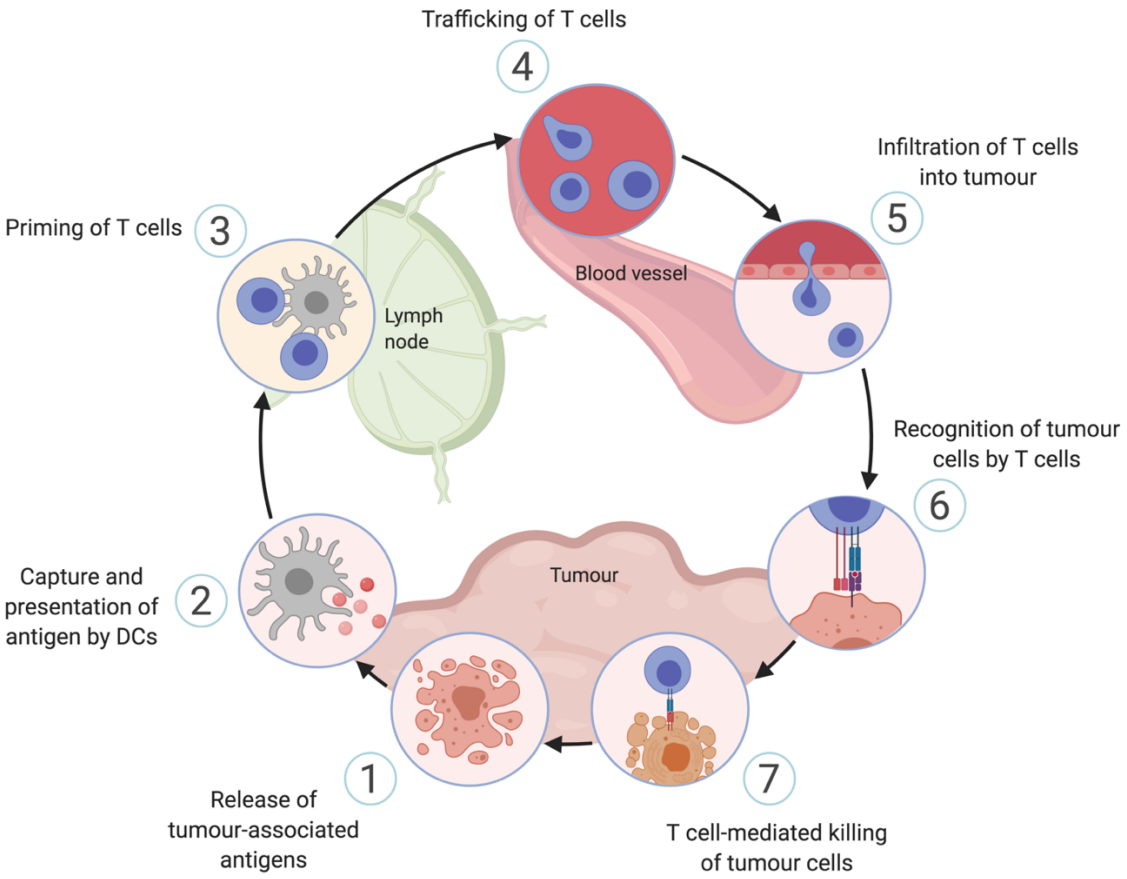

Figure 1.3. The cancer-immunity cycle. A sequence of events occurs in a self-propagating cyclic process in the generation of an optimal anti-tumour immune response. The cycle is divided in seven major steps, as illustrated above. Each step occurs at a particular anatomical site and is carefully regulated by a balance of stimulatory and inhibitory factors. This framework helps with the identification of points of failure in anti-tumour immune responses and the design of strategies to overcome them. Figure adapted from Chen and Mellman, 2013.

1.4.2 Immune checkpoint blockade

The two major modern breakthroughs in cancer immunotherapy that have dramatically redefined our paradigm on approaching cancer treatment are antibody-based immune checkpoint inhibitors and chimeric antigen receptor (CAR) T cells (Couzin-Frankel, 2013). Although the efficacy of CAR T cells in solid cancers has not been as profound as in haematological malignancies, antibody-based immune checkpoint inhibitors have demonstrated impressive results. The observation that treatment of metastatic melanoma with ipilimumab (an anti-CTLA-4 antibody) generated durable clinical responses in 20-30% of patients that translated to survival of greater than 10 years was unparalleled by any other cancer treatment modality (Schadendorf *et al.*, 2015). This led to the rapid approval of ipilimumab for clinical use by the United States Food and Drug Administration (FDA) in 2011. Since then, immune checkpoint inhibitors targeting the PD-1/PD-L1 axis such as nivolumab, pembrolizumab and durvalumab have also been approved after

demonstrating significant therapeutic gains across multiple solid cancers, including urothelial, renal cell, head and neck, hepatocellular carcinomas and non-small cell lung cancers (Ribas and Wolchok, 2018).

Informed by our understanding of the CTLA-4/CD28 and PD-1/PD-L1 signalling pathways, it is reasonable to extrapolate that blockade of CTLA-4 and PD-1/PD-L1 address steps 3 and 7 in the cancer-immunity cycle, respectively (*Figure 1.3*). Therefore, anti-CTLA-4 therapy is thought to primarily act in tumour draining lymph nodes to promote the priming of new T cell responses, whereas anti-PD-1 and anti-PD-L1 therapy are thought to primarily act peripherally in the tumour to reinvigorate T cells. However, many aspects of the underlying biology of CTLA-4 and PD-1/PD-L1 blockade remain to be elucidated (Wei *et al.*, 2018). For example, the possibility that anti-CTLA-4 therapy may be relevant within the tumour microenvironment in addition to draining lymph nodes is raised by two observations. Firstly, tumour-associated tertiary lymphoid structures have been described in cancers and correlated with improved survival, in which APCs could potentially process and cross-present tumour-associated antigens to prime T cells directly within tumours (Dieu-Nosjean *et al.*, 2008; Engelhard *et al.*, 2018). Secondly, depletion of Tregs by anti-CTLA-4 antibodies via ADCC is an important mechanism of action that contributes to their anti-tumour effect in mouse models (Bulliard *et al.*, 2013; Selby *et al.*, 2013; Simpson *et al.*, 2013). However, the currently available humanised anti-CTLA-4 antibodies ipilimumab and tremelimumab were not designed to deplete Tregs, and studies examining their ability to mediate Tregs clearance have thus far yielded conflicting results (Romano *et al.*, 2015; Arce Vargas *et al.*, 2018; Sharma *et al.*, 2019). Another potential mechanism of action of anti-CTLA-4 therapy is the broadening of the peripheral TCR repertoire. Given that CTLA-4 normally restricts TCR synapse signalling, loss of CTLA-4 may lower the threshold for TCR ligation required for T cell activation, allowing the emergence of T cell responses to antigens with weaker TCR affinity (Cha *et al.*, 2014; Robert *et al.*, 2014). Nonetheless, although this may confer better anti-tumour activity, it could also account for increased immune-related adverse events seen in patients receiving ipilimumab (Oh *et al.*, 2017).

PD-1 blockade induces the expansion and cytotoxic function of $CD8^+$ T cells, but the discrete subset of $CD8^+$ T cells that mediate tumour rejection remains to be fully elucidated. Studies have suggested that $CD8^+$ T cells with stem-like properties, as defined by the transcription factor Tcf1 and surface marker CXCR5, constitute the proliferative response to PD-1 blockade (Im *et al.*, 2016; Siddiqui *et al.*, 2019), whereas terminally exhausted $CD8^+$ T cells have acquired irreversible epigenetic changes that limit their reinvigoration (Pauken *et al.*, 2016; Philip *et al.*, 2017). The anti-tumour effects of PD-1 and PD-L1 blockade may also extend beyond changes to T cells. Intriguingly, selective PD-1 ablation on myeloid cells was recently reported to result in elevated T effector memory cell frequency and function despite preserved expression of PD-1 on T cells, leading to more effective control of tumours than selective PD-1 ablation on T cells (Strauss *et al.*, 2020). Another important recent study uncovered that PD-L1 expression and ligation on T cells could in fact induce inhibitory signalling within T cells, dampening Th1 polarisation in $CD4^+$ T cells and inducing an anergic phenotype in $CD8^+$ T cells (Diskin *et al.*, 2020). In that study, PD-

$L1^+$ T cells also engaged PD-1^+ macrophages which generated a tolerogenic immune contexture in the tumour microenvironment. However, although PD-1 and PD-L1 expression on macrophages is well-described in the cancer setting, much remains to be clarified regarding their role in anti-tumour responses (Hartley *et al.*, 2018; Lu *et al.*, 2019). PD-1 can also be expressed on a subpopulation of tumour cells, which promotes tumour growth through modulation of tumour cell-intrinsic mTOR signalling (Kleffel *et al.*, 2015). Collectively, these findings present new perspectives in understanding the mechanisms of action of anti-PD-1 and anti-PD-L1 therapy.

1.4.3 Overcoming resistance to cancer immunotherapy

The impressive and durable responses observed with immune checkpoint blockade therapy are currently restricted to specific patient subgroups and only in certain cancer types. Therapeutic resistance can be classified as: 1) primary, whereby the cancer lacks a pre-existing contexture that is permissive for immunotherapeutic intervention; 2) adaptive, whereby the cancer is recognised by the immune system but is able to protect itself from immune attack through modifications; or 3) acquired, whereby the cancer had initially responded to immunotherapy for a period of time before relapsing (Sharma *et al.*, 2017). Mechanisms of therapeutic resistance overlap with those described in Section 1.3 and include low tumour mutational burden, altered antigen presentation machinery, increased cellular stemness, and an unfavourable contexture of immune cell subsets and molecules in the tumour microenvironment. Importantly, they are shaped by continuous and constantly evolving interactions between tumour cell-intrinsic and -extrinsic factors. In recent years, alongside significant gains in the understanding of these therapeutic barriers, there have also been considerable efforts to address them (Sharma *et al.*, 2017; Galon and Bruni, 2019).

The effectiveness of a multi-pronged approach in overcoming resistance to cancer immunotherapy was clearly demonstrated by the finding that dual therapy with ipilimumab and nivolumab (an anti-PD-1 antibody), which have non-overlapping mechanisms of action, generated significantly improved response rates of up to 60% in patients with metastatic melanoma (Larkin *et al.*, 2015). An explosion of clinical trials testing the combination of immune checkpoint blockade with other therapies for mechanistic synergy have ensued, such as the pairing with cancer vaccines, adoptive cell transfer, targeted therapies, and epigenetic modifiers (Sharma *et al.*, 2017). Among these potential strategies, radiation therapy (RT) has steadily emerged as a promising candidate to complement cancer immunotherapy. As reviewed below, RT is a potent cytotoxic modality that also induces a range of immunomodulatory effects, which include release of tumour-associated antigens in an inflammatory environment, increased visibility of surviving tumour cells to T and NK cells, and greater infiltration of immune cells into tumours. Thus, RT could potentially re-initiate or further promote steps 1, 5 and 7 of the cancer-immunity cycle (*Figure 1.3*). Importantly, compared to other modalities, RT is unique in that it is fundamentally different in nature (a

physical rather than pharmacological intervention), geographically precise, potentially curative as monotherapy, readily accessible, and importantly, is inexpensive and free from commercial patents.

2. Radiation for the treatment of cancer

The use of ionising radiation, especially X-rays (photons), for the treatment of cancer is a well-established and major cancer treatment modality. Modern RT is an alternative to surgery in the curative-intent treatment of many cancer types. In addition, it is also used extensively in the adjuvant and palliative settings of cancer treatment. It is estimated that RT contributes to 40% of all cancer cures (Ringborg *et al.*, 2003), and at least 1 in 2 cancer patients will benefit from RT during their course of illness (Delaney *et al.*, 2005). Significant advances in radiobiology, radiation physics, and computer technology in the late 20th century have transformed RT into a highly sophisticated, precise and effective cancer treatment modality (Bernier *et al.*, 2004).

2.1 Radiation dose-fractionation

When X-rays were first adopted for treatment of tumours in the 1900's, large single-dose techniques were commonplace, which controlled tumours but at the cost of severe radiation toxicity. Pivotal work by Regaud, Coutard and colleagues in the 1920's confirmed that fractionation, or the dividing of a radiation dose into multiple daily fractions, could greatly increase the therapeutic window between tumour control and normal tissue toxicity (Bernier *et al.*, 2004). Subsequent foundational radiobiological work in the 1970's has allowed a better understanding of this phenomenon by proposing the "four R's" of radiation fractionation: repair, reoxygenation, reassortment, and repopulation (Joiner and Kogel, 2018). Briefly, repair refers to the restoration of sublethal DNA damage in normal tissues between fractions, in contrast to tumour cells which usually have defective DNA repair pathways. Reoxygenation describes the phenomenon whereby central hypoxic parts of the tumour become increasingly oxygenated as the tumour shrinks with each fraction, which increases the lethality of radiation-induced DNA damage due to chemical interactions with molecular oxygen. Reassortment, also called redistribution, refers to the entry of tumour cells previously in radioresistant phases of the cell cycle into radiosensitive phases between fractions. Lastly, repopulation means that fractionation allows time for rapidly dividing normal tissues, such as epithelia, to replenish between fractions, thereby decreasing acute radiation toxicity.

Thus, fractionation exploits differences between tumour and normal tissues to maximise tumour cell death but minimise normal tissue damage. In light of this, conventionally fractionated radiation regimens, which typically use multiple fractions of less than 4Gy per fraction (often over many weeks), have dominated clinical practice for a long time. More recently, technological advances in image guidance, motion tracking, and dose calculation algorithms have reintroduced the delivery of high doses in one or a few fractions, referred to as severely hypofractionated or ablative regimens (usually above 8Gy per fraction) (Pan *et al.*, 2011). The implementation of such radiation techniques is termed stereotactic radiosurgery

(SRS) or stereotactic ablative body radiotherapy (SABR) for intracranial and extracranial treatments, respectively. Although the differential cell kill between tumour and normal tissues is lost with such regimens, this is compensated by geographic and dosimetric precision in radiation delivery. Therefore, SRS and SABR are suitable only for smaller lesions with well-defined margins. The unique roles of these techniques in the armamentarium against cancer were first tested and established for the treatment of metastases, in which a major advantage of SRS and SABR is the convenience afforded to the patient by reducing the number of treatment sessions while achieving durable local control. Beyond mere convenience, a recent phase 2 randomised trial reported that an aggressive use of SABR to target metastases could double the median progression free survival with an increase in overall survival, serving as clinical support for using SABR within the oligometastatic paradigm to hamper systemic disease progression (Palma *et al.*, 2019). Concurrently, clinical evidence for the safety and efficacy of SABR regimens as an alternative to conventionally fractionated regimens in the non-metastatic, curative setting has been mounting in a variety of cancer types (Loblaw *et al.*, 2013; Crane, 2016; Ball *et al.*, 2019).

It is evident that radiation dose-fractionation regimens have been evolving since the beginning of radiation oncology. The selection of the most appropriate radiation regimen to afford the best chance of tumour control in a given context will therefore be guided by continual advances in the clinical evidence and biological understanding of radiation dose-fractionation.

2.2 Molecular mechanisms of radiation-induced cell death

Radiation kills cells primarily by damaging nuclear DNA. DNA lesions are sensed by the kinases ataxia-telangiectasia mutated (ATM) and ataxia-telangiectasia and Rad3-related protein (ATR), which initiate the DNA damage response, placing the cell into cell cycle arrest for DNA repair (Joiner and Kogel, 2018). The lethality of radiation-induced DNA lesions is dependent on a combination of radiation, cell-intrinsic and microenvironmental factors, including radiation quality, the proximity of DNA lesions to each other, the phase of the cell cycle at the time of DNA damage, cell type, and oxygen tension of the cellular microenvironment (Joiner and Kogel, 2018). While most DNA lesions are repaired, complex chromosomal aberrations resulting from interactions between broken DNA strands lead to irreparable damage and cell death, which can occur either in interphase or at a delayed time point when the cell enters mitosis. Radiation-induced cell death has several major types, but in classical radiobiology, the primary measure of biological effect by radiation is the loss of cellular replicative capacity, as determined by clonogenic assays. However, an understanding of the different types of radiation-induced cell death and their underlying molecular mechanisms is vital when considering downstream effects and when combining with other cancer treatment modalities.

2.2.1 Mitotic catastrophe and mitotic death

Mitotic catastrophe is an interim cellular state of replicative stasis resulting from failed or aberrant mitosis, and is the most common mechanism of tumour control in solid cancers after irradiation (Eriksson and Stigbrand, 2010). The exact mechanisms for the initiation of mitotic catastrophe are unclear, but tumour cells often have dysfunctional cell cycle checkpoints that allow premature entry into mitosis with misrepaired DNA. Almost always, mitotic catastrophe leads to either regulated cell death (most commonly apoptosis) or cellular senescence, but rarely do cells escape mitotic catastrophe (Gascoigne and Taylor, 2008; Vakifahmetoglu *et al.*, 2008). Mitotic death refers to the secondary death types when preceded by mitotic catastrophe (Galluzzi *et al.*, 2018). Therefore, mitotic catastrophe is not a bona fide cell death type, even though there is a long history of recognising it as a type of cell death in classical radiobiology. Factors affecting the decision of final cell fate after mitotic catastrophe are poorly defined at present. Several attempted cell divisions can occur before sufficient genetic damage is accumulated, underlining the clinical observation that most solid tumours display delayed regression post irradiation.

2.2.2 Apoptosis

Apoptosis can be triggered by radiation through the intrinsic and extrinsic pathways. A third pathway, called the ceramide pathway, has been proposed but is less well-described. The intrinsic pathway, also known as the mitochondrial pathway, is activated when the DNA damage repair machinery upregulates pro-apoptotic factors over anti-apoptotic factors. The tipping of balance results in release of cytochrome c from the mitochondria into the cytoplasm to activate caspase 9 (Eriksson and Stigbrand, 2010). In contrast, the extrinsic pathway is initiated upon binding of TNF family of ligands, such as TNF, TRAIL and the Fas ligand, to their cognate death receptors on the cell surface, which leads to downstream activation of caspase 8. Because radiation upregulates the expression of death receptors, irradiated cells have increased susceptibility to death via this pathway (Wu *et al.*, 1997; Chakraborty *et al.*, 2003; Sheard *et al.*, 2003). The ceramide pathway can be triggered by radiation through activation of acid sphingomyelinase in the plasma membrane, which hydrolyses sphingomyelin to produce ceramide (Pettus *et al.*, 2002). Additionally, ceramide can also be synthesised *de novo* by activation of mitochondrial ceramide synthase by radiation-induced DNA damage. Ceramide acts as a second messenger in a complex signalling network that initiates the apoptotic programme (Pettus *et al.*, 2002; Kolesnick and Fuks, 2003).

2.2.3 Necrosis

Necrosis is an unregulated, chaotic form of cell death, triggered by unfavourable conditions such as extreme changes in pH, energy loss and ion imbalance within the cell and its microenvironment during infection, inflammation, or following irradiation (Kroemer *et al.*, 2009). Because necrosis lacks characteristic biochemical markers, it is often a diagnosis of exclusion based largely on morphological changes, which include a gain in cellular volume, plasma membrane rupture, organelle breakdown and

mitochondrial dysfunction, release of lysosomal enzymes, and spill of intracellular contents. Necrosis has been traditionally thought to be pro-inflammatory, although this association is no longer considered absolute (Green *et al.*, 2009; Galluzzi *et al.*, 2017).

2.2.4 Senescence

Senescence refers to permanent cell cycle arrest and is usually differentiated by its cause: replicative, oncogene-induced, or stress-induced. Stress-induced senescence after radiation exposure is triggered by DNA damage and the induction of the p53/p21$^{WAF1/CIP1}$ and pRb/p16^{INK4A} pathways which block progression through the cell cycle, although other factors including oxidative stress may also be relevant triggers in the irradiation context (Sabin and Anderson, 2011; Li *et al.*, 2018b). While senescence is a form of replicative "death", senescent cells continue to be viable and metabolically active. Importantly, senescent cells develop the senescence-associated secretory phenotype (SASP) over time, characterised by a specific expression pattern of immuno-modulatory cytokines, growth factors, and matrix metalloproteinases (Lasry and Ben-Neriah, 2015). Both pro- and anti-tumour effects of SASP have been described (Xue *et al.*, 2007; Coppe *et al.*, 2010; Iannello *et al.*, 2013). It was recently elucidated that SASP is a result of the extrusion of cytosolic chromatin fragments in senescent cells due to decreased nuclear membrane integrity, which activates the stimulator of interferon genes (STING) pathway to drive expression of interferon and NF-kB elements (Dou *et al.*, 2017; Gluck *et al.*, 2017).

2.2.5 Autophagic cell death

Autophagy describes the process of sequestrating damaged or old cytoplasmic organelles within vesicles for lysosomal degradation in response to cellular stress. It is usually a cytoprotective process, but autophagic cell death occurs when the autophagic response is excessive (Kroemer and Levine, 2008). The autophagic machinery is a highly regulated pathway involving the ATG genes. The exact mechanisms by which radiation triggers autophagy is unclear, but likely involves the endoplasmic stress module and mTOR pathway (Tam *et al.*, 2017).

2.2.6 Other types of cell death

More recently described forms of regulated cell death have been identified in response to radiation exposure, including necroptosis and ferroptosis, although the extent to which these occur *in vivo* are uncertain (Gong *et al.*, 2019; Lang *et al.*, 2019; Lei *et al.*, 2019). Necroptosis was for a long time confused with necrosis due their similar morphological changes, however necroptosis is activated by death receptors and signalled through caspase-independent pathways converging on RIPK3 and MLKL. Because necroptosis occurs when caspase 8 is non-functional, it has been suggested that necroptosis is a back-up death pathway to apoptosis. Ferroptosis is a type of cell death triggered by the accumulation of lipid peroxides due to decreased degradation by glutathione peroxidase (GPX). In the irradiation context, this

can occur via ATM-mediated repression of the cystine-glutamate antiporter system xc-, resulting in decreased glutathione, a co-factor for GPX4 (Lang *et al.*, 2019).

2.3 The shift of focus from classical radiobiology

Classical radiobiology, which studies how radiation interacts with cellular and microenvironmental factors to induce DNA damage and cell death, has led to cornerstone clinical gains such as the development of altered fractionation and the use of hypoxic modifiers (Ang, 1998; Marcu, 2010; Overgaard, 2011). Indeed, if cancer is purely a cell-autonomous predicament, the ultimate aim of RT in curative-intent treatment is to achieve replicative sterilisation of all cancer stem cells within the radiation field. Several lines of observation however challenge the DNA-centric dogma of classical radiobiology. For example, induction of biological effects have been observed in tissues not directly traversed by ionising radiation but in close proximity, as well as distant, to irradiated tissues — termed the radiation bystander and abscopal effects respectively (Prise *et al.*, 2005). Importantly, it has been noted since the 1970's that an intact host immune system improves the tumour control probability of RT (Stone *et al.*, 1979). These phenomena suggest that the tumouricidal activity of RT must extend beyond the direct cytotoxicity of damaging DNA in irradiated cancer cells. The concept of "non-targeted effects" of RT has been conceived to refer to the downstream consequences of irradiation that are not directly related to cellular energy deposition (Prise *et al.*, 2005; Formenti and Demaria, 2009).

The immunological effects of RT constitute a principal component of its non-targeted effects. The interaction between RT and the host immune system in controlling tumours has been demonstrated by several key studies. The previously mentioned report by Stone *et al.* provides early evidence for this, in which a 1.67-fold higher dose of radiation was required to achieve comparable tumour control in immunodeficient mice compared to immunocompetent mice (Stone *et al.*, 1979). Consistent with this finding, Dunn *et al.* reported that whole-body irradiation of immunocompetent mice mediated rejection of established tumours, whereas this effect was not observed in immunodeficient mice (Dunn and North, 1991). Furthermore, the radiation abscopal effect was demonstrated by Demaria *et al.* to be mediated by $CD8^+$ T cells (Demaria *et al.*, 2004). More recently, immense interest in the immunological effects of RT was heightened following clinical reports of increased abscopal events in patients receiving RT and cancer immunotherapy (Postow *et al.*, 2012; Golden *et al.*, 2015). Owing to a large body of mechanistic work, we now have greater insight into the mechanisms by which RT can evoke anti-tumour immune responses to support its therapeutic activity. For the purposes of this review, these processes are categorised into: 1) radiation-induced immunogenic cell death, 2) generation of $CD8^+$ T cell responses, 3) immune infiltration of tumours, 4) modulation of immune recognition and killing of tumour cells, and 5) negative regulation of radiation-induced immune responses.

2.4 Radiation-induced immunogenic cell death (ICD)

2.4.1 Observations of radiation-induced ICD

The discovery that conventional cancer modalities such as chemotherapy and RT can evoke forms of cell death that are able to induce host immune responses via peri-mortem processes has shifted our perspective on cell death to one from a functional aspect. The Nomenclature Committee on Cell Death (NCDD) defines immunogenic cell death (ICD) as a type of regulated cell death that is sufficient to evoke an adaptive immune response in immunocompetent hosts (Galluzzi *et al.*, 2018). Although the immunogenicity of cell death has historically been ascribed based on the type of cell death (Green *et al.*, 2009), this has now been re-evaluated. A range of cell death types, including necrosis and apoptosis, have been shown capable of inducing ICD (Galluzzi *et al.*, 2018). Therefore, the current mechanistic understanding of ICD disengages from traditional cell death types, but specifies two requirements for immunogenicity: adjuvanticity and antigenicity (Galluzzi *et al.*, 2017). Adjuvanticity is mediated by the exposure of danger signals, or DAMPs, from the dying cell, which activates APCs involved in immune surveillance. Antigenicity is achieved when tumour-associated antigens are captured by APCs and cross-presented to the adaptive immune arm for priming. Because neither the release of DAMPs nor the tumour cell type reliably predicts for adjuvanticity or antigenicity upon death *in vivo*, the gold standard approach for confirming ICD relies on *in vivo* vaccination assays (Galluzzi *et al.*, 2017). Surrogate measures, including the detection of DAMPs, DC maturation and phagocytosis assays, cytotoxic T cell killing assays, and tumour control monitoring, are of value but do not unequivocally prove that bona fide ICD has taken place.

The capacity for radiation to evoke ICD has been demonstrated both directly, using *in vivo* vaccination assays, and indirectly, by surrogate measures as outlined above. Several landmark papers have demonstrated the induction of ICD by irradiation with X-rays and alpha particles using *in vivo* vaccination assays in mouse models (Apetoh *et al.*, 2007; Obeid *et al.*, 2007; Gorin *et al.*, 2014). Complementing this, a large body of work has provided indirect support for radiation-induced ICD across different murine and human cell lines. These include early experiments in which DCs that had been loaded with protein lysates derived from irradiated tumour cells could evoke tumour-specific immune responses (Kurokawa *et al.*, 2001; Strome *et al.*, 2002), and more recent *in vitro* and *in vivo* studies that demonstrated induction of DAMP release, DC maturation and T cell priming by radiation (Demaria *et al.*, 2004; Deng *et al.*, 2014b; Gameiro *et al.*, 2014; Golden *et al.*, 2014; Ko *et al.*, 2014; Lim *et al.*, 2014; Vanpouille-Box *et al.*, 2017). Collectively, these direct and indirect observations have led to the hypothesis that radiation cell kill and the resultant exposure of tumour-associated antigens and immune adjuvants can potentially convert the irradiated tumour into an *in situ* vaccine capable of evoking host anti-tumour immune defences (Formenti and Demaria, 2012).

2.4.2 Molecular mechanisms of adjuvanticity in radiation-induced ICD

The observation that tumour cells lysed by freeze-thawing or by boiling were unable to induce host immunity indicates that ICD involves cellular processes beyond mere spillage of intracellular content (Goldszmid *et al.*, 2003; Casares *et al.*, 2005; Aaes *et al.*, 2016). Three molecular pathways for the peri-mortem release of DAMPs are classically described with radiation: 1) the surface exposure of calreticulin, 2) the release of HMGB1, and 3) the secretion of adenosine triphosphate (ATP) into the extracellular space (Ma *et al.*, 2010; Golden *et al.*, 2012).

Calreticulin is an endoplasmic reticulum chaperone that becomes an "eat me" signal for APCs when exposed on the surface of dying cells by interaction with the CD91 receptor on APCs (Basu *et al.*, 2001). The translocation of calreticulin to the cell surface occurs early in the pre-apoptotic process as part of the unfolded protein response in stressed cells. The requirement of this event for ICD have been shown to be relevant in the irradiation context by multiple groups (Obeid *et al.*, 2007; Gameiro *et al.*, 2014; Golden *et al.*, 2014). HMGB1 is a nuclear chromatin-binding protein that binds to the TLR4 receptor on DCs when in the extracellular space, which promotes type I IFN expression and DC cross-presentation function. Although HMGB1 is actively secreted by some immune cells, release of HMGB1 by tumour cells is thought to be passive and occurs with late apoptosis, autophagy, or necrosis (Lotze and Tracey, 2005). The relevance of HMGB1 in radiation-induced ICD has also been well-demonstrated (Apetoh *et al.*, 2007; Golden *et al.*, 2014; Werthmoller *et al.*, 2015). ATP that has been secreted into the extracellular space attracts DCs and activates the DC inflammasome via interaction with the purinergic receptors P2RY2 and P2RX7 (Lopez-Castejon and Brough, 2011). This leads to generation of the pro-inflammatory IL-1β cytokine, which enhances T cell priming and differentiation. Optimal secretion of ATP in both chemotherapy and radiation-induced ICD is active and dependent on intact pre-mortem autophagic machinery for the accumulation of ATP within autolysosomes (Ohshima *et al.*, 2010; Michaud *et al.*, 2011; Golden *et al.*, 2014; Ko *et al.*, 2014).

Cytosolic double-stranded DNA (dsDNA) is a recently described radiation-induced DAMP that has received significant attention. dsDNA is commonly thought to be released directly into the cytoplasm from the nucleus and/or mitochondria as a consequence of radiation damage, where it binds to the innate DNA sensor cyclic GMP-AMP synthase (cGAS). However, it was recently shown that unstable chromosomes resulting from radiation-induced DNA double-strand breaks form micronuclei during mitosis, and the subsequent loss of micronuclear envelope integrity allows co-localisation with cGAS (Harding *et al.*, 2017). Thus, the sensing of cytosolic dsDNA following irradiation may be dependent on cell cycling, which provides a link between the rapid kinetics of DNA damage responses with the delayed onset of downstream inflammatory processes (minutes to hours *vs*. days, respectively). Binding of dsDNA with cGAS catalyses the production of 2',3'-cyclic GMP-AMP (cGAMP), which activates STING, initiating a cascade that culminates in the nuclear recruitment of interferon regulatory factor 3 (IRF3) to drive expression of type I IFN (reviewed in Kwon and Bakhoum, 2020) (*Figure 1.4*). Cytosolic dsDNA does

not necessarily activate STING in a cell-intrinsic fashion, but dsDNA or cGAMP can be released into the extracellular space and, through mechanisms that are still being defined, taken up by myeloid cells, resulting in activation of STING within those cells (Woo *et al.*, 2014; Diamond *et al.*, 2018; Schadt *et al.*, 2019). Thus, cytosolic dsDNA constitutes an important DAMP in the radiation setting through a "viral mimicry" pathway that culminates in the generation of type I IFN, which in turn promotes the efficient cross-presentation function of DCs (Burnette *et al.*, 2011; Deng *et al.*, 2014b; Vanpouille-Box *et al.*, 2017). Besides priming T cell responses, recent data suggests tumour cell cGAS-dependent STING activation also induces NK cell-mediated tumour cell kill (Marcus *et al.*, 2018).

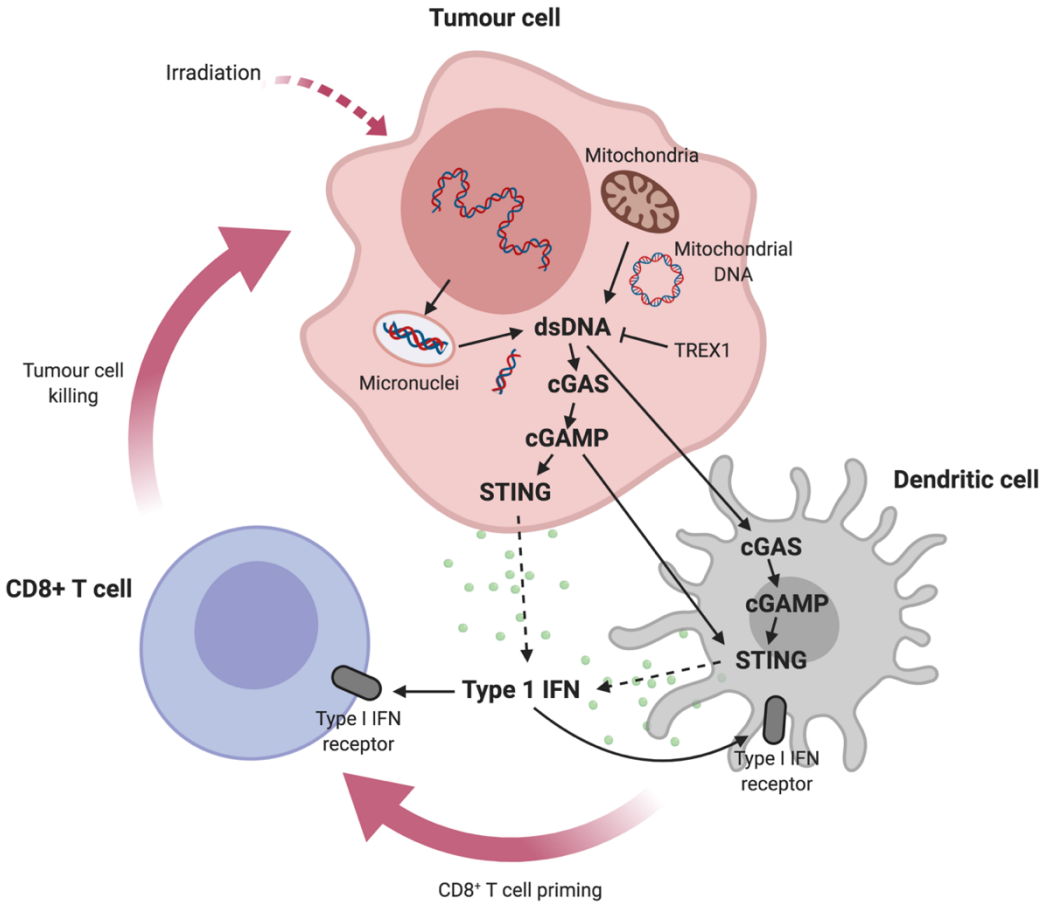

Figure 1.4. Cytosolic dsDNA sensing by the cGAS-STING axis in the induction of CD8+ T cell responses following irradiation. Radiation damage to tumour cells results in the release of nuclear and mitochondrial double-stranded DNA (dsDNA) into the cytoplasm. There, it is sensed by cyclic GMP-AMP synthase (cGAS), which catalyses production of 2',3'-cyclic GMP-AMP (cGAMP). cGAMP then activates stimulator of interferon genes (STING), initiating a cascade that ultimately drives expression of type 1 interferons (IFN), among other gene products. Intermediary steps in this pathway are not depicted in the diagram. Importantly, tumour-derived dsDNA can activate both cell-intrinsic and -extrinsic STING. In the latter, tumour dsDNA or cGAMP can be taken up by neighbouring myeloid cells such as dendritic cells (DCs) to trigger STING-mediated type I IFN production in those cells. Both type I IFN production and responsiveness is required in DCs to efficiently prime tumour cell-reactive

$CD8^+$ T cell responses following irradiation (reviewed in Section 2.5.3). As a homeostatic mechanism, STING activation can be regulated by the exonuclease TREX1, which degrades cytosolic dsDNA.

STING signalling could potentially be shut down by the exonuclease TREX1, which degrades cytosolic dsDNA. Vanpouille-Box *et al.* demonstrated that higher radiation doses when delivered as a single fraction generated larger amounts of STING-activating cytosolic dsDNA within tumour cells, but this was accompanied by induction of TREX1 expression as a homeostatic mechanism (Vanpouille-Box *et al.*, 2017). At a threshold of 10-12Gy in a single fraction, TREX1 was sufficiently upregulated in a range of mouse and human tumour cell lines such that cytosolic dsDNA was degraded to a level below the detection of cGAS, leading to loss of tumour cell-intrinsic STING activation and IFN-β production. *In vivo*, this abrogated the ability of RT and anti-CTLA-4 therapy to control unirradiated TSA mammary carcinoma tumours. However, reactive oxygen species generated by radiation can induce DNA modifications that render DNA resistant to degradation by TREX1, yet still capable of activating cGAS-STING signalling (Gehrke *et al.*, 2013). Indeed, another recent study found that a single fraction of 20Gy generated similar levels of cytosolic dsDNA compared to a single fraction of 8Gy in CT26 mouse colon carcinoma cells (Schadt *et al.*, 2019). Moreover, in this study, tumour cell cGAS activation of STING in tumour-associated DCs, rather than in tumour cells, was found to be critical for radiation-induced $CD8^+$ T cell responses in CT26 tumours. Therefore, the requirement of tumour cell-intrinsic STING activation for $CD8^+$ T cell responses and its regulation by TREX1 modulation are likely tumour model-dependent and remain to be clarified.

Other DAMPs have also been identified in the context of ICD induced by cancer treatment modalities other than radiation, such as the heat shock protein 70 kDa (HSP70) and heat shock protein 90 kDa (HSP90), F-actin, and IL-33 (Krysko *et al.*, 2012; Galluzzi *et al.*, 2017). Although their role in the radiation setting has not been formally tested, it is conceivable that they may have a role to play in radiation-induced ICD too. It is also likely that the DAMPs involved in the priming of adaptive immune responses will be tumour and context-dependent. For example, the cGAS-STING axis, but not HMGB1, was shown to be essential for adaptive anti-tumour immune responses after irradiation of MC38 mouse colon carcinoma tumours with a single fraction of 20Gy (Deng *et al.*, 2014b).

2.4.3 Molecular mechanisms of antigenicity in radiation-induced ICD

Cancers by nature of their inherent genomic instability are potential antigenic entities, accumulating somatic mutations as they evolve (Schumacher and Schreiber, 2015). Additionally, radiation also increases tumour antigenicity via several mechanisms. Firstly, irradiation can induce the expression of potentially antigenic but normally silent genes. Sharma *et al.* showed that irradiation of various cancer cell lines with a single fraction of 20Gy *in vitro* upregulated mRNA expression of normally silent cancer testis antigens, and was able to corroborate this in paired pre- and post-RT biopsies from sarcoma patients (Sharma *et al.*,

2011). Secondly, radiation can result in an altered intracellular peptide pool through upregulation of the mTOR protein translation machinery, detectable on examination of the repertoire of peptides presented on surface MHC-I, as demonstrated by Reits *et al.* (further described in Section 2.7) (Reits *et al.*, 2006). Thirdly, radiation-induced inflammatory cues lead to formation of immunoproteasomes that process peptides differently than standard proteasomes in non-inflammatory settings (Morel *et al.*, 2000). Importantly, the immunological impact of these observations is reflected in mouse and human studies showing that RT broadens the diversity of circulating and tumour-infiltrating TCR clonotypes (Twyman-Saint Victor *et al.*, 2015; Rudqvist *et al.*, 2018; Phillips *et al.*, 2020). A recent clinical trial combining RT with immune checkpoint blockade reported a patient case of complete response who had expansion of T cell clones against a tumour-associated neoantigen, the expression of which was upregulated by irradiation (Formenti *et al.*, 2018). This represents the first in-human proof of benefit for radiation-induced exposure of immunogenic tumour mutations to the immune system.

Collectively, these mechanistic findings explain the ability of RT to induce ICD by both promoting adjuvanticity through the peri-mortem release of DAMPs and enhancing antigenicity through the increase in expression of tumour-associated antigens.

2.5 Generation of CD8$^+$ T cell responses by RT

2.5.1 The radiosensitivity of T cells

RT has long been considered immunosuppressive due to the inherent susceptibility of lymphocytes to radiation-induced apoptosis. Since the 1950's, it has been observed that exposure to 0.5-2Gy irradiation is sufficient to eradicate significant proportions of lymphocytes in human blood and mouse lymphoid organs (Trowell, 1952; Heylmann *et al.*, 2014). Furthermore, Tregs are consistently found to be one of the most radioresistant subsets, reinforcing the notion that RT is an immunosuppressive modality (Heylmann *et al.*, 2014). This conclusion however is an oversimplification and is in contrast with the observations of T cells potentiating the anti-tumour effects of RT. Subsequent investigations have determined that antigen-experienced and memory T cells are more radioresistant than naïve T cells (Dunn and North, 1991; Grayson *et al.*, 2002). An important study by Arina *et al.*, using longitudinal *in vivo* imaging and functional analysis in two mouse tumour models, showed that pre-existing tumour-associated T cells survived up to two weeks after 5x1.8Gy and even 1x20Gy irradiation (Arina *et al.*, 2019). In fact, these pre-existing T cells retained their motility and demonstrated increased production of IFN-γ *in vivo* after irradiation, and were critical for the full therapeutic effects of RT. Most of these T cells were CD8$^+$ and transcriptionally resembled resident memory T cells (T_{RM}), although not all demonstrated a T_{RM} surface marker phenotype. These observations overturn the long-standing assumption that lymphocytes are universally highly sensitive to radiation killing or become functionally impaired after irradiation. Rather, T cells exhibit remarkable subset and site-specific radioresistance that likely contribute to the anti-tumour effects of RT.

2.5.2 Radiation-induced priming of CD8$^+$ T cells by DCs

Studies have shown that radiation-induced anti-tumour CD8$^+$ T cell responses are dependent on tumour antigen-specific priming by DCs. In a landmark study by Demaria *et al.*, 67NR mammary carcinoma cells were inoculated in both flanks of immunocompetent Balb/c mice to form tumours, and localised tumour irradiation (1x2Gy or 1x6Gy) was delivered to only one side (Demaria *et al.*, 2004). Mice were also treated with the DC growth factor fms-like tyrosine kinase 3 (FLT3) ligand to promote the cross-presentation function of DCs. Only the combination of tumour irradiation and FLT3 ligand treatment could evoke abscopal responses that delayed the growth of unirradiated 67NR tumours in the same mice. These abscopal responses were confirmed to be tumour-specific since the growth of unirradiated A20 lymphoma tumours was not affected. Furthermore, mice deficient of T cells did not mount such abscopal responses. Together, these findings were the first to suggest that RT promoted tumour antigen-specific priming of T cells through stimulation of DCs. Other *in vivo* studies using B16 mouse melanoma tumours have since correlated tumour irradiation with increased numbers and cross-presentation function of DCs in draining lymph nodes, as well as expansion of antigen-specific CD8$^+$ T cells and their infiltration into tumours (Lugade *et al.*, 2005; Lee *et al.*, 2009; Sharabi *et al.*, 2015a). Importantly, Gupta *et al.* found that depletion of DCs or blockade of the DC co-stimulatory molecule CD70 reduced the number of tumour-associated CD8$^+$ T cells, resulting in poorer tumour control following irradiation (1x10Gy) of B16 tumours (Gupta *et al.*, 2012). In the same study, B16 tumour cells were engineered to express the diphtheria toxin (DT) receptor so that they could be killed by DT treatment in mice. Triggering of tumour cell death in this sterile context failed to prime CD8$^+$ T cell responses, highlighting the requirement of radiation-induced inflammation for DC maturation and induction of CD8$^+$ T cell responses.

2.5.3 The requirement of Type I IFN

In line with the selective requirement of type I IFN for the cross-presentation function of cCD1s (reviewed in Section 1.2.1), radiation-induced DC priming of CD8$^+$ T cell responses has also been reported to be type I IFN-dependent. Burnette *et al.* showed that in irradiated B16 tumours, IFN-β mRNA and protein expression levels were elevated in immune cells, and expression of the IFN-α/β receptor alpha chain (IFNAR1) in tumour-associated DCs, but interestingly not in lymph node DCs or tumour cells, was critical in driving radiation-induced T cell expansion and tumour control (Burnette *et al.*, 2011). Further to this, Deng *et al.* reported that in irradiated MC38 tumours, the source of IFN-β was DCs and central to their ability to produce IFN-β was activation of the STING signalling pathway (Deng *et al.*, 2014b). These findings suggest that induction of CD8$^+$ T cell responses by radiation requires DCs to both produce and respond to type I IFN (*Figure 1.4*). Vanpouille-Box *et al.* subsequently confirmed that radiation-induced STING signalling for type I IFN production was activated by increases in cytosolic dsDNA (reviewed in Section 2.4.3) (Vanpouille-Box *et al.*, 2017).

2.6 Immune infiltration of irradiated tumours

Besides priming $CD8^+$ T cell responses, radiation also promotes the recruitment of T cells into tumours through evoking the release of chemoattractants such as the IFN-γ inducible chemokines CXCL9 and CXCL10 (Lugade *et al.*, 2008; Lim *et al.*, 2014). Additionally, in an *in vitro* migration assay, CXCL16 from irradiated mouse and human breast cancer cells was identified as an important factor for the recruitment of activated $CD8^+$ T and NK cells (Matsumura *et al.*, 2008; Yoon *et al.*, 2016). Radiation-induced DNA damage can also trigger the activation of the canonical NF-kB pathway, when ATM, after recruitment to sites of DNA damage in the nucleus, translocates to the cytoplasm to interact with the p50/p65 complex of NF-kB (Brach *et al.*, 1991; Piret *et al.*, 1999). This leads to expression of a host of pro-inflammatory cytokines, including TNF-α, IL-1α, IL-1β, IL-6, and CXCL1.

Radiation-induced changes to tumour vasculature also contribute to the trafficking of immune cells into tumours. Several reports have described upregulation of the vascular endothelial cell adhesion molecules VCAM-1, ICAM-1 and CD31 following irradiation, which may aid in the extravasation of immune cells into tumours (Heckmann *et al.*, 1998; Quarmby *et al.*, 2000; Lugade *et al.*, 2008). Furthermore, Ganss *et al.* reported normalisation of previously irregular tumour capillary networks in a RIP-Tag5 insulinoma model thirty-eight days after whole body irradiation with a single fraction 10Gy, which facilitated an increased T cell infiltration into the tumours (Ganss *et al.*, 2002). Interestingly, there was no obvious endothelial cell death to explain the vasculature remodelling, but enhanced expression of CXCL9 and CXCL10 was noted, which also had angiostatic properties. Therefore, radiation-induced CXCL9 and CXCL10 could have a dual role of inhibiting disorderly angiogenesis to re-establish normal vasculature, as well as promoting lymphocyte chemotaxis. Altogether, the potential for radiation to enhance immune infiltration of tumours is a promising strategy for converting “cold” (non-inflamed) tumours into “hot” (inflamed) tumours for synergy with cancer immunotherapy (Galon and Bruni, 2019).

2.7 Modulation of immune recognition and killing of tumour cells

Radiation may also modulate the recognition of tumour cells by immune cells. Multiple studies have demonstrated that radiation upregulates MHC-I expression on tumour cells both *in vitro* and *in vivo* in a dose-dependent manner (Santin *et al.*, 1997; Garnett *et al.*, 2004; Reits *et al.*, 2006; Lugade *et al.*, 2008; Sharabi *et al.*, 2015a). This can potentially counteract the downregulation of MHC-I as a pathway hijacked by tumour cells for immune escape. Reits *et al.* also demonstrated *in vitro* that irradiated cells have an altered repertoire of peptides presented on MHC-I, creating an additional mechanism by which RT may increase the visibility of tumour cells to T cells (Reits *et al.*, 2006). In these studies, radiation-induced increases in MHC-I expression on tumour cells correlated with higher recognition by antigen-specific $CD8^+$ T cells both *in vitro* and *in vivo*. Interestingly, Zheng *et al.* showed that a by-product of greater antigen release following irradiation was the transient appearance of tumour-specific MHC-peptide complexes on stromal cells, which sensitised stromal cells to $CD8^+$ T cell killing (Zhang *et al.*, 2007).

Beyond T cells, radiation as a genotoxic agent induces the expression of stress-induced ligands on tumour cells, making them targets for NK cells. Gasser *et al.* used a NKG2D tetramer to demonstrate *in vitro* that NKG2D ligands, including RAE-1, were upregulated in murine ovarian epithelial carcinoma cell lines following irradiation with a single fraction of 40Gy, in a process that was linked with the ATM pathway in response to radiation-induced DNA damage (Gasser *et al.*, 2005). Additionally, Kim *et al.* examined various human tumour cell lines following irradiation with a single fraction of 20Gy *in vitro* and also found increased expression of the human NKG2A ligands MICA, MICB, ULBP1, ULBP2 and ULBP3 (Kim *et al.*, 2006). In this study, irradiated tumour cells were more prone to NK cell-mediated killing, although there were differences in magnitude across the cell lines. Of note, very high doses of radiation were used by both these groups.

The sensitivity of tumour cells to immune cell killing can be enhanced by radiation through the upregulation of death receptors linked with the DNA damage response pathway, which include Fas/CD95 and DR5 (Wu *et al.*, 1997; Chakraborty *et al.*, 2003; Sheard *et al.*, 2003; Chakraborty *et al.*, 2004; Garnett *et al.*, 2004). In one study, increased surface expression of Fas in MC38 tumours *in vivo* was seen up to eleven days after irradiation, suggesting that tumour cells could be sensitised to immune cell killing for a prolonged duration (Chakraborty *et al.*, 2004). Upregulation of these receptors correlated with higher granzyme/perforin-independent killing by $CD8^+$ T cells, although the sensitisation effect may not apply to all tumour cell types (Sheard *et al.*, 2003; Garnett *et al.*, 2004).

2.8 Negative regulation of radiation-induced immune responses

Because radiation can promote the infiltration and function of immune cells, it is no surprise that the inflammatory response generated would upregulate PD-L1 expression in both tumour and host cells, due to increased IFN-γ levels in the tumour microenvironment (Deng *et al.*, 2014a; Dovedi *et al.*, 2014; Twyman-Saint Victor *et al.*, 2015). This constitutes a radiation-induced mechanism of adaptive resistance to immune-mediated tumour cell killing. Besides tumour cell-intrinsic adaption, radiation also evokes suppressive immune responses that hamper the net anti-tumour effect. It is well demonstrated that tumour-associated and circulating Tregs can be enriched by radiation over other effector T cell subsets in both human and mouse settings (reviewed in Persa *et al.*, 2015). The mechanisms for this selective increase in Tregs are uncertain, but the relative radioresistance of Tregs, peripheral Treg conversion by radiation-induced TGF-β expression, and increased Treg proliferative capacity have been proposed as possibilities (Persa *et al.*, 2015). An interesting mechanism of radiation-induced Treg expansion was reported by Price *et al.*, who showed that whole body irradiation of mice with a single fraction of 6Gy activated epidermal Langerhans cells, a specialised subset of DCs, which migrated to draining lymph nodes and there induced the proliferation of Tregs (Price *et al.*, 2015). The relevance of this mechanism to local irradiation in tumour settings however is unknown. Data surrounding the impact of radiation on Treg function is also conflicting, with studies variously reporting diminished (Qu *et al.*, 2010; Balogh *et al.*, 2013), similar

(Kachikwu *et al.*, 2011), or enhanced (Muroyama *et al.*, 2017) suppressive capabilities. Furthermore, no clear correlation with radiation doses could be extrapolated from these studies. Significantly improved therapeutic activity has nonetheless been consistently reported with concurrent tumour irradiation and Treg depletion (Kachikwu *et al.*, 2011; Bos *et al.*, 2013; Twyman-Saint Victor *et al.*, 2015).

MDSCs are a heterogeneous group of immunosuppressive cells, comprised primarily of neutrophils and inflammatory monocytes. Tissue damage caused by irradiation can initiate a wound repair response, driven by infiltrating MDSCs that limit inflammation and immune activity (Tibbs, 1997; Rodriguez *et al.*, 2004; Gough *et al.*, 2013). An early study by Ahn *et al.* reported that large numbers of MDSCs were recruited into MT1A2 mouse mammary tumours and RIF fibrosarcomas at day 5 post RT (1x20Gy) (Ahn and Brown, 2008). These MDSCs expressed matrix metalloproteinase-9 (MMP-9) which promoted vasculogenesis, tumour growth and metastatic spread. The effects of radiation on tumour-associated MDSCs remain to be clarified and are most likely dependent on tumour model and radiation dose (reviewed in Vatner and Formenti, 2015). For example, Deng *et al.* showed that tumour-associated MDSCs were reduced at day 10 post RT (1x12Gy) in TUBO mammary tumours, but Xu *et al.* observed an increase at day 19 post RT (5x3Gy) in the prostate carcinoma models RM-1 and Myc-CaP (Xu *et al.*, 2013; Deng *et al.*, 2014a). Furthermore, radiation-induced recruitment of MDSCs into tumours can be mediated by type I IFN resulting from STING activation, which suggests that STING signalling can be a double-edged sword (reviewed in Section 2.4.3) (Liang *et al.*, 2017).

Alongside MDSCs, tumour-associated macrophages (TAMs) are a subset of myeloid cells that exhibit either a pro-inflammatory (M1) or immunosuppressive (M2) phenotype. Shiao *et al.* found that irradiation with a single fraction of 8Gy, but not a single fraction of 2Gy, significantly increased TAMs at day 14 post irradiation in an autochthonous MMTV-PyMT mouse mammary carcinoma model (Shiao *et al.*, 2015). This was associated with an increase in expression of macrophage colony-stimulating factor (CSF1), which upon neutralisation or blockade of the receptor significantly improved tumour control after irradiation. Using a spontaneous pancreatic cancer mouse model, Seifert *et al.* also demonstrated an increase in TAMs at day 3 following irradiation (1x12Gy) of pre-malignant pancreatic lesions, leading to accelerated tumourigenesis (Seifert *et al.*, 2016). However, Klug *et al.*, using the RIP1-Tag5 mouse model of pancreatic cancer, showed that low dose irradiation with a single fraction of 2Gy could reprogram TAMs into the anti-tumour M1 phenotype by upregulating inducible nitric oxide synthase (iNOS) (Klug *et al.*, 2013). These M1 TAMs were essential for recruiting T cells and generating anti-tumour Th1 responses. As an additional layer of complexity, radiation-induced M1 or M2 polarisation of TAMs was found to be different between mice of different genetic backgrounds, suggesting that the host genotype may also be an important determinant (Coates *et al.*, 2008). Altogether, the effect of radiation on myeloid cells is ill-defined, no doubt due to the complexity of studying these cells.

Radiation also increases intra-tumoural levels of TGF-β, a potent cytokine that dampens antigen cross-presentation by DCs and effector differentiation of T cells (Wrzesinski *et al.*, 2007). TGF-β is secreted into the extracellular space in an inactive form, bound to the latency associated peptide (LAP). TGF-β levels are increased by radiation both via increased expression of the TGF-β-LAP protein complex (Martin *et al.*, 2000) as well as release of its active form through interaction with radiation-induced reactive oxygen species (Jobling *et al.*, 2006). Various sources of TGF-β in the irradiated tumour have been implicated, including tumour cells, tumour-associated stromal cells, Tregs, M2 TAMs and MDSCs (Barcellos-Hoff, 1993; Huynh *et al.*, 2002; Moses *et al.*, 2009). Consistent with the immunosuppressive role of TGF-β, disruption of the TGF-β pathway not only radiosensitises tumour cells by altering the tumour cell-intrinsic DNA damage response, but also improves $CD8^+$ T cell-mediated tumour control (Bouquet *et al.*, 2011; Vanpouille-Box *et al.*, 2015). However, Arina *et al.* found that tumour-associated T cells depended on TGF-β for their reprogramming into radioresistant T_{RM}-like subsets, which were also critical for tumour control (Arina *et al.*, 2019). Although TGF-β blockade elevated the number of tumour-associated T cells in unirradiated tumours at baseline, it paradoxically decreased the survival of tumour-associated T cells after irradiation, which possibly reflected a reduced proportion of baseline T_{RM}-like T cells due to TGF-β blockade.

3. Combining radiation and cancer immunotherapy

3.1 Pre-clinical evidence

While radiation can support anti-tumour immune responses, they are rarely sufficient to offset the immune evasion mechanisms co-opted by tumour cells. Over the last decade, an extensive body of pre-clinical work has accumulated substantiating the potential of combining cancer immunotherapy with RT to overcome immunological barriers and achieve immune-mediated tumour rejection. The arsenal of cancer immunotherapy includes cytokine therapy, cancer vaccines, adoptive cellular transfer, and immune checkpoint blockade, but the following review focuses on the use of immune checkpoint blockade in combination with RT.

Having demonstrated that the abscopal effect is immune-mediated, Demaria *et al.* reported the first pre-clinical study of combining RT with immune checkpoint blockade, in which RT (1x12Gy) and anti-CTLA-4 therapy in the poorly immunogenic and metastatic 4T1 mouse mammary carcinoma model inhibited lung metastases in a $CD8^+$ T cell-dependent manner (Demaria *et al.*, 2005). This was followed by a study by the same group showing that the addition of anti-CTLA-4 therapy to RT (3x8Gy and 5x6Gy) improved control of irradiated TSA and MC38 tumours, but also significantly inhibited the growth of unirradiated tumours growing in the same mice (Dewan *et al.*, 2009). IFN-γ levels in both the draining lymph nodes of the primary irradiated tumour and in the secondary non-irradiated tumours were increased by this dual treatment (Dewan *et al.*, 2009; Vanpouille-Box *et al.*, 2017). Besides CTLA-4 blockade, the combination of RT and anti-PD-1 therapy have also shown therapeutic synergy for both local (Verbrugge *et al.*, 2012;

Zeng *et al.*, 2013; Sharabi *et al.*, 2015b) and distant tumour control (Park *et al.*, 2015; Vanpouille-Box *et al.*, 2015). Mechanistically, $CD8^+$ T cells exhibited higher PD1 expression after irradiation, consistent with greater TCR engagement, and concurrent PD1 blockade expanded the pool of tumour antigen-specific $CD8^+$ T cells within tumours.

Various groups have also tested the combination of RT with anti-PD-L1 therapy. Dovedi *et al.* demonstrated that irradiation (5x2Gy) of CT26 tumours upregulated tumour cell PD-L1 expression, which was due to $CD8^+$ T cell-derived IFN-γ (Dovedi *et al.*, 2014). This dampened further control by $CD8^+$ T cells, but could be circumvented with concurrently administered PD-L1 blockade, resulting in long-term tumour control and generation of T cell memory. Crucially, the timing of PD-L1 blockade influenced outcomes, whereby sequential therapy, as opposed to concurrent therapy, with anti-PD-L1 antibodies did not evoke combinatorial effects (Dovedi *et al.*, 2014). Deng *et al.* also observed radiation-induced upregulation of PD-L1 on tumour cells in subcutaneous TUBO mouse mammary carcinoma tumours, but reported an additional mechanism of synergy between RT and anti-PD-L1 therapy, beyond addressing radiation-induced immune resistance (Deng *et al.*, 2014a). In this study, the combinatorial effects of RT (1x12Gy) and anti-PD-L1 therapy were critically mediated by a reduction in tumour-associated MDSCs, which were killed by TNF derived from activated $CD8^+$ T cells. Neutralisation of TNF abrogated the clearance of MDSCs and reduced tumour control. The inverse relationship between T cells and MDSCs post irradiation was also described by Filatenkov *et al.*, who demonstrated in CT26 tumours that 1x30Gy irradiation significantly reduced MDSCs at day 14, an effect that was lost with depletion of either $CD8^+$ or $CD4^+$ T cells (Filatenkov *et al.*, 2015).

Complementing all these data, Twyman-Saint *et al.* tested the triple combination of RT, anti-CTLA-4 and anti-PD-L1 and found complementary, non-redundant mechanisms of action that contributed to tumour cures (Twyman-Saint Victor *et al.*, 2015). The study demonstrated that anti-CTLA-4 therapy abrogated the radiation-induced increase in Treg numbers and promoted expansion of $CD8^+$ T cells, RT shaped the TCR repertoire of peripheral T cell clones, and anti-PD-L1 reversed T cell exhaustion. Along a similar paradigm, other groups have reported improved anti-tumour responses when RT was applied concurrently with immune stimulatory antibodies such as anti-CD137 and anti-OX40 (Shi and Siemann, 2006; Yokouchi *et al.*, 2008), or with the combination of stimulatory and inhibitory antibodies (Verbrugge *et al.*, 2012; Rodriguez-Ruiz *et al.*, 2016). These pre-clinical data provide a compelling argument for testing these mechanisms of synergy in the clinic.

3.2 Clinical evidence

RT in combination with immunotherapeutic agents such as cytokine therapy and cancer vaccines has been investigated in the clinic over the previous decades, demonstrating only mediocre toxicity and efficacy profiles (reviewed in Kang *et al.*, 2016). However, the advent of antibody-based immune checkpoint inhibitors and increased reports of abscopal responses in patients receiving RT and ipilimumab have

reignited the interest in combining RT with cancer immunotherapy in patients (Hiniker *et al.*, 2012; Postow *et al.*, 2012; Golden *et al.*, 2013; Stamell *et al.*, 2013; Chandra *et al.*, 2015). Notably, those anecdotal reports of abscopal responses were in cases of melanoma and non-small cell lung cancer (NSCLC), which are among the most immunogenic tumours with high baseline tumour mutational burdens (Schumacher and Schreiber, 2015). A proof-of-principle single-arm basket trial around this time enrolled patients with metastatic cancer of various histologies for RT (10x3.5Gy) and granulocyte-macrophage colony-stimulating factor (GM-CSF) therapy (Golden *et al.*, 2015). Abscopal responses were observed in more than 25% of patients in this study, compared to what would be considered a very rare event with either RT or GM-CSF alone. Another phase I study of patients with advanced melanoma receiving RT (in a dose-escalation design based on anatomical site, ranging from 2x6Gy to 3x8Gy) and ipilimumab showed 18% of the patients had an abscopal response, again higher than historical controls (Twyman-Saint Victor *et al.*, 2015). Besides anti-CTLA-4 therapy and single-site RT, increased abscopal responses with pembrolizumab (an anti-PD-1 antibody) and multi-site SABR were also seen in a basket trial of various histologies (Luke *et al.*, 2018). Importantly, translational studies in humans have corroborated pre-clinical mechanistic work, in which clinically responding patients receiving combination therapy showed increases in serum antibodies against tumour-associated antigens and higher serum IFN-β and $CD8^+$ T cell levels (Postow *et al.*, 2012; Golden *et al.*, 2013; Twyman-Saint Victor *et al.*, 2015).

These early clinical results led to a rapid proliferation of clinical trials testing RT with various immunotherapeutic agents (Kang *et al.*, 2016). In the last few years, several randomised trials have started to mature, reporting exciting results suggesting combinatorial efficacy, such as the PEMBRO-RT, PACIFIC, and CA184-043 trials. The PEMBRO-RT study was a randomised phase 2 trial which assigned patients with metastatic NSCLC to receive pembrolizumab with or without induction SABR (Theelen *et al.*, 2019). SABR was given in 3x8Gy to a single metastatic site within 7 days before starting pembrolizumab. Although the study did not reach the pre-specified endpoint, impressive trends towards a doubling of objective response rates (36% *vs*. 18%, p=0.07), progression free survival (PFS) and overall survival (OS) were observed. A criticism of this trial is the unbalanced proportion of patients with PD-L1 positive (>50%) tumours between the arms (13% *vs.* 28% in the control and experimental arms, respectively), given that studies of anti-PD-L1 monotherapy have suggested tumour PD-L1 status to be predictive for response (Abdel-Rahman, 2016). Nonetheless, patients who derived the largest benefit from combination therapy on subgroup analysis were intriguingly patients with PD-L1 negative (<1%) tumours. A provocative explanation for this finding is the hypothesis that RT could convert a "cold" tumour into a "hot" tumour, thereby allowing anti-PD-1 therapy to be effective. The combination of the two modalities did not result in increased toxicity.

In the landmark randomised phase 3 PACIFIC trial, patients with unresectable Stage III NSCLC received chemoradiation with sequential durvalumab (an anti-PD-L1 antibody) or placebo (Antonia *et al.*, 2018). Chemoradiation was in the form of conventionally fractionated RT (54-66Gy in 1.8-2.0Gy per fraction)

and concurrent platinum-based chemotherapy. Durvalumab was started after completion of chemoradiation within 1-42 days. At two years, there was a doubling of PFS that translated into significantly longer OS in patients who received sequential durvalumab, an improvement that is not easily achieved in this group of patients. A small increase in pneumonitis was seen with combination therapy (4.8% *vs.*2.6% in the durvalumab and placebo groups, respectively). An open question posed by this trial is whether the initiation of immunotherapy upon relapse, rather than in the adjuvant setting, would have conferred similar outcomes. Subgroup analysis however suggested that patients who started durvalumab within two weeks after chemoradiation derived the most benefit (Antonia *et al.*, 2017).

The CA184-043 trial was a randomised phase 3 trial in which patients with metastatic prostate cancer received RT (1x8Gy) within two days before initiation of either ipilimumab or placebo (Kwon *et al.*, 2014). At a median follow up of 10 months, a near-significant improvement in OS was observed with patients who received RT and ipilimumab (p=0.053). Importantly, the hazard ratio for OS changed over time, demonstrating that patients who survived beyond 12 months derived a statistically significant survival benefit from combination therapy. Longer follow-up data in the future may elucidate if durable responses were achieved. Minimal added toxicity was seen with the combination treatment.

A clinical trial that did not report synergy between RT and cancer immunotherapy was the TONIC trial (Voorwerk *et al.*, 2019). This was a phase 2 randomised, non-comparative trial exploring if conventional cancer treatments could induce a tumour microenvironment that was more favourable for response to nivolumab therapy in patients with metastatic triple negative breast cancer. Induction strategies tested were RT (3x8Gy to a single site, given 2 weeks before starting nivolumab), cyclophosphamide, cisplatin and doxorubicin. It was observed that prior treatment with cisplatin or doxorubicin elevated response rates to nivolumab, but RT did not. Although this was a phase 2 trial with limited cohort sizes (12-17 patients per cohort), this trial illustrates that RT and immune checkpoint blockade combinations do not universally synergise, and that the underlying factors determining combinatorial efficacy are poorly understood. Some of the open questions are outlined below, of which the potential impact of radiation dose-fractionation is a major consideration.

3.3 The undefined impact of radiation dose-fractionation

Despite its promise, the optimal combination of RT and immune checkpoint blockade for the treatment of cancer is ill-defined in several aspects, which can be broadly categorised into host, tumour, and treatment factors. Patients with metastatic disease are generally more immunosuppressed than patients with localised disease, due to a higher systemic tumour burden and the likelihood of having received more lines of myelosuppressive systemic therapy. The lower volume of disease in earlier stages of cancer may also make it easier for host immune responses to eradicate or control tumours. Supporting these conjectures, patients with visceral disease in addition to bone metastases in the CA184-043 trial, who are often in more advanced stages of prostate cancer, had poorer responses to RT and ipilimumab on subgroup analysis compared to

patients with bone metastases only (Kwon *et al.*, 2014). Additionally, in the aforementioned early basket trial examining single-site RT in combination with GM-CSF therapy, the rate of abscopal responses correlated inversely with the number of lesions present at baseline, and no responses were observed in patients with six or more lesions (Golden *et al.*, 2015). Whether metastatic status and tumour burden are valid biomarkers of response for RT and cancer immunotherapy will need to be confirmed. Tumour characteristics are likely an important factor too. It is known that tumour mutational burden and immune contexture are important determinants of response in the setting of cancer immunotherapy as monotherapy (Sharma *et al.*, 2017). As discussed earlier, a hypothesis generating finding from the PEMBRO-RT trial was that patients with PD-L1 negative tumours derived the largest benefit from RT and pembrolizumab, suggesting that certain baseline tumour characteristics are more suited for this combination approach (Theelen *et al.*, 2019). Just as important are how treatment parameters such as the choice of immunotherapeutic agent, radiation dose-fractionation, radiation volume and site(s), and scheduling of modalities affect anti-tumour immune responses. For example, elective nodal irradiation is frequently performed in the clinical setting to eradicate potential microscopic spread, but whether this dampens priming of anti-tumour T cell immune responses and thus affects overall immune-mediated control of cancer is unknown. Perhaps more urgent however, given the wide range of radiation regimens that are currently used in clinical practice, is to gain an understanding of how radiation dose-fractionation impacts on host anti-tumour immune responses and how these differences affect combination strategies with checkpoint blockade immunotherapy. This aspect of radiation dose-fractionation formed the focus of research for this PhD project.

3.3.1 Comparing between radiation dose-fractionation regimens

Although classical radiobiology has made great strides in explaining how radiation dose-fractionation affects cell survival in different tissue types, the impact of dose-fractionation on the immunological effects of radiation is unclear. Several complexities surround this issue. Firstly, the majority of pre-clinical and clinical studies in this field have used hypofractionated, ablative regimens rather than conventionally fractionated regimens, which has biased the impression that SABR-like regimens are better inducers of cancer immunity (Demaria and Formenti, 2012). Conventionally fractionated regimens are less investigated because they are often temporally protracted and thus present technical and logistical difficulties for *in vitro* cell work and *in vivo* animal experiments. Secondly, comparisons between studies are often confounded by the different experimental models and methodologies used.

Thirdly, and importantly, the relationship between radiation dose and cell kill is non-linear (*Figure 1.5a*). As such, the total cytotoxic effect of a radiation regimen is not the arithmetic sum of the doses per fraction, which complicates comparison of biological sequelae between dose-fractionations. Methods have been devised to estimate the relationship between radiation dose and cell kill. The linear quadratic model is the most widely adopted in clinical use, being a mathematical fitting of the cell survival curve with a second-

order polynomial (*Figure 1.5b*) (McMahon, 2018). The ratio of the α (linear) and β (quadratic) parameters (α/β ratio) describes the tissue of interest's radiation response characteristics to dose per fraction (DPF). Tissues with low α/β ratios are more sensitive to high radiation DPFs (exhibiting a more downward-arched cell survival curve), while tissues with higher α/β ratio are less so (exhibiting a straighter cell survival curve). Traditionally, α and β have been described to reflect the formation of DNA double strand breaks by single and double tracks of electrons respectively, but these mechanistic attributions have not been proven. More practically, the linear quadratic model allows calculation of the biological effective dose (BED), which is a method for standardising the effects of fractionation by assuming the delivery of a radiation dose over an infinite number of fractions (*Figure 1.5c*) (Fowler, 1989). In its most basic formulation, the BED equation does not take into account parameters such as inter-fraction repair and repopulation, but is simple and reasonably accurate as a surrogate for total dose. Thus, the BED is commonly used to compare the expected biological effect of different radiation dose-fractionation regimens (Fowler, 2010).

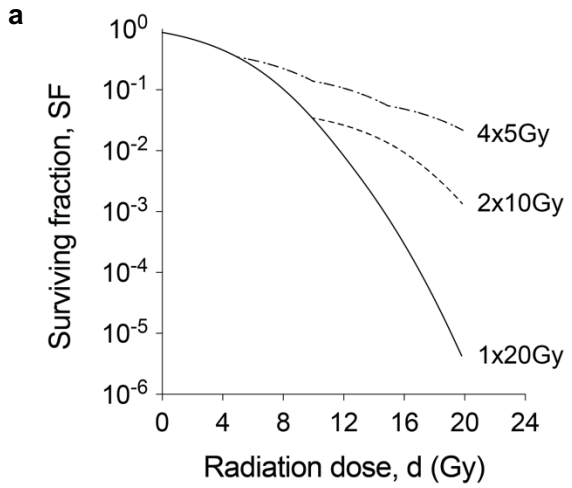

b

$$SF = e^{-\alpha d - \beta d^2}$$

c

$$BED_{\alpha/\beta} = nd\left(1 + \frac{d}{\alpha/\beta}\right)$$

Figure 1.5. The linear-quadratic model and biological effective dose (BED) equation. a, Example cell survival curves illustrating the non-linear relationship between the surviving fraction (SF) (the proportion of cells with preserved clonogenic potential) and absorbed radiation dose. The SF is depicted on a logarithmic scale on the *y*-axis against radiation dose on the *x*-axis. Because the "shoulder" of the curve is recapitulated with each fraction, the SF after 1x20Gy is not equivalent to the SFs after 2x10Gy or 4x5Gy. **b**, The linear-quadratic equation, a widely adopted mathematical approximation of the radiation cell survival curve. According to this model, the survival curve is dominated by the linear α parameter at low radiation doses, followed by increasing curvature as the quadratic β parameter becomes more significant. The degree of curvature is frequently defined in terms of the α/β ratio. **c**, The BED equation. The BED of a given radiation dose-fractionation is the total dose required to give the same cell kill as the dose-fractionation with infinitely small fractions. It is commonly used as a surrogate for total dose to allow comparison between dose-fractionation regimens. *SF: surviving fraction, n: number of fractions*, *d: dose per fraction.*

3.3.2 Critical appraisal of current data

Few studies examining the immunomodulatory effects of RT have conducted side-by-side comparisons using different radiation dose-fractionation regimens. In order to guide clinical practice, comparing between dose-fractionation regimens in pre-clinical studies will also need to take into account whether an observed difference in a particular readout could be due to differences in DPF or in total dose, as represented by BED. *Table 1.2* summarises a list of key studies discussed in this review that looked at immunological endpoints evoked by radiation as a single modality, divided according to whether non-ablative (defined as ≤8Gy) or ablative (>8Gy) radiation DPFs were employed. As is evident, a wide range of radiation dose-fractionation regimens and tumour models have been used across different studies. In general, many of the reported immunological effects can be detected with either non-ablative or ablative radiation DPFs.

The previously mentioned study by Dewan *et al.* was an important pre-clinical study that investigated the impact of radiation dose-fractionation on downstream immunological effects and synergy with checkpoint blockade therapy (Dewan *et al.*, 2009). In that study, only the fractionated regimens of 3x8Gy and 5x6Gy, but not 1x20Gy, in combination with anti-CTLA-4 therapy were able to induce abscopal effects in TSA and MC38 tumours. Mechanistically, this phenomenon was found to be due to the shutting down of tumour cell-intrinsic STING activation via induction of TREX1 by radiation DPFs above 10-12Gy (Vanpouille-Box *et al.*, 2017). Nonetheless, as alluded to in Section 2.4.2, this model of regulation is challenged by observations made by other groups. Park *et al.* and Harding *et al.* were able to induce abscopal responses in B16 tumours using the high DPF regimens of 1x15Gy and 1x10Gy, respectively, in combination with immune checkpoint blockade (Park *et al.*, 2015; Harding *et al.*, 2017). Similarly, STING or type I IFN-dependent $CD8^+$ T cell responses for local tumour control could be evoked with the 1x20Gy regimen in B16, MC38 and CT26 tumours without the addition of immunotherapy (Lee *et al.*, 2009; Burnette *et al.*, 2011; Deng *et al.*, 2014b; Schadt *et al.*, 2019). In humans, published reports of abscopal responses have used single-fraction doses as high as 1x26Gy, among a wide range of other dose-fractionations (*Table 1.3*). Therefore, it is uncertain if high radiation DPF regimens are truly poor inducers of anti-tumour immune responses.

By contrast, some pre-clinical studies have reported large single-fraction doses to be more effective than fractionated regimens at supporting the induction of anti-tumour responses. Lugade *et al.* and Lee *et al.* demonstrated greater levels of $CD8^+$ T cell infiltration into B16 tumours irradiated with 1x15Gy compared to 3x5Gy, and 1x20Gy compared to 5x4Gy, respectively (Lugade *et al.*, 2005; Lee *et al.*, 2009). Filatenkov *et al.* showed that 1x30Gy irradiation of CT26 tumours conferred better survival than 10x3Gy irradiation (Filatenkov *et al.*, 2015). It is important to note that in these studies, the difference in outcomes between dose-fractionations do not necessarily point to the superiority of single-fraction regimens, but could be due to differences in the cumulative effect of radiation. For example, the 1x20Gy regimen would have a BED that is very much higher than the 5x4Gy regimen. Indeed, Verbrugge *et al.* found similar levels of

therapeutic synergy between dual anti-CD137/anti-PD-1 therapy and radiation regimens of much more comparable BED values (1x12Gy, 4x4Gy and 4x5Gy) in AT3 mouse mammary tumours (Verbrugge *et al.*, 2012). Moreover, although most clinical trials showing benefit with combination RT and immune checkpoint blockade have employed hypofractionated, high DPF regimens, the aforementioned PACIFIC trial reported combinatorial efficacy using conventionally fractionated regimens with a high BED (54-66Gy in 1.8-2.0Gy per fraction) (Antonia *et al.*, 2018).

Therefore, despite the large body of pre-clinical and clinical data emerging on the immunological effects of RT, the question of how radiation dose-fractionation affects such processes and their synergy with cancer immunotherapy is still poorly understood, and no general rules can at present be extrapolated from existing literature. Very likely this will be a complex issue determined by a range of host, tumour and treatment factors. More balanced side-by-side comparisons of radiation dose-fractionations, coupled with deeper interrogation of host and tumour cell-intrinsic determinants of immune responses, will help towards resolving this outstanding gap in knowledge.

Target of interest	Reference	Dose-fractionation	Time point (post irradiation)	*In vivo / in vitro*	Tumour model	Observation
Reported only with non-ablative doses per fraction (≤ 8Gy per fraction)						
ATP	(Ohshima *et al.*, 2010)	1x0.5Gy-8Gy	5 minutes	*In vitro*	B16 (melanoma)	Increased 1.5-2.5x fold, no dose dependent pattern
MDSCs	(Xu *et al.*, 2013)	5x3Gy	19 days	*In vivo*	RM-1 and Myc-CaP (prostate)	Increased in tumours
TAMs	(Klug *et al.*, 2013)	1x2Gy	10 days	*In vivo*	Spontaneous pancreatic carcinoma (RIP1-Tag5)	Reprogramming of TAMs into anti-tumour M1 phenotype
Reported only with ablative doses per fraction (> 8Gy per fraction)						
Calreticulin	(Obeid *et al.*, 2007)	1x75Gy	1, 4, 24 hours	*In vitro*	CT26 (colon)	Detectable as early as 1-hour post RT
NK ligands	(Gasser *et al.*, 2005)	1x40Gy	3-24 hours	*In vitro*	C1 and C2 (ovarian epithelial)	Pan NKG2D ligands (including RAE-1) increased, peaked at 24 hours post RT
	(Kim *et al.*, 2006)	1x20Gy	24 hours	*In vitro*	A375 (human melanoma), KM12 (human colon), NCI-H23 (human NSCLC), HeLa (human cervical)	Increased (MICA/B, ULBP1-3)
Fas/CD95	(Chakraborty *et al.*, 2003)	10-50Gy (10Gy increments)	48 hours	*In vitro*	MC38 (colon)	Increased, no dose dependent pattern

Organisation of tumour vasculature	(Ganss *et al.*, 2002)	1x10Gy (whole body irradiation)	7 days	*In vivo*	Pancreatic insulinoma	Irregular tumour vasculature normalised only in mice receiving irradiation
MDSCs	(Deng *et al.*, 2014a)	1x12Gy	10 days	*In vivo*	TUBO (prostate)	Reduced in tumours
	(Filatenkov *et al.*, 2015)	1x30Gy	14 days	*In vivo*	CT26 (colorectal)	Reduced in tumours
Trex1 expression	(Vanpouille-Box *et al.*, 2017)	1x12-30Gy	24 hours	*In vitro*	TSA (mammary), MC38 (colorectal), 4T1 (mammary), MDA-MB-231 (human breast), 4175TR (human NSCLC)	Increased *Trex1* expression (by PCR), associated with decrease in cytosolic dsDNA and *Ifnb1* expression
Reported with both non-ablative and ablative doses per fraction						
NF-kB	(Brach *et al.*, 1991)	1x2-50Gy	2, 4 hours	*In vitro*	KG1 (human myeloid leukaemia)	Increased expression and binding activity
HMGB1	(Apetoh *et al.*, 2007)	1x12Gy	18, 24 hours	*In vitro*	EG7 (thymoma), TS/A (mammary)	Increased
	(Rubner *et al.*, 2014)	5x2Gy	48 hours	*In vitro*	U87MG, T98G, U251 (human glioblastoma)	Increased
MHC-I	(Reits *et al.*, 2006)	1x1-25Gy	18-96 hours	*In vitro*	MelJuSo (human melanoma), MC38 (colon)	Increased in dose-dependent fashion, peaked at 48 hours post irradiation
		1x25Gy	24 hours	*In vivo*	Normal tissue (kidney)	Increased
	(Santin *et al.*, 1997)	1x25Gy, 1x50Gy	2 days	*In vitro*	CaSki (cervical)	Increased
	(Garnett *et al.*, 2004)	1x10Gy	3 days	*In vitro*	WiDr, SW620, HCT116 (all human colorectal)	Increased

PD-L1 expression	(Deng *et al.*, 2014a)	1x12Gy	3 days	*In vivo*	TUBO (mammary)	Increased
	(Dovedi *et al.*, 2014)	5x2Gy	1-7 days	*In vivo*	CT26 (colon)	Increased, peaked at day 3 post irradiation
		1x2.5-10Gy	Not reported	*In vitro*	CT26 (colon)	Increased, only in presence of IFN-γ
Tregs	(Kachikwu *et al.*, 2011)	1x2-20Gy	2 days	*In vivo*	Normal tissue (right leg)	Proportion of circulating Tregs increased, no dose dependent pattern
	(Qu *et al.*, 2010)	1x5Gy (total body irradiation)	12 hours, 5 days, 15 days	*In vivo*	Normal tissue (whole body)	Proportion of circulating Tregs increased, absolute numbers decreased
	(Muroyama *et al.*, 2017)	1x10Gy	7, 10, 16 days	*In vivo*	B16 (melanoma), MC38 (colorectal), RENCA (renal)	Increased in tumours
	(Schaue *et al.*, 2012)	1x5-15Gy	7 days	*In vivo*	B16 (melanoma)	Proportion of circulating Tregs increased, no dose dependent pattern
Lymph node DCs	(Lugade *et al.*, 2005)	3x5Gy, 1x15Gy	14 days	*In vivo*	B16-OVA (melanoma)	Number of APCs in draining lymph nodes increased (1x15Gy > 3x5Gy)
	(Sharabi *et al.*, 2015b)	3x7Gy, 1x15Gy	4 days	*In vivo*	B16-OVA (melanoma)	Increased DC cross-presentation function

Table 1.2. The impact of radiation dose-fractionation on the immunomodulatory effects of radiation, without concurrent immunotherapy. Data is compiled from selected key studies, categorised by the radiation DPFs employed. Cell lines are of mouse origin unless otherwise specified.

Year	Sex	Age	Histology	Primary site	Treatment of primary	RT treated sites	RT dose/fractions	Site of abscopal regression	Time to abscopal response
2013	F	78	Adenocarcinoma	Lung	SABR	Primary	26Gy/1fx	Bone and adrenal metastases	12 mth
2012	M	61	RCC	Kidney	Nephrectomy	Brain and bone metastases	18Gy/1fx (brain), 40Gy/8fx (bone)	Lung and bone metastases	1 mth
2012	M	72	Medullary carcinoma	Thyroid	Thyroidectomy	Mediastinal LN	30Gy/3fx	Mediastinal LN	1 mth
2011	M	63	HCC	Liver	Hepatic Lobectomy	Mediastinal LN	60.75Gy/27fx	Lung metastases	1 mth
2011	M	70	Merkel cell carcinoma	Calf	Excision + adjuvant EBRT	In-transit cutaneous M+	12 Gy/2fx	Cutaneous metastases	≤ 1 mth
2009	F	65	Lymphocytic leukaemia	Axillar LN	Chemotherapy	Axillar LN	24Gy/12fx	Cervical LN	≤ 1 mth
2008	M	79	HCC *	Liver	Embolisation	Inferior vena cava lesion	48Gy/NR	Hepatic metastases	5 mth
2007	F	69	SCC	Cervix	EBRT + Brachytherapy	Primary tumour	50.8Gy/27fx (EBRT) + 24Gy/4fx (brachytherapy)	Para-aortic LN	NR
2006	F	83	RCC *	Kidney	SABR	Primary tumour	32Gy/4fx	Lung metastases and abdominal LN	24 mth
2006	F	64	RCC	Kidney	Nephrectomy	Lung metastases	NR	Lung metastases	5 mth
2006	M	69	RCC	Kidney	Nephrectomy	Lung metastases	30Gy/2fx	Lung metastases	3 mth
2006	F	55	RCC	Kidney	SABR	Primary tumour	32Gy/4fx	Abdominal LN	5 mth
2005	M	65	HCC	Liver	None	Bone metastases	30Gy/NR	Hepatic and bone metastases	10 mth

1998	M	76	HCC	Liver	Resection/Embolisation	Bone metastases	36Gy/NR	Hepatic and bone metastases	10 mth
1995	M	77	CLL	N/A	Chemotherapy	Neck/supraclavicular LN	32.4Gy/NR	Splenomegaly	≤ 1 mth
1994	M	58	RCC	Kidney	EBRT	Primary tumour	20Gy/10fx	Lung metastases and mediastinal LN	6 mth
1983	M	49	Adenocarcinoma	Oesophagus	EBRT	Primary tumour	40Gy/20fx	Lung metastases	6 mth
1983	M	56	Adenocarcinoma	Lung	EBRT	Primary tumour	35Gy/10fx	Cutaneous metastases	≤ 1 mth
1981	F	73	RCC	Kidney	Nephrectomy	Groin metastases	40Gy/15fx	Lung metastases	≤ 12 mth
1977	M	44	Lymphocytic lymphoma	LN	EBRT	Mantle field	30Gy/20fx	Abdominal LN	≤ 1 mth
1977	M	40	Lymphocytic lymphoma	LN	EBRT	Mantle field	30 Gy/20fx	Abdominal LN	≤ 1 mth
1975	M	28	Melanoma	Knee	Wide excision	Right inguinal LN	14.4Gy/12fx	Para-aortic LN	2 mth
1973	F	35	Adenocarcinoma	CUP	N/A	Neck/Supraclavicular LN	40Gy/20fx	Mediastinal mass	NR

***** No pathological diagnosis was reported. Tentative diagnosis based on imaging and disease presentation.

Table 1.3. Published reports of radiation abscopal responses in humans, without concurrent immunotherapy. Table adapted from (Reynders *et al.*, 2015). References for individual cases can be found in the publication. *Fx: fractions; RCC: renal cell carcinoma; HCC: hepatocellular carcinoma; SCC: squamous cell carcinoma; CLL: chronic lymphocytic leukaemia; LN: lymph node; EBRT: external beam radiation therapy; SABR: stereotactic ablative body radiotherapy; NR: not reported; fx: fraction, mths: months.*

4. Hypothesis and aims

This literature review has presented data arguing that radiation evokes pleiotropic immunomodulatory effects on the tumour microenvironment, which creates opportunities for mechanistic synergy with cancer immunotherapy. Nonetheless, how these effects are impacted by radiation dose-fractionation, in particular by radiation DPF and total dose (BED), is presently poorly defined. This question is clinically pertinent and urgent in light of the mounting interest in integrating RT with cancer immunotherapy. Mouse models of cancer present a good avenue to systematically interrogate this question and its underlying mechanisms. Deeper insights gained into these processes will help guide the rational design of combination RT and cancer immunotherapy strategies in the clinic.

The hypothesis of this PhD project was that radiation dose-fractionation regimens are not equivalent in their capacity to evoke anti-tumour immune responses, and therefore do not similarly support cancer immunotherapy. To test this hypothesis, the specific aims of the project were as follows:

1. To dissect the differential impact of radiation DPF and BED on anti-tumour $CD8^+$ T and NK cell responses

2. To interrogate radiation-induced changes in the tumour cells and in the tumour immune microenvironment that contribute to these responses

3. To determine the differential capacities of radiation dose-fractionation regimens to support immune checkpoint blockade

Results from these aims are reported across three data chapters, which focused on anti-tumour $CD8^+$ T cell responses, NK cell responses, and immune checkpoint combinations, respectively.

Chapter 2: Methods and Materials

1. Cell lines

The AT3 cell line was generated by Dr. Trina Stewart from an autochthonous mammary carcinoma isolated from a C57BL/6 MMTV-PyMT transgenic mouse (Stewart and Abrams, 2007). This line was retrovirally transduced to express chicken ovalbumin (OVA) and GFP as described in (Mattarollo *et al.*, 2011). The MC38 cell line, derived from a methylcholanthrene-induced colon carcinoma isolated from a C57BL/6 mouse, was originally obtained from American Type Culture Collection, VA, USA. These cell lines were periodically authenticated by morphologic inspection and were confirmed Mycoplasma negative by polymerase chain reaction (PCR) tests (PMCC Genotyping Core Facility, Melbourne).

AT3, AT3-OVA and MC38 cells are adherent cell lines that were grown in tissue culture flasks (Corning®, Thermo Fisher, USA) unless otherwise specified, and passaged under sterile conditions when approximately 75% confluent. Cells were trypsinised at the time of passaging and centrifugation was performed at 1400 rpm for 4 minutes. The AT3 and AT3-OVA cell lines were cultured in Dulbecco's Modified Eagle's Medium (DMEM) (Gibco™, Thermo Fisher, USA), 10% (v/v) foetal bovine serum (FBS) (Commonwealth Serum Laboratories, Parkville, Melbourne), 0.1 mM non-essential amino acids (Gibco™, Thermo Fisher, USA), 1 mM sodium pyruvate (Gibco™, Thermo Fisher, USA), 2 mM L-glutamine (Gibco™, Thermo Fisher, USA), and 2 mM penicillin/streptomycin (Gibco™, Thermo Fisher, USA), and incubated at 37º C in 5% CO_2. The MC38 cell line was cultured in DMEM, 10% (v/v) FBS, and 2 mM penicillin/streptomycin and incubated at 37º C in 10% CO2.

2. Cell irradiation

Tumour cells were irradiated using the X-RAD 320 irradiator (Precision X-ray, CT, USA). The machine was set at 320 kV and 12.5 mA, and a beam filter with a half value layer (HVL) value equivalent to 3.84 mm copper was used for beam hardening. The output dose rate was approximately 1 Gy/minute. Cell culture flasks were placed on a 4 cm Perspex slab for water-equivalent backscatter, at a surface to source distance (SSD) of 46cm. Mock irradiated tumour cells were taken out of the incubator for the same duration of time as cells being irradiated. As much as feasible, radiation fractions were given at the same time each day at 24-hour intervals.

3. Clonogenic assays

Cultured AT3-OVA and MC38 tumour cells were seeded into 60 mm or 100 mm dishes (CELLSTAR®, Greiner Bio-One, Kremsmünster, Austria) at a density based on the intended radiation dose exposure (*Table 2.1*).

Radiation dose	**Number of cells seeded**	
	AT3-OVA	**MC38**
0 Gy	250	150
2 Gy	250	500
4 Gy	1.5×10^3	1.0×10^3
6 Gy	7.5×10^3	5.0×10^3
8 Gy	3.0×10^4	2.0×10^4
10 Gy	6.0×10^4	8.0×10^4
12 Gy	1.2×10^5	3.2×10^5

Table 2.1. Clonogenic assay cell seeding densities.

For AT3-OVA tumour cells, 2-8 Gy samples were plated onto 60 mm tissue culture dishes and 10-12 Gy samples onto 100 mm tissue culture dishes. 0 Gy samples were plated onto both 60 mm or 100 mm for determination of the respective plating efficiencies. For MC38 tumour cells, all samples were plated onto 60 mm tissue culture dishes. All cells were given at least 4 hours to adhere and were irradiated. Irradiated cells were incubated for 9 days and the culture medium was supplemented as required. To quantify the number of cell colonies formed post irradiation, cells were washed twice with PBS, stained with crystal violet dye (50% (v/v) methanol, 50% (v/v) distilled H_2O, 1 g/L crystal violet) for 2 minutes and then washed twice again with PBS. Colonies of more than 50 cells were counted manually under an inverted microscope. The surviving fraction was calculated according to the formula below, where plating efficiency was the surviving fraction for 0 Gy.

$$Surviving\ fraction = \frac{No.of\ colonies\ formed}{No.of\ cells\ seeded\ \times\ Plating\ efficiency}$$

The linear quadratic equation was fitted by non-linear regression with $1/Y^2$ weighting using GraphPad Prism (version 8.3.1, GraphPad Software, USA). Based on this, the biological effective

dose (BED) was calculated as a surrogate for the total dose of a given radiation regimen, as is common in clinical practice (Fowler, 2010). An extended BED equation that included secondary parameters such as overall treatment time and tumour repopulation was not deemed necessary, as the calculated BED values correlated well with the tumour control achieved and allowed sufficient distinction between the impact of radiation dose per fraction and that of total dose.

4. Cell death assays

4.1 Annexin V/PI flow cytometry assay

AT3-OVA tumour cells were seeded into 60 mm tissue culture dishes (CELLSTAR®, Greiner Bio-One, Kremsmünster, Austria) at a density based on the intended radiation dose exposure (*Table 2.2*). Irradiation was performed following 20-24 hours of incubation. 24 or 48 hours after irradiation, cells were harvested and washed twice in Annexin V binding buffer (10 mM HEPES, 125 mM NaCl, 5 mM $CaCl_2$ in H_20 at pH 7.4) before being stained with 100-150 µL of staining cocktail containing Annexin V (APC-conjugated, BD Pharmingen™, CA, USA at 1:150 dilution in Annexin V binding buffer) and propidium iodide (PI) (20µg/mL, Thermo Fisher, USA, at 1:50 dilution in Annexin V binding buffer). Samples were quantified for levels of cell death within an hour of processing using a BD FACSCanto™ II flow analyser (BD Biosciences, CA, USA).

Radiation dose	Number of cells seeded
3x0 Gy	500
3x4 Gy	2.0×10^4
1x0 Gy	1.5×10^4
1x20 Gy	4.0×10^4

Table 2.2. Annexin V / PI flow cytometry assay cell seeding densities.

4.2 Real-time apoptosis and necrosis assay

AT3-OVA tumour cells were plated at $1x10^4$ cells/well into a single flat-bottom, white-wall, 96-well microplate (Corning® 3903, Merck, Darmstadt, Germany) and given 4 hours to adhere prior to being irradiated with 0, 2, 4, 8, 12, and 20 Gy. To achieve differential radiation exposure to different wells on the same microplate, 3mm-thick lead pieces wrapped in wet gauze were used to shield the different areas of the microplate from the 320kVp X-ray beam in the X-RAD 320

irradiator (Precision X-ray, CT, USA). For positive controls, AT3-OVA cells were treated with 10% sodium dodecyl sulfate (SDS). Wells with no cells were used as background controls. Each treatment group was run in triplicate. Induction of apoptosis and necrosis were measured in using the RealTime-Glo™ Annexin V Apoptosis and Necrosis Assay Kit (Promega, WI, USA) as per the manufacturer's instructions. Briefly, cells were treated with a preparation containing two Annexin V fusion proteins each attached to a luciferase subunit, time-released luciferase substrates, and a cell-impermeant pro-fluorescent DNA dye. Exposure of phosphatidylserine in early apoptosis brings the two luciferase subunits together to emit a luminescent signal, while exposure of DNA due to necrosis results in a fluorescent signal. The microplate was incubated at 37º C in 5% O_2 for the duration of the assay. Every 3 hours over 68 hours, the microplate was temporarily taken out of the incubator and placed in a plate-based multi-mode reader (Cytation™ 5, BioTek Instruments, VT, USA) for detection of luminescence and fluorescence signals.

5. Chromium-release killing assays

5.1 Preparation of effector cells (OT-1 T cells)

Spleens from C57BL/6 OT-1 transgenic mice were harvested and mechanically dissociated through a 70 µm EASYstrainer™ strainer (Greiner Bio-One, Kremsmünster, Austria) each into 10 mL of T cell medium (RPMI-1640 medium (Gibco™, Thermo Fisher, USA) supplemented with 10% (v/v) FBS, 100 µg/mL penicillin/streptomycin, 2 mM L-glutamine, 1 mM sodium pyruvate, 50 µM 2-mercaptoethanol). Each splenocyte preparation was resuspended in T cell medium plus ACK lysis buffer (*Table 2.3*) at a 1:9 ratio to lyse red blood cells. Once washed in T cell medium, the cells were resuspended in 50 mL of T cell medium supplemented with $1x10^6$ U/mL recombinant IL-2 (Sigma-Aldrich, Merck, Darmstadt, Germany) and 10 nM OVA 257-264 (SIINFEKL) peptide (InvivoGen™, Thermo Fisher, USA), and transferred to a 175 cm^2 angled neck cell culture flask (Corning®, Merck, Darmstadt, Germany), which was placed in an upright position in a 37°C, 5% CO_2 incubator. After 2-3 days, the cells were split across 2-4 flasks with each containing 50 mL of fresh T cell medium supplemented with $1x10^6$ U/mL recombinant IL-2. After 7-8 days of incubation, the culture largely comprised of activated OT-1 $CD8^+$ T cells. All of the aforementioned steps were performed under sterile conditions.

Reagent	Concentration
NH_4Cl (Ammonium chloride)	0.15 M
$KHCO_3$ (Potassium bicarbonate)	1 mM
Ethylenediaminetetraacetic acid (EDTA)	0.1 mM
Made up in distilled H2O, and adjusted to pH 7.2-7.4 with HCl	

Table 2.3. ACK lysis buffer recipe.

5.2 Preparation of effector cells (NK cells)

Spleens from wildtype C57BL/6 mice were harvested and mechanically dissociated as described above, each into 10mL of isolation buffer (PBS containing 2% (v/v) FBS plus 1mM ethylenediaminetetraacetic acid [EDTA]). The splenocyte preparations were red blood cell lysed in isolation buffer plus ACK lysis buffer at a 1:4 ratio. An EasySep™ Mouse NK Cell Isolation Kit (STEMCELL, Canada) was used to negatively enrich for splenic NK cells as per the manufacturer's instructions. The NK cells retrieved were quantified before being resuspended in NK cell growth medium (RPMI-1640 medium with 10% (v/v) FBS, 100µg/mL penicillin/streptomycin, 2 mM L-glutamine, 1mM sodium pyruvate, 50 µM 2-mercaptoethanol, 1000 U/mL recombinant IL-2 (Sigma-Aldrich, Merck, Darmstadt, Germany)) at a final concentration of $4x10^5$ cells/mL. Cells were plated out into a 12-well plate in 2 mL aliquots per well and incubated at 37ºC in 5% CO_2 for 5-6 days prior to use. All of the aforementioned steps were performed under sterile conditions.

5.3 Preparation of target cells

Two target cell types were used: tumour cells that had been cultured *in vitro* as detailed above in Section 1, and primary cancer associated fibroblasts (CAFs), the generation of which is detailed below in Section 9.3.

Tumour cells or primary cancer-associated fibroblasts were cultured until approximately 75% confluent before being irradiated. Where indicated, recombinant IFN-γ (Sigma-Aldrich, Merck, Darmstadt, Germany) was added into the culture medium at 1 ng/mL final concentration 24 hours prior to irradiation to better mimic a physiological environment. The target cells were harvested 24 or 48-hours after irradiation and labelled with 50 µCi $Na_2{}^{51}CrO_4$ (^{51}Cr). After a 30-60-minute incubation at 37ºC, the cells were washed 2-3 times in medium (RPMI-1640 plus 2% (v/v) FBS)

and resuspended at $1x10^6$ cells/mL in T or NK cell medium, as described above. The ^{51}Cr-labelled targets were plated into 96-well U-bottom microplates (Corning®, Darmstadt, Germany) at $2x10^4$ cells per well. Activated OT-1 T cells or NK cells were harvested and resuspended at $2.2x10^6$ cells/mL before being co-cultured with the targets at specific effector:target ratios. For spontaneous ^{51}Cr release readouts, target cells were incubated in medium alone. Targets were treated with 10% SDS to quantify total ^{51}Cr release. A sample set-up of the assay is depicted in *Table 2.4*. Each group had 3-6 technical repeats.

Effector:target ratio	**Spont.**	**0.25:1**	**0.5:1**	**1:1**	**10:1**	**20:1**
Target cells ($2x10^4$ cells/well) ($1x10^6$ cells/mL)	20 µL	20 µL	20 µL	20 µL	20 µL	20 µL
Effector cells ($2.22x10^6$ cells/mL)	-	2.2 µL	4.5 µL	9 µL	90 µL	180 µL
Assay media	180 µL	177.8 µL	175.5 µL	171µL	90 µL	-

Table 2.4. Sample set up of ^{51}Cr release assays. *Spont.: spontaneous; SDS: sodium dodecyl sulfate.*

The assay was incubated at 37º C, 5% CO_2 for 4 and/or 24 hours. At the time of harvest, the plates were centrifuged at 1400 rpm for 4 minutes and the supernatants were transferred carefully using a micropipette into 5mL round-bottom polysterene tubes (Falcon®, STEMCELL, Canada). Levels of ^{51}Cr released into the supernatant were detected using a Wallax Wizard 1470 Automatic Gamma Counter (Skudtek Scientific, Australia). All radioactive waste was disposed in accordance to institutional guidelines. Cytotoxicity was expressed as a percentage of specific ^{51}Cr release using the following calculation:

$$Specific\ release = \frac{(Sample\ release - Spontaneous.release)}{(Total\ release - Spontaneous\ release)} \times\ 100\%$$

6. Mice

C57BL/6 mice were obtained from the Walter and Eliza Hall Institute of Medical Research (WEHI), Australia. C57BL/6-Tg(Foxp3-DTR/EGFP) (DEREG), C57BL/6 *Batf3*$^{-/-}$ and C57BL/6 *Ifnar1*$^{-/-}$ mice were bred in-house and genotyped at the Peter MacCallum Cancer Centre (PMCC),

Australia. All mice were used at 6-12 weeks of age and maintained under pathogen-free conditions in the PMCC animal facility. All mouse experiments were conducted in accordance with institutional protocols and guidelines.

7. Tumour implantation and irradiation

AT3 and AT3-OVA tumour cells were injected orthotopically into the left 4th mammary fat pad of female C57BL/6 mice. A total of 1.5-1.8x10^6 cells in 100 µL PBS mice were injected per mouse. Mice were anaesthetised with isoflurane for mammary fat pad injection. A total of 1.8x10^6 MC38 tumour cells in 100 µL PBS were injected subcutaneously into the left flank of female C57BL/6 mice. Tumour growth was measured 2-3 times a week using electronic callipers. Tumour area (length x width) was recorded as a representative measure of tumour growth. Treatment of AT3 and MC38 tumours was initiated when they reached 25-35mm^2 and 40-50mm^2, respectively. Mice were culled when tumours reached 100-150mm^2 in size, or at other pre-defined time points for tumour or organ harvest. Survival of remaining mice were monitored until at least day 50 post initiation of treatment.

For tumour irradiation, mice were anaesthetised with a ketamine/xylazine mix (ketamine 100 mg/kg (Baxter Pharmaceuticals, India) + xylazine 20 mg/kg (Troy Laboratories, Australia) in 200ml PBS, injected intraperitoneally). Mice were positioned under a specially designed Perspex plate and covered by a 3mm thick lead shield containing 0.8 cm^2 exposure holes in designated areas to allow localised radiation to be delivered to the site of tumour growth while minimising radiation exposure of the rest of the animal (*Figure 2.1*). Irradiation was delivered using a 6 MeV electron beam at a dose rate of 20 Gy/minute using a megavoltage medical linear accelerator (Varian Medical Systems, USA). A senior physicist from within the Physical Sciences Department at PMCC was in charge of administering the radiation treatment. Quality assurance measurements using thermoluminiscent dosimeters on phantoms of similar thickness to experimental mice (approximately 1.5cm) confirmed that the dose received on entry was more than 95% of the prescribed dose, and on exit around 50% of the prescribed dose. A negligible amount of radiation (approximately 1.5% of the prescribed dose) was transmitted through the lead shielding. Radiation regimens used for this project were 3x4Gy, 9x4Gy, 3x8Gy, 1x12Gy, 1x20Gy. Control mice were anaesthetised but not exposed to radiation. Post treatment, mice were left to recovery in their cages on a heat pad to ensure normal body temperature was maintained.

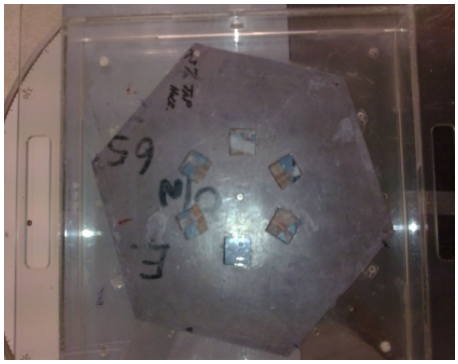

Figure 2.1. Specially designed Perspex plate with lead shielding for localised tumour irradiation.

8. Antibody / drug treatments

Antibody or drug treatments used alone or in combination with radiation are detailed in *Table 2.5*. All reagents were made up in 200 µL of sterile PBS on the day of injection and administered intraperitoneally. Unless specified, treatments were routinely initiated concurrently with the start of tumour irradiation. Control mice were treated with an isotype control using the same protocol as the test antibody or drug.

Antibody	**Clone**	**Isotype / Control**	**Source**	**Dose**	**Frequency***
Anti-asialoGM1	Rabbit polyclonal	PBS	Wako Chemicals, Japan	10 µL/mouse	Every 3 days from day of irradiation, until end of experiment
Anti-CD8β	53-5.8	Rat IgG1	BioXCell, USA	100 µg/mouse	Every 3 days from day of irradiation, until end of experiment
Anti-CTLA-4	9H10	Syrian Hamster IgG	BioXCell, USA	150 µg/mouse for the 1st injection, 100 µg/mouse thereafter	Days 0, 4, 8, and 12

Anti-CTLA-4 (depleting) **	9D9	Mouse IgG2a	Bristol-Myers Squibb, USA	150 µg/mouse for the 1st injection, 100 µg/mouse thereafter	Days 0, 4, 8, and 12
Anti-CTLA-4 (non-depleting) **	9D9 D265A	Mouse IgG1	Bristol-Myers Squibb, USA	150 µg/mouse for the 1st injection, 100 µg/mouse thereafter	Days 0, 4, 8, and 12
Anti-CXCR3	CXCR3-173	Armenian Hamster IgG	BioXCell, USA	150 µg/mouse	Every 3 days from day of irradiation, until end of experiment
Anti-CD96 **	NS	Mouse IgG1	Bristol-Myers Squibb, USA	200 µg/mouse for the 1st injection, 150 µg/mouse thereafter	Days 0, 4, 8, 12, and 16
Anti-FcR	2.4G2	Rat IgG2b	BioXCell, USA	200 µg/mouse for the 1st injection, 150 µg/mouse thereafter	Days 10, 13, 16,19
Anti-IFNAR1	MAR1-5A3	Mouse IgG1	BioXCell, USA	300 µg/mouse for the 1st injection, 150 µg/mouse thereafter	Days 0, 3, 6, 9, 12, and 15
Anti-Ly49C/I **	NS	Mouse IgG1	Bristol-Myers Squibb, USA	200 µg/mouse for the 1st injection, 150 µg/mouse thereafter	Days 0, 4, 8, 12, and 16
Anti-NKG2A **	NS	Mouse IgG1	Bristol-Myers Squibb, USA	200 µg/mouse for the 1st injection, 150 µg/mouse thereafter	Days 0, 4, 8, 12, and 16; or Days 10, 14, 18, 22, and 26
Anti-TIGIT **	NS	Mouse IgG1	Bristol-Myers Squibb, USA	200 µg/mouse for the 1st injection, 150 µg/mouse thereafter	Days 0, 4, 8, 12, and 16
Anti-TIM-3 **	NS	Mouse IgG1	Bristol-Myers Squibb, USA	200 µg/mouse for the 1st injection, 150 µg/mouse thereafter	Days 0, 4, 8, 12 and 16

Anti-PD-1	RMP1-14	Rat IgG2a	BioXCell, USA	150 µg/mouse for the 1st injection, 100 µg/mouse thereafter	Days 0, 4, 8, 12, and 16
Anti-PD-L1	10F.9G2	Rat IgG2b	BioXCell, USA	150 µg/mouse for the 1st injection, 100 µg/mouse thereafter	Days 0, 4, 8, 12, and 16
Anti-PD-L1 ***	6E11	Mouse IgG1	Roche Pharmaceuticals, Switzerland	150 µg/mouse for the 1st injection, 100 µg/mouse thereafter	Days 0, 4, 8, 12, and 16
Diphtheria toxin	-	PBS	Thermo Fisher, USA	0.5 µg/mouse	Day 3

Table 2.5. Details of *in vivo* treatment reagents. * Relative to day of first radiation fraction. ** Kindly provided by Bristol-Myers Squibb, CA, USA, through the International Immuno-oncology Network (IION). *** Kindly provided by Roche Pharmaceuticals, Basel, Switzerland, through the ImCORE Scientific Collaboration Network. *NS: not specified*

9 Processing of *ex vivo* mouse samples

9.1 Generation of single cell suspensions from mouse tumours, lymph nodes and spleens

Mice were euthanised by CO_2 asphyxiation or cervical dislocation at pre-defined experimental time points. Tumours, spleen and lymph nodes were excised from mice and each mechanically cut into small pieces and suspended in a 5mL collagenase preparation (0.625mg/mL collagenase type IV (Worthington Biochemical Corporation, NJ, USA) in DMEM containing 2% FBS and 0.1% (v/v) recombinant DNase I (Sigma-Aldrich™, Merck, Darmstadt, Germany)). Samples were placed on a rotator and incubated at 37°C for 25-35 minutes for enzymatic dissociation, prior to the addition of 5mM EDTA for 5 minutes to cease the enzymatic activity of the collagenase. The samples were then passed through a 70µm EASYstrainer™ strainer (Greiner Bio-One, Kremsmünster, Austria), washed and red blood cell lysed in ACK lysis buffer, if necessary, and resuspended in DMEM plus 2% FBS. Centrifugation for pelleting was performed at 1400 rpm for 4 minutes. All samples were stored at 4ºC post processing.

9.2 Processing of mouse blood

Mice were euthanised by CO_2 asphyxiation. Once dead, the abdomen of the mouse was opened and organs moved to expose the inferior vena cava. A 29-gauge insulin syringe was inserted into the blood vessel to collect 0.5-0.8 mL of blood. The blood was transferred into microcentrifuge tubes containing 10µL of 10mM EDTA to prevent coagulation. Blood samples were red blood cell lysed using ACK lysis buffer (*Table 2.3*), washed and resuspended in assay medium as per requirements and stored at 4º C.

9.3 Isolation of primary cancer-associated fibroblasts

To generate CAFs for use in *in vitro* ^{51}Cr release assays, untreated AT3-OVA tumours were harvested and processed into single cell suspensions as described above but with the following differences: procedures were done under sterile conditions, tumours were each placed in 10 mL of collagenase IV preparation instead of 5 mL, and centrifugation for pelleting was performed at 250 x g for 5 minutes. Single cell suspensions were red blood cell lysed using sterile ACK lysis buffer (*Table 2.3*) for 5 minutes at room temperature twice, resuspended in DMEM supplemented with 10% (v/v) FBS and transferred into 75 cm^2 angled-neck tissue culture flasks and incubated at 37º C in 5% CO_2 for one hour, which is sufficient time for fibroblasts to adhere firmly to the plastic. To remove all other non-essential cells, the flasks were gently shaken in a horizontal plane. The supernatant was suctioned off and the flask was rinsed once with DMEM medium. Fibroblast growth media was then added (Gibco™ Dulbecco's Modified Eagle Medium: Nutrient Mixture F-12 (DMEM/F-12) (Gibco™, Thermo Fisher, USA), 10% (v/v) FBS, 2 mM L-glutamine, 2 mM penicillin/streptomycin, 0.2 U/mL insulin (from bovine pancreas, Sigma-Aldrich™, Merck, Darmstadt, Germany), and 2.25 ng/mL recombinant human basic fibroblast growth factor (rh-bFGF) (Sigma-Aldrich™, Merck, Darmstadt, Germany)) and the cells were incubated at 37ºC in 5% CO_2 and 5% O_2 to create a hypoxic environment. The CAFs were checked every 2-3 days and passaged when necessary by differential trypsinisation, where fibroblasts, which detach quicker, were harvested quickly after 1 minute of trypsinisation. Fibroblasts were used within 2 weeks of preparation.

10. Splenocyte transfer

To examine the ability of RT to generate systemic anti-tumour immune responses, spleens were harvested from AT3-OVA tumour-bearing mice at post irradiation endpoints as described in Section 7. The spleens were each passed through a 70µm EASYstrainer™ strainer (Greiner Bio-One, Kremsmünster, Austria) into DMEM containing 2% FBS, red blood cell lysed using ACK

lysis buffer (*Table 2.3*), and passed through a 70µm EASYstrainer™ strainer again to remove undissolved cellular debris. After two washes in sterile PBS, the splenocytes were resuspended in approximately 500 µL of sterile PBS. The splenocyte preparations were injected into the tail vein of recipient mice at 200 µL per mouse.

11. Flow cytometric analysis

Single cell suspensions were aliquoted onto 96-well U-bottom microplates (Corning®, Merck, Darmstadt, Germany). Where required, Flow-Count™ Fluorospheres counting beads (Beckman Coulter, CA, USA) were added to each well as per manufacturer's instructions. Pelleted cells were resuspended in cold FACS buffer (2% (v/v) FBS in PBS, 1mM EDTA and 0.1% (w/v) sodium azide in PBS)) supplemented with 2% (v/v) normal mouse serum (NMS; Jackson ImmunoResearch, PA, USA) and incubated on ice for 10 minutes to saturate Fc receptors. Following a single wash in FACS buffer, the cells were stained for 30 minutes with the fluorescently labelled flow cytometry antibodies against extracellular markers, where are listed in *Table 2.6*.

Specificity	**Conjugate**	**Dilution**	**Clone**	**Source**	**Catalogue no.**
B220	eFluor 450	1/200	RA3-RB2	eBioscience	48-0452-82
CD4	APC-Cy7	1/200	RM4-5	eBioscience	17-0042-81
CD4	FITC	1/100	GK1.5	BD	553729
CD8α	BV480	1/300	53-6.7	BD	566096
CD8α	BV711	1/600	53-6.7	BioLegend	100747
CD8α	PE-Cy7	1/200	53-6.7	BD	552877
CD11b	APC-eFluor 780	1/150	M1/70	eBioscience	47-0112-82
CD11b	BV711	1/200	M1/70	BioLegend	101242
CD11c	BV510	1/100	HL3	BD	562949
CD19	eFluor 450	1/200	1D3	eBioscience	48-0193-82
CD27	APC	1/100	LG.7F9	eBioscience	17-0271-82
CD45.2	BUV395	1/200	104	BD	564616
CD45.2	BV650	1/200	104	BD	740490

CD45.2	eFluor 450	1/200	104	eBioscience	48-0454-82
CD49b	FITC	1/50	DX5	BD	553857
CD62L	AF700	1/500	MEL-14	BioLegend	104441
CD62L	APC-Cy7	1/200	MEL-14	BD	560514
CD62L	BV510	1/200	MEL-14	BD	563117
CD69	APC	1/200	H1.2F3	eBioscience	17-0691-82
CD69	FITC	1/100	H1.2F3	eBioscience	11-0691-82
CD86	FITC	1/100	GL1	eBioscience	11-0862-82
CD103	BUV395	1/200	M290	BD	740238
CD103	PE-CF594	1/100	M290	BD	565849
CD112	BV711	1/100	829038	BD	748049
CD155	PE-Cy7	1/100	TX56	BioLegend	131511
CTLA-4	APC	1/80	UC10-4B9	BioLegend	106310
CTLA-4	PE	1/100	UC10-4B9	eBioscience	12-1522-81
DNAM1	APC	1/100	10E5	eBioscience	17-2261-80
F4/80	APC	1/100	BM8	eBioscience	17-4801-82
F4/80	FITC	1/100	BM8	eBioscience	11-4801-82
H2-D^b	PE-Cy7	1/100	28-14-8	eBioscience	25-5999-82
H2-K^b	PE	1/100	AF6-88.5	BD	553570
H60	Alexa Fluor 405	1/100	205326	R&D	FAB1155V
LAG-3	BV711	1/100	C9B7W	BD	563179
Ly6C	PE-Cy7	1/2000	HK1-4	BioLegend	128018
Ly6G	BV605	1/400	RB6-8C5	BioLegend	108439
Ly6G	BV421	1/400	1A8	BD	562737
MHC-II	APC	1/600	M5/114.15.2	eBioscience	17-5321-82
MHC-II	BV786	1/15	M5/114.15.2	BD	742894
MULT-1	Alexa Fluor 405	1/100	237104	R&D	FAB2588V

NK1.1	BV510	1/100	PK136	BioLegend	408738
NK1.1	BV421	1/100	PK136	BD	562921
NK1.1	PE-Cy7	1/100	PK136	eBioscience	25-5941-82
NKG2A/C/E	BV480	1/100	20D5	BD	746584
NKG2D	PE	1/100	CX5	BD	558403
NKp46	BV421	1/100	29A1.4	BD	562850
Neuropilin-1	PE	1/200	3DS304M	eBioscience	17-3041-82
OVAtet*	PE	1/400	-	University of Melbourne	
PD-1	BV786	1/80	J43	BD	744548
PD-1	FITC	1/150	J43	eBioscience	11-9981-81
PD-L1	APC	1/100	10F.9G2	BioLegend	124311
PD-L1	PE	1/100	MIH5	eBioscience	12-5982-83
PD-L1	PE-Cy7	1/100	MIH5	eBioscience	25-5982-82
Qa1	BV711	1/100	6A8.6F10.1A6	BD	744389
RAE-1	PE	1/25	186107	R&D	FAB17582P
Streptavidin	APC	1/500	-	eBioscience	17-4317-82
Streptavidin	APC-Cy7	1/500	-	BD	554063
TCRβ	BUV737	1/200	H57-597	BD	564799
TCRβ	PB	1/100	H57-597	eBioscience	48-5961-82
TIGIT	BV605	1/200	1G9	BD	744212
TRAIL	Biotin	1/200	N2B2	eBioscience	13-5951-82
TIM-3	PE	1/100	5D12	BD	563179

Table 2.6. List of extracellular flow cytometry antibodies. * The PE-labelled OVA tetramer (OVAtet) (PE-conjugated tetrameric H2-Kb/SIINFEKL complex) was produced and purchased from Dr. Andrew Brooks' laboratory in the Department of Microbiology and Immunology, Peter Doherty Institute for Infection and Immunity, University of Melbourne. *BD: BD Biosciences, USA; BioLegend: BioLegend, CA, USA; eBioscience: eBioscience™, Thermo Fisher, USA; R&D: R&D Systems, MN, USA*

Upon completion of antibody staining the cells were resuspended in FACS buffer containing a viability dye for 20 minutes. *Table 2.7* lists the different viability dyes used.

Reagent	Dilution	Source	Catalogue no.
LIVE/DEAD™ Fixable Near-IR Dead Cell Stain Kit	1/1000	Invitrogen	L10119
BD Horizon™ Fixable Viability Stain 700	1/1000	BD	564997
4',6-diamidino-2-phenylindole (DAPI)	1/1000	Invitrogen	D3571
Propidium iodide (PI)	1/200	Sigma-Aldrich	P4864

Table 2.7. List of viability dyes for flow cytometry. *BD: BD Biosciences, USA; Invitrogen: Invitrogen™, Thermo Fisher, USA; Sigma-Aldrich: Sigma-Aldrich™, Merck, Darmstadt, Germany.*

For the detection of intracellular proteins, after staining for extracellular markers the cells were fixed and permeabilised (eBioscience™ Foxp3/Transcription Factor staining Buffer Set, Thermo Fisher, USA; or BD Cytofix/Cytoperm™ Fixation/Permeabilization Solution Kit, BD Biosciences, USA) as per the manufacturer's instructions. Intracellular staining antibodies (*Table 2.8*) were then added in permeabilisation buffer and the cells incubated on ice for 20-25 minutes before being washed and resuspended in ice-cold FACS buffer.

Specificity	Conjugate	Dilution	Clone	Source	Catalogue no.
FoxP3	eFluor 450	1/100	FJK-16S	eBioscience	48-5773-82
FoxP3	BV421	1/100	MF23	BD	562996
Granzyme B	Alexa Fluor 647	1/100	GB11	BD	560212
IFN-γ	BUV737	1/100	XMG1.2	BD	612769
IFN-γ	BV421	1/100	XMG1.2	BD	563376

Table 2.8. List of intracellular flow cytometry antibodies. *BD: BD Biosciences, USA; eBioscience: eBioscience™, Thermo Fisher, USA.*

Single stain compensation controls were set up for each experiment. Flow analysis was performed within 2 days of staining on a flow cytometer (BD FACSCanto™ II, BD LSRFortessa™ or BD FACSymphony™; BD Biosciences, USA). Flow cytometry data were analysed using FlowJo software (Tree Star Incorporated, USA).

12. Detection of radiation-induced cellular senescence

12.1 X-gal staining

Cultured AT3-OVA tumour cells were seeded into 60mm or 100mm tissue culture dishes (CELLSTAR®, Greiner Bio-One, Kremsmünster, Austria) as per *Table 2.1* and were given at least 4 hours to allow adherence prior to being irradiated. After 6 days of incubation, the tissue culture medium was aspirated and samples were rinsed twice with PBS. The fixation solution (2% formaldehyde and 0.2% glutaraldehyde in PBS) was then added for 3 minutes at a volume sufficient to cover the entire surface of the tissue culture dish, followed by two PBS rinses. The X-gal staining solution (*Table 2.9*) was then applied to cover the entire surface of the dish. Preparation of each reagent in the solution was performed beforehand in accordance to the protocol in (Debacq-Chainiaux *et al.*, 2009). Samples were sealed with Parafilm (Sigma-Aldrich, Merck, Darmstadt, Germany), wrapped in aluminium foil, and placed at 37° C in a non-humidified, non-CO_2 injected incubator overnight for at least 12 hours. The samples were then rinsed twice with PBS and permeabilised for 5 minutes with 0.5% Triton™ X-100 (Merck, Darmstadt, Germany) in PBS, followed by a PBS rinse and 5 minutes stain in 0.5 µg/mL 4',6-diamidino-2-phenylindole (DAPI; Thermo Fisher, USA). Following another 2-3 PBS rinses, the cells were imaged for X-gal and DAPI staining. Bright field images for X-gal staining and fluorescent images for DAPI staining were acquired using the Olympus V120 microscope (Olympus IMS, MA, USA) within 5 days. The number of X-gal stained cells were quantified manually by counting cells with greater than 50% cytoplasmic staining. The total number of cells was quantified by automatic counting of DAPI-stained nuclei using ImageJ software (National Institutes of Health, USA).

Reagent	**Concentration**
$C_6H_8O_7$ / $NaPO_4$ (Citric acid / sodium phosphate) buffer at pH 6.0	0.2M
$K_4[Fe(CN)_6]$ (Potassium ferrocyanide)	100mM
$K_3[Fe(CN)_6]$ (Potassium ferricyanide)	100mM

NaCl (Sodium chloride)	5M
MgCl2 (Magnesium chloride)	1M
5-bromo-4-chloro-3-indolyl-β-D-galactopyranoside (X-gal) – **added last**	20mg/mL (in dimethylformamide)
Made up in distilled H_2O	

Table 2.9. X-gal staining solution recipe. X-gal was sourced from Thermo Fisher, USA (Catalogue number B1690). The other reagents were sourced from communal laboratory stocks.

12.2 DDAOG staining

Single cell AT3-OVA tumour suspensions were aliquoted out into 96-well U-bottom microplates (Corning®, Merck, Darmstadt, Germany) and resuspended in 250 µL of DMEM (Gibco™, Thermo Fisher, USA) supplemented with 1 µM bafilomycin A1 (Cayman Chemicals, MI, USA). The microplate was wrapped in aluminium foil and incubated at 37ºC in a non-humidified, non-CO_2-injected incubator for 30 minutes. The cells were then treated with 10 µM of 9H-(1,3-dichloro-9,9-dimethylacridin-2-one-7-yl) β-D-galactopyranoside (DDAOG) (Invitrogen™, Thermo Fisher, USA) and further incubated under the same conditions for a further 60 minutes. The samples were washed twice and resuspended in FACS buffer containing a viability dye (*Table 2.7*). The samples were analysed on a flow cytometer (BD FACSCanto™ II, BD LSRFortessa™ or BD FACSymphony; BD Biosciences, USA) on the same day. Flow cytometry data were analysed using FlowJo software (Tree Star Incorporated, USA).

13. Antibody titre assay

On days 0 and 13 post completion of irradiation, blood was collected via tail vein bleed. Blood samples were left to coagulate in 1.5 mL Eppendorf® microcentrifuge tubes (Merck, Darmstadt, Germany) at room temperature for 45 minutes, after which they were centrifuged at 3000 rpm for 4 minutes. The supernatants, being the sera, were collected and re-centrifuged to remove all unwanted particulates. The serum samples were either used immediately or stored at -80º C for future use. To determine whether the serum samples contained tumour cell-reactive antibodies, cultured AT3-OVA tumour cells were harvested, washed three times in PBS to remove all protein contaminates and aliquoted into 96-well U-bottom microplates (Corning®, Merck, Darmstadt, Germany) at 1.5 x10^4 cells/well. The cell pellets were resuspended in 30 µL of Fc blocking reagent (Clone 2.4G2, BD Pharmingen™, CA, USA) for 10 minutes on ice before being washed and

resuspended in ice-cold PBS supplemented with 0.1% bovine serum albumin (BSA). The serum samples were thawed on ice and diluted serially (1:10, 1:25, 1:100, 1:300, 1:900, 1:2700, 1:27000) in ice-cold PBS plus 0.1% BSA before being added to the AT3-OVA tumour cells. After 30 minutes of incubation on ice, the cells were washed twice in PBS prior to being incubated with a PE-conjugated anti-mouse IgG antibody (Invitrogen™, Thermo Fisher, USA) to detect any bound mouse antibodies (antibody used at a 1:200 dilution in PBS supplemented with 0.1% BSA). After 30 minutes, the cells were washed and resuspended in FACS buffer containing a viability dye (*Table 2.6*). Samples were analysed on a flow cytometer (BD FACSCanto™ II, BD LSRFortessa™ or BD FACSymphony; BD Biosciences, USA). The percentages of PE-staining live cells were determined using FlowJo software (Tree Star Incorporated, USA) and were plotted against serum dilution factors and fitted with a 4-parameter logistic regression curve in GraphPad Prism (version 8.3.1, GraphPad Software, USA). The serum dilution that yielded 50% of cells positive for antibody binding was used as a measure of antibody titre.

14. RNAseq analysis

14.1 Preparation of mouse tumour samples and extraction of RNA

To examine how radiation can alter the transcriptional landscape of the tumour, stromal and immune cell compartments, irradiated AT3-OVA tumours were harvested, processed into single cell suspensions and stained for the pan-leukocyte marker CD45.2 as detailed above. BD FACSAria™ Fusion or BD FACSAria™ II was used to sort and enrich for $CD45^{+}GFP^{-}$ immune cells, $CD45^{-}GFP^{+}$ tumour cells and $CD45^{-}GFP^{-}$ tumour/stromal cells. Sorted cells were spun down at 400 x g for 5 minutes at 4ºC, resuspended in 1mL of ice-cold PBS, and transferred into 1.5mL Eppendorf® microcentrifuge tubes (Merck, Darmstadt, Germany), and spun down again. The PBS supernatant was carefully removed, and the cell pellet resuspended in 350 µL of QIAzol™ lysis reagent (QIAGEN, Germany). These samples were snap frozen in liquid nitrogen and stored at -80ºC. For extraction of RNA, QIAzol™-treated samples were thawed gently on ice and processed using the Direct-zol™ RNA MicroPrep kit (Zymo Research, USA) as per the manufacturer's instructions. Prior to sequencing, the quality of extracted RNA was assessed using the Aligent 2100 Bioanalyzer (Aligent Technologies, USA). Only samples with an RNA integrity number (RIN) of greater than 8.5 were processed for library preparation.

14.2 Library preparation and 3'-mRNA sequencing

Library preparation and RNA sequencing were performed by the PMCC Molecular Genomics Core Facility. Briefly, the QuantSeq 3'mRNA-Seq Library Prep Kit for Illumina (Lexogen, USA)

was used to generate libraries, as per manufacturer's instructions. Paired-end sequencing was performed on the Nextseq (Illumina, USA) to generate approximately 5 million 75bp paired-end reads per sample.

14.3 Analysis of mouse tumour sequencing data

RNA sequencing reads were trimmed using Trimmomatic (Bolger *et al.*, 2014) to remove adapter sequences, primers, poly-A tails and other short read sequences generated from the Illumina platform (Lexogen, USA). Reads were aligned to the reference mouse genome (GRCm38/mm10) using HISAT2 (Kim *et al.*, 2015), and features were counted using HTseq (Anders *et al.*, 2015) according to the Ensembl gene annotation version 90. Overlapping reads were resolved using the *intersection-nonempty* mode. Lowly expressed transcripts were filtered based on a threshold of 1 count per million across 4 samples (corresponding to the smallest sample group). Differential gene expression analysis was performed using limma-voom (Law *et al.*, 2014). Gene set analyses were performed using Gene Set Enrichment Analysis (GSEA version 3.0, Broad Institute Inc., USA) with genes pre-ranked by *t* value (Subramanian *et al.*, 2005) and Rotation Gene Set Test (ROAST) (Wu *et al.*, 2010). Gene sets were obtained from the Molecular Signatures Database (MSigDB). Gene ontology (GO) enrichment analysis was performed using PANTHER (Mi *et al.*, 2019). Where required, mouse genes were converted into human orthologues based on Ensembl annotations.

14.4 Analysis of human transcriptomic data

Publicly accessible human transcriptomic data were downloaded from the Gene Expression Omnibus (GEO). Normalisation of the human pancreatic ductal adenocarcinoma dataset (GSE129492) was performed using the default settings on nCounter Advanced Analysis 2.0 (NanoString Technologies®, Inc., USA). Downstream analyses were performed using the in-built Differential Expression, Pathway Scoring and Cell Type Profiling modules. An IFN-γ signature was calculated from this dataset by averaging the $\log_{10}$-transformed expression values of *IDO1*, *CXCL10*, *CXCL9*, *HLA-DRA*, *STAT1*, and *IFNG*, as per Ayers *et al.*, 2017. For analysis of the human rectal adenocarcinoma dataset (GSE15781), probe annotations for the Human Genome Survey Microarray v.2.0 (Applied Biosystems Inc., USA) were obtained from GEO. Multiple probes that matched to a single gene were filtered by selecting the probe with the highest expression value. Normalisation was performed using quantile normalisation. Differential gene expression analysis was performed using limma (Law *et al.*, 2014). Gene set analyses were performed as per Section 14.3.

15. Statistics

Unless otherwise stated, unpaired Student's *t* test and log rank test were used for group comparison and Kaplan-Meier survival analyses, respectively, using GraphPad Prism (version 8.3.1, GraphPad Software, USA). All error bars represent standard error of the mean (SEM). For RNAseq analyses, adjusted *p* values were calculated using the Benjamini-Hochberg procedure. A *p* value cut-off of less than 0.05 was used for statistical significance.

Chapter 3: The impact of radiation dose-fractionation on anti-tumour $CD8^+$ T cell responses

Abstract

Radiation therapy (RT) can induce host immune responses that contribute to tumour control. $CD8^+$ T cells play a pivotal role in these responses, capable of mediating control of tumours within and distant to the radiation volume. How these responses are dictated by radiation dose-fractionation remains unclear. In this chapter, the AT3-OVA mouse model of non-metastatic, triple-negative breast cancer was used to examine the impact of radiation dose-fractionation on the ability of RT to evoke local anti-tumour $CD8^+$ T cell responses. By comparing a series of rationally-selected radiation dose-fractionation regimens in the context of $CD8^+$ T cell depletion, radiation-induced $CD8^+$ T cell responses were found to be regulated by radiation dose per fraction (DPF), rather than total dose, as represented by biological effective dose (BED). Radiation regimens with low-to-moderate DPFs such as 3x4Gy (BED_{16} 15Gy), 9x4Gy (BED_{16} 45Gy), and 3x8Gy (BED_{16} 36Gy) were able to induce $CD8^+$ T cell-mediated tumour control, while radiation regimens with high DPFs such as 1x12Gy (BED_{16} 21Gy) and 1x20Gy (BED_{16} 45Gy) could not. Tumour cell-intrinsic changes evoked by radiation, including death and expression of immunomodulatory ligands or death receptors, were similar across radiation dose-fractionations and therefore were unlikely to have accounted for the modulation of $CD8^+$ T cell responses by radiation DPF. However, RT induced a transient accumulation of tumour-associated regulatory T cells (Tregs), the kinetics and amplitude of which were proportional to the radiation DPF employed. These Tregs suppressed $CD8^+$ T cells directly and indirectly via restricting the function of type 1 conventional DCs within tumours. Depletion of radiation-induced Tregs rescued anti-tumour $CD8^+$ T cell responses following irradiation with the high DPF 1x20Gy regimen, resulting in tumour cures and the generation of protective immunological memory. By contrast, radiation-induced enrichment of Tregs was not observed in MC38 colon carcinoma tumours, correlating with the ability of the 1x20Gy regimen to independently evoke $CD8^+$ T cell responses in those tumours. Thus, in some tumour types, radiation dose-fractionation regimens do not similarly support $CD8^+$ T cell responses not because of differences in tumour cell-intrinsic immunogenicity, but because of differences in the tumour immune regulatory environment. Identifying tumour factors predictive of radiation-induced Treg responses could be valuable to guide RT and cancer immunotherapy strategies.

Introduction

Cancer immunotherapy has seen a dramatic resurgence in the last decade, and $CD8^+$ T cells have been at the forefront of this wave. The radiation abscopal response, defined as the regression of a tumour lesion distant to the irradiated site, is mediated by $CD8^+$ T cells and is an archetypal demonstration of the potential of radiation therapy (RT) to modulate host immunity for significant clinical benefit (Reynders *et al.*, 2015). Although combination RT and immunotherapy strategies have resulted in higher proportions of abscopal events, their rates remain low at 10-30%, reflecting the inefficiency of the underlying processes (Golden *et al.*, 2015; Formenti *et al.*, 2018; Luke *et al.*, 2018). Because abscopal responses are a function of effective circulating T cell responses and must have originated from changes occurring within the irradiated tumour, a deeper understanding of the effects of radiation on the local tumour immune microenvironment is crucial.

The generation of anti-tumour $CD8^+$ T cell responses by radiation putatively stems from the induction of immunogenic cell death (ICD) within the tumour, leading to the release of danger associated molecular patterns (DAMPs) that can promote dendritic cell (DC) antigen uptake, maturation, and migration to secondary lymphoid organs, whereupon they interact with and prime $CD8^+$ T cells (Lugade *et al.*, 2005; Lee *et al.*, 2009; Vanpouille-Box *et al.*, 2017). While the role of lymph node DCs is undisputed and has been the subject of significant focus, the importance of a specialised subset of tumour-associated DCs in supporting T cell-mediated immune rejection has also recently been recognised (Broz *et al.*, 2014; Bottcher and Reis, 2018). These tumour-associated type 1 conventional DCs (cDC1s) play key roles in the further recruitment, restimulation and repositioning of T cells within the tumour. Furthermore, tumour-associated DCs can exhibit significant cross-talk with regulatory T cells (Tregs) to influence the immunogenic or tolerant nature of the tumour immune contexture (Delgoffe *et al.*, 2013; Jang *et al.*, 2017). How these local interactions within the tumour are affected by radiation dose-fractionation is nonetheless presently ill-defined.

Clarifying the impact of radiation dose-fractionation is made more urgent given the increasing adoption of stereotactic ablative radiotherapy (SABR) into clinical practice, which involves the delivery of high radiation doses in one or a few fractions (usually above 8Gy per fraction), in contrast to conventionally fractionated regimens which typically employ an extended number of fractions of less than 4Gy per fraction. Landmark pre-clinical work from Demaria and colleagues have shown that large single-fraction doses above 10-12Gy were incapable of evoking T cell-mediated abscopal responses (Dewan *et al.*, 2009; Vanpouille-Box *et al.*, 2017). This was demonstrated to be due to the induction of exonuclease TREX1 by high DPFs, which degraded

cytosolic double-stranded DNA (dsDNA), resulting in abrogation of tumour cell-intrinsic STING signalling and the production of type I interferon (IFN) required for $CD8^+$ T cell priming. However, a large single-fraction dose of 20Gy was able evoke STING and/or type I IFN-dependent $CD8^+$ T cell responses in other pre-clinical tumour models (Lee *et al.*, 2009; Deng *et al.*, 2014b; Schadt *et al.*, 2019), and in humans, abscopal responses have been reported with single-fraction doses as high as 26Gy (Siva *et al.*, 2013). Therefore, regulatory pathways other than the tumour cell-intrinsic TREX1 induction likely exist in determining host anti-tumour $CD8^+$ T cell responses.

To address inconsistencies in the field, this chapter examined the impact of radiation dose-fractionation on tumour cell-intrinsic and tumour immune microenvironmental changes that drive $CD8^+$ T cell responses, dissecting the contributions of dose per fraction (DPF) from total dose, as expressed by the biological effective dose (BED). Using AT3-OVA mammary carcinoma cells as the primary model of investigation, radiation-induced $CD8^+$ T cell responses were found to be regulated by radiation DPF, not BED, in a tumour-type dependent manner. The inability of high radiation DPFs to evoke $CD8^+$ T cell responses was due to radiation DPF-dependent Treg responses, which suppressed tumour-associated cDC1s and $CD8^+$ T cells. Depletion of radiation-induced Tregs rescued anti-tumour $CD8^+$ T cell responses regardless of the radiation regimen employed, indicating a tumour cell-extrinsic rather than tumour cell-intrinsic mechanism of regulation. By contrast, radiation-induced $CD8^+$ T cell responses were not regulated by radiation DPF in MC38 murine colon carcinomas because such Treg responses were absent. Understanding these interactions across different tumour types will help with the rational selection of immune-permissive radiation dose-fractionation regimens for combination with cancer immunotherapy.

Results

1. Radiation-induced CD8+ T cell responses are regulated by radiation DPF rather than BED

To study the immunological effects of tumour irradiation, AT3 triple negative mammary carcinoma cells retrovirally transduced to express membrane-bound ovalbumin and GFP (AT3-OVA) (as described in Mattarollo *et al.*, 2011) were implanted into the mammary fat pads of wildtype C57BL/6 female mice. Based on previous work in the laboratory, AT3-OVA tumours were left to grow to 25-35mm^2 before being locally irradiated with an electron beam delivered by a medical linear accelerator (linac). At this size, the tumours were refractory to control by CD8$^+$ T and NK cells as well as checkpoint blockade therapy (Verbrugge *et al.*, 2012).

To select the radiation dose-fractionation regimens for study, the radiation cell survival curve of the AT3-OVA tumour cell line was generated using *in vitro* clonogenic survival assays and fitted using the linear-quadratic model (Joiner and Kogel, 2018) (*Figure 3.1a*). The α/β ratio, which is a mathematical description of the curve shape representing the dose at which the number of cells killed by the linear component (α) is equal to the cells killed by the quadratic component (β), was determined to be 16Gy. Using this ratio, the BED values for different dose-fractionation regimens could be calculated as an expression of total dose (total clonogenic cell kill) for the AT3-OVA tumour cell line (Fowler, 2010). The ability to account for the BED of different radiation regimens avoids confusing the effects of DPF with total dose, and vice versa.

Prior to this PhD project, the 3x4Gy and 1x20Gy regimens had been employed for *in vivo* work in AT3-OVA tumours and were therefore used as starting points for selecting comparative dose-fractionation regimens. It was determined that 9x4Gy (BED_{16} 45Gy, 4Gy per fraction) had the same DPF as 3x4Gy (BED_{16} 15Gy, 4Gy per fraction) but a similar BED to 1x20Gy (BED_{16} 45Gy, 20Gy per fraction). 9x4Gy thus served as a control regimen for DPF and BED between the 3x4Gy and 1x20Gy regimens, permitting the contributions of DPF and BED toward CD8$^+$ T cell responses to be independently dissected. For comparison with other published studies (Dewan *et al.*, 2009; Vanpouille-Box *et al.*, 2017), the 3x8Gy regimen (BED_{16} 36Gy, 8Gy per fraction) was also investigated. 1x12Gy, a high DPF but low BED regimen (BED_{16} 21Gy, 12Gy per fraction), was also tested as another commonly used ablative regimen in clinic. These radiation regimens and the experimental schema incorporating their use in AT3-OVA tumours in combination with CD8$^+$ T cell depleting antibodies are presented in *Figure 3.1b-c*.

a

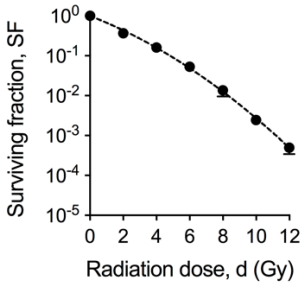

$$SF = \exp(-\alpha d - \beta d^2)$$

$\alpha \sim 0.37$

$\beta \sim 0.022$

$\alpha/\beta \sim 16\text{Gy}$

b

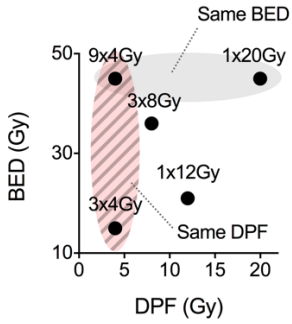

$$BED_{\alpha/\beta} = n \times d\left(1 + \frac{d}{\alpha/\beta}\right)$$

Dose-fractionation (n x d)	BED_{16}
3x4Gy	15Gy
9x4Gy	45Gy
3x8Gy	36Gy
1x12Gy	21Gy
1x20Gy	45Gy

c

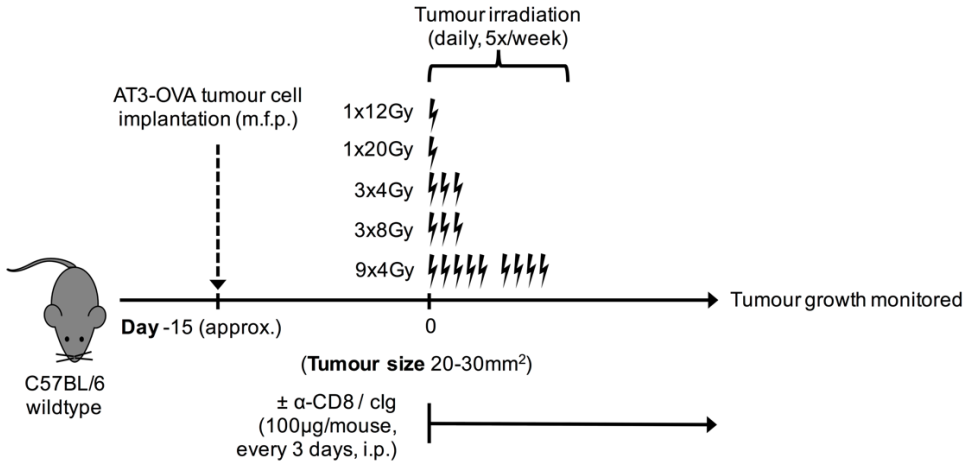

Figure 3.1. Selection of radiation dose-fractionation regimens for investigation, based on DPF and BED. a, *Left*: Radiation cell survival curve of AT3-OVA tumour cells, as established by *in vitro* clonogenic survival assays following radiation exposure at the indicated doses. *n*=6 replicates combined from 2 independent experiments. Data presented as mean ± SEM. *Right*: The linear-quadratic equation and the best-fit α and β parameters. **b,** *Left*: The selected dose-fractionation regimens in biological effective dose (BED) and dose per fraction (DPF) dimensions. *Right*: The BED equation, which is an expression of total dose based on the linear-quadratic model. The BED estimates for the different radiation regimens are shown in table format. **c,** Experimental schema of *in vivo* $CD8^+$ T cell depletion experiments. AT3-OVA

tumour cells were injected into the mammary fat pads (m.f.p.) of C57BL/6 wildtype mice (1.5-1.8x10^6 cells/mouse) to allow orthotopic tumours to form. Tumours were irradiated when they reached 25-35mm^2 in size, which took approximately 14-16 days. RT was given daily, 5 fractions per week. Mice were culled when tumours reached 100-150mm^2. Survival of remaining mice were monitored until at least day 50 post initiation of treatment. $CD8^+$ T cell depleting or isotype control antibodies were administered intra-peritoneally (i.p.) at 100μg/mouse, every 3 days from start of RT to end of experiment. *n: number of fractions, d: dose per fraction*

AT3-OVA tumours in mice reached experimental endpoint (100-150mm^2) by approximately 3 weeks with mock-irradiation, but RT slowed the growth of tumours in a manner that was proportional to the BED estimate of the radiation regimen employed (*Figure 3.2a*). Irradiated tumours decreased in size with all radiation regimens, but took longer to grow back to their pre-RT sizes when treated with higher BED regimens (3x8Gy, 9x4Gy, 1x20Gy) than with lower BED regimens (3x4Gy, 1x12Gy). The role of $CD8^+$ T cells in mediating tumour control was determined using a $CD8^+$ T cell depleting antibody, which depleted more than 80% of circulating $CD8^+$ T cells (*Figure 3.2b*). Depletion of $CD8^+$ T cells did not affect the growth of mock-irradiated tumours, indicating that these tumours had escaped $CD8^+$ T cell control at treatment initiation (*Figure 3.2a*). A role for $CD8^+$ T cells in supporting the anti-tumour effects of RT was observed with radiation regimens of low-to-moderate DPF (3x4Gy, 9x4Gy and 3x8Gy) (*Figure 3.2a*). Notably, $CD8^+$ T cell-depleted and non-depleted tumour growth curves separated at around 10-15 days after completion of RT, consistent with the time required for priming and trafficking of T cells from draining lymph nodes back into the tumour (Paul, 2013). In contrast, there was little or no impact of $CD8^+$ T cell depletion on tumour control with radiation regimens of high DPF (1x12Gy and 1x20Gy) (*Figure 3.2a*). Since the 9x4Gy and 1x20Gy regimens were isoeffective (having similar BED values) yet differed in their ability to evoke host anti-tumour $CD8^+$ T cell responses, this suggests that radiation DPF was a more critical parameter than radiation BED in the regulation of radiation-induced anti-tumour $CD8^+$ T cell responses.

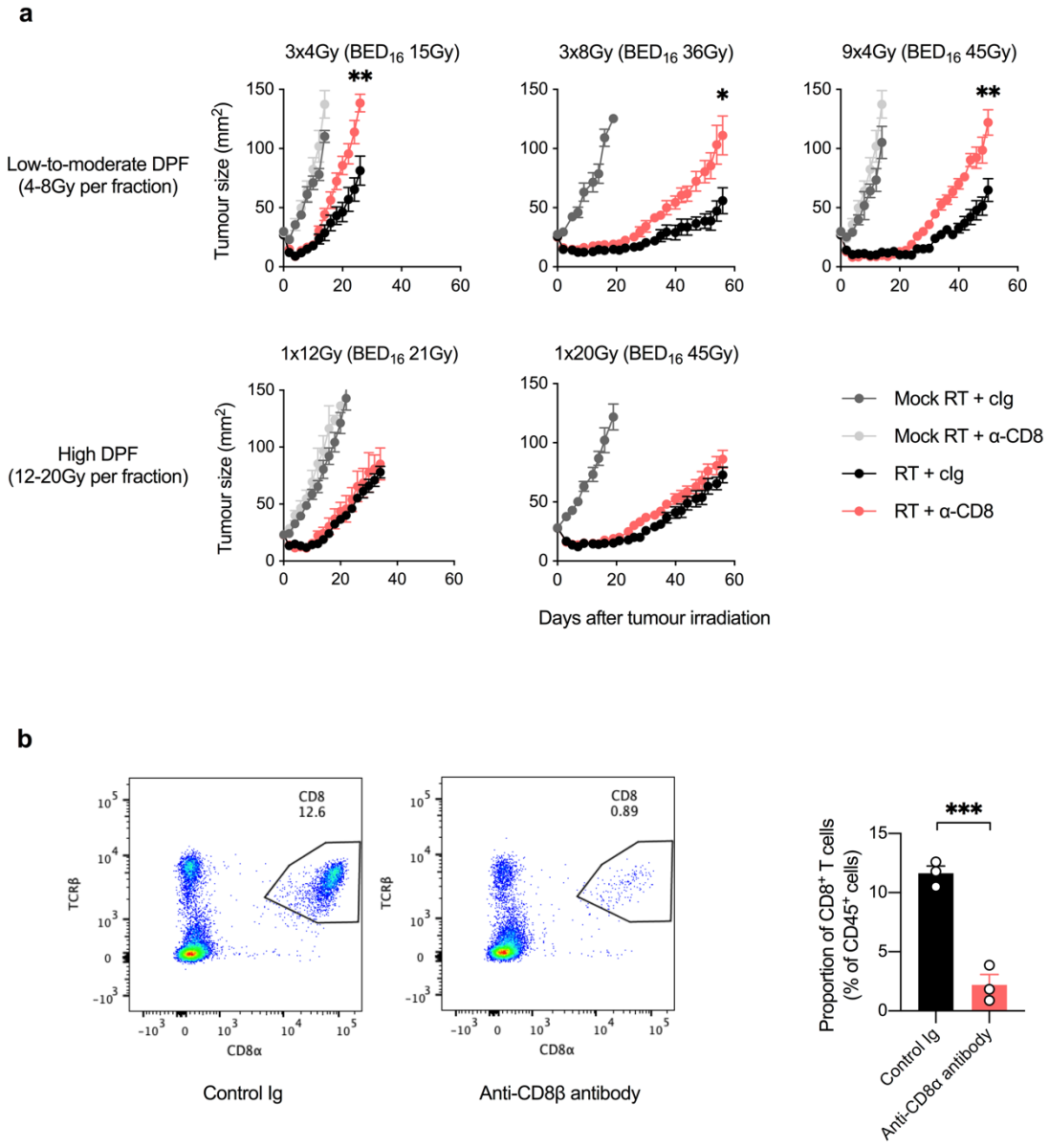

Figure 3.2. Radiation regimens with low-to-moderate DPFs but not high DPFs evoke anti-tumour CD8+ T cell responses. a, AT3-OVA tumour growth after RT in mice treated with $CD8^+$ T cell depleting or isotype control antibodies. Tumour growth is presented from start of RT. Because RT was delivered daily, 5 fractions a week, the 3x4Gy and 3x8Gy regimens were delivered over 3 days, and the 9x4Gy regimen over 11 days. Statistical comparisons were made between the RT + anti-CD8 and RT + cIg groups. *n*=4-6 mice per group, representative of 2 independent experiments. Data presented as mean ± SEM. **b,** Depletion of $CD8^+$ T cells by anti-$CD8^+$ T cell depleting antibodies. *Left*: Representative flow cytometry plots of splenocytes at 24 hours after a single dose of anti-$CD8^+$ T cell depleting or isotype control antibodies. *Right*: Quantification of data in left panel. *n*=3 mice, representative of 1 experiment. Data presented as mean ± SEM. * $p<0.05$, ** $p<0.01$, *** $p<0.001$

2. Radiation-induced CD8+ T cell responses are cDC1-dependent

Across various cancer models, anti-tumour $CD8^+$ T cell responses critically require cDC1s for priming (Bottcher and Reis, 2018). Type I IFN facilitates this process by promoting the efficient cross-presentation of antigens by DCs to T cells (Diamond *et al.*, 2011; Fuertes *et al.*, 2011). To test the role of cDC1s in radiation-induced $CD8^+$ T cell responses observed in AT3-OVA tumours, the control of irradiated tumours grown in wildtype and *Batf3*$^{-/-}$ mice, which are deficient for cDC1, was compared. For logistical reasons, 3x4Gy and 1x20Gy were selected as representative low-to-moderate and high DPF regimens, respectively. Interestingly, control of tumour growth in *Batf3*$^{-/-}$ mice was impaired compared to wildtype mice following irradiation with the 3x4Gy regimen but not with the 1x20Gy regimen, consistent with the capacity of the respective radiation regimens to evoke anti-tumour $CD8^+$ T cell responses (*Figure 3.3a*).

To determine if type I IFN signalling was essential for $CD8^+$ T cell responses, the control of irradiated tumours grown in wildtype and type I IFN-α/β receptor deficient (*Ifnar1*$^{-/-}$) mice was next compared. A non-statistically significant trend towards poorer tumour control in *Ifnar1*$^{-/-}$ mice compared to wildtype mice was observed following irradiation with the 3x4Gy regimen but not with the 1x20Gy regimen (*Figure 3.3b*). As an extension to these experiments, wildtype mice bearing AT3-OVA tumours were treated with an anti-IFNAR1 blocking antibody from the start of RT. Under these experimental conditions, in which both the host and tumour cells could not respond to type I IFN, no discernible difference in tumour control was evident between anti-IFNAR1 and isotype control antibody-treated mice (*Figure 3.3c*).

Altogether, these findings suggest that radiation regimens with low-to-moderate DPFs have a greater capacity to prime anti-tumour $CD8^+$ T cell immune responses than radiation regimens with high DPFs. However, type I IFN signalling was not critical to the stimulatory activity of cDC1s in the AT3-OVA tumour model.

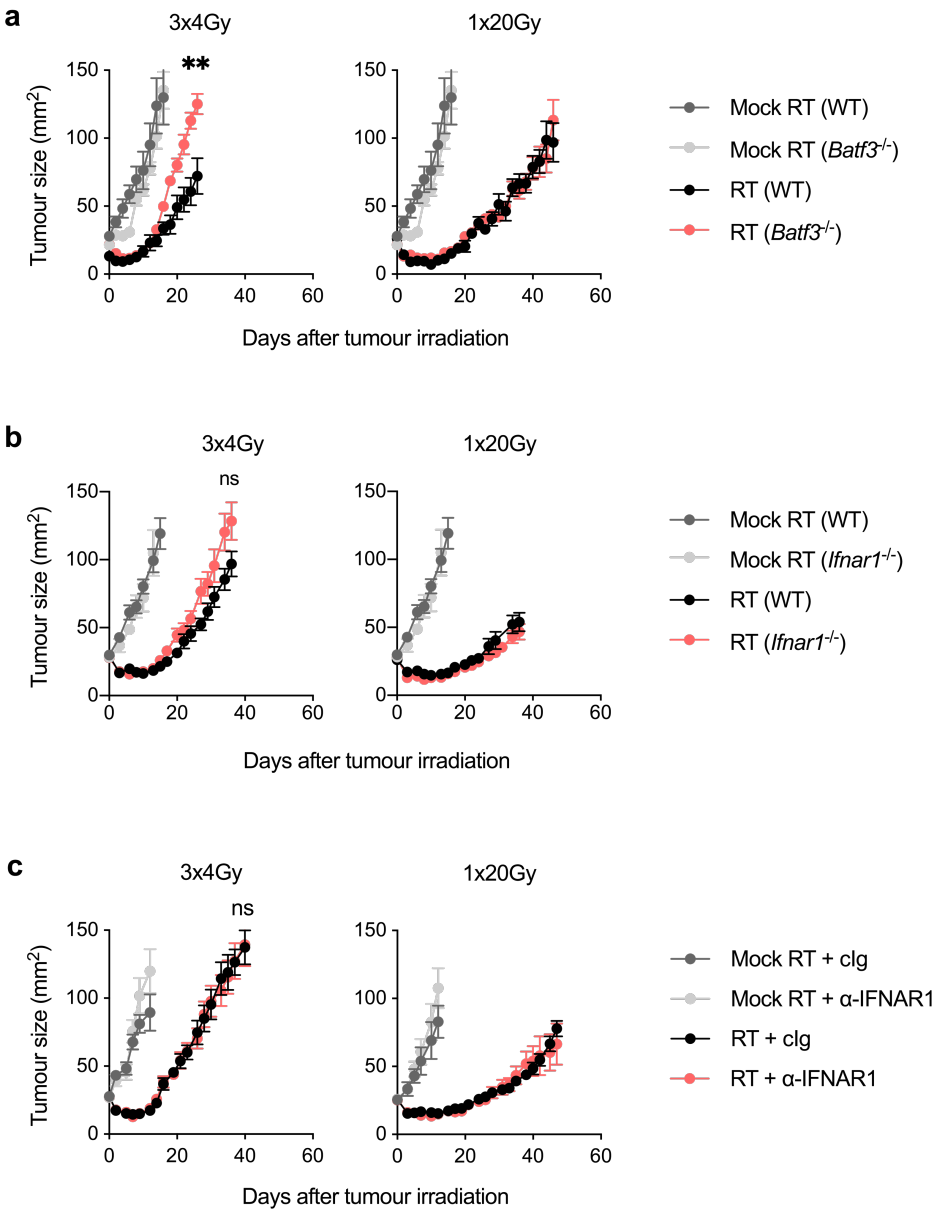

Figure 3.3. Lack of *Batf3* but not type I IFN signalling affects the anti-tumour activity of radiation regimens with low-to-moderate DPFs. a-b, AT3-OVA tumour growth post RT in (**a**) *Batf3*$^{-/-}$ and (**b**) *Ifnar1*$^{-/-}$ mice compared to wildtype (WT) mice. The experimental set up for *Batf3*$^{-/-}$ and *Ifnar1*$^{-/-}$ mice was similar to that of wildtype mice described in *Figure 3.1c*. 3x4Gy and 1x20Gy irradiation was performed in one experiment with shared mock-irradiated controls. Statistical comparisons were made between the RT (*Ifnar1*$^{-/-}$ or *Batf3*$^{-/-}$) and RT (WT) groups. *n*=4-6 mice per group, representative of 2 independent experiments. **c**, AT3-OVA tumour growth post RT in WT mice treated with anti-IFNAR1 or isotype control antibodies (300 µg/mouse for the first injection, 150 µg/mouse thereafter), administered every 3 days from start of RT, for a total of 8 injections. Statistical comparison was made between the RT + anti-IFNAR1 and RT + cIg groups. *n*=4-6 mice per group, representative of 2 independent experiments. Data presented as mean ± SEM. *ns: non-significant, ** p<0.01*

3. Tumour cell-intrinsic effects of radiation dose-fractionation on cell death type and kinetics

To test whether differences in the type and kinetics of radiation-induced tumour cell death may have accounted for why the 3x4Gy regimen was better than the 1x20Gy regimen at priming anti-tumour $CD8^+$ T cell responses, *in vitro* AT3-OVA tumour cells were stained for Annexin V and propidium iodide (PI) 24 and 48 hours post irradiation to track differences in apoptosis and necrosis (*Figure 3.4a-b*). These *in vitro* experiments examined the tumour cell-intrinsic effects of RT, detached from the tumour cell-extrinsic effects of the tumour microenvironment *in vivo*. Early apoptosis was defined as Annexin V^+ PI^- and necrosis (either primary necrosis or secondary necrosis resulting from late apoptosis) was defined as any PI^+ staining (Wlodkowic *et al.*, 2011). As expected, 48 hours after irradiation, a larger proportion of dead cells (any Annexin V^+ or PI^+) was detected in the 1x20Gy group (*Figure 3.4c*). Nevertheless, the number of cells undergoing early apoptosis relative to total death was higher in the 3x4Gy group at 24 hours (*Figure 3.4d*). Because the assay time points were synchronised to post completion of irradiation, the 24-hour time point was in fact 72 hours after the first fraction of 3x4Gy (*Figure 3.4a*). Therefore, more cells could have been initiated to undergo apoptosis over the course of the 3x4Gy regimen by this time. Alternatively, 1x20Gy irradiation may have pushed more cells into primary necrosis at the early 24-hour time point, resulting in a correspondingly lower proportion of cells in early apoptosis.

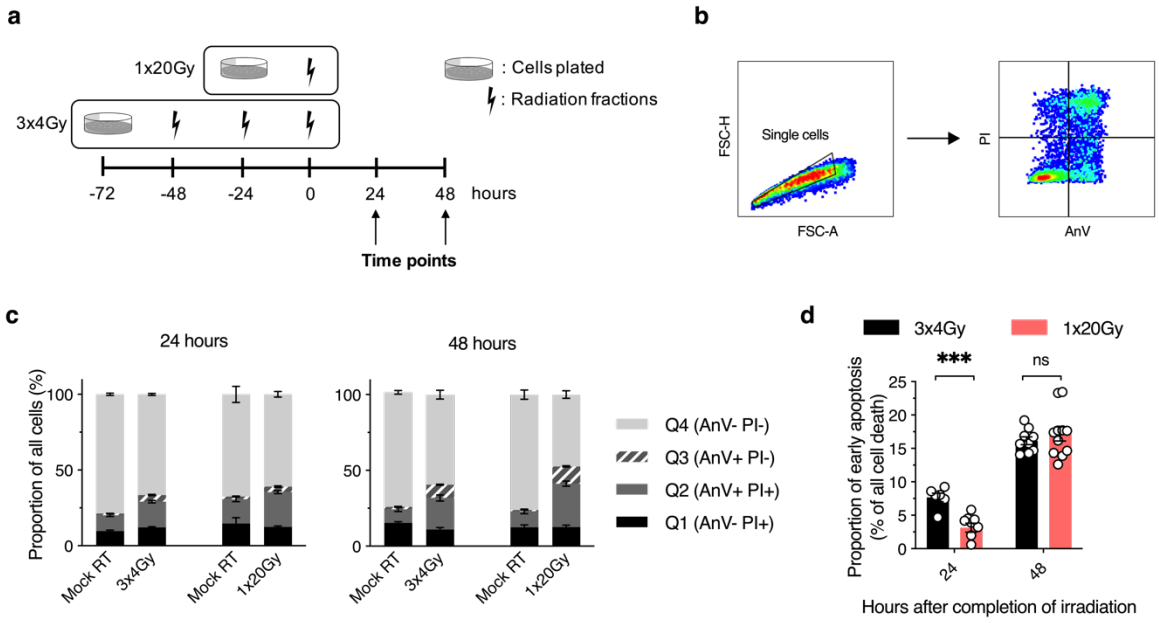

Figure 3.4. ***In vitro*** **radiation exposure induces apoptotic and necrotic responses in AT3-OVA tumour cells. a,** Experimental schema for *in vitro* assays. AT3-OVA tumour cells in each group were plated 24 hours before being irradiated, and processed at 24 and 48-hour time points after completion of RT. **b,** Representative flow cytometry plots and gating strategy for Annexin V (AnV) and propidium iodide (PI) staining of cultured AT3-OVA cells. **c,** Proportion of AnV and PI staining AT3-OVA cells, as determined by flow cytometry, after *in vitro* radiation exposure. *n*=6-11 replicates per group combined from 2 independent experiments. **d,** Number of early apoptotic (AnV+ PI-) cells as proportion of all dead/dying (AnV+ and/or PI+) cells after irradiation, from data presented in (**c**). Data presented as mean ± SEM. *ns: non-significant, *** p<0.001*

To discern between the two possibilities, a live-cell real-time assay system was used, where Annexin V and PI staining was monitored continuously for 48 hours using luminescence and fluorescence as a measure of apoptosis and necrosis (both primary and secondary necrosis), respectively. Compared to a single fraction of 4Gy, the 1x20Gy regimen induced higher amounts of apoptosis and necrosis, but the shape of the response curves was similar for both regimens, indicating that the majority of cell death occurred approximately 36 hours after irradiation regardless of radiation dose (*Figure 3.5a*). This delayed entry into cell death explains why the increased amount of overall death with 1x20Gy irradiation over 3x4Gy was only apparent at 48 hours but not at 24 hours (*Figure 3.4b*).

Because the initial gradient of the necrosis curve following irradiation with 1x20Gy was similar to that with 1x4Gy, it is unlikely that higher DPFs evoked more primary necrosis in AT3-OVA tumour cells. However, as these were single-fraction experiments, a "double-hit" effect could have been missed, where cells might be sensitised after the first fraction to undergo necrosis when exposed to a second fraction of radiation. To test this, a second fraction of radiation was given at the 24-hour time point and the rates of apoptosis and necrosis were observed. There was an expected subsequent increase in apoptotic events, but the gradient of the necrosis curve stayed unchanged compared to single-fraction treatment (*Figure 3.5b*), indicating that cells were not driven towards necrosis by consecutive radiation fractions. Other intermediate doses were also tested, demonstrating dose-proportional amounts of apoptosis and necrosis, but with similar curve shapes (*Figure 3.5c*). The peak in apoptosis events at 8Gy likely represented saturation of the assay's detection range.

Collectively, these data suggest that while the amount of tumour cell death was proportional to the total radiation dose, the type and kinetics of death were not different between dose-fractionations. A high DPF regimen did not push cells towards primary necrosis, but rather the predominant type of radiation-induced cell death for AT3-OVA tumour cells was apoptosis regardless of the radiation DPF employed. Moreover, the rates of apoptosis and necrosis were almost identical across the DPFs tested, primarily occurring around 36 hours after radiation exposure. It is therefore unlikely that the type and kinetics of radiation-induced tumour cell death underpinned the differential capacities of 3x4Gy and 1x20Gy to evoke anti-tumour $CD8^+$ T cell responses.

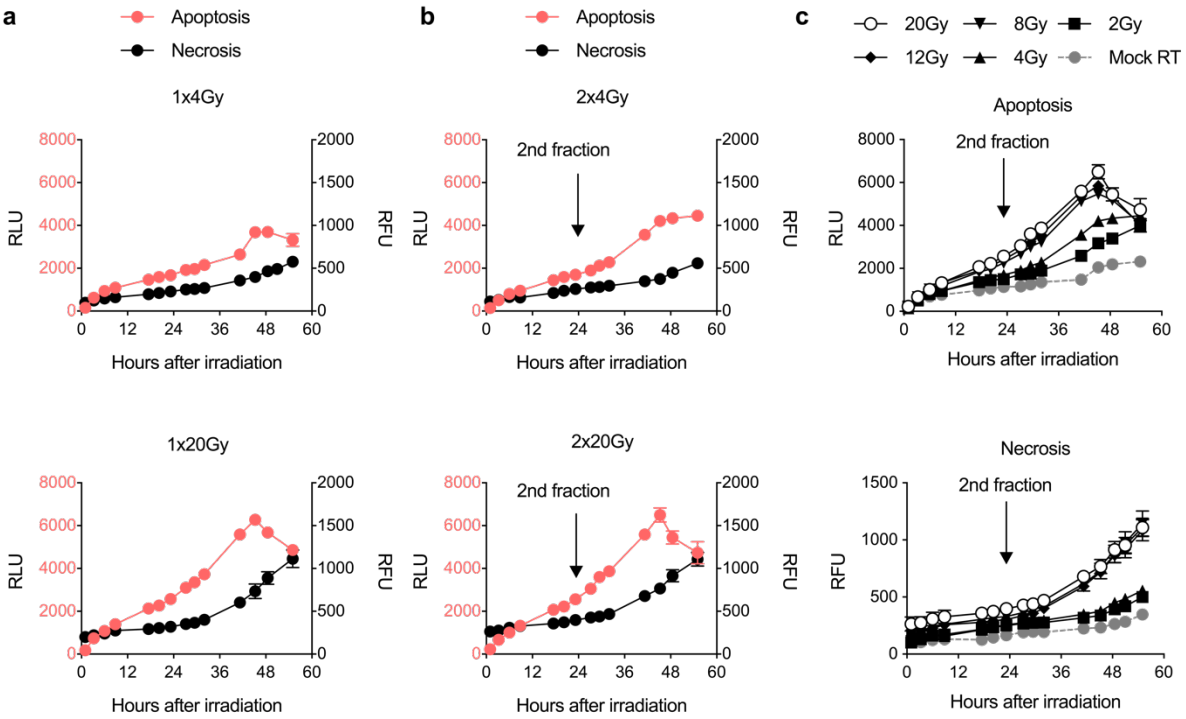

Figure 3.5. The kinetics of radiation-induced apoptotic and necrotic responses are similar between radiation DPFs. a-c, Real-time measurement of apoptosis (Annexin V staining) and necrosis (PI staining) events by luminescence and fluorescence readouts, respectively, in AT3-OVA cell cultures following exposure to 1 or 2 fractions of radiation. A single fraction of radiation was given in **a**, while two fractions of the same dose were given 24 hours apart in **b** and **c**. *n*=3 replicates per group, representative of 1 experiment. Data presented as mean ± SEM. *RFU: relative fluorescent units, RLU: relative luminescence units*

4. Radiation-induced changes in tumour cell expression of immunomodulatory ligands and death receptors

Having detected no differences in the type and kinetics of cell death between radiation dose-fractionation regimens, the expression of immunomodulatory ligands and receptors on the surface of surviving AT3-OVA cells post 3x4Gy and 1x20Gy irradiation was examined *in vitro*. Compared to mock-irradiated cells, expression of the MHC-I haplotypes H2-K^b and H2-D^b, the co-stimulatory molecule CD80, the inhibitory ligand PD-L1, and the death receptors Fas and DR5 were upregulated within 48 hours of irradiation with both 3x4Gy and 1x20Gy regimens (*Figure 3.6a*). 1x20Gy-irradiated cells demonstrated modestly greater upregulation of H2-K^b, H2-D^b, CD80 and Fas compared to 3x4Gy-irradiated cells. To test if this translated to differential sensitivity to $CD8^+$ T cell killing, irradiated AT3-OVA cells were labelled with chromium-51 (^{51}Cr) and co-cultured with IL-2-activated OVA-reactive OT-1 $CD8^+$ T cells for 24 hours at increasing effector:target ratios. Levels of ^{51}Cr release into the culture supernatant was used as a readout of specific tumour cell lysis. No significant increases in $CD8^+$ T cell tumour cell killing of either 3x4Gy or 1x20Gy-irradiated cells relative to mock-irradiated cells were detected (*Figure 3.6b*). This experiment was repeated with the addition of IFN-γ to emulate a more physiologically-relevant microenvironment. The addition of IFN-γ upregulated MHC-I expression on mock-irradiated cells, but did not further increase the levels of MHC-I induced by radiation (*Appendix Figure 1*). Exposure to IFN-γ increased the sensitivity of AT3-OVA cells to $CD8^+$ T cell killing, but the amount of cell kill between mock-irradiated and irradiated cells remained comparable (*Figure 3.6c*).

To determine if the pattern of modulation of these molecules was maintained *in vivo*, AT3-OVA tumours grown in mice were harvested 2 days post completion of irradiation and processed into single cell suspensions. Tumour cells ($CD45^-GFP^+$) were selectively examined. In contrast to that observed on *in vitro* cultured AT-3-OVA cells, expression of H2-Kb, CD80 and PD-L1 was significantly higher in the 3x4Gy group compared to the 1x20Gy group (*Figure 3.6d*), reflecting tumour cell-extrinsic influences in response to the 3x4Gy regimen. This suggests that low-to-moderate DPF regimens generated a more immune-stimulatory tumour microenvironment compared to high DPF regimens. Indeed, the 1x20Gy regimen appeared to reverse the PD-L1 status of tumour cells relative to the mock-irradiated tumours, suggesting a potential shut down of immune activity within the tumours.

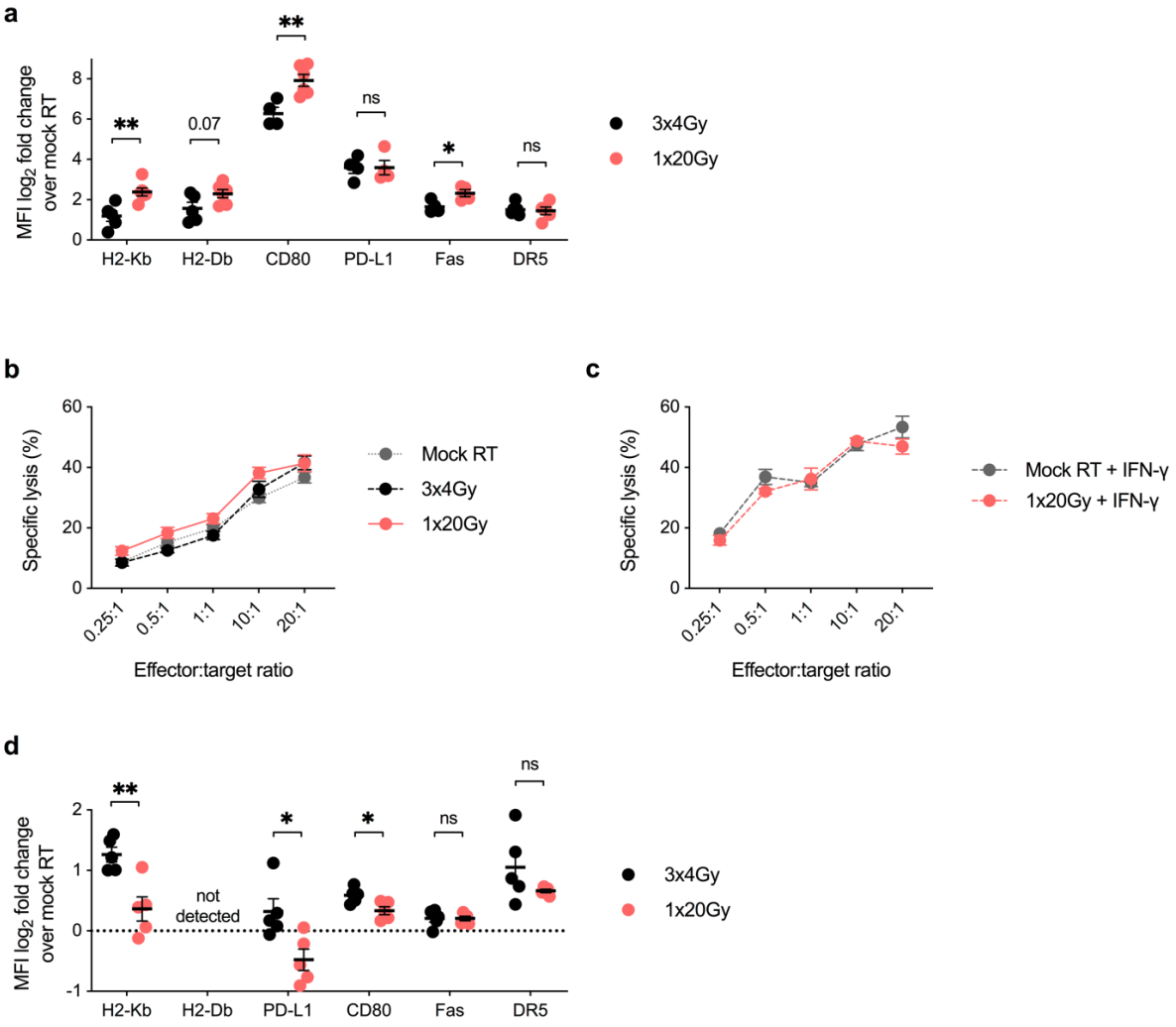

Figure 3.6. Tumour cell expression of immunomodulatory ligands and death receptors are increased by radiation *in vitro* but this does not translate to increased sensitivity to CD8$^+$ T cell killing. a, Flow cytometric analysis of radiation-induced changes to the expression of H2-Kb, H2-Db, CD80, PD-L1, Fas and DR5 on cultured AT3-OVA tumour cells at day 2 post completion of RT. Log fold change in MFI relative to mock-irradiated controls is presented. *n*=4 replicates per group, combined from 2 independent experiments. **b-c,** Specific killing of *in vitro* irradiated AT3-OVA cells by IL-2 activated OT-1 T cells, as determined using a ^{51}Cr release killing assay. At 48 hours post completion of RT, AT3-OVA cells were co-cultured with OT-1 T cells for 24 hours at the indicated effector:target ratios. In (**c**), IFN-γ (1ng/mL) was added to the AT3-OVA cell cultures 24 hours prior to irradiation. (**b**) *n*=11-15 replicates per group, combined from 3 independent experiments; (**c**) *n*=4 replicates per group, representative of 1 experiment. **d,** Flow cytometric analysis of radiation-induced changes to the expression of H2-Kb, H2-Db, CD80, PD-L1, Fas and DR5 gated on tumour cells (CD45$^-$GFP$^+$) in AT3-OVA tumours harvested from mice at day 2 post completion of RT. Log fold change in MFI relative to mock-irradiated controls (dotted line) is presented. *n*=4 tumours per group, combined from 2 independent experiments. All data is presented as mean ± SEM. *MFI: mean fluorescence intensity, ns: non-significant, * p<0.05, ** p<0.01*

5. Modulation of CD8+ T cell frequency and functional status by radiation dose-fractionation

Modulation of the tumour immune microenvironment by radiation DPF to account for differences in anti-tumour $CD8^+$ T cell activity was next investigated. Tumours were harvested and processed into single cell suspensions at days 1, 3, 5, 7, 9 and 13 post completion of RT and analysed by flow cytometry. Focus was directed towards analysis of the major αβ T cell subsets ($CD8^+$ and $CD4^+$ effector T cells, and Tregs). $CD8^+$ T cells comprised a major proportion (around 30%) of immune cells infiltrating the tumours at baseline (data not shown). Irradiation with either 1x20Gy or 3x4Gy regimens did not evoke a significant change in $CD8^+$ T cell numbers relative to that observed in mock-irradiated tumours (*Figure 3.7a*). However, significant increases in $CD4^+$ effector T cell ($CD4^+Foxp3^-$) and Treg ($CD4^+Foxp3^+$) numbers were observed in 3x4Gy and 1x20Gy-irradiated tumours relative to mock-irradiated tumours up to two weeks post RT (*Figure 3.7a*). Intriguingly, the timing of these changes synchronised to the completion, rather than commencement, of RT, noting that the 3x4Gy regimen was delivered over 3 days and the 1x20Gy regimen over 1 day. Although $CD4^+$ effector T cells were more enriched in 1x20Gy-irradiated tumours at day 1 post completion of RT compared to that observed in 3x4Gy-irradiated tumours, there were otherwise no differences in $CD4^+$ effector T cell numbers between the two irradiated groups (*Figure 3.7a*). The amplitude and kinetics of Treg accumulation in AT3-OVA tumours were however differentially modulated by radiation dose-fractionation. Tumour-associated Treg numbers peaked significantly higher and earlier following 1x20Gy irradiation compared to 3x4Gy irradiation (*Figure 3.7a*).

Despite little to no radiation-induced change in tumour-associated $CD8^+$ T cell numbers relative to mock irradiation, elevated levels of intracellular granzyme B within the $CD8^+$ T cell compartment were evident in 3x4Gy but not 1x20Gy-irradiated tumours (*Figure 3.7b*). In addition, there were higher proportions of programmed cell death protein 1-positive ($PD\text{-}1^+$) $CD8^+$ T cells in 3x4Gy-irradiated tumours compared to 1x20Gy-irradiated tumours, suggesting increased tumour-reactivity of $CD8^+$ T cells in response to the 3x4Gy regimen (*Figure 3.7c*). Interestingly, the frequency of tumour-associated OVA-tetramer staining ($OVAtet^+$) $CD8^+$ T cells were not different between mock, 3x4Gy, and 1x20Gy-irradiated tumours (*Figure 3.7d*). Almost all of these cells were $PD\text{-}1^+$, with no differences observed between groups (*Figure 3.7e*). A fluorescently labelled H2Kb-SIINFEKL antibody was trialled to track radiation-induced changes in tumour cell expression of OVA, but no staining was achieved (data not shown).

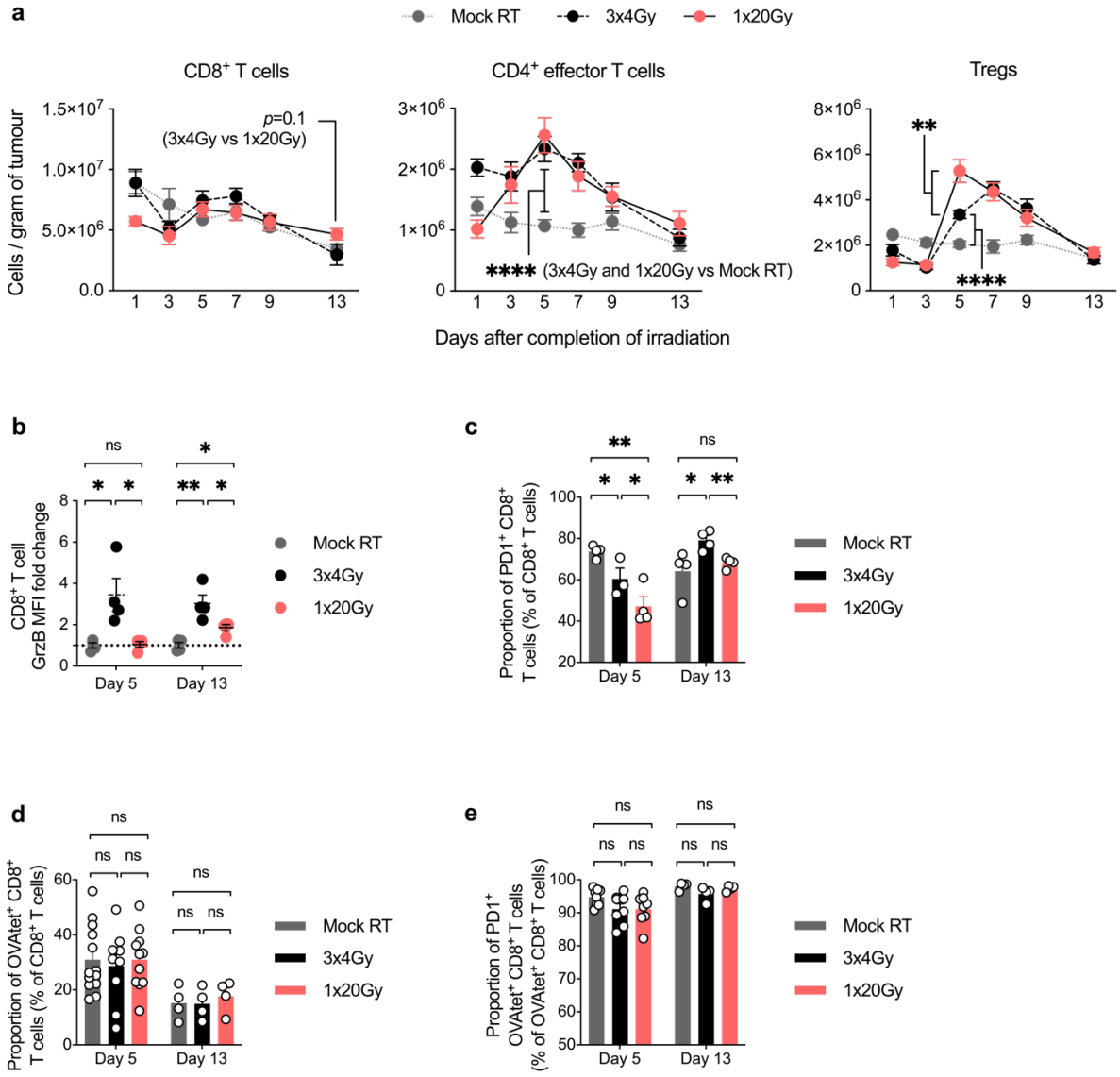

Figure 3.7. Differential modulation of T cells in AT3-OVA tumours by radiation dose-fractionation. AT3-OVA tumours were irradiated at 25-35mm^2 and harvested at time points that were aligned to post completion of RT for flow cytometric analysis. **a,** Absolute numbers of tumour-associated CD8$^+$ (CD45$^+$ TCRβ$^+$ CD8$^+$) CD4$^+$ effector T cells (CD45$^+$ TCRβ$^+$ CD4$^+$ Foxp3$^-$) and Tregs (CD45$^+$ TCRβ$^+$ CD4$^+$ Foxp3$^+$) over time post RT. *n*=4-17 tumours per group, combined from 4 independent experiments. Data presented as mean ± SEM. **b,** Granzyme B expression in CD8$^+$ T cells in tumours at days 5 and 13 post completion of RT, presented as fold change in MFI relative to mock-irradiated controls (dotted line). Data is representative of 2 independent experiments. **c,** Proportion of PD-1$^+$ CD8$^+$ T cells in tumours at days 5 and 13 post completion of RT. Data is representative of 2 independent experiments. **d,** Proportion of OVAtet$^+$ CD8$^+$ T cells in tumours at days 5 and 13 post completion of RT. Data is combined from 2 independent experiments. **e,** Proportion of PD-1$^+$ OVAtet$^+$ CD8$^+$ T cells in tumours at days 5 and 13 post completion of RT. Data is combined from 2 independent experiments. Data is presented as mean ± SEM. *MFI: mean fluorescence intensity, ns: non-significant, * p<0.05, ** p<0.01, *** p<0.005*

Similar analyses were performed on the inguinal lymph node isolated from the tumour-bearing mammary fat pad. The frequency of $CD8^+$ T cells and the proportion of $PD\text{-}1^+$ $CD8^+$ T cells trended higher in the irradiated groups compared to the lymph nodes isolated from the mock-irradiated group, but no differences between the dose-fractionation regimens were observed (*Figure 3.8a-b*). $OVAtet^+$ $CD8^+$ T cells in the lymph nodes formed a negligible proportion (around 1% of all $CD8^+$ T cells), and no differences in their numbers or PD-1 expression were observed either following RT or between dose-fractionation regimens (data not shown). Notably, analysis of the spleens out to two weeks post RT revealed no significant changes in frequency within any of the T cell subsets analysed (*Figure 3.8c*).

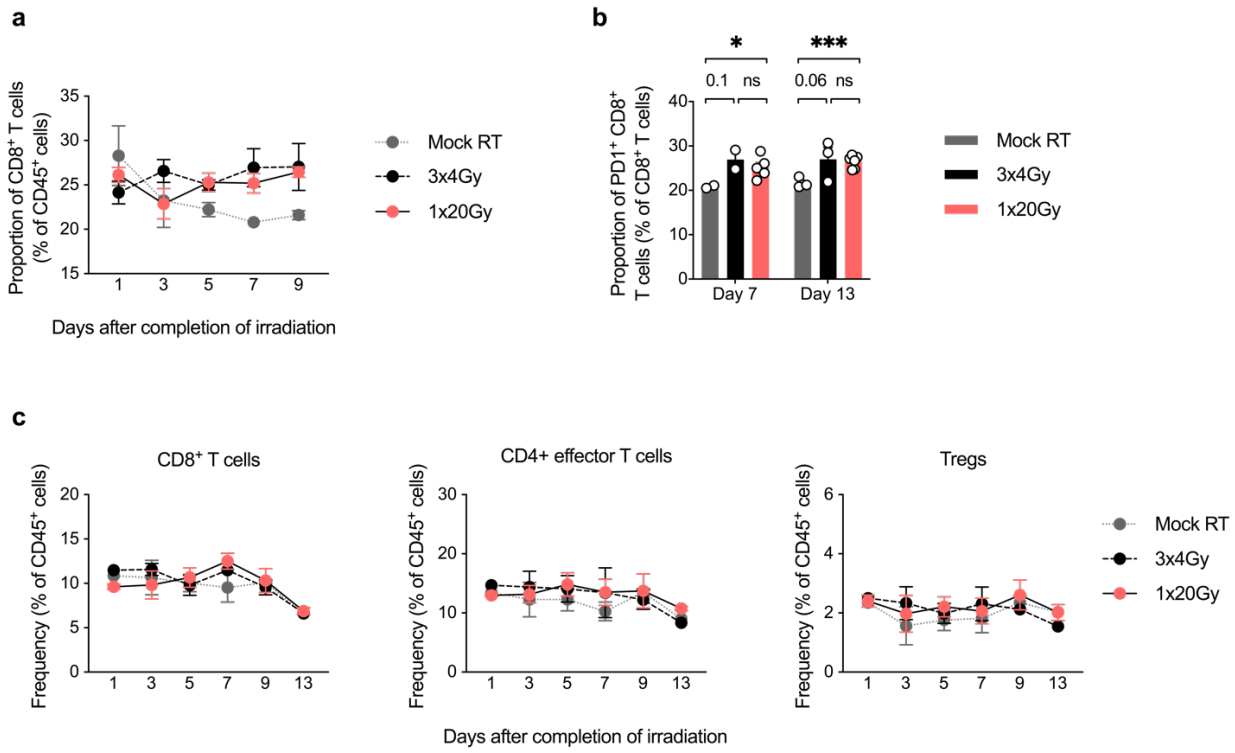

Figure 3.8. Differential modulation of T cells in lymph nodes and spleens by radiation dose-fractionation. Inguinal lymph nodes isolated from the tumour-bearing mammary fat pad of mice in *Figure 3.7a* as well as spleens from the same mice were harvested together with the tumours for flow cytometric analysis. **a,** Relative frequencies of $CD8^+$ T cells in the inguinal lymph nodes after tumour irradiation. *n*=2-4 samples per group, each sample represents lymph nodes pooled from 4-6 mice in each group. Data is combined from 2 independent experiments. **b,** Proportion of $PD\text{-}1^+$ $CD8^+$ T cells in inguinal lymph nodes at days 7 and 13 post completion of tumour irradiation. Each sample represents lymph nodes pooled from 4-6 mice. Data is combined from 2 independent experiments. **c,** Relative frequencies of $CD8^+$, $CD4^+$ effector T cells and Tregs in spleens of AT3-OVA tumour-bearing mice after tumour irradiation. Spleens were harvested at pre-determined time points after irradiation and processed for flow cytometry. *n*=2-3 samples per group, each sample represents spleens pooled from 4-6 mice in each group. Data is combined from 3 independent experiments. Data point is presented as mean ± SEM. *MFI: mean fluorescence intensity, ns: non-significant, * $p<0.05$, ** $p<0.01$, *** $p<0.005$*

6. The accumulation of Tregs in tumours is influenced by radiation dose-fractionation

In contrast to $CD8^+$ and $CD4^+$ effector T cells, only Tregs were differentially modulated in their tumour-associated numbers by radiation dose-fractionation, demonstrating a more rapid and more significant accumulation following 1x20Gy irradiation compared to 3x4Gy irradiation (*Figure 3.7a*). To determine if this difference was a function of the high DPF or high BED of the 1x20Gy regimen, tumour-associated Treg numbers were also quantified at days 1, 3 and 5 post irradiation with the 9x4Gy regimen, which had the same DPF as the 3x4Gy regimen but a similar BED to the 1x20Gy regimen. Remarkably, the kinetics and amplitude of the Treg response following completion of the 9x4Gy regimen were almost identical to that of the 3x4Gy regimen, suggesting that radiation-induced Treg responses were predominantly influenced by radiation DPF rather than BED (*Figure 3.9a*).

Compared to Tregs in mock-irradiated tumours, phenotypic analysis of Tregs in irradiated tumours revealed significantly elevated surface expression of cytotoxic T-lymphocyte-associated protein 4 (CTLA-4) and lymphocyte-activation gene 3 (LAG-3), but not T cell immunoreceptor with Ig and ITIM domains (TIGIT), raising the possibility that radiation may increase the regulatory function of tumour-associated Tregs (*Figure 3.9b*). However, no differences in the expression of these molecules were observed between the dose-fractionation regimens. To determine if Tregs were ontologically distinct between irradiated and mock-irradiated tumours, surface expression of neuropilin-1 (Nrp1) was examined, since natural Tregs (nTregs) have heightened expression of Nrp1 whereas on induced Tregs (iTregs) its expression is typically low (Weiss *et al.*, 2012; Yadav *et al.*, 2012). $Nrp1^+$ Tregs (nTregs) made up approximately 50-60% of all Tregs in mock-irradiated tumours, which increased to approximately 70% in 3x4Gy and 1x20Gy-irradiated tumours (*Figure 3.9c*). Differences in the proportion of $Nrp1^+$ Tregs between 3x4Gy and 1x20Gy-irradiated tumours were modest. Therefore, the observed accumulation of Tregs in AT3-OVA tumours post RT was more likely due to newly recruited and/or expanded nTregs rather than *in situ* conversion of $CD4^+$ effector T cells into iTregs.

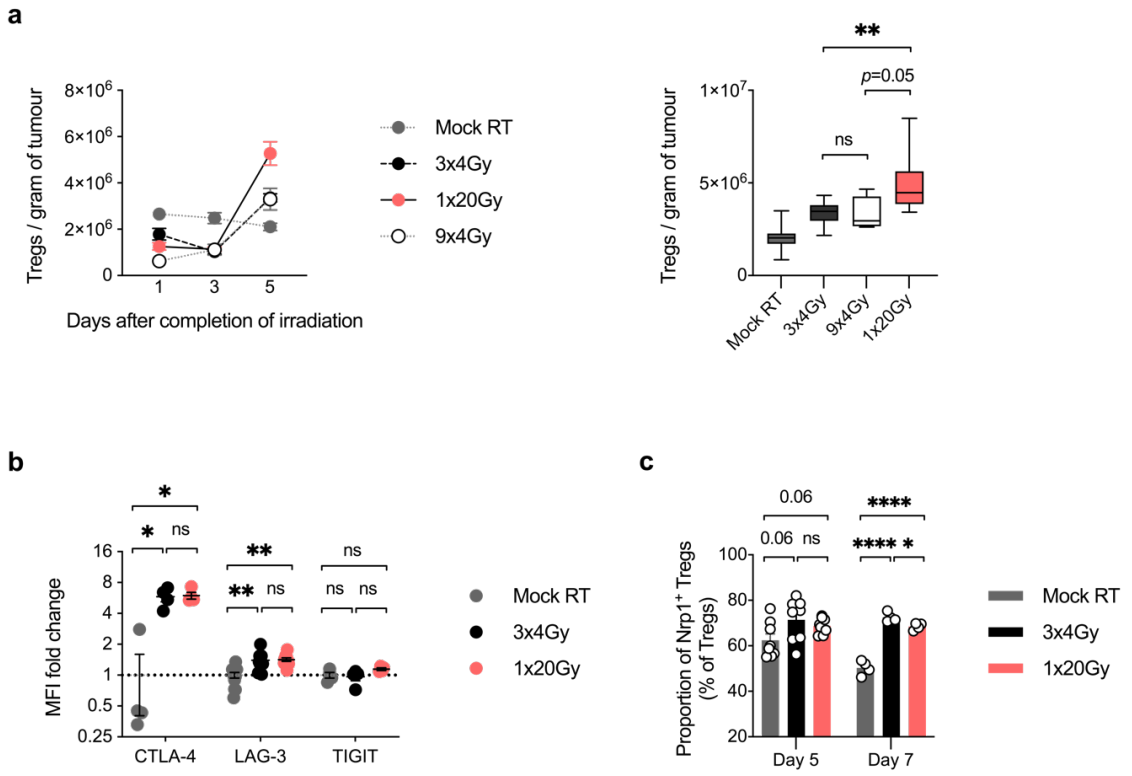

Figure 3.9. Radiation-induced Tregs are influenced by radiation DPF and express elevated levels of suppressive checkpoints. a, *Left*: Absolute numbers of Tregs in mock-irradiated and irradiated AT3-OVA tumours at days 1, 3 and 5 post completion of RT, as quantified by flow cytometry. *Right*: Box plot of Treg numbers in AT3-OVA tumours at day 5 after completion of RT. *n*=4-17 mice per group, combined from 4 independent experiments, which includes data presented in *Figure 3.7a*. **b,** Flow cytometric analysis of CTLA-4, LAG-3 and TIGIT expression on Tregs in mock-irradiated and irradiated AT3-OVA tumours, presented as fold change in MFI relative to mock-irradiated controls (dotted line). Data is representative of 2 independent experiments. **c,** Proportion of neuropilin-1^{+} (Nrp1^{+}) Tregs in mock-irradiated and irradiated tumours, as determined by flow cytometry. Data is combined from 2 independent experiments. Analysis of (**b**) and (**c**) were performed on tumours that were included in *Figure 3.7a. MFI: mean fluorescence intensity, ns: non-significant, * p<0.05, ** p<0.01, *** p<0.005, **** p<0.001*

7. Transcriptional changes in the post irradiation tumour immune microenvironment relating to T cell responses

To gain a more in-depth insight into the immunological effects of radiation dose-fractionation, bulk RNA sequencing (RNAseq) was performed on sorted $CD45^+$ and $CD45^-$ cells from AT3-OVA tumours irradiated with the 3x4Gy and 1x20Gy regimens. Mock-irradiated tumours from mice anaesthetised with ketamine/xylazine as per their irradiated counterparts were used as controls (3x0Gy and 1x0Gy, respectively). Because changes in tumour-associated immune cell frequencies aligned with the completion, rather than commencement, of RT, tumours were harvested at time points synchronised to the completion of the respective radiation regimens (*Figure 3.10a*).

At day 1, all groups were separated on the multi-dimensional scaling (MDS) plot, suggesting distinct immune transcriptional profiles in each group (*Figure 3.10b*). Interestingly, the mock-irradiated groups (3x0Gy and 1x0Gy) were also located apart from each other, which may indicate transcriptional changes induced by the additional ketamine/xylazine injections received in the 3x0Gy group over the 1x0Gy group. When compared directly to their respective mock-irradiated controls, the 3x4Gy group demonstrated enrichment of gene signatures for danger signals and innate immune responses, consistent with the capacity of the radiation regimen to prime T cell responses, whereas these signatures were not enriched in the 1x20Gy group (*Figure 3.10c-d*). Rather, there was an overwhelming amount of DNA damage repair and cell cycle signatures present in the 1x20Gy group at this time point, which likely masked the detection of any immune processes (*Figure 3.10d*). Some of these signatures were still present at day 5 (*Figure 3.11e*), reflecting greater overall genotoxic stress exerted by the higher BED of 1x20Gy.

At day 5, the immune transcriptional profiles of irradiated groups were distinct to those of mock-irradiated groups as demonstrated on the MDS plot, but the 3x4Gy and 1x20Gy groups overlapped with each other (*Figure 3.11a*). The mock-irradiated groups were also no longer separated, potentially suggesting a wash-out period from the effects of ketamine/xylazine. Consistent with their MDS clustering, the 3x4Gy and 1x20Gy groups shared a large proportion of common differentially expressed genes when compared to their respective mock-irradiated controls (*Figure 3.11b*). Although there were differentially expressed genes unique to each radiation regimen, these differences were not large enough to reach statistical significance on pair-wise comparison (no “difference of differences”). T cell response gene signatures, especially those pertaining to $CD4^+$ T cells, were the most commonly and strongly expressed signatures for both radiation regimens, corroborating the flow cytometry findings (*Figure 3.11c*).

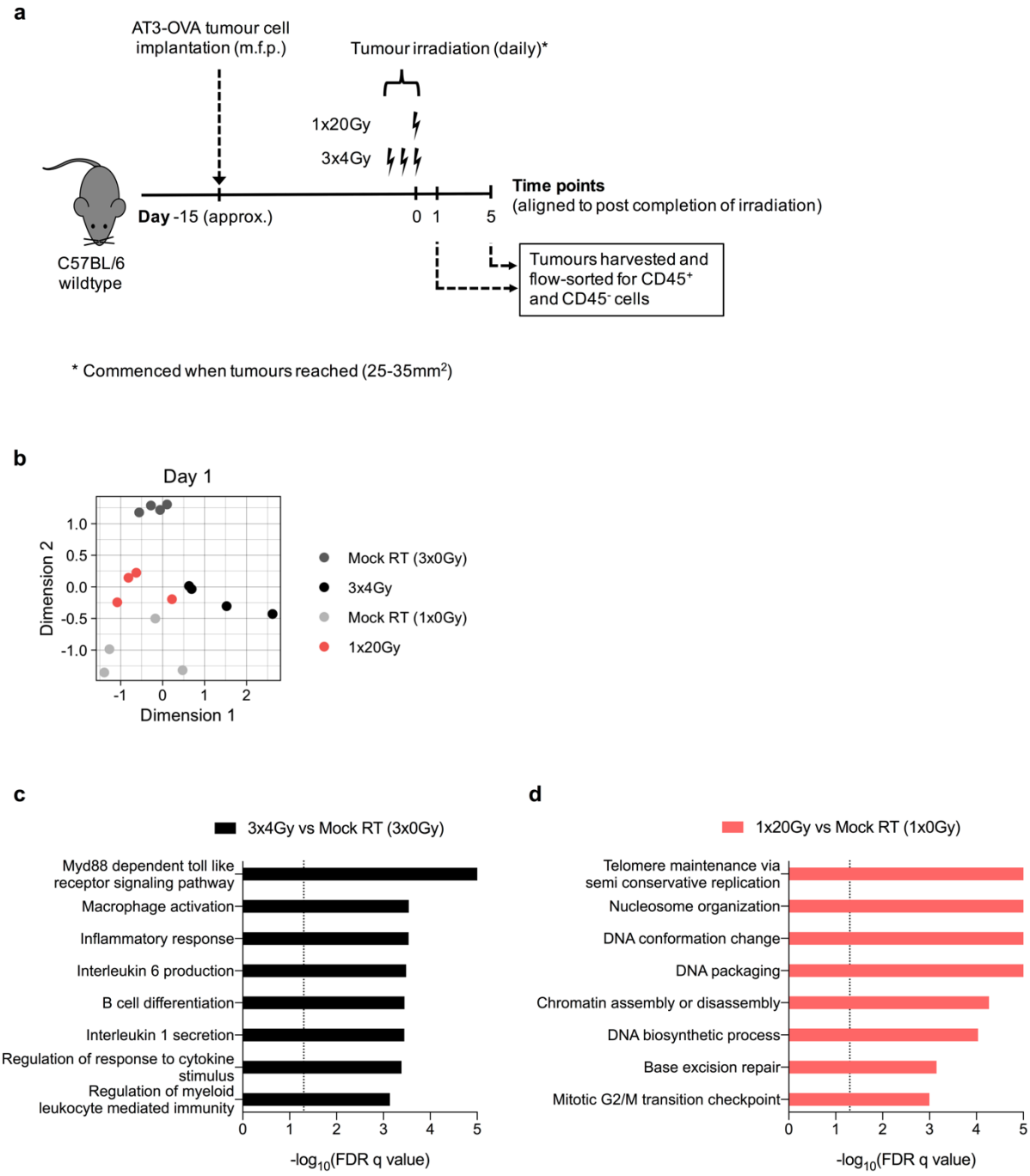

Figure 3.10. Gene signatures for danger signals and innate immune responses are enriched by the 3x4Gy regimen but not the 1x20Gy at day 1 post completion of RT. a, Experimental schema for RNAseq experiments. AT3-OVA tumours were irradiated (3x4Gy and 1x20Gy) at 25-35mm^2 and harvested at time points that were aligned to post completion of RT. Mock-irradiated tumours from mice anaesthetised as per their irradiated counterparts (3x0Gy and 1x0Gy) were used as controls. CD45$^+$ cells were flow-sorted from single cell AT3-OVA tumour suspensions and processed for RNAseq analysis. *n*=4-6 tumours per group. **b,** Multi-dimensional scaling (MDS) plot of mock-irradiated (3x0Gy, 1x0Gy) and irradiated (3x4Gy,

1x20Gy) RNAseq samples at day 1 post completion of RT. **c-d,** Gene Ontology-Biological Processes (GO-BP) terms enriched in the immune compartment of (**c**) 3x4Gy and (**d**) 1x20Gy-irradiated AT3-OVA tumours at day 1 RT, compared to their respective mock-irradiated controls. Analysis was performed using Gene Set Enrichment Analysis (GSEA). Dotted line delineates FDR *q* value of 0.05. *FDR: false discovery rate.*

To tease out distinctions in the distribution of gene signatures between the two radiation regimens, gene signatures with the largest discrepancy in enrichment between the 3x4Gy and 1x20Gy groups were examined. This revealed that signatures pertaining to myeloid cell processes were predominantly associated with the 3x4Gy group rather than the 1x20Gy group (*Figure 3.11d*). Significantly, such signatures included the activation of the STING axis by cytosolic dsDNA (as represented by the regulation of defence response to virus and IFN-β production signatures), which is a well-described mechanism by which radiation activates myeloid cells, including DCs (Deng *et al.*, 2014b; Vanpouille-Box *et al.*, 2017).

Conversely, gene signatures selectively associated with 1x20Gy irradiation opposed Th1 immune responses, including the negative regulation of IL-12 and production of TGF-β (*Figure 3.11e*). As the 1x20Gy regimen evoked more pronounced Treg responses on flow cytometric analysis than the 3x4Gy regimen (*Figure 3.7a*), a set of core genes associated with Tregs (Zemmour *et al.*, 2018) as well as genes for suppressive ligands known to be expressed by Tregs were also examined. There was a trend for increased expression of these genes in the 1x20Gy group compared to the 3x4Gy group when compared to their respective controls, including *Ctla4*, *Foxp3*, *Tnfrsf18* (encoding for glucocorticoid-induced TNFR-related protein, GITR), and *Il10* (*Figure 3.11f*). Interestingly, *Lag3* gene transcripts were found to be reduced in the irradiated groups, which contrasted with what was observed for this checkpoint protein when tumour-associated Tregs were analysed *ex vivo* by flow cytometry (*Figure 3.9b*). This difference between the two assays was likely linked to the RNAseq analysis being run on bulk tumour-associated $CD45^+$ cells, thus masking any selective regulation of LAG-3 expression in Tregs.

Collectively, these data demonstrated that although the immune transcriptional profiles of both 3x4Gy and 1x20Gy-irradiated tumours were enriched for T cell gene signatures at day 5 post completion of RT, myeloid cell signatures were enriched only with the 3x4Gy regimen, while immunosuppressive signatures were more prominent with the 1x20Gy regimen.

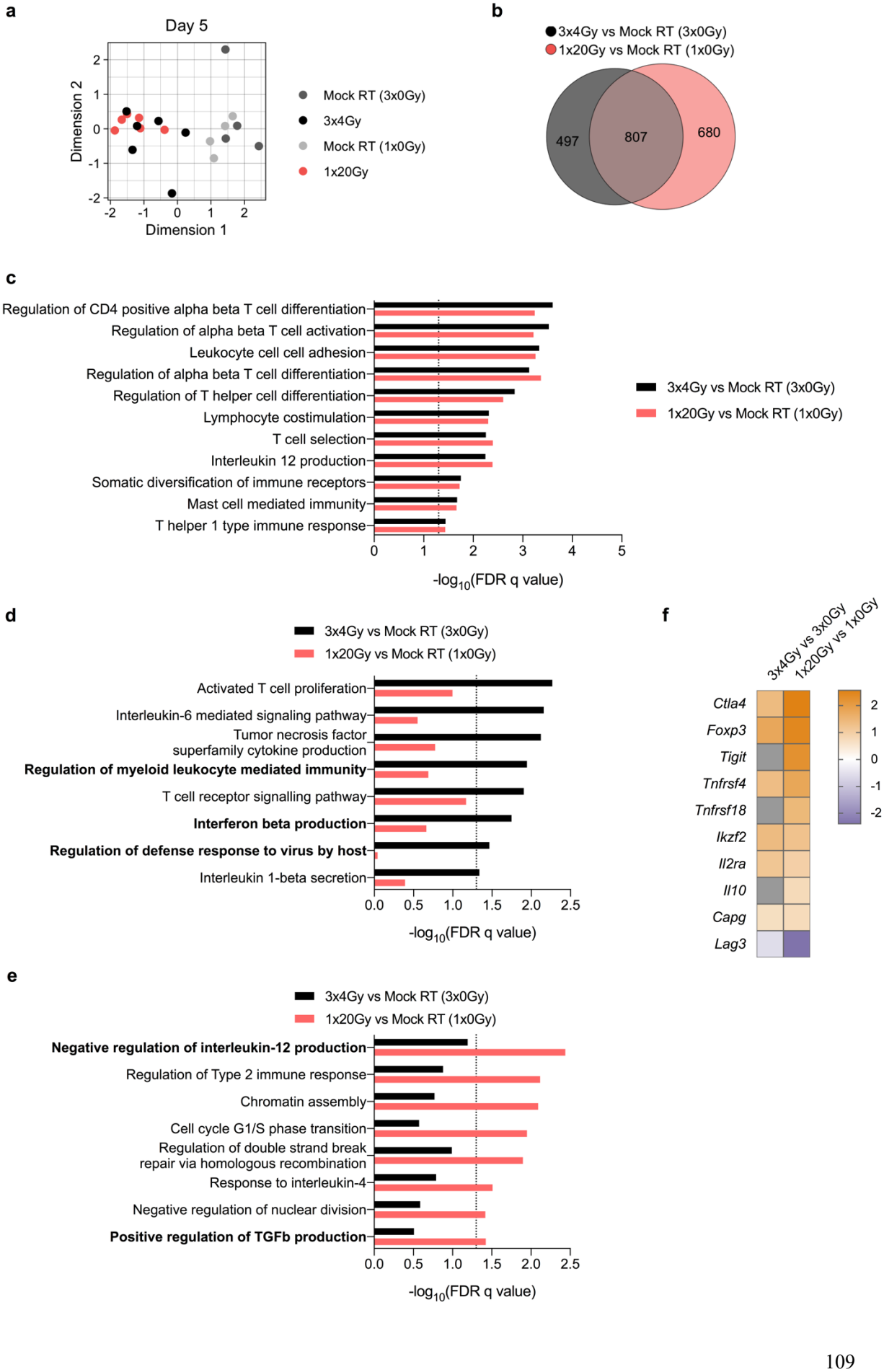
a
Day 5
Dimension 2
Dimension 1
Mock RT (3x0Gy)
3x4Gy
Mock RT (1x0Gy)
1x20Gy
b
3x4Gy vs Mock RT (3x0Gy)
1x20Gy vs Mock RT (1x0Gy)
497
807
680
c
Regulation of CD4 positive alpha beta T cell differentiation
Regulation of alpha beta T cell activation
Leukocyte cell cell adhesion
Regulation of alpha beta T cell differentiation
Regulation of T helper cell differentiation
Lymphocyte costimulation
T cell selection
Interleukin 12 production
Somatic diversification of immune receptors
Mast cell mediated immunity
T helper 1 type immune response
-log10(FDR q value)
3x4Gy vs Mock RT (3x0Gy)
1x20Gy vs Mock RT (1x0Gy)
d
3x4Gy vs Mock RT (3x0Gy)
1x20Gy vs Mock RT (1x0Gy)
Activated T cell proliferation
Interleukin-6 mediated signaling pathway
Tumor necrosis factor superfamily cytokine production
Regulation of myeloid leukocyte mediated immunity
T cell receptor signalling pathway
Interferon beta production
Regulation of defense response to virus by host
Interleukin 1-beta secretion
-log10(FDR q value)
e
3x4Gy vs Mock RT (3x0Gy)
1x20Gy vs Mock RT (1x0Gy)
Negative regulation of interleukin-12 production
Regulation of Type 2 immune response
Chromatin assembly
Cell cycle G1/S phase transition
Regulation of double strand break repair via homologous recombination
Response to interleukin-4
Negative regulation of nuclear division
Positive regulation of TGFb production
-log10(FDR q value)
f
3x4Gy vs 3x0Gy
1x20Gy vs 1x0Gy
Ctla4
Foxp3
Tigit
Tnfrsf4
Tnfrsf18
Ikzf2
Il2ra
Il10
Capg
Lag3

Figure 3.11. Gene signatures for myeloid cell and immunosuppressive processes are differentially enriched by the 3x4Gy and 1x20Gy regimens at day 5 post RT. a, MDS plot of mock-irradiated (3x0Gy and 1x0Gy) and irradiated (3x4Gy and 1x20Gy) RNAseq samples at day 5 post completion of RT. **b,** Euler diagram showing the number of common and unique differentially expressed genes between the immune compartment of 3x4Gy and 1x20Gy-irradiated AT3-OVA tumours at day 5 post RT, compared to their respective mock-irradiated controls. **c-e,** GO-BP terms enriched in the immune compartment of 3x4Gy and 1x20Gy-irradiated AT3-OVA tumours at day 5 post RT, compared to their respective mock-irradiated controls, as analysed by GSEA. Dotted line delineates a FDR *q* value of 0.05. **c,** Terms most commonly enriched by both 3x4Gy and 1x20Gy regimens. **d,** Terms most selectively enriched by the 3x4Gy regimen over the 1x20Gy regimen. Bold terms indicate gene signatures relating to myeloid cell processes. **e,** Terms most selectively enriched by the 1x20Gy regimen over the 3x4Gy regimen. Bold terms indicate gene signatures relating to negative regulation of immune responses. **f,** Differential expression of Treg core genes and genes of Treg-associated suppressive ligands in the immune compartment of 3x4Gy and 1x20Gy-irradiated AT3-OVA tumours at day 5 post RT, compared to their respective mock-irradiated controls. Log_2-fold change in expression with adjusted $p<0.1$ is expressed. Grey squares represent non-significant modulation in expression ($p>0.1$). *FDR: false discovery rate.*

8. Depletion of Tregs significantly enhances radiation tumour control

It is possible that the Treg responses evoked by 1x20Gy irradiation were suppressing $CD8^+$ T cell responses (*Figure 3.12a*). To examine the *in vivo* suppressive activity of radiation-induced Tregs on concurrent anti-tumour immune responses, DEREG transgenic mice, which can be selectively depleted of $Foxp3^+$ Tregs with administration of diphtheria toxin (DT), were used for investigation (Lahl and Sparwasser, 2011). DEREG mice bearing established AT3-OVA tumours were injected with a single dose of DT at day 3 post completion of 3x4Gy and 1x20Gy irradiation, just prior to the expected rise in tumour-associated Tregs, to achieve 95-98% clearance of Tregs for up to 7 days (Christiaansen *et al.*, 2014). Although a single dose of DT without RT only transiently slowed tumour growth, it was sufficient to profoundly enhance the long-term tumour control when given with both 1x20Gy and 3x4Gy irradiation (*Figure 3.12b*). Tumour control with the low BED 3x4Gy regimen coupled with Treg depletion exceeded that of the high BED 1x20Gy regimen as single modality, and the high BED 1x20Gy regimen coupled with Treg depletion cured 3 of 5 mice, in which no tumours were palpable out to day 90 after initiating RT.

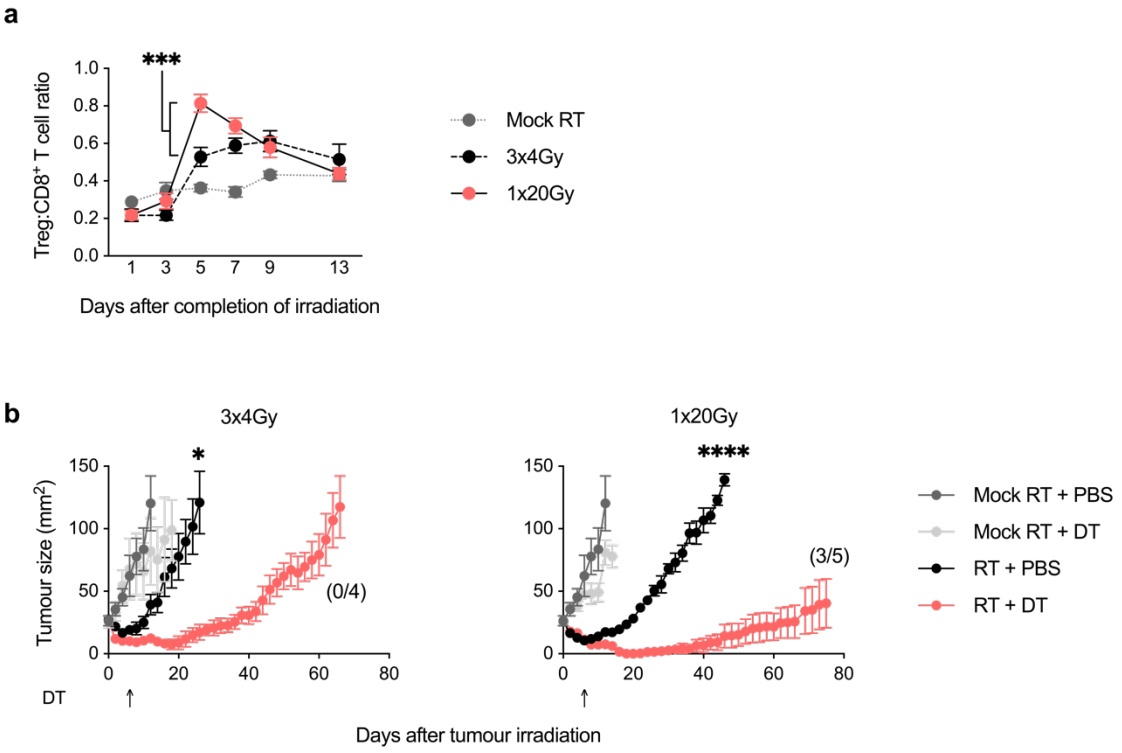

Figure 3.12. Short-term, rationally-timed depletion of Tregs in DEREG mice significantly improves tumour control by RT. a, Changes in tumour-associated Treg:CD8$^+$ T cell ratios in mock, 3x4Gy, and 1x20Gy-irradiated AT3-OVA tumours. Data is derived from experiments presented in *Figure 3.7a*. **b,** AT3-OVA tumour growth post RT in DEREG mice treated with diphtheria toxin (DT) or phosphate-buffered saline (PBS). The experimental set up was similar to that of wildtype mice described in *Figure 3.1c*. A single injection of DT (0.5µg/mouse) or PBS (200 µL) was administered at day 3 post completion of RT. Numbers in parentheses indicate the fraction of tumour-free mice at day 90 from the start of RT. Arrow indicates the time of DT treatment. Statistical comparisons were made between the RT + DT and RT + PBS groups. *n*=4-5 mice per group, representative of 2 independent experiments. Data is presented as mean ± SEM. * $p<0.05$, *** $p<0.001$, **** $p<0.0001$

To determine if this observation could be replicated in a wildtype setting, wildtype mice bearing established AT3-OVA tumours were treated with an anti-CTLA-4 antibody (9H10 clone, Syrian Hamster IgG isotype, Bio X Cell) that has been reported to induce Treg depletion through antibody-dependent cellular cytotoxicity (ADCC) (Simpson *et al.*, 2013). Treatment with the 9H10 anti-CTLA-4 antibody initiated at the start of RT prevented the accumulation of Tregs in irradiated AT3-OVA tumours (*Figure 3.13a*). Interestingly, Treg numbers in mock-irradiated tumours and in spleens of irradiated and mock-irradiated mice were not affected by this treatment (*Figure 3.13a-b*). The selective depletion of Tregs in irradiated tumours may reflect their higher surface expression of CTLA-4 compared to Tregs in mock-irradiated tumours (*Figure 3.9b*). $CD8^+$ and $CD4^+$ effector T cell numbers were also not impacted by 9H10 anti-CTLA-4 antibody treatment (*Figure 3.13a*). Strikingly, short-term 9H10 anti-CTLA-4 antibody treatment when given alone (a total of 4 doses, every 4 days) demonstrated no activity against AT3-OVA tumours, but when used in conjunction with 3x4Gy and 1x20Gy irradiation achieved long-term tumour control, phenocopying what was observed in DT-treated DEREG mice (*Figure 3.13c*). A similarly profound combinatorial effect was seen with 9x4Gy irradiation (*Figure 3.13c*), suggesting that therapeutic synergy was achieved irrespective of the radiation dose-fractionation employed. Notably, 5 of 6 mice co-treated with 9H10 anti-CTLA-4 antibodies and 9x4Gy and 1x20Gy irradiation were cleared of their tumours (*Fig 3.13c*). A single dose of 9H10 anti-CTLA-4 antibody treatment given at day 3 post 1x20Gy irradiation also resulted in better tumour control compared to RT alone, but no tumours were cured (*Figure 3.13d*). The reduced potency of a single dose of 9H10 anti-CTLA-4 antibody to deplete Tregs, compared to a single dose DT in DEREG mice, was most likely due to restricted clearance of tumour-associated Tregs post RT in contrast to bulk Treg depletion, respectively. Importantly, these data demonstrate that short-term depletion of tumour-associated Tregs can be achieved with clinically relevant antibodies, leading to significantly improved outcomes with RT.

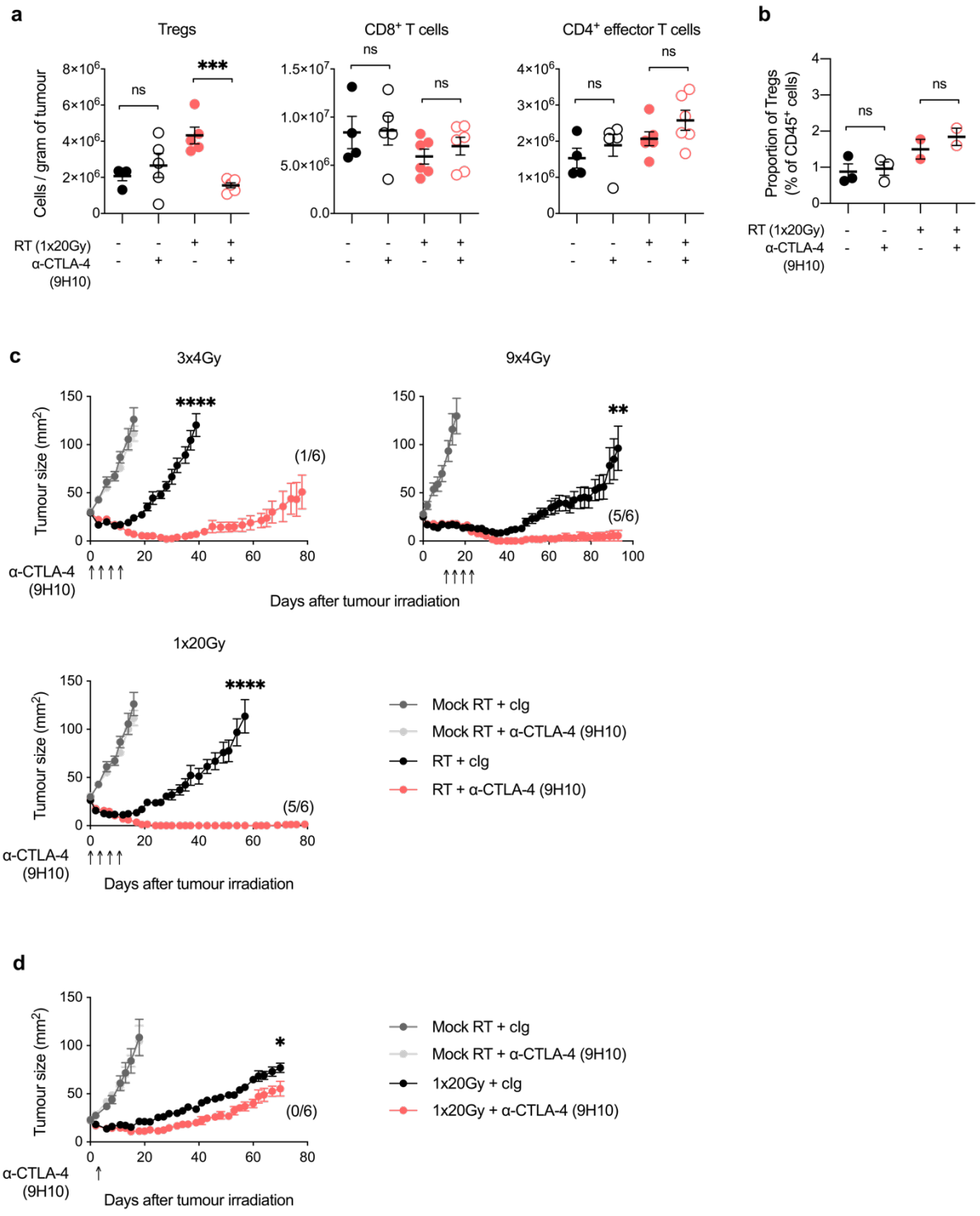

Figure 3.13. Treatment with 9H10 anti-CTLA-4 antibodies in wildtype mice selectively targets tumour-associated Tregs and improves tumour control by RT. a-b, AT3-OVA tumours in wildtype mice were irradiated with the 1x20Gy regimen at 25-35mm^2 and harvested at day 5 post completion of RT. Spleens from the same mice were also harvested. Mice were treated with 9H10 anti-CTLA4 or isotype

control antibodies (150μg/mouse for the first injection, 100μg/mouse thereafter), administered every 4 days from start of RT. Data is combined from 2 experiments. **a,** Absolute numbers of tumour-associated Tregs, $CD8^+$ and $CD4^+$ effector T cells. **b,** Relative frequency of splenic Tregs. Each sample in (**b**) was pooled from 2-4 mouse spleens. **c,** AT3-OVA tumour growth after RT in wildtype mice treated with 9H10 anti-CTLA4 or isotype control antibodies, administered every 4 days either from start of RT (3x4Gy and 1x20Gy) or from day 10 post completion of RT (9x4Gy), for a total of 4 injections. The experimental set up was similar to that described in *Figure 3.1c.* Numbers in parentheses indicate the fraction of tumour-free mice at day 90 from the start of RT. Arrows indicate the time of antibody treatment. Statistical comparisons were made between the RT + anti-CTLA-4 and RT + cIg groups. *n*=5-6 mice per group, representative of 3 independent experiments. **d,** AT3-OVA tumour growth post 1x20Gy irradiation in WT mice treated with 9H10 anti-CTLA4 or isotype control antibodies, administered once at day 3 post RT. Numbers in parentheses indicate the fraction of tumour-free mice at day 90 from the start of RT. Arrow indicates the time of antibody treatment. Statistical comparison was made between the 1x20Gy + anti-CTLA-4 and 1x20Gy + cIg groups. *n*=5-6 mice per group, representative of 1 experiment. Data presented as mean ± SEM. *ns: non-significant, * $p<0.05$, *** $p<0.001$, **** $p<0.0001$*

To further interrogate the combinatorial effect of RT and Treg depletion, a second anti-CTLA-4 antibody (9D9 clone, mouse IgG2a isotype, kindly provided by Bristol Myers Squibb (BMS)) was tested. Treatment with this antibody demonstrated significant activity against AT3-OVA tumours even when given alone, and when given with 1x20Gy irradiation resulted in tumour cures and long-term survival (*Figure 3.14a*). Unlike the 9H10 anti-CTLA-4 antibody, the 9D9 anti-CTLA-4 antibody depleted baseline Tregs even in mock-irradiated tumours, which potentially underpinned its strong single agent activity (*Figure 3.14b*). Tumour-associated $CD8^+$ and $CD4^+$ effector T cells and peripheral Tregs were also not affected by the 9D9 anti-CTLA-4 antibody, highlighting the specificity of the antibody for tumour-associated Tregs (*Figure 3.14b-c*). To confirm that the effects of 9D9 anti-CTLA-4 antibody treatment were critically due to Treg depletion and not a product of CTLA-4 checkpoint blockade, a version of the antibody engineered with a non-Fcγ receptor-binding D265A mutation (9D9 clone, IgG1 D265A, BMS), which was incapable of triggering ADCC, was used. As expected, the 9D9 D265A anti-CTLA-4 antibody had no depleting effect on tumour-associated and peripheral Tregs (*Figure 3.14b-c*). Indeed, treatment with this antibody demonstrated no single agent activity against AT3-OVA tumours and could only enhance the anti-tumour activity of the 3x4Gy regimen in a $CD8^+$ T cell dependent manner, but not that of the 1x20Gy regimen (*Figure 3.14d-e*). Thus, depletion of Tregs significantly improved tumour control following both 3x4Gy and 1x20Gy regimens.

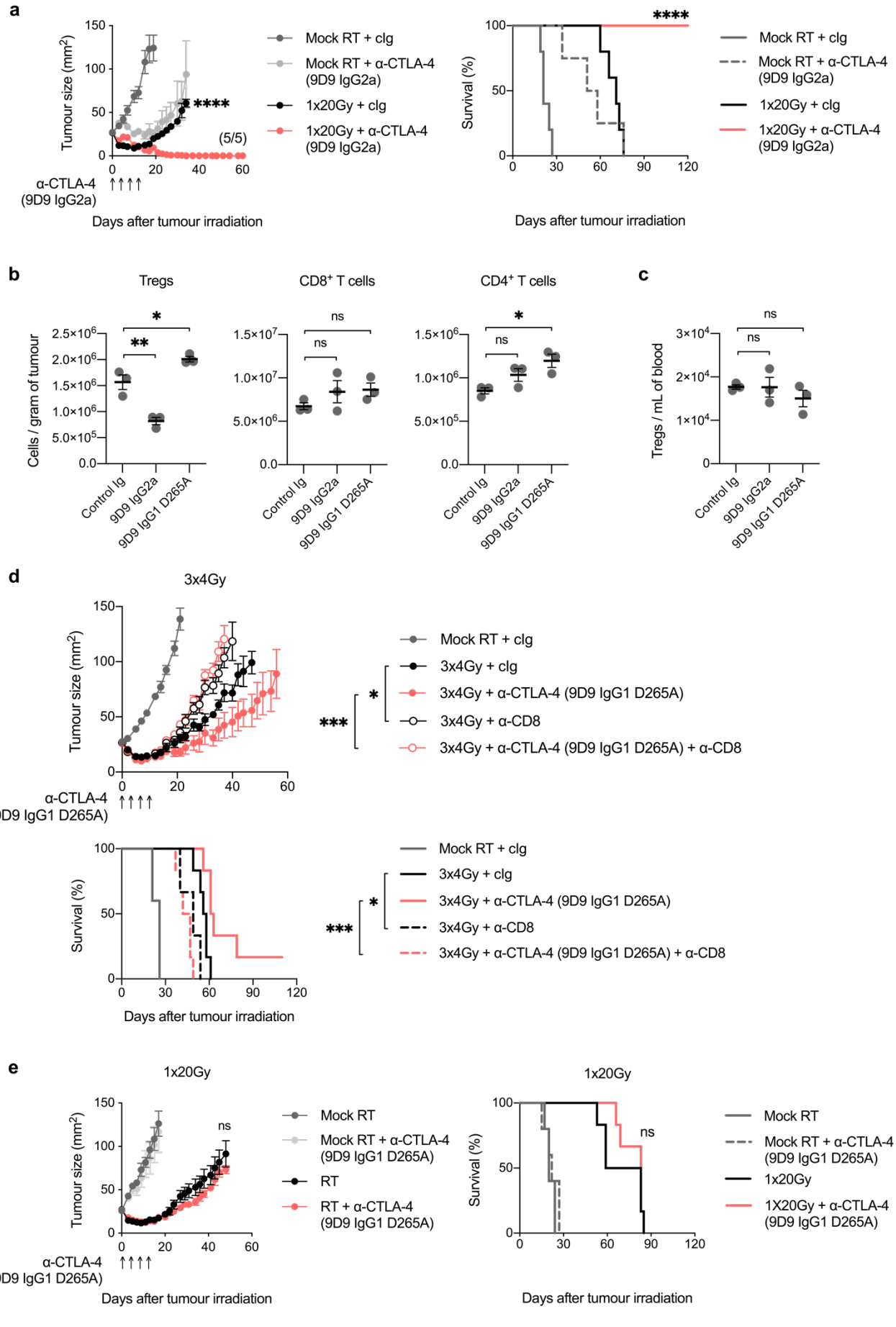
a
Tumour size (mm²)
****
(5/5)
α-CTLA-4
(9D9 IgG2a)
Days after tumour irradiation
Mock RT + clg
Mock RT + α-CTLA-4 (9D9 IgG2a)
1x20Gy + clg
1x20Gy + α-CTLA-4 (9D9 IgG2a)
Survival (%)
****
Days after tumour irradiation
b
Tregs
CD8⁺ T cells
CD4⁺ T cells
Cells / gram of tumour
Control Ig
9D9 IgG2a
9D9 IgG1 D265A
c
Tregs / mL of blood
d
3x4Gy
Tumour size (mm²)
α-CTLA-4
(9D9 IgG1 D265A)
Mock RT + clg
3x4Gy + clg
3x4Gy + α-CTLA-4 (9D9 IgG1 D265A)
3x4Gy + α-CD8
3x4Gy + α-CTLA-4 (9D9 IgG1 D265A) + α-CD8
Survival (%)
Days after tumour irradiation
e
1x20Gy
Tumour size (mm²)
α-CTLA-4
(9D9 IgG1 D265A)
Mock RT
Mock RT + α-CTLA-4 (9D9 IgG1 D265A)
RT
RT + α-CTLA-4 (9D9 IgG1 D265A)
Survival (%)
1x20Gy
1X20Gy + α-CTLA-4 (9D9 IgG1 D265A)

Figure 3.14. Combinatorial effects of 1x20Gy irradiation and anti-CTLA-4 antibodies depend on Treg depletion. a, AT3-OVA tumour growth and mouse survival post RT in mice treated with 9D9 anti-CTLA4 or isotype control antibodies (150μg/mouse for the first injection, 100μg/mouse thereafter), administered every 4 days from start of RT, for a total of 4 injections. The experimental set up was similar to that described in *Figure 3.1c.* Numbers in parentheses indicate the fraction of tumour-free mice at day 120 from the start of RT. Arrows indicate the time of antibody treatment. Statistical comparisons were made between the 1x20Gy + 9D9 anti-CTLA-4 and 1x20Gy + cIg groups. *n*=5-6 mice per group, representative of 2 independent experiments. **b-c,** Absolute numbers of Tregs, $CD8^+$ and $CD4^+$ T cells in **(b)** non-irradiated AT3-OVA tumours and **(c)** peripheral blood of mice, 24 hours after a single treatment of depleting (9D9), non-depleting (9D9 D265A) anti-CTLA-4 or isotype control (for 9D9) antibodies. Data is representative of 1 experiment. **d-e,** AT3-OVA tumour growth and mouse survival post RT in mice treated with and without 9D9 D265A anti-CTLA-4 antibodies, (**e**) in conjunction with $CD8^+$ T cell depleting or control isotype antibodies. 9D9 D265A anti-CTLA4 antibodies (150μg/mouse for the first injection, 100μg/mouse thereafter) were administered every 4 days from start of RT, for a total of 4 injections. $CD8^+$ T cell depleting or control isotype antibodies were administered every 3 days from start of RT to end of experiment. In (**e**), statistical comparisons were made between the RT + 9D9 D265A anti-CTLA-4 and RT groups. Arrows indicate the time of anti-CTLA-4 antibody treatment. *n*=5-6 mice per group, representative of 1 experiment. *ns: non-significant, * $p<0.05$, *** $p<0.001$, **** $p<0.0001$*

9. Radiation-induced Tregs restrict tumour-associated cDC1s maturation and CD8+ T cell responses

To confirm that radiation-induced Tregs were suppressing $CD8^+$ T cell responses, $CD8^+$ T cells were concurrently depleted with RT and 9H10 anti-CTLA-4 antibody treatment. The therapeutic benefit of 9H10 anti-CTLA-4 antibody treatment was entirely lost with depletion of $CD8^+$ T cells following both 3x4Gy and 1x20Gy irradiation (*Figure 3.15a*), indicating that the anti-tumour activity of $CD8^+$ T cells was significantly potentiated in the absence of radiation-induced Tregs irrespective of the dose-fractionation employed. In line with this, flow cytometric analysis revealed elevated granzyme B levels in tumour-associated $CD8^+$ T cells at day 5 post RT when given with 9H10 antibody treatment, compared to RT alone (*Figure 3.15b*). Notably, no modulation of granzyme B levels was observed when 9H10 antibody treatment was administered without RT, highlighting the essential role of radiation in reinvigorating anti-tumour $CD8^+$ T cell responses.

Because radiation-induced $CD8^+$ T cell responses were dependent on cDC1s, the impact of radiation-induced Treg responses on cDC1 maturation and activity was next examined. Flow cytometric analysis of the AT3-OVA tumours at day 5 post co-treatment with RT and 9H10 antibodies found that while the number of tumour-associated cDC1s (as defined as $CD45^+$ $lineage^-$ $MHCII^+$ $CD11c^+$ $F4/80^-$ $CD11b^-$ $CD103^+$) did not increase in response to Treg depletion (*Figure 3.16a-b*), expression of the co-stimulatory ligand CD86 on cDC1s was significantly elevated (*Figure 3.16c*), suggesting that Tregs were restricting the maturation and/or activity of cDC1s within irradiated tumours. This was most striking in 1x20Gy-irradiated tumours, in which RT alone caused a significant loss of CD86 expression on cDC1s that could be prevented by Treg depletion (*Figure 3.16c*). Notably, the levels of CD86 expression on cDC1s across the 3x4Gy and 1x20Gy groups were inverse to the abundance of Tregs in those groups (*Figure 3.16c-d*). Indeed, Treg:cDC1 ratios in individual tumours across all groups that received RT demonstrated a strong negative correlation with the induction of CD86 expression on cDC1s (*Figure 3.16e*). Interestingly, the MHC-II expression status of tumour-associated cDC1s did not change in response to any of the treatment conditions (*Figure 3.16f*). As an extension to this work, cDC1s in the inguinal lymph nodes isolated from the tumour-bearing mammary fat pat were analysed. No significant change in CD86 expression was detected in response to RT, suggesting that the suppression of DC maturation and/or activity was exclusively mediated by radiation-induced Tregs within tumours (*Figure 3.16g)*.

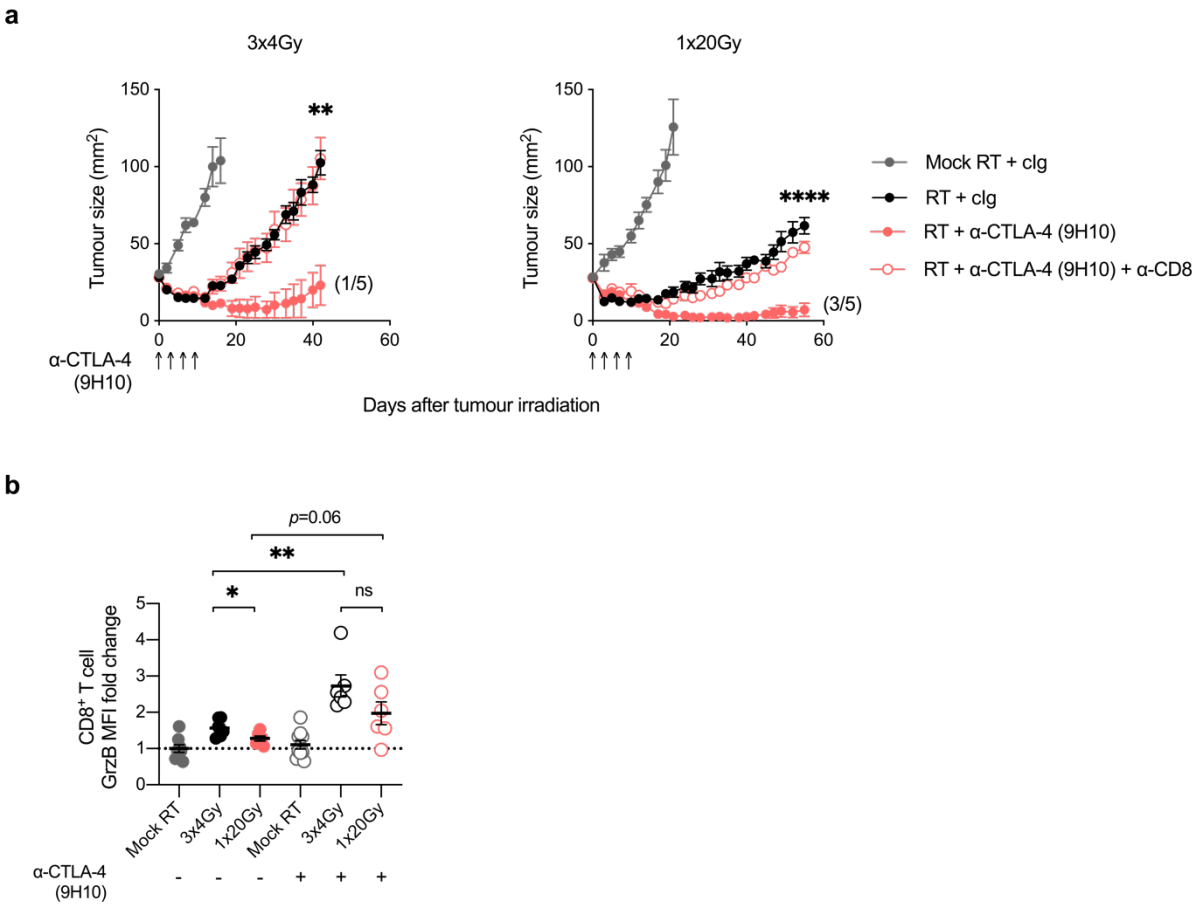

Figure 3.15. Depletion of radiation-induced Tregs rescues the ability of RT to evoke anti-tumour CD8+ T cell responses. a, AT3-OVA tumour growth post RT in mice treated with 9H10 anti-CTLA-4 and $CD8^+$ T cell depleting antibodies, or with their respective isotype control antibodies. 9H10 anti-CTLA-4 or isotype control antibodies were administered every 4 days from start of irradiation, for a total of 4 total injections. $CD8^+$ T cell depleting or control isotype antibodies were administered every 3 days from start of RT to end of experiment. Arrows indicate the time of 9H10 anti-CTLA-4 antibody treatment. Statistical comparisons were made between the RT + anti-CTLA-4 + anti-CD8 and RT + anti-CTLA-4 + cIg groups. Numbers in parentheses indicate fraction of tumour-free mice at day 90 from start of RT. *n*=5 per group, representative of 2 independent experiments. Data is presented as mean ± SEM. **b,** Flow cytometric analysis of granzyme B expression in $CD8^+$ T cells in mock or 1x20Gy-irradiated AT3-OVA tumours at day 5 post RT, harvested from mice treated with 9H10 anti-CTLA4 or isotype control antibodies. Fold change in MFI relative to mock-irradiated controls (dotted line) is presented. 9H10 anti-CTLA-4 antibodies were administered every 4 days from start of RT for a total of 2 injections. Data is representative of 1 experiment. *MFI: mean fluorescence intensity, ns: non-significant, * p<0.05, ** p<0.01, **** p<0.0001*

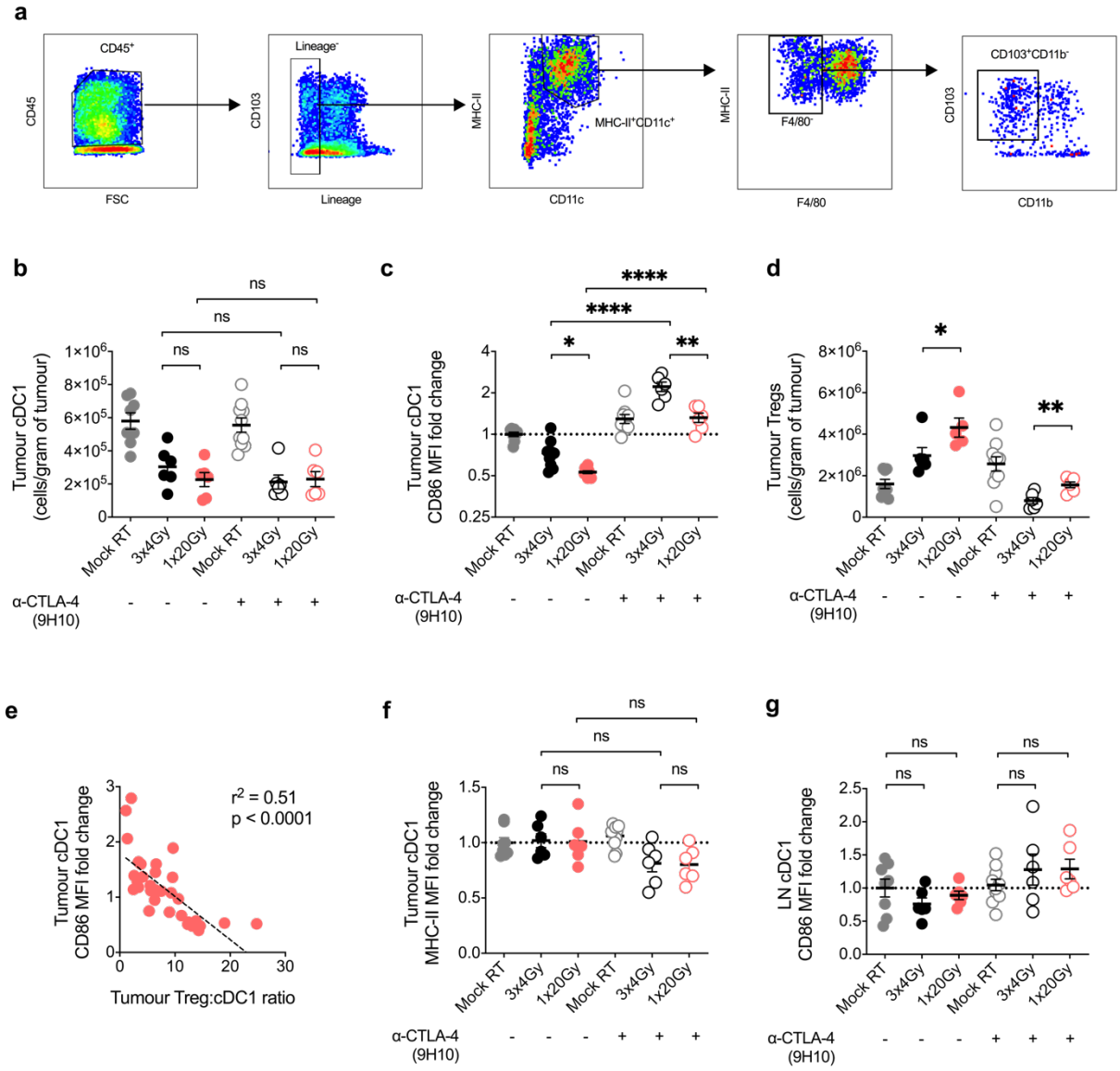

Figure 3.16. Radiation-induced Tregs restrict tumour-associated cDC1 maturation. AT3-OVA tumours were irradiated at 25-35mm^2 and harvested at day 5 post completion of RT. Inguinal lymph nodes isolated from the tumour-bearing mammary fat pad were also harvested. Mice were treated with 9H10 anti-CTLA4 or isotype control antibodies, administered every 4 days from start of RT. **a,** Flow cytometry gating strategy for cDC1s, defined as CD45$^+$ lineage$^-$ MHCII$^+$ CD11c$^+$ F4/80$^-$ CD11b$^-$ CD103$^+$. Lineage markers include TCRβ, CD19, NK1.1, and Ly6G. **b & d,** Absolute numbers of tumour-associated (**b**) cDC1s and (**d**) Tregs. **c & f,** (**c**) CD86 and (**f**) MHC-II expression in tumour-associated cDC1s. Fold change in MFI relative to mock-irradiated controls (dotted line) is presented. **e,** Correlation between the ratio of tumour-associated Treg:cDC1 frequencies and the induction of CD86 expression in cDC1s (expressed as fold change over respective control groups) across all irradiated tumours, with and without 9H10 anti-CTLA-4 treatment. **g,** CD86 expression in cDC1s in inguinal lymph nodes. Data is representative of 1 experiment. *MFI: mean fluorescence intensity, ns: non-significant, * p<0.05, ** p<0.01, **** p<0.0001*

10. Radiation dose-fractionation influences the induction of anti-tumour immunological memory

Having demonstrated that depletion of Tregs could unmask local immunoadjuvant effects of the 3x4Gy and 1x20Gy regimens in AT3-OVA tumours, the subsequent impact of Treg depletion on the generation of immunological memory responses was examined. Spleens were harvested from all groups of DT-treated DEREG mice (mock RT + DT, 3x4Gy + DT and 1x20Gy + DT) used in the experiment presented in *Fig 3.12b* once the tumours reached experimental endpoint. Since all mice in that experiment were disease-burdened, a tumour rechallenge experiment to test memory induction was not feasible. To circumvent this, splenocyte transfers were employed with the goal of transferring immunity from one mouse to another. Each splenocyte preparation was injected intravenously into two separate treatment-naïve wildtype mice, as shown in *Figure 3.17a*. After at least one week of reconstitution, AT3-OVA tumour cells were injected orthotopically into the mammary fat pad of one mouse, and AT3-parental tumour cells into the other. Growth of these tumours was then monitored over time. No additional therapeutic intervention was used in this experiment.

Inhibition of AT3-OVA tumour growth was evident in recipients of splenocytes from 3x4Gy + DT and 1x20Gy + DT mice relative to recipients of splenocytes from mock RT + DT mice, suggesting that both 3x4Gy and 1x20Gy regimens in the context of Treg depletion could evoke memory responses capable of protecting against disease recurrence (*Figure 3.17b*). Intriguingly, inhibition of AT3-parental tumour growth was only observed in recipients of splenocytes from 1x20Gy + DT mice. To confirm these observations, a similar experiment was repeated using splenocytes from AT3-OVA tumour-bearing wildtype mice receiving RT and 9H10 antibody therapy from the experiment presented in *Figure 3.13c*. A similar pattern of AT3-OVA and AT3-parental tumour growth modulation was observed across the groups (*Figure 3.17c*). Ongoing work in the laboratory during the preparation of this thesis has revealed that the induction of memory responses with the 3x4Gy and 1x20Gy regimens was indeed dependent on depletion of Tregs (data not shown).

Collectively, these data highlight the suppressive impact of radiation-induced Tregs on the ability of RT to evoke immunological memory responses. Depletion of Tregs effectively rescued the ability of both low-to-moderate and high DPF regimens to induce long-term protective anti-tumour immunity. More importantly, the demonstration of a memory response against AT3-parental tumours in recipients of splenocytes from 1x20Gy-irradiated mice, but not from 3x4Gy-irradiated mice, suggests a differential induction of antigenic spread and diversification of the T cell receptor (TCR) repertoire within irradiated tumours by radiation dose-fractionation.

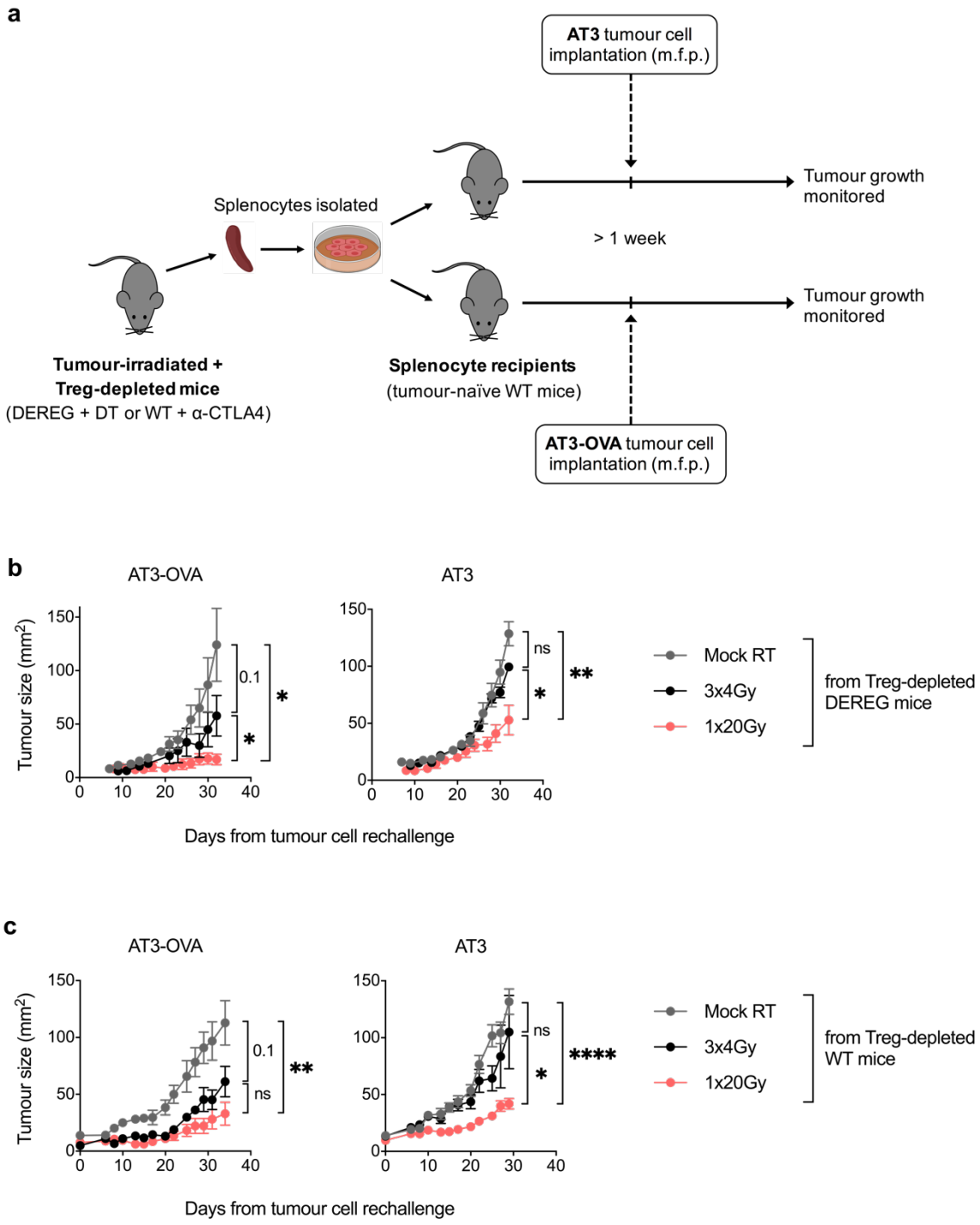

Figure 3.17. RT in the context of Treg depletion can evoke protective immunological memory responses. a, Experimental schema for testing the generation of anti-tumour immunological memory. Spleens were harvested from Treg-depleted DEREG mice in *Figure 3.12b* and Treg-depleted wildtype (WT) mice in *Figure 3.13c* once tumours reached experimental endpoint. Each splenocyte preparation were injected intravenously into two separate treatment-naive wildtype mice. After at least one week, AT3-OVA tumour cells were injected orthotopically into the mammary fat pad (m.f.p.) of one mouse, and AT3-parental tumour cells into the other. Growth of these tumours was monitored over time, with no further

therapy given. **b-c,** AT3-OVA and AT3 tumour growth in recipient mice with splenocytes transferred from (**b**) Treg-depleted DEREG mice, *n*=4-5 mice per group, data representative of 2 independent experiments; and (**c**) Treg-depleted WT mice, *n*=3-6 mice per group, data representative of 2 independent experiments. Data is presented as mean ± SEM. *ns: non-significant, * p<0.05, ** p<0.01, **** p<0.0001*

11. The regulation of CD8+ T cell responses by radiation DPF is tumour type-dependent

To determine if Treg-mediated inhibition of $CD8^+$ T cell responses by high radiation DPF was a phenomenon specific to AT3-OVA tumours, examination of the immunological effects of RT was extended to the MC38 colorectal carcinoma cell line. *In vitro* clonogenic assays of MC38 tumour cells revealed a lower α/β ratio of 4Gy and a higher surviving fraction after 2Gy (SF2) of 0.49 compared to 16Gy and 0.36 for AT3-OVA tumour cells, respectively (*Figure 3.18a-b*). These parameters suggest that MC38 tumour cells were more radioresistant to lower radiation DPFs but were more radiosensitive to higher DPFs than AT3-OVA tumour cells. In line with this, subcutaneously implanted MC38 tumours in mice were poorly responsive to the 3x4Gy regimen and highly sensitive to the 1x20Gy regimen (*Figure 3.19a*). Interestingly, depletion of $CD8^+$ T cells at the time of starting RT did not affect tumour control by the 3x4Gy regimen, but severely compromised tumour control by the 1x20Gy regimen, suggesting that high DPF regimens could evoke anti-tumour $CD8^+$ T cell responses in MC38 tumours (*Figure 3.19a*). Induction of $CD8^+$ T cell responses in MC38 tumours by RT was likely dependent on the cross-priming activity of cDC1s since *Batf3* deficiency in mice also resulted in loss of tumour control by the 1x20Gy regimen, compared to the growth of tumours in wildtype mice (*Figure 3.19b*).

To test if the disparity between the ability of the 1x20Gy regimen to evoke anti-tumour $CD8^+$ T cell responses in MC38 and AT3-OVA tumours was due to a difference in tissue niche (subcutaneous *vs.* mammary fat pad), mice with subcutaneously-implanted AT3-OVA tumours were locally irradiated with the 1x20Gy regimen and concurrently treated with $CD8^+$ T cell depleting antibodies. No impact of $CD8^+$ T cell depletion was observed on the growth of these tumours following RT when compared to tumours in mice treated with RT alone (*Figure 3.19c*), suggesting that the regulation of radiation-induced $CD8^+$ T cell responses by dose-fractionation was tumour type-dependent, not tumour niche-dependent.

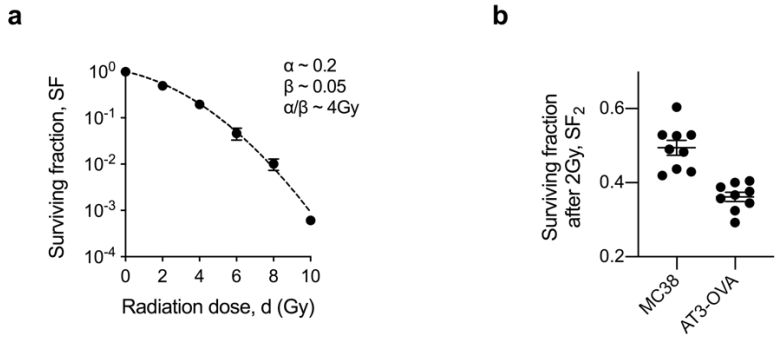

Figure 3.18. MC38 tumour cells are more radioresistant to low radiation DPFs and more radiosensitive to high DPFs than AT3-OVA tumour cells. a, Radiation cell survival curve of MC38 tumour cells, as established by *in vitro* clonogenic survival assays following radiation exposure at the indicated doses. *n*=6 replicates combined from 2 independent experiments. Data presented as mean ± SEM. **b,** Surviving fraction after 2Gy (SF2) of MC38 and AT3-OVA tumour cells *in vitro*. Data is collated from (**a**) for MC38 tumour cells and from *Figure 3.1a* for AT3-OVA tumour cells.

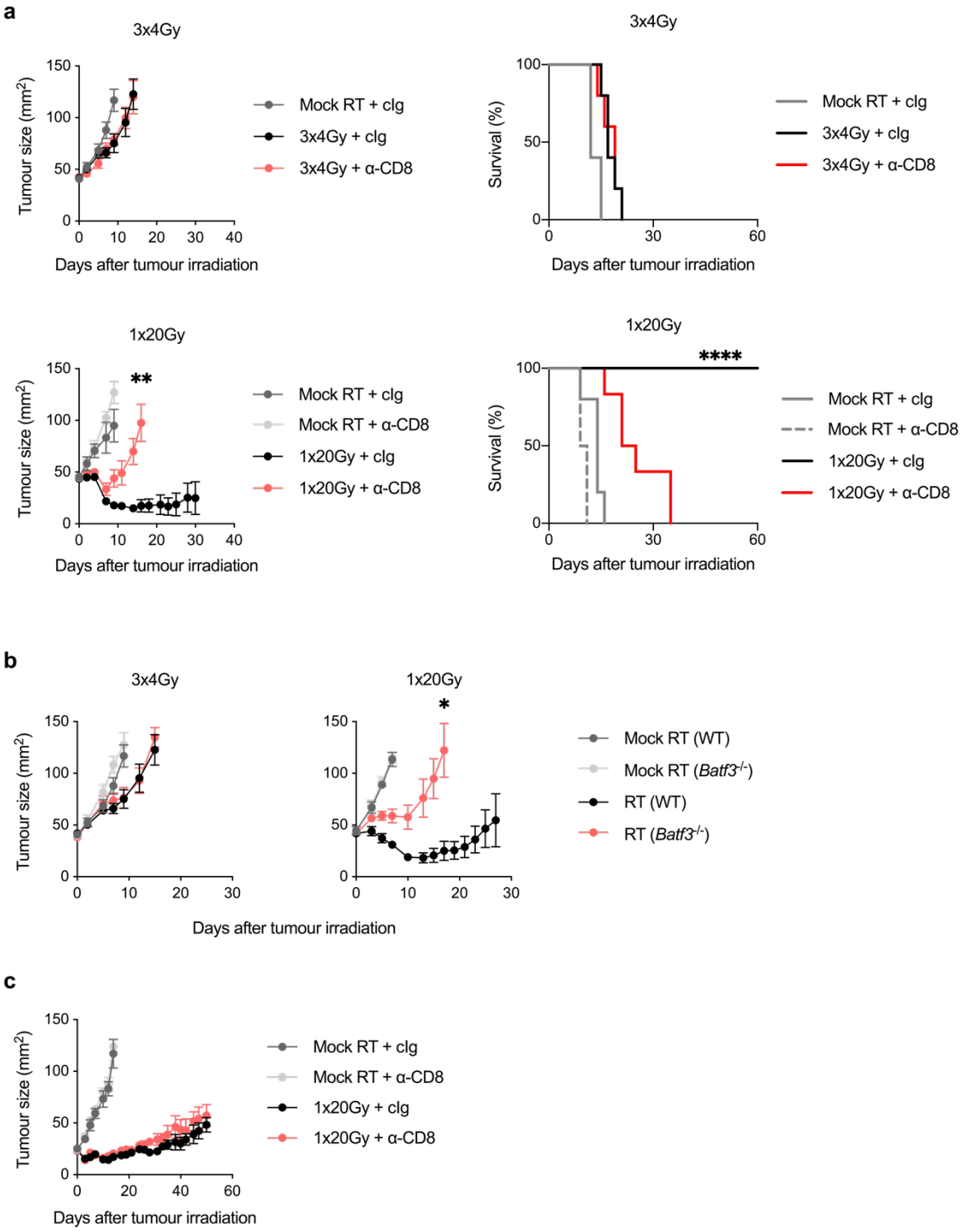

Figure 3.19. 1x20Gy irradiation can evoke anti-tumour CD8$^+$ T cell responses in MC38 tumours. a-b, MC38 tumour cells were injected subcutaneously into the flanks of C57BL/6 wildtype (WT) or *Batf3*$^{-/-}$ mice (1.8x10^6 cells/mouse). Tumours were irradiated when they reached 40-50mm^2. **a,** MC38 tumour growth and mouse survival curves post RT in WT mice treated with CD8$^+$ T cell depleting or isotype control antibodies, administered every 3 days from start of RT to end of experiment. Statistical comparisons were made between the RT + anti-CD8 and RT + cIg groups. *n*=5 mice per group, representative of 2 independent

experiments. **b,** MC38 tumour growth post RT in WT and *Batf3*$^{-/-}$ mice. Statistical comparisons were made between the RT (*Batf3*$^{-/-}$) and RT (WT) groups. *n*=5 mice per group, representative of 1 experiment. **c,** AT3-OVA tumour cells were injected subcutaneously into the flanks of C57BL/6 WT mice ($1.8x10^6$ cells/mouse) and left to grow to 25-35mm^2 before being irradiated. AT3-OVA tumour growth post RT in mice treated with CD8$^+$ T cell depleting or isotype control antibodies, administered every 3 days from start of RT to end of experiment. *n*=5-6 mice per group, representative of 1 experiment. Tumour growth data is presented as mean ± SEM., *** $p<0.01$, *** $p<0.001$

Since radiation-induced Tregs were a key barrier to the ability of 1x20Gy irradiation to prime $CD8^+$ T responses in AT3-OVA tumours, the impact of the radiation regimen on Tregs in MC38 tumours was next examined. Flow cytometric analysis of MC38 tumours at days 5 and 10 after 1x20Gy irradiation revealed no radiation-induced enrichment of tumour-associated Tregs, but rather increases in $CD8^+$ T cell frequencies (*Figure 3.20a*). The proportion of $PD\text{-}1^+$ $CD8^+$ T cells were also increased relative to the mock-irradiated tumours (*Figure 3.20b*). Moreover, Treg:$CD8^+$ T cell ratios after 1x20Gy irradiation did not rise above those observed for mock-irradiated controls (*Fig 3.20c*). These data suggest that in contrast to AT3-OVA tumours, MC38 tumours did not support the radiation-induced accumulation of Tregs, thus permitting the dominance of $CD8^+$ T cell activity following irradiation of these tumours.

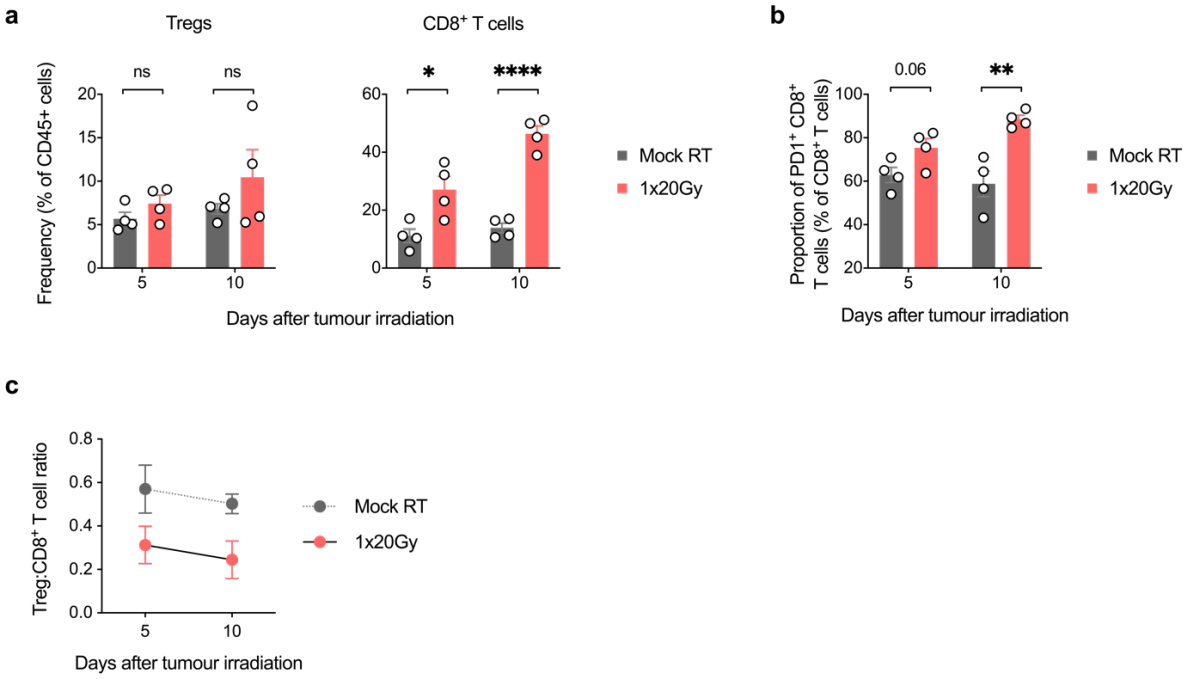

Figure 3.20. 1x20Gy irradiation does not alter the Treg:CD8$^+$ T cell ratio in MC38 tumours. MC38 tumours in wildtype mice were irradiated at 40-50mm^2 as described in *Figure 3.18* and harvested at days 5 and 10 post RT for flow cytometric analysis. **a,** Frequencies of tumour-associated Tregs and CD8$^+$ T cells at days 5 and 10 post RT. **c,** Proportion of PD-1$^+$ CD8$^+$ T cells at days 5 and 10 post RT. **b,** Ratio of tumour-associated Treg:CD8$^+$ T cell frequencies, presented as mean ± SEM. All data is representative of 1 experiment. *ns: non-significant, * p<0.05, ** p<0.01, **** p<0.0001*

Discussion

An exciting revolution in our understanding of the immunological effects of RT has occurred in recent years, especially as the mechanisms by which radiation modulates DC and $CD8^+$ T cell function are uncovered. Using a series of radiation dose-fractionation regimens that allowed the immunological impact of radiation DPF to be dissected from that of total dose (as represented by BED), this chapter demonstrated that radiation-induced priming of $CD8^+$ T cell responses in AT3-OVA tumours was regulated by radiation DPF, rather than BED. Examination of tumour cell-intrinsic changes evoked by radiation, such as death and expression of immunomodulatory molecules or death receptors, did not reveal significant changes between radiation regimens, suggesting that they were not key factors determining the differential effects of radiation dose-fractionation on host adaptive immune responses. Radiation-induced accumulation of Tregs in tumours was however proportional to the radiation DPF employed, showing heightened amplitude and kinetics with the 1x20Gy (BED_{16} 45Gy) regimen compared to the 3x4Gy (BED_{16} 15Gy) and 9x4Gy (BED_{16} 45Gy) regimens. No obvious phenotypic differences were detected in the Tregs across radiation regimens. While radiation-induced Tregs dampened the anti-tumour activity of all radiation regimens tested, the functional status of tumour-associated cDC1s were most severely suppressed by Treg responses induced by 1x20Gy irradiation, which correlated with the lack of effective $CD8^+$ T cell responses generated by that radiation regimen. Correspondingly, depletion of Tregs rescued the capacity of 1x20Gy irradiation to prime $CD8^+$ T cell responses, resulting in compete regression of irradiated AT3-OVA tumours. In MC38 tumours that did not demonstrate an enrichment of tumour-associated Tregs following RT, the 1x20Gy regimen was able to independently evoke effective anti-tumour $CD8^+$ T cell responses. Thus, radiation-induced $CD8^+$ T cell responses can be shaped by tumour cell-extrinsic factors that are dependent on radiation dose-fractionation and tumour type.

Few studies have performed side-by-side mechanistic investigation of the differential immunological effects induced by radiation dose-fractionation. Seminal pre-clinical studies by Demaria and colleagues have reported that large single-fraction doses are poor inducers of T cell immunity and in turn lack the ability to support the anti-tumour activity of anti-CTLA-4 and anti-PD-1 therapy (Dewan *et al.*, 2009; Vanpouille-Box *et al.*, 2017). By increasing expression of the exonuclease TREX1, single-fraction high DPF regimens such as 1x20Gy limited the radiation-induced accumulation of cytosolic dsDNA within tumour cells and failed to stimulate tumour cell-intrinsic STING signalling and production of type I IFN (Vanpouille-Box *et al.*, 2017). By contrast, fractionated radiation regimens with lower DPFs such as 3x8Gy and 5x6Gy did not induce sufficiently high TREX1 expression to prevent STING activation, thus supported abscopal

control of TSA mammary carcinomas in a type I IFN-dependent manner when used in conjunction with anti-CTLA-4 antibody (9H10 clone) therapy. This has in part led to the common use of the 3x8Gy regimen with immune checkpoint inhibitors across human trials, which have promisingly corroborated heightened immunological responses (Formenti *et al.*, 2018; Theelen *et al.*, 2019), although not consistently across all studies (Voorwerk *et al.*, 2019).

Results presented in this chapter also demonstrated the inability of high DPF regimens (1x12Gy and 1x20Gy) to evoke anti-tumour $CD8^+$ T cell responses in AT3-OVA tumours, whereas low-to-moderate DPF regimens (3x4Gy, 9x4Gy and 3x8Gy) could. However, there are several key differences in this study compared to the aforementioned work by Demaria and colleagues. Most importantly, rather than an abrogation of tumour cell-intrinsic immunogenicity with high DPF regimens, this study identified the loss of $CD8^+$ T cell priming with high DPF regimens to be due to tumour cell-extrinsic immunosuppressive factors, namely the induction of a greater and more rapid accumulation of Tregs within irradiated tumours, which suppressed the maturation of tumour-associated cDC1s. Although the recruitment and priming capacity of tumour-associated cDC1s in TSA tumours were also more suppressed by the 1x20Gy regimen compared to the 3x8Gy regimen in work by Demaria and colleagues, other changes in the tumour immune microenvironment were not reported for comparison (Vanpouille-Box *et al.*, 2017). By contrast, results in this study suggest that tumour cell-intrinsic immunogenicity was unperturbed by high DPF regimens, since depletion of Tregs restored the ability of the 1x20Gy regimen to potently prime $CD8^+$ T cell responses in AT3-OVA tumours, resulting in tumour cures and the generation of long-term immunological memory. Interestingly, upregulation of *Trex1* transcripts was detected using RNAseq in the tumour/stromal compartment ($CD45^-$ cells) of AT3-OVA tumours following 1x20Gy but not 3x4Gy irradiation (*Appendix Figure 2*). Whether this could be linked with the absence of STING signalling and type I IFN production gene signatures in the immune compartment of the same tumours following 1x20Gy irradiation, compared to 3x4Gy irradiation, remains to be determined (*Figure 3.11d*). However, a more severe suppression by tumour-associated Tregs is a more likely explanation, given the concurrent enrichment of gene signatures for negative regulation of IL-12 production and positive regulation of TGF-β production, which was not detected in response to 3x4Gy irradiation (*Figure 3.11e*). Of note, Schadt *et al.* recently reported that a single fraction of 20Gy generated similar levels of STING-stimulatory cytosolic dsDNA compared to a single fraction of 8Gy in CT26 mouse colon carcinoma cells, although TREX1 levels were not assessed in that study (Schadt *et al.*, 2019). Indeed, it has been reported that radiation-induced reactive oxygen species can induce DNA modifications that render DNA resistant to degradation by TREX1 (Gehrke *et al.*, 2013). In other published work, 1x20Gy irradiation was able to prime anti-tumour $CD8^+$ T cell responses that could control the growth of

CT26, MC38 and B16 melanoma tumours (Lee *et al.*, 2009; Deng *et al.*, 2014b; Schadt *et al.*, 2019). Therefore, it is likely that not all tumour types exhibit a similar regulation of tumour cell-intrinsic immunogenicity by TREX1 following RT.

In contrast to other studies pointing to the key requirement of type I IFN for radiation-induced priming of $CD8^+$ T cells (Burnette *et al.*, 2011; Deng *et al.*, 2014b), type I IFN signalling did not appear to be critical for this process in AT3-OVA tumours, since the anti-tumour effects of the 3x4Gy regimen, which was in part mediated by $CD8^+$ T cell responses, was not compromised in *Ifnar1*$^{-/-}$ mice or in wildtype mice treated with anti-IFNAR1 blocking antibodies. As both type I IFN and IFN-γ can promote maturation of DCs (Parker *et al.*, 2016), sufficient compensation by IFN-γ in AT3-OVA tumours could potentially have circumvented the requirement for type I IFN. In support of this conjecture, the administration of ketamine/xylazine to anaesthetise mice in preparation for irradiation was found to evoke the maturation and activation of DCs within AT3-OVA tumours in conjunction with responses to IFN-γ signalling – but notably not responses to type I IFN (*Appendix Figure 3a-c*). These findings were derived from comparing the transcriptional profile of the immune compartment of 1x0Gy tumours (unirradiated but treated with one dose of ketamine/xylazine) with that of untreated tumours (unirradiated and not treated with ketamine/xylazine). Because RNA from these samples was extracted and sequenced together, batch effect could be excluded as a contributing factor to the observed transcriptional differences. While it is known that all anaesthetic agents can exert immunomodulatory effects (Anderson *et al.*, 2014), whether IFN-γ production could truly circumvent the requirement of type I IFN to promote DC function needs further investigation. The independent immunomodulatory effects of mouse anaesthesia however emphasise the necessity for a rigorous comparison between irradiated samples and respective control groups that received the same number of anaesthetic treatments, especially for sensitive assays such as RNAseq.

Another point of difference between this study and work by Demaria and colleagues is that this study focused on local $CD8^+$ T cell responses against irradiated tumours, rather than abscopal responses against tumours outside the radiation volume. Nonetheless, this study did demonstrate that irradiation of AT3-OVA tumours with either the 3x4Gy or 1x20Gy regimen, together with Treg depletion, led to the generation of immunological memory that could be adoptively transferred into treatment-naïve mice, endowing them with protective responses against similar tumours. It is anticipated that such memory responses would also translate into abscopal responses, although this will need to be confirmed. Intriguingly, the 1x20Gy regimen but not the 3x4Gy regimen evoked memory responses against AT3-parental tumours in addition to AT3-OVA tumours, suggesting differences in the antigenic repertoire of circulating immunological

memory generated between dose-fractionation regimens. Pointing to the potential translatability of this finding, in the clinical setting, SABR has been shown to broaden the diversity of peripheral and tumour-infiltrating T cell clones with and without concurrent immunotherapy (Twyman-Saint Victor *et al.*, 2015; Rudqvist *et al.*, 2018; Phillips *et al.*, 2020). Whether a similar effect on the TCR repertoire could be achieved with low-to-moderate DPF but high BED regimens is however unknown. Further work using AT3 and AT3-OVA tumours to determine the dependency of this effect on radiation DPF versus BED as well as the immune cell subsets mediating these memory responses will be pursued beyond this PhD project.

Collectively, results in this chapter highlight radiation-induced Treg responses as a key tumour cell-extrinsic determinant for the priming of $CD8^+$ T cell by radiation. However, although both 3x4Gy and 1x20Gy regimens evoked a local accumulation of Tregs that restricted the maturation of tumour-associated cDC1s and anti-tumour function of $CD8^+$ T cells, the 3x4Gy regimen was still able to independently prime $CD8^+$ T cell responses that could be further leveraged with CTLA-4 checkpoint blockade, whereas the 1x20Gy regimen could not. This is likely linked to the greater and more rapid accumulation of tumour-associated Tregs following 1x20Gy irradiation compared to 3x4Gy irradiation, which might have been sufficient to completely block $CD8^+$ T cell priming. Indeed, the expression of the co-stimulatory ligand CD86 on tumour-associated cDC1s in AT3-OVA tumours was significantly more supressed at day 5 post irradiation with the 1x20Gy regimen than with the 3x4Gy regimen, an effect that was reversed when tumour-associated Tregs were depleted (*Figure 3.16c*, *Figure 3.8a*). The observation that the 1x20Gy regimen could evoke anti-tumour $CD8^+$ T cell responses in MC38 tumours, which did not exhibit radiation-induced Treg responses, lends further support to this notion. Given that the upregulation of CTLA-4 and LAG-3 expression on Tregs, which contribute to Treg suppressor function (Sakaguchi *et al.*, 2008), was not different in AT3-OVA tumours following irradiation with the 3x4Gy and 1x20Gy regimens, it is possible that the regulation of $CD8^+$ T cell priming by radiation DPF was principally due to differences in the quantity rather than the function of Tregs. However, this will need to be validated. Further characterisation of the Tregs in 3x4Gy and 1x20Gy-irradiated tumours, including examination of their cytokine secretory activity and their suppressive function using *in vitro* Treg suppression assays, will help clarify this.

Although radiation-induced enrichment of tumour-associated Tregs has been well-described in various tumours, the underlying mechanisms for this phenomenon are not fully clear (Persa *et al.*, 2015). In irradiated AT3-OVA tumours, given that a higher proportion of the Tregs were $Nrp1^+$, it is likely that newly recruited and/or expanded nTregs accounted for the majority of the increase in Treg numbers, rather than the radiation-induced conversion of $CD4^+$ effector T cells into iTregs

in situ. The parallel enrichment of other immune subsets such as $CD4^+$ effector T cells and NK cells (described in Chapter 4) within tumours over the same timeframe suggests an inflammatory response induced by radiation tissue damage. Tregs express similar homing receptors to other T cell subsets that allow them to traffic into inflamed tissues and tumours (Sakaguchi *et al.*, 2008). In line with this, AT3-OVA tumours demonstrated higher gene expression of inflammatory cytokines and receptors following irradiation, including *Cxcl1*, *Cxcl2*, *Csf1*, and *Ccr2* (discussed in Chapter 4, *Figure 4.8, Figure 4.13, Appendix Tables 1-4*). Muroyama *et al.* demonstrated that Tregs in irradiated B16-F10 tumours were more actively proliferating as determined by Ki67 staining than Tregs in mock-irradiated tumours, which suggests that RT can promote the expansion of Tregs within tumours (Muroyama *et al.*, 2017). Interestingly, the authors also examined MC38 tumours and reported that 1x10Gy irradiation increased the proportion of tumour-associated Tregs from 20-30% of all $CD4^+$ T cells, as detected in mock-irradiated tumours, to 40-50% at day 7 post RT. This is in contrast to work presented in this chapter, which observed Tregs to comprise 60-70% of all $CD4^+$ T cells in MC38 tumours, a proportion that was unchanged by 1x20Gy irradiation at day 5. The reasons for this discrepancy are unclear.

Increasingly, it is recognised that the composition of Tregs within tumours can be significantly shaped by the non-immune tumour stroma. For example, CCL5 production by cancer-associated fibroblasts has been reported to preferentially recruit Tregs due to higher expression of CCR1 by Tregs (Tan et al., 2011). Upregulation of the common lymphatic endothelial and vascular endothelial receptor 1 (CLEVER1), mucosal vascular addressin cell adhesion molecule 1 (MADCAM1) and CD166 have also been shown to facilitate the extravasation of Tregs into tumours (Nummer et al., 2007; Shetty et al., 2011). Additionally, increased expression of Fas ligand in the tumour vasculature can evoke selective apoptosis of $CD8^+$ T cells but spare Tregs, which express higher levels of the apoptosis inhibitor c-FLIP (Motz et al., 2014). How the tumour stroma compartment is affected by radiation dose-fractionation parameters such as DPF and BED, and how this influences Treg responses within the tumour is at present poorly understood. Given the likely heterogeneity of tumour stroma between tumour types, it is also possible that this compartment may account for the observed differences in radiation-induced Treg responses between AT3-OVA and MC38 tumours. Discovering factors within the tumour microenvironment that dictate whether a tumour will respond to radiation by transiently enriching for Tregs may lead to the identification of important biomarkers to guide selection of radiation dose-fractionation and immunotherapeutic agent. For example, for tumours with radiation DPF-dependent Treg responses similar to that of AT3-OVA tumours, low-to-moderate DPF radiation regimens may be more effective in harnessing anti-tumour immune responses than high DPF regimens. Such tumours may also be well-suited for co-treatment with RT and Treg-directed

interventions such as antibody-based Treg depletion. By contrast, these considerations may not be as critical for tumours that do not exhibit Treg responses following irradiation.

While this chapter has focused on the interplay between $CD8^+$ T cells, cDC1s and Tregs, it is important to acknowledge that the immune system is a far more complex network of cellular subsets that could collectively influence immune responses following RT. Indeed, results from exploratory experiments and analyses in this PhD project suggest that intriguingly, $CD4^+$ effector T cells were more important to the anti-tumour activity of the 1x20Gy regimen than that of the 3x4Gy regimen in AT3-OVA tumours (data not shown). Additionally, tumour-associated macrophages in AT3-OVA tumours were more significantly depleted by the 3x4Gy regimen than by the 1x20Gy regimen (data not shown). These preliminary findings suggest additional layers of regulation that were beyond the scope of this PhD project and could not be studied in depth.

Overall, work herein adds to our current state of knowledge surrounding the impact of radiation dose-fractionation on $CD8^+$ T cell responses. Significantly, this chapter represents a comprehensive side-by-side pre-clinical comparison and mechanistic interrogation of the immunomodulatory effects of radiation dose-fractionation, and one of the few studies to examine such effects independent of immunotherapy. The translational implications of these findings on combining RT with immune checkpoint blockade are discussed in Chapter 5.

Chapter 4: The impact of radiation dose-fractionation on anti-tumour NK cell responses

Abstract

Natural killer (NK) cells form the primary cytotoxic subset in the innate arm of the immune system and their abundance in tumours is prognostic for improved survival in a wide range of human cancers. Radiation therapy (RT) has the potential to augment the anti-tumour activity of NK cells by increasing recruitment of NK cells into tumours and upregulating tumour cell expression of NK cell-activating stress-induced ligands. Nonetheless, how anti-tumour NK cell responses are influenced by radiation dose-fractionation is unclear. Results in this chapter demonstrated that for AT3-OVA murine mammary carcinoma tumours, the induction of effective anti-tumour NK cell responses by radiation required a sufficiently high total dose, as represented by biological effective dose (BED), rather than dose per fraction (DPF). NK cell responses following high BED radiation were also observed in MC38 murine colorectal carcinoma tumours and in publicly accessible transcriptomic data of human pancreatic and rectal adenocarcinomas. In AT3-OVA tumours, a rapid accumulation of NK cells that peaked within 5 days post RT was observed, regardless of the radiation dose-fractionation employed. These early NK cell responses were functionally restricted by a transient but concurrent increase in tumour-associated regulatory T cells (Tregs) that lasted for about 2 weeks post RT. However, sustained NK cell responses up to 3 weeks post RT were selectively evoked by the 1x20Gy regimen (BED_{16} 45Gy) but not by the 3x4Gy regimen (BED_{16} 16Gy). These late-phase NK cell responses were the primary source of interferon-γ within the tumours and exhibited heightened activation markers. Gene expression profiling of AT3-OVA tumours and human rectal adenocarcinomas revealed a putative link between sustained NK cell infiltration and radiation-induced cellular senescence. Collectively, these results suggest that the impact of radiation dose-fractionation on NK cell responses is dictated by a highly dynamic interaction between effector and suppressor subsets within the tumour immune microenvironment. An increased understanding of the regulation and kinetics of these responses will likely reveal opportunities for combining RT and NK cell-directed immunotherapy strategies.

Introduction

Natural killer (NK) cells are the primary cytotoxic subset in the innate arm of the immune system and are early immune responders to danger. In contrast to T cells which show specificity in antigenic recognition and require cross-presentation by dendritic cells (DCs) for priming, NK cells rely on an array of germline-encoded activating and inhibitory receptors to engage and spontaneously kill damaged, infected, and transformed cells (Paul, 2013). Fc receptor-expressing NK cells also exert antibody-dependent cellular cytotoxicity (ADCC) through recognition and lysis of cells that have been coated with host IgG antibodies in response to activation of humoral immunity. Together with T cells, NK cells constitute an important source of interferon (IFN)-γ, which drives a diverse range of inflammatory processes in the immune microenvironment (Paul, 2013).

A limited number of studies have investigated the immunomodulatory effects of RT on NK cell responses in solid cancers. *In vitro* studies have described upregulation of stress ligands on irradiated tumour cell lines that sensitised cells for NK cell killing (Gasser *et al.*, 2005; Kim *et al.*, 2006). It was also reported that radiation exposure of cultured human breast cancer cell lines induced the expression of CXCL16 *in vitro*, correlating with increased migration of $CXCR6^{+}$ activated NK cells in a chemotaxis assay (Yoon *et al.*, 2016). However, *in vitro* assays can be unreliable predictors of *in vivo* efficacy (Kim *et al.*, 2019). Studies examining the impact of RT on anti-tumour NK cell responses *in vivo* have largely used RT coupled with adoptive NK cell transfer in immunodeficient xenograft models. Synergistic effects were seen between the two, resulting in better control of the primary tumour and less metastatic dissemination (Canter *et al.*, 2017; Kim *et al.*, 2019). These findings led to a single-arm proof-of-principle trial in companion dogs with spontaneous sarcoma tumours, which showed that local tumour irradiation with autologous NK cell transfer resulted in favourable metastases-free survival (Canter *et al.*, 2017). Alongside these studies, NK cells have been reported to be important players in mediating the synergy between RT and immune checkpoint inhibitors (Dovedi *et al.*, 2014; Benci *et al.*, 2019; Watanabe *et al.*, 2019). Nonetheless, the mechanistic underpinnings of radiation-induced NK cell responses and the impact of radiation dose-fractionation on anti-tumour NK cell responses remain poorly understood. These questions are particularly important when considering RT as a synergistic partner with NK cell-directed immunotherapy, which is increasingly investigated as a strategy to circumvent resistance to T cell-directed immunotherapy (Guillerey *et al.*, 2016; Freeman *et al.*, 2019).

In this chapter, using syngeneic models of solid cancer in wildtype immunocompetent mice, the induction of effective anti-tumour NK cell responses by RT was found to be dependent on a sufficiently high biological effective dose (BED), rather than dose per fraction (DPF). This observation could be validated in transcriptomic data of human cancers post RT. In AT3-OVA murine mammary carcinoma tumours, the radiation BED-dependency of NK cell responses was a function of the sustained enrichment of tumour-associated NK cells following high BED radiation which outlasted radiation-induced regulatory T cell (Treg) responses. Gene expression profiling of these tumours revealed a putative link between persisting NK cell infiltration and radiation-induced cellular senescence. Importantly, results herein constitute the first body of work examining the impact of radiation dose-fractionation on NK cell responses and point to a window for leveraging radiation-induced NK cell responses for therapeutic synergy.

Results

1. Radiation-induced NK cell responses in mouse and human cancers are dependent on radiation BED, not DPF

To examine the impact of radiation dose-fractionation on the ability of RT to evoke host anti-tumour NK cell responses, AT3-OVA tumour-bearing mice were locally irradiated and concurrently treated with the NK cell-depleting antibody anti-asialo-GM1 (*Figure 4.1a*). Anti-asialo-GM1 treatment was confirmed to result in depletion of more than 80% of tumour-associated NK cells (*Figure 4.1b*). The same radiation dose-fractionation regimens detailed in Chapter 3 (*Figure 3.1b*) were used to dissect the effects of radiation DPF from total dose, as represented by BED. Although depletion of NK cells did not affect the growth of mock-irradiated AT3-OVA tumours, it resulted in poorer tumour control following irradiation with the 9x4Gy, 3x8Gy, and 1x20Gy regimens (BED_{16} 36-45Gy), but not the 3x4Gy and 1x12Gy regimens (BED_{16} 15-21Gy). The loss in ability of the higher BED regimens to slow tumour growth in the NK cell-depleted context was modest but consistently observed, suggesting that a radiation BED threshold of approximately 36Gy was needed for RT to evoke effective anti-tumour NK cell responses in AT3-OVA tumours (*Figure 4.1c*). Notably, this requirement was independent of radiation DPF and immunotherapy. In line with this, in MC38 tumours, a role for NK cells in supporting the anti-tumour activity of RT was only observed for the 1x20Gy regimen (BED_4 120Gy), but not the 3x4Gy regimen (BED_4 24Gy) (*Figure 4.2*).

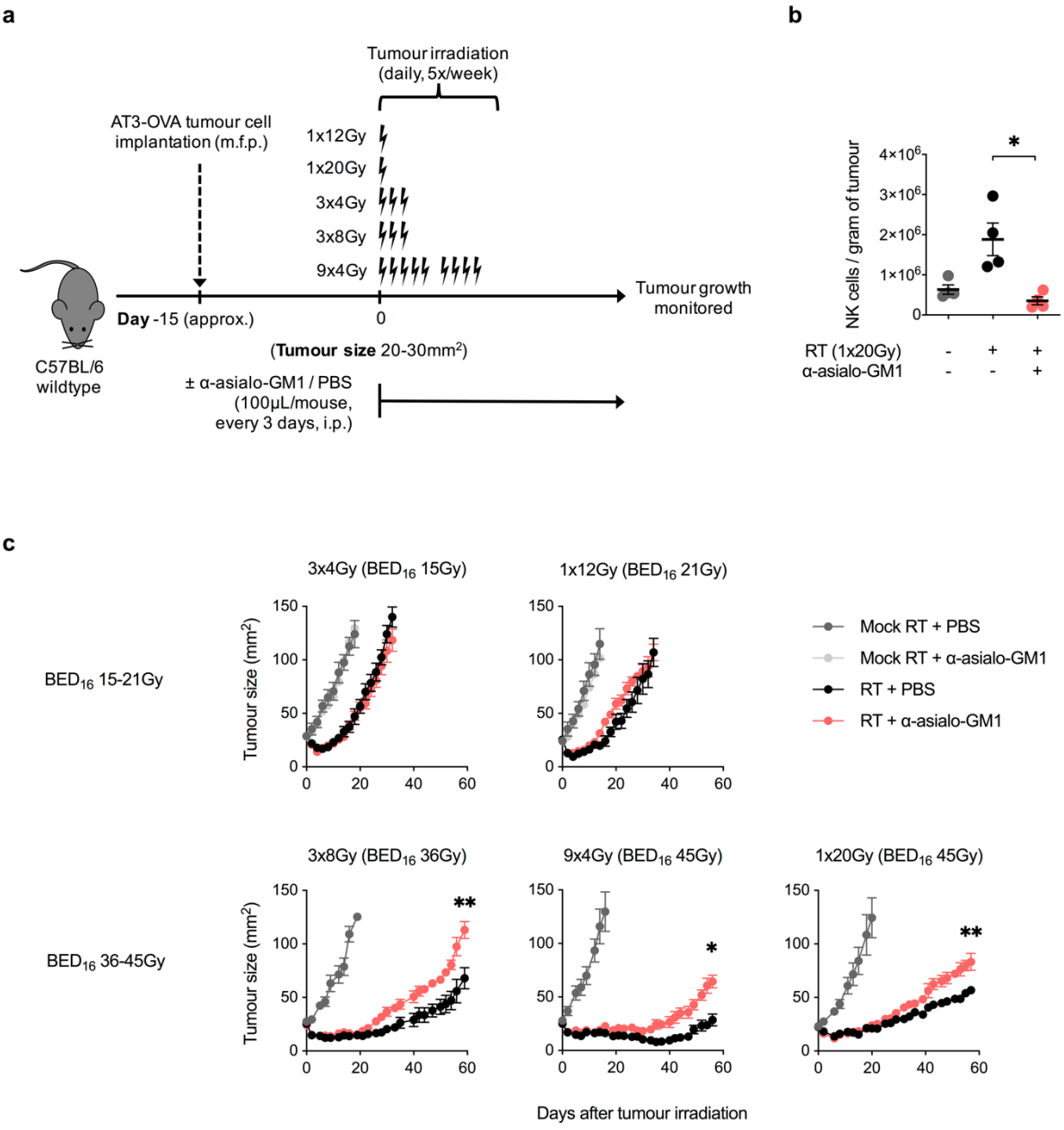

Figure 4.1. Radiation regimens with a sufficiently high BED can evoke anti-tumour NK cell responses independent of immunotherapy. a, Experimental schema of *in vivo* NK cell depletion experiments. AT3-OVA tumour cells were injected into mammary fat pads (m.f.p.) of C57BL/6 wildtype mice (1.5-1.8x10^6 cells/mouse) to allow orthotopic tumours to form. Tumours were irradiated when they reached 25-35mm^2 in size, which took approximately 14-16 days. RT was given daily, 5 fractions per week. Mice were culled when tumours reached 100-150mm^2. Survival of remaining mice were monitored until at least day 50 post initiation of treatment. Anti-asialo-GM1 antibodies were administered intra-peritoneally (i.p.) at 100µL/mouse, every 3 days from the day of RT to end of experiment for NK cell depletion. Phosphate-buffered saline (PBS) was used as control treatment. **b,** Depletion of tumour-associated NK cells by anti-

asialo-GM1 treatment. AT3-OVA tumours were harvested at day 5 post RT from mice treated with anti-asialo-GM1 antibodies or PBS, administered on day 0 and 3 post RT. Tumours were analysed by flow cytometry and NK cells were defined as $CD45^+$ $TCR\beta^-$ $NK1.1^+$. **c,** AT3-OVA tumour growth post RT in mice treated with anti-asialo-GM1 antibodies or PBS, as per (**a**). Statistical comparison was made between the RT + anti-asialo-GM1 and RT + PBS groups. *n*=4-6 mice per group, representative of 2 independent experiments. Data is presented as mean ± SEM, * $p<0.05$, ** $p<0.01$

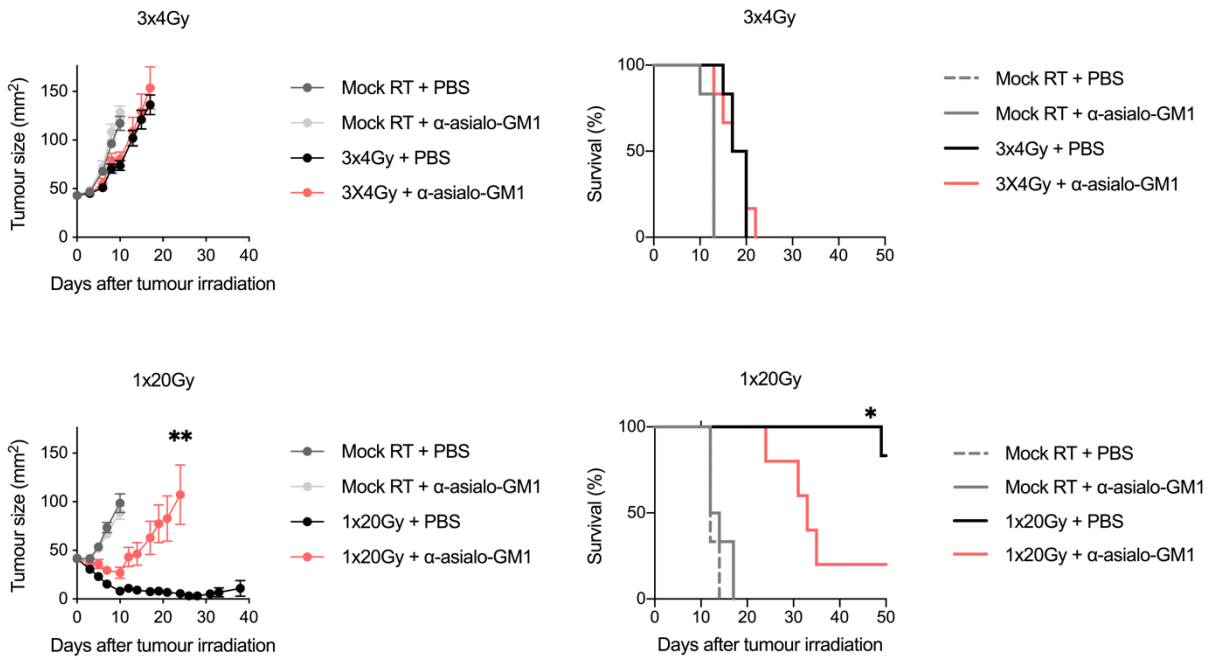

Figure 4.2. NK cells contribute significantly to the anti-tumour activity of 1x20Gy irradiation in MC38 tumours. MC38 tumour cells were injected subcutaneously into the flanks of C57BL/6 wildtype mice ($1.8x10^6$ cells/mouse). Tumours were irradiated when they reached 40-50mm^2. MC38 tumour growth (left) and mouse survival curves (right) post RT in mice treated with anti-asialo-GM1 antibodies or PBS, administered every 3 days from start of RT to end of experiment. Statistical comparisons were made between the RT + anti-asialo-GM1 and RT + PBS groups. *n*=4-6 mice per group, representative of 2 independent experiments. Tumour growth data is presented as mean ± SEM. * $p<0.05$, ** $p<0.01$

To confirm if these observations had translational significance, publicly accessible human transcriptomic data on the Gene Expression Omnibus (GEO) were screened for tissue samples taken after RT. Two datasets were found, one comprising of pancreatic ductal adenocarcinoma (PDAC) tumour samples (GSE129492) and the other rectal adenocarcinoma tumour samples (GSE15781). In GSE129492 dataset, archival tissue was obtained as a retrospective study from 24 patients who had surgical resection of PDAC tumours between 2011 and 2016 (Farren *et al.*, 2020). Of those patients, six patients received neoadjuvant folinic acid, 5-fluorouracil, irinotecan and oxaliplatin (FOLFORINOX) chemotherapy followed by SABR prior to surgery (chemoSABR + S), six received neoadjuvant chemotherapy followed by conventionally fractionated RT prior to surgery (chemoXRT + S), six received neoadjuvant chemotherapy only prior to surgery (chemo + S), and six received surgery alone without neoadjuvant therapy (S) (*Figure 4.3a*). The radiation regimen for conventionally fractionated RT was 50Gy in 2Gy per fraction, and for SABR 45Gy in 5-9Gy per fraction, depending on the location of the tumour (private communication with corresponding author). The time from completion of neoadjuvant therapy to surgical resection ranged from 2.9 - 18.3 weeks. Gene expression profiles were generated using the PanCancer Immune Profiling Panel (Nanostring Inc., Seattle WA), which analysed 730 selected genes pertaining to the immune response. Multi-dimensional scaling (MDS) analysis demonstrated that chemoradiotherapy (chemoRT) groups (chemoXRT + S and chemoSABR + S) clustered together and away from the non-irradiated groups (chemo + S and S), indicating a distinct radiation-induced immune-related gene expression profile (*Figure 4.3b*). Because the Nanostring panel only surveyed a select number of transcripts, testing of gene sets that were derived from whole transcriptomic data (such as MSigDB gene sets) was not performed to avoid selection bias. Instead, pathway analyses were performed using the in-built gene sets in the nSolver Advanced Analysis package, developed specifically for the Nanostring platform. In these analyses, both chemoRT groups demonstrated higher NK cell scores compared to non-irradiated groups (*Figure 4.3c*). The similarity in NK cell scores following either conventionally fractionated RT or SABR corroborated the pre-clinical observations above that radiation BED, not DPF, was the key dose-fractionation parameter determining effective NK cell responses. Interestingly, no differences in T cell scores were detected between any treatment groups (*Figure 4.3d*).

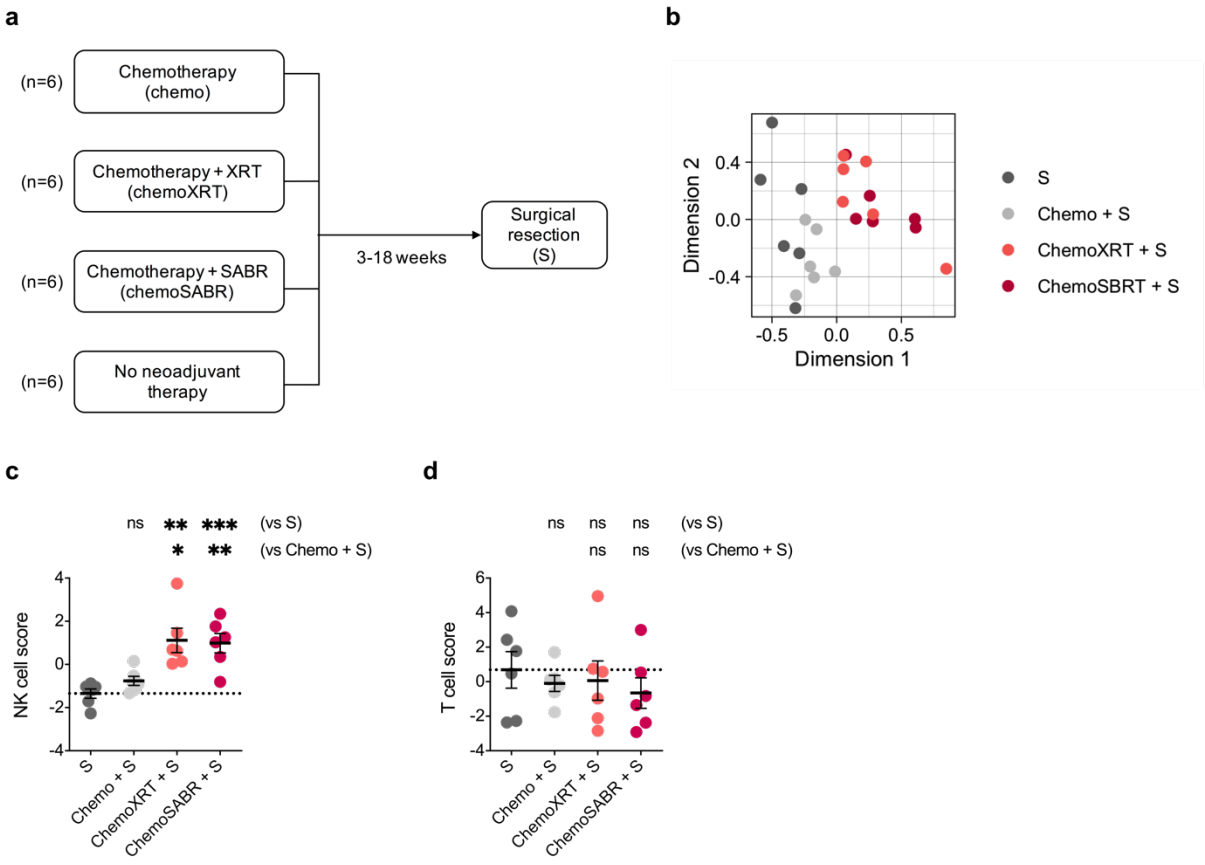

Figure 4.3. NK cell gene signatures are increased by RT in human pancreatic ductal adenocarcinoma cancers. a, Schematic of the GSE129492 study design. XRT: conventionally fractionated RT, 50Gy in 2Gy per fraction; SABR: stereotactic ablative body RT, average 45Gy in 5-9Gy per fraction. The chemotherapy regimen was folinic acid, 5-fluorouracil, irinotecan and oxaliplatin (FOLFORINOX). Gene expression profiles were generated using the PanCancer Immune Profiling Panel (Nanostring Inc., Seattle WA). **b,** MDS plot of samples by treatment modality. **c-d,** (**c**) NK cell and (**d**) T cell scores, presented relative to samples that received surgical resection only (the S group) (dotted line). Scores represent a weighted average of the gene expression values in the pathway of interest, calculated using the Pathway Scoring module in the nSolver Advanced Analysis package.

In the GSE15781 dataset, tumour specimens were collected from patients with rectal adenocarcinomas treated with neoadjuvant chemoRT prior to surgical resection, or with surgical resection alone (*Figure 4.4a*) (Snipstad *et al.*, 2010). The radiation regimen employed was 50Gy in 2Gy per fraction and concurrent chemotherapy was in the form of oral capecitabine. Surgery followed neoadjuvant therapy 4-6 weeks later. Thirteen tumours received surgery alone and nine tumours received neoadjuvant chemoRT with surgery. Gene expression profiling was performed using the Human Genome Survey Microarray 2.0 platform (Applied Biosystems Inc., USA). Tumours that received chemoRT prior to surgery demonstrated a distinct gene expression profile and were strongly enriched for NK cell activation, NK cell-mediated cytotoxicity, and T cell activation signatures compared to tumours that received surgery alone (*Figure 4.4b-d*). Because NK cells share many common transcripts with T cells, the enrichment of NK and T cell signatures might not be independent. To be confident that the enrichment of NK cell gene signatures was not confounded by T cell responses, a NK cell infiltration gene signature developed by Cursons *et. al* was used, which was curated from RNAseq data of sorted cell populations and single cells for specificity towards NK cells only (referred here as the "WEHI NK cell infiltration" gene set) (Cursons *et al.*, 2019). Tumours that received chemoRT prior to surgery showed higher expression of genes in this NK cell-specific gene set compared to tumours that received surgery alone, with a statistically significant enrichment of the gene set on Gene Set Enrichment Analysis (GSEA) (*Figure 4.4e-f*).

Collectively, these human cancer datasets re-affirm the importance of the BED parameter for the induction of tumour-associated NK cell responses by radiation, and importantly validate the pre-clinical approach used to study of the immunological effects of RT.

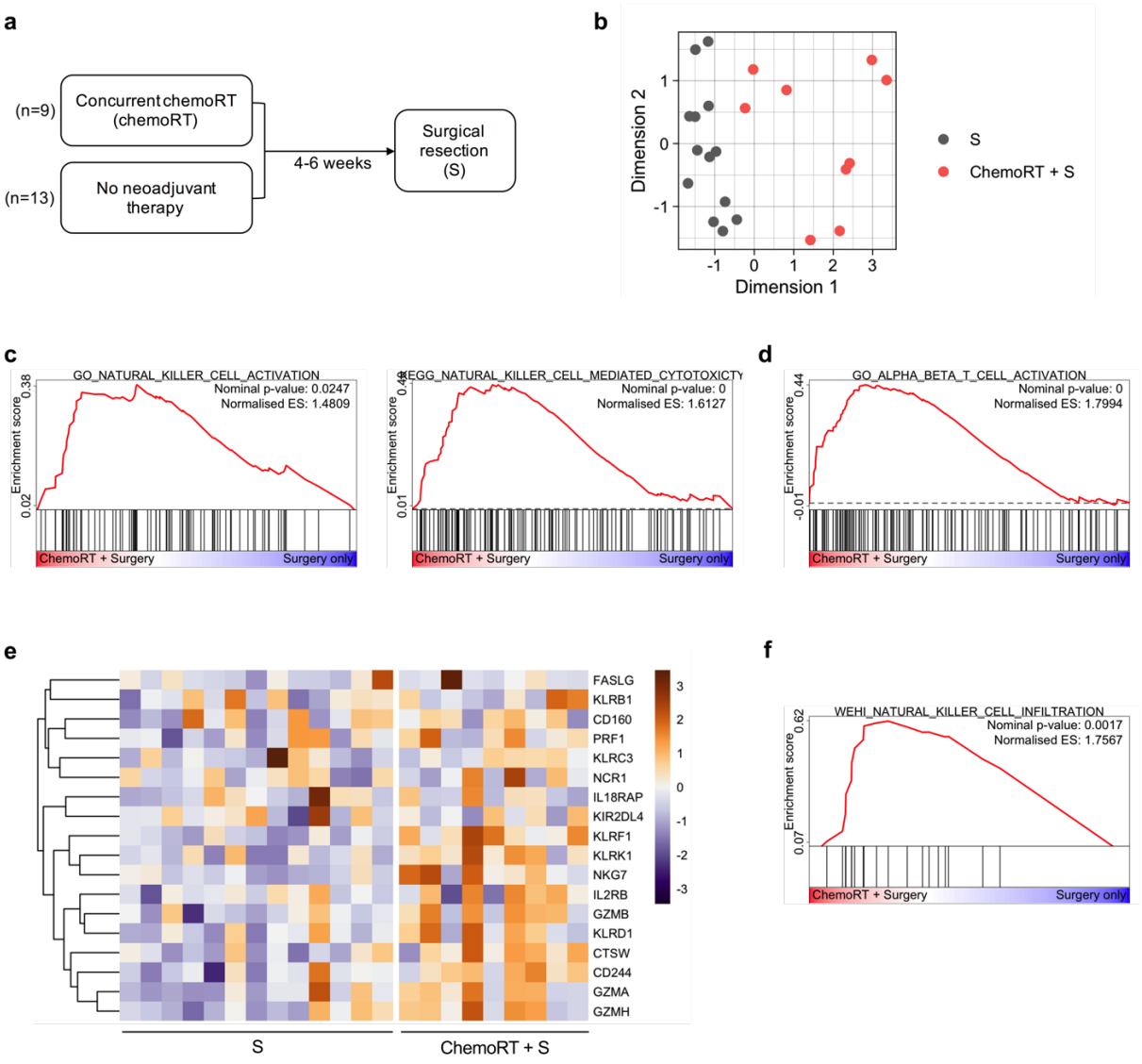

Figure 4.4. NK cell gene signatures are enriched by RT in human rectal adenocarcinomas. a, Schematic of the GSE15781 dataset study design. RT was given in a conventionally fractionated regimen, 50Gy in 2Gy per fraction. Chemotherapy was in the form of oral capecitabine**.** Gene expression profiling was performed using the Human Genome Survey Microarray 2.0 platform (Applied Biosystems Inc., USA). **b,** MDS plot of samples by treatment modality. **c, d & f,** Gene Set Enrichment Analysis (GSEA) plots of NK cell activation (Gene Ontology-Biological Processes, GO-BP), NK cell-mediated cytotoxicity (KEGG), αβ T cell activation (GO-BP) and WEHI NK cell infiltration gene sets. Tumours that received chemoRT and surgery (the chemoRT + S group) were compared to tumours that received surgery only (the S group). **e,** Expression of genes in the WEHI NK cell infiltration gene set in the chemoRT + S and S tumours. The WEHI NK cell infiltration gene set was curated for specificity towards NK cells.

2. Tumour-associated NK cells in the early post irradiation phase are suppressed by Tregs

To investigate why radiation BED was important for the induction of NK cell responses, the impact of radiation dose-fractionation on NK cells in AT3-OVA tumours was examined. Tumours were harvested and processed for flow cytometry at days 1, 3, 5, 7, 9 and 13 post completion of RT using the 3x4Gy and 1x20Gy regimens as representative low and high BED regimens, respectively. Both regimens induced a similar enrichment of tumour-associated NK cells within the first 9 days post RT, relative to that observed in mock-irradiated tumours (*Figure 4.5a, left panel*). Interestingly, the dynamics of this response closely resembled that of radiation-induced Treg responses, with their peaks aligning at days 5-7 post completion of RT (*Figure 4.5a, right panel*). Therefore, the concurrent suppression of NK cells by Tregs in 3x4Gy and 1x20Gy-irradiated tumours may account for the lack of induction in NK cell granzyme B levels over mock-irradiated tumours at day 5 post RT (*Figure 4.5b*). To confirm if radiation-induced Treg responses were restricting the anti-tumour function of NK cells, AT3-OVA tumour-bearing mice were depleted of radiation-induced Tregs using the 9H10 anti-CTLA-4 antibody (as described in Chapter 3, *Figure 3.13a*) together with depletion of NK cells. The therapeutic synergy of RT and 9H10 anti-CTLA-4 antibody-mediated depletion of Tregs was lost in mice that were concurrently depleted of NK cells (*Figure 4.6a*), highlighting that Treg suppression of NK cell function prevented long-term NK cell-mediated control of irradiated AT3-OVA tumours, irrespective of the radiation dose-fractionation employed. Notably, the divergence in the growth rate of NK cell-depleted and non-depleted irradiated tumours occurred at day 10-15 post RT (*Figure 4.6a*), in contrast to the non-Treg-depleted setting, in which the divergence between the NK cell-depleted and non-depleted 1x20Gy-irradiated tumours occurred at days 20-25 post RT (*Figure 4.1c*). Together, these data suggest that Treg depletion unleashed the anti-tumour activity of NK cell responses early in the post irradiation phase. Consistent with this, while Treg depletion did not alter the number of NK cells in 3x4Gy and 1x20Gy-irradiated AT3-OVA tumours at day 5 post RT (*Figure 4.6b*), it did heighten their intracellular granzyme B levels (*Figure 4.6c*). The suppression of NK cell function by Tregs following RT may explain why MC38 tumours, which did not demonstrate radiation-induced Treg responses (*Figure 3.20c*), were highly sensitive to NK cell-mediated tumour control following 1x20Gy irradiation (*Figure 4.2*).

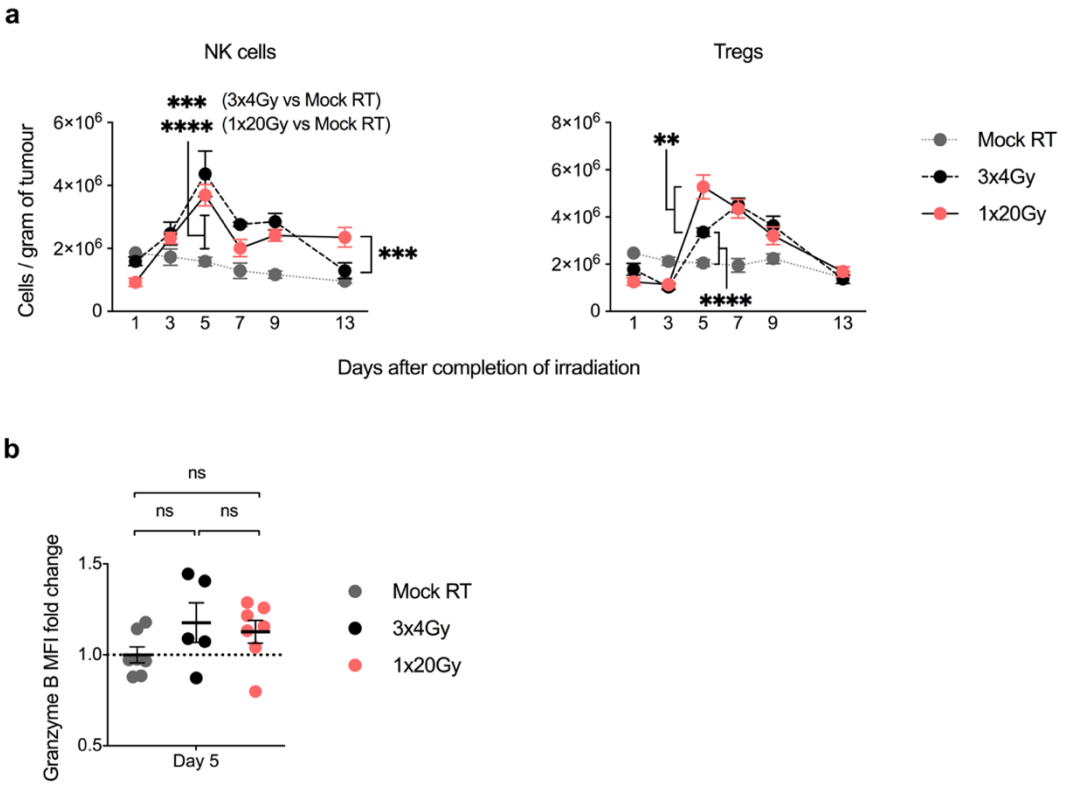

Figure 4.5. RT induces the enrichment of NK cells in AT3-OVA tumours but not their cytotoxic potential, regardless of dose-fractionation. AT3-OVA tumours were irradiated at 25-35mm^2 and harvested at time points that were aligned to post completion of RT for flow cytometric analysis. **a,** Absolute numbers of tumour-associated NK cells (CD45$^+$ TCRβ$^-$ NK1.1$^+$) and Tregs (CD45$^+$ TCRβ$^+$ CD4$^+$ Foxp3$^+$). *n*=4-17 tumours per group, combined from 4 independent experiments. The data for tumour-associated Tregs was reproduced from *Figure 3.7a* for comparison here. Data presented as mean ± SEM. **b,** Granzyme B expression in tumour-associated NK cells at day 5 post completion of RT, presented as fold change in MFI relative to mock-irradiated controls (dotted line). Data is combined from 2 independent experiments. *ns: non-significant, *** p<0.001*

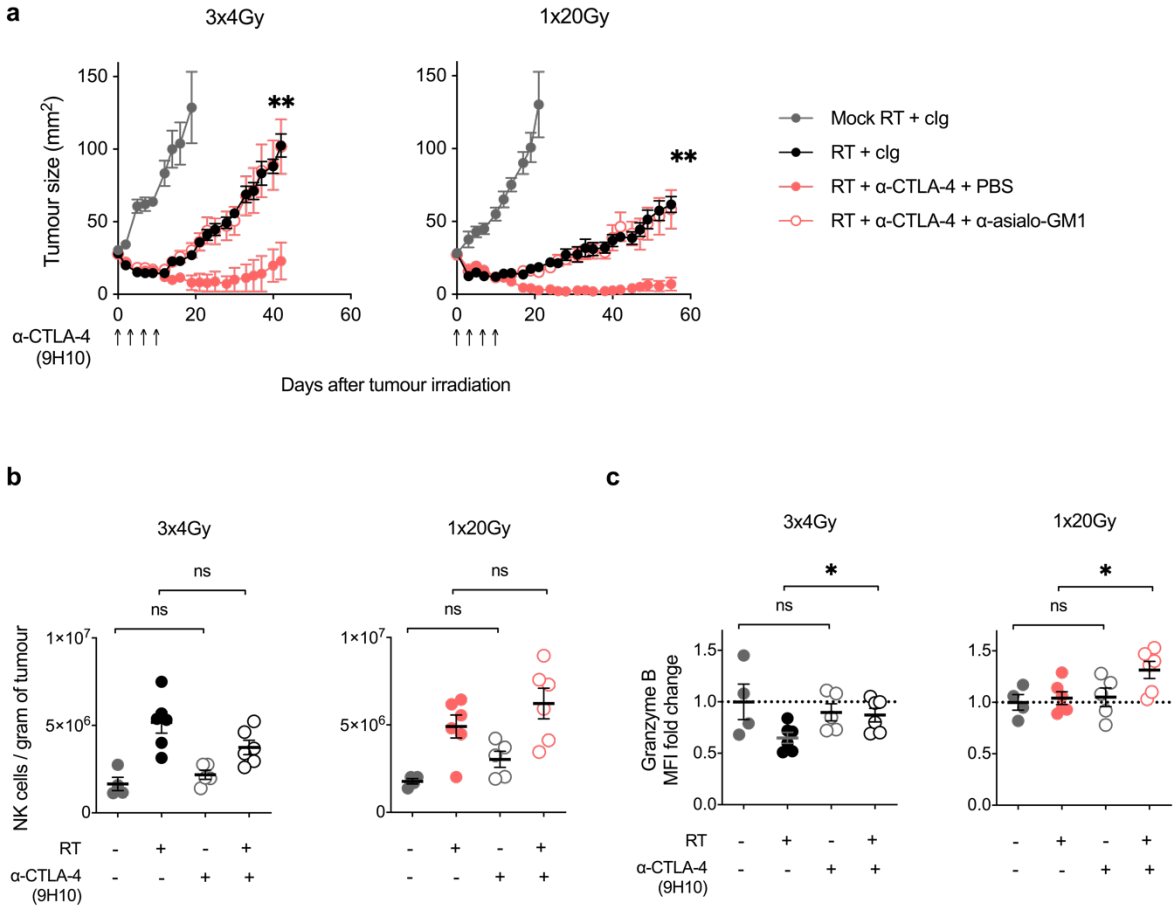

Figure 4.6. Radiation-induced Treg responses suppress the function of NK cells in AT3-OVA tumours. a, AT3-OVA tumour growth post RT in mice treated with 9H10 anti-CTLA-4 and anti-asialo-GM1 antibodies, or with control isotype antibodies or PBS. 9H10 anti-CTLA-4 or isotype control antibodies were administered every 4 days from start of irradiation, for a total of 4 total injections. Anti-asialoGM1 antibodies or PBS were administered every 3 days from start of RT to end of experiment. Arrows indicate the time of antibody treatment. Statistical comparisons were made between the RT + anti-CTLA-4 + cIg and RT + anti-CTLA-4 + anti-asialo-GM1 groups. *n*=5 per group, representative of 2 independent experiments. This experiment was performed simultaneously with the experiment in *Fig 3.15a*, using the same control mice. Data is presented as mean ± SEM. **b & c,** Flow cytometric analysis of (**b**) absolute NK cell numbers and (**c**) granzyme B expression in NK cells in mock, 3x4Gy or 1x20Gy-irradiated AT3-OVA tumours at day 5 post RT, harvested from mice treated with 9H10 anti-CTLA4 or isotype control antibodies. Granzyme B expression in (**c**) is presented as fold change in MFI relative to mock-irradiated controls (dotted line) is presented. 9H10 anti-CTLA-4 antibodies were administered every 4 days from start of RT for a total of 2 injections. Data is representative of 1 experiment. *MFI: mean fluorescence intensity, ns: non-significant, * p<0.05, ** p<0.01*

3. High BED radiation supports sustained tumour-associated NK cell responses

The divergence in the growth kinetics of NK cell-depleted and non-depleted AT3-OVA tumours at day 20-25 post 1x20Gy irradiation (*Figure 4.1c*) suggests that late, rather than early, NK cell responses following high BED radiation were exerting anti-tumour effects. Indeed, NK cells remained enriched in 1x20Gy-irradiated tumours at day 13 post RT compared to both 3x4Gy and mock-irradiated tumours (*Fig 4.5a, left panel*). Higher numbers of NK cells, but not of T cell subsets, continued to be detectable out to day 21 post RT in 1x20Gy-irradiated tumours compared to mock-irradiated tumours, although the increase had diminished at this point (*Figure 4.7a*). Given that radiation-induced Treg responses had completely subsided by day 13 (*Figure 4.5a, right panel*), it is possible that late-phase NK cell responses generated by high BED regimens were controlling AT3-OVA tumours at this point. In support of this, elevated surface expression of the activation markers NKG2D, NKG2A, NKp46, DNAM1 and intracellular levels of IFN-γ were detected in tumour-associated NK cells at day 13 post 1x20Gy irradiation, compared to that observed with 3x4Gy and mock irradiation (*Figure 4.7b*). Intriguingly, elevated intracellular IFN-γ levels were detected exclusively in NK cells and not in T cells at this time point (*Figure 4.7b-c*), suggesting that NK cells were the principal source of tumour-associated IFN-γ in the late phase following irradiation with high BED regimens. Validating these findings, NK cell activation and NK cell-mediated cytotoxicity gene signatures were enriched within the immune ($CD45^+$) compartment of AT3-OVA tumours at day 5 post irradiation with both 3x4Gy and 1x20Gy regimens compared to their respective mock-irradiated controls, but only the immune compartment of 1x20Gy-irradiated tumours continued to show enrichment of these signatures at day 13 (*Figure 4.7d*). However, most striking was the difference in selective enrichment of the IFN-γ production gene signature between the two regimens. At day 5, this signature was enriched in the immune compartment of 3x4Gy-irradiated but not 1x20Gy-irradiated tumours, but this pattern was reversed at day 13, when it was enriched in the immune compartment of 1x20Gy-irradiated but not 3x4Gy-irradiated tumours (*Figure 4.7d*). Altogether, these findings suggest that distinctions in the tumour immune microenvironment occurring in the late post irradiation phase, but not earlier, underpinned the capacity of high BED regimens to support effective anti-tumour NK cell responses.

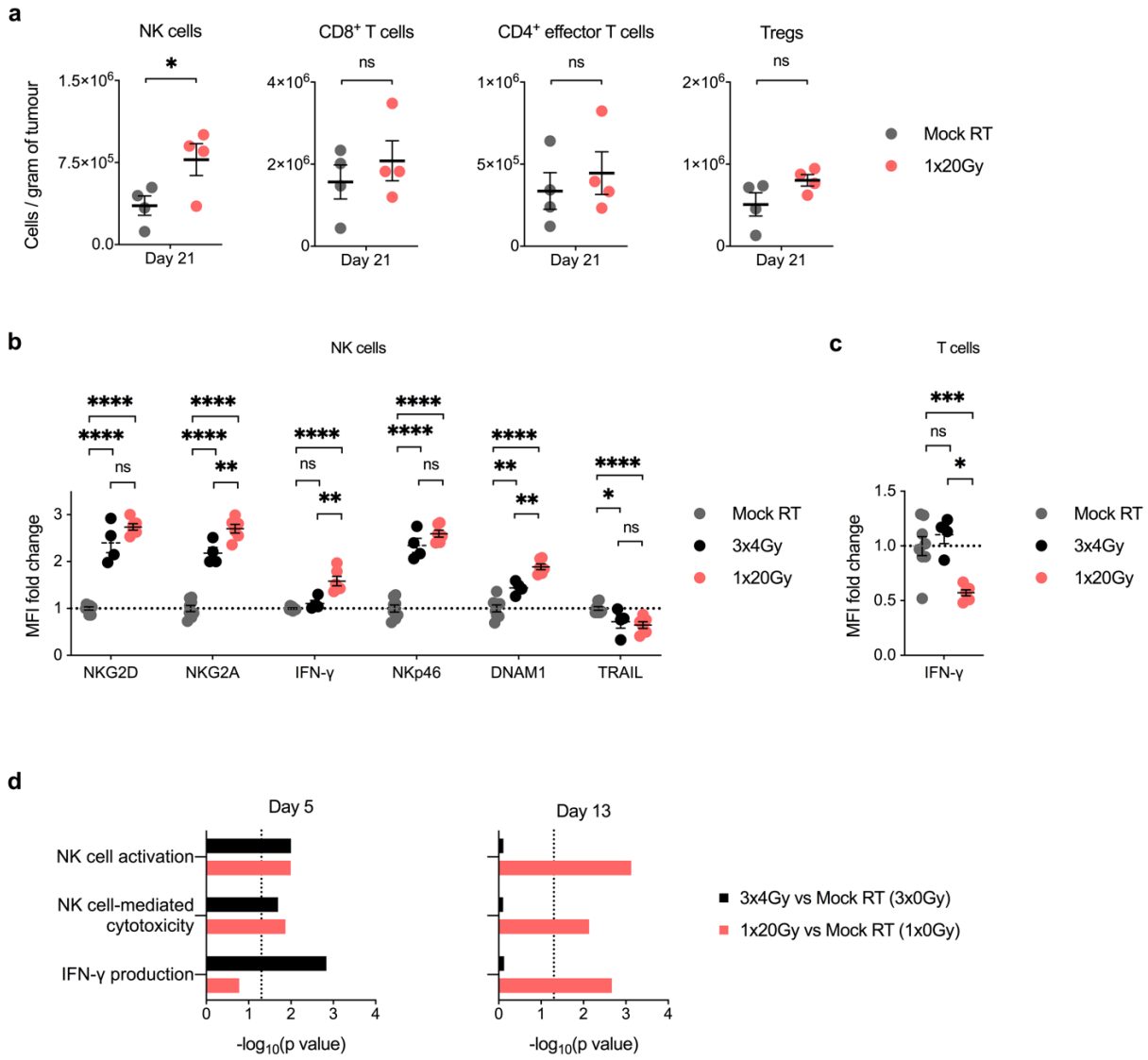

Figure 4.7. High BED radiation regimens promote sustained NK cell function and IFN-γ signalling in AT3-OVA tumours. AT3-OVA tumours were irradiated at 25-35mm^2 and harvested at time points that were aligned to post completion of RT for (**a-c**) flow cytometric analysis or (**d**) RNAseq. **a,** Absolute numbers of tumour-associated NK cells, CD8$^+$, CD4$^+$ effector T cells and Tregs at day 21 post 1x20Gy irradiation. Data is representative of 1 experiment. **b & c,** Expression of (**b**) functional activation and cytotoxic markers on NK cells and (**c**) intracellular IFN-γ levels in T cells (TCRβ$^+$ cells) at day 13 post completion of RT, presented as fold change in MFI relative to mock-irradiated controls (dotted line). Data is representative of 1 experiment. **d,** NK cell activation (GO-BP), NK cell-mediated cytotoxicity (KEGG), and IFN-γ production (GO-BP) gene set testing in the immune compartment of 3x4Gy and 1x20Gy-irradiated AT3-OVA tumours at days 5 and 13 post RT, compared to their respective mock-irradiated controls. Samples were processed for RNAseq as described in *Figure 3.10a*. Analysis was performed using Rotational Gene Set Testing (ROAST). Dotted line represents $p<0.05$. *ns: non-significant, * $p<0.05$, ** $p<0.01$, *** $p<0.001$, **** $p<0.0001$*

4. CXCR3 signalling does not underpin the impact of radiation BED on NK cell responses

Given the strong IFN-γ production gene signature detected within the immune compartment of 1x20Gy-irradiated tumours at day 13 post RT, the role of IFN-γ signalling in sustaining radiation-induced NK cell responses was next examined. CXCR3 is a chemokine receptor that binds to the IFN-γ-inducible chemokines CXCL9, CXCL10, and CXCL11, playing an instrumental role in directing immune recruitment into inflamed tissues sites (Lacotte *et al.*, 2009). Differential gene expression analysis by RNAseq identified *Cxcr3* as the only chemokine receptor gene to be upregulated in the immune compartment of AT3-OVA tumours at both days 5 and 13 post 1x20Gy irradiation (*Figure 4.8*). By contrast, modulation of CXCR3 gene expression was not detected in 3x4Gy-irradiated tumours (*Figure 4.8*). To test the importance of CXCR3 signalling for the recruitment of NK cells into 1x20Gy-irradiated tumours, AT3-OVA tumour-bearing mice were injected with anti-CXCR3 blocking antibodies at the time of RT and every 3 days thereafter. CXCR3 blockade even without RT reduced the numbers of tumour-associated $CD4^+$ T effector cells, Tregs and NK cells (*Figure 4.9a*). In the context of 1x20Gy irradiation, the most profound effects of CXCR3 blockade were in the reduction of tumour-associated $CD4^+$ T effector and NK cells (*Figure 4.9a*). However, it is noteworthy that the proportions of T and NK cell subsets within the lymphocyte population were largely unaffected by CXCR3 blockade. Counterintuitively, despite the general reduction in tumour-associated immune cell numbers caused by CXCR3 blockade, no effect on the control of AT3-OVA tumours following either mock or 1x20Gy irradiation was observed (*Figure 4.9b*). As both effector T and NK cells in AT3-OVA tumours were sensitive to Treg control, it is possible that the parallel reduction in Treg numbers within the tumour could have sufficiently potentiated the anti-tumour activity of local residual immune effector cells, although this needs to be further investigated. Overall, while these findings highlight a critical role for the CXCR3 receptor in promoting the general homing of T and NK cells into tumours, it is unlikely that CXCR3 signalling significantly influenced the differential ability of high and low BED radiation regimens to evoke anti-tumour NK cell responses. Other cytokine receptors relevant to NK cell trafficking and function such as CXCR6 and IL-18 also had their respective transcripts elevated in the immune compartment of AT3-OVA tumours at day 13 post 1x20Gy irradiation, which offer alternate avenues for ongoing investigation (Dinarello *et al.*, 2013; Yoon *et al.*, 2016) (*Figure 4.8*).

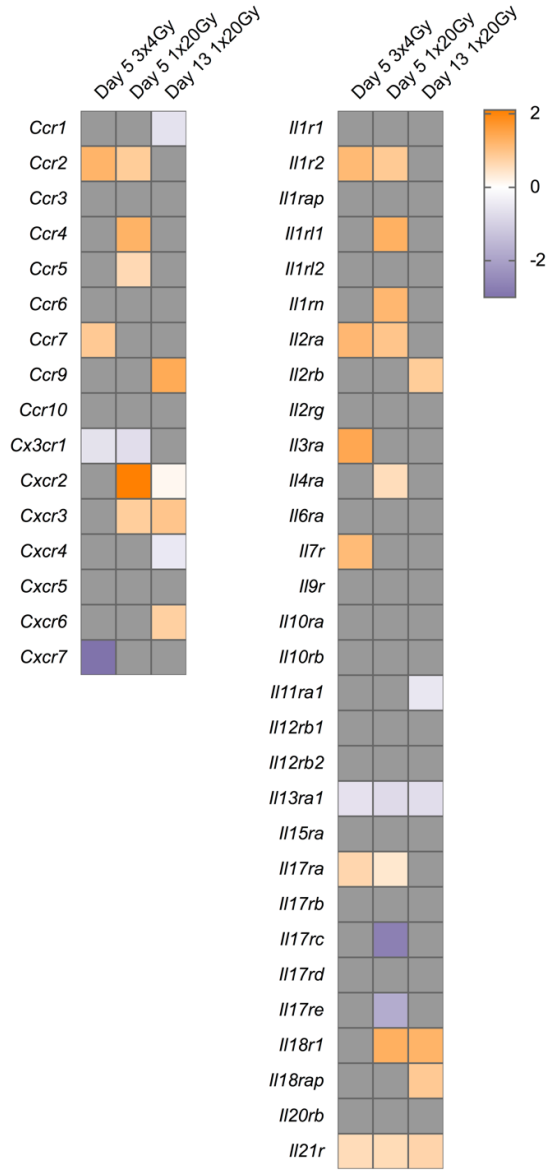

Figure 4.8. Expression of cytokine receptor transcripts in immune cells after irradiation. a, Heat map of differentially expressed genes for chemokine and interleukin receptors in the immune compartment of 3x4Gy and 1x20Gy-irradiated AT3-OVA tumours, compared to their respective mock-irradiated controls. Log_2-fold change in expression with adjusted $p<0.1$ is expressed. Grey squares represent non-significant modulation. Samples were processed for RNAseq as described in *Figure 3.10a*. Essentially, AT3-OVA tumours were irradiated and harvested at time points that were aligned to post completion of RT. Mock-irradiated tumours from mice anaesthetised as per their irradiated counterparts (3x0Gy and 1x0Gy) were used as controls. $CD45^+$ cells were flow-sorted from single cell AT3-OVA tumour suspensions and processed for RNAseq analysis. n=4-6 tumours per group.

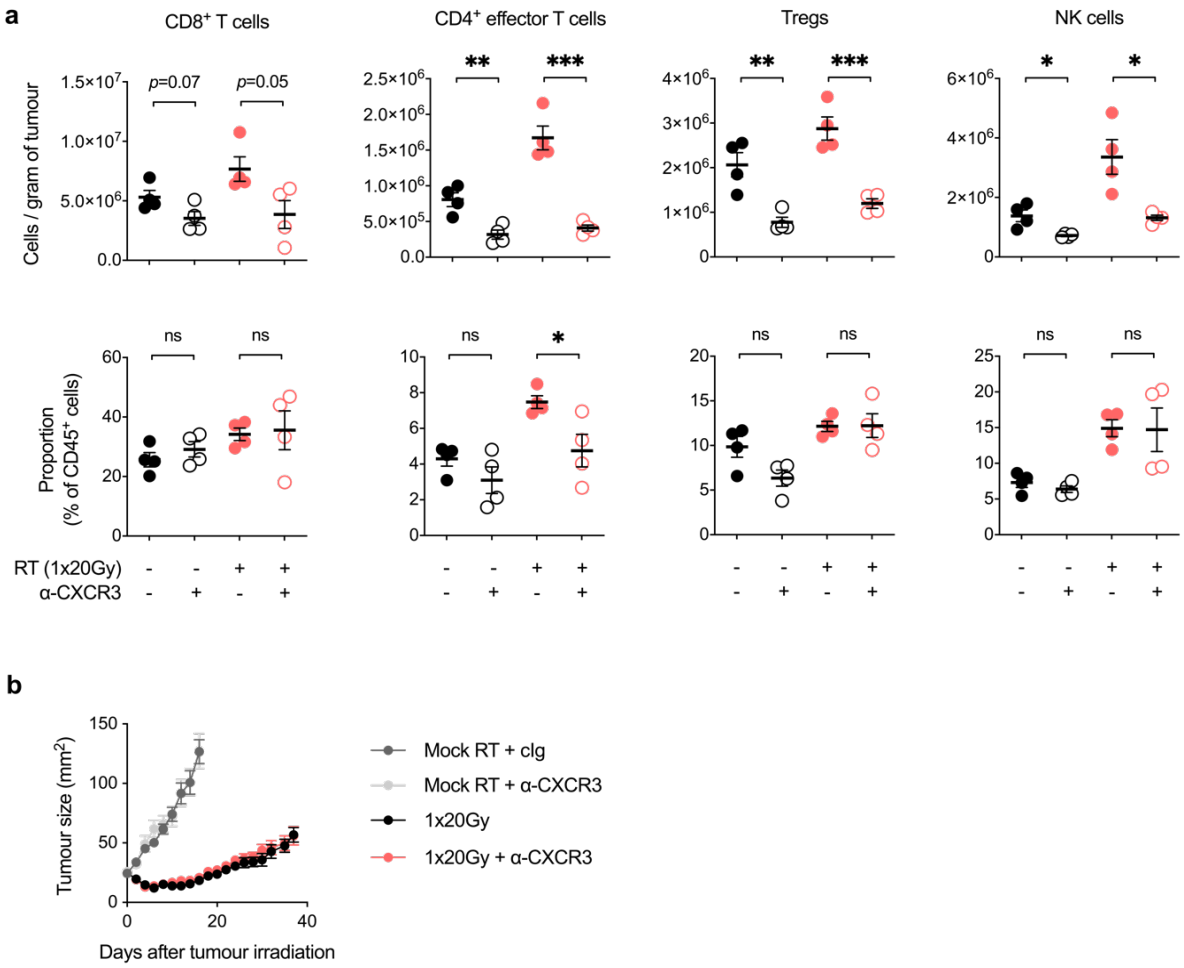

Figure 4.9. CXCR3 blockade results in widespread abrogation of tumour-infiltrating lymphocytes but does not affect tumour control by 1x20Gy irradiation. a, Flow cytometry analysis of absolute numbers and relative frequencies of $CD8^+$, $CD4^+$ effector T cells, Tregs and NK cells in mock or 1x20Gy-irradiated AT3-OVA tumours at day 13 post RT, harvested from mice treated with anti-CXCR3 or isotype control antibodies. Anti-CXCR3 or isotype control antibodies (150µg/mouse) were administered every 3 days from start of RT to end of experiment. Data is representative of 1 experiment. **b,** AT3-OVA tumour growth post 1x20Gy irradiation in mice treated with anti-CXCR3 or isotype control antibodies, administered every 3 days from start of RT to end of experiment. *n*=5-6 mice per group, representative of 1 experiment. Data is presented as mean ± SEM. *ns: non-significant, * p<0.05, ** p<0.01, *** p<0.001*

5. High BED radiation does not alter tumour and stromal cell susceptibility to killing by NK cells

To demonstrate whether radiation-induced changes in the susceptibility of tumour and/or stromal cells to NK cell killing could contribute to the persistence of NK cell responses following high BED irradiation, *in vitro* 24-hour 51-chromium (^{51}Cr) release killing assays involving the co-culture of IL-2 activated NK cells with irradiated tumour or stromal cells were employed. Although AT3-OVA cells were susceptible to killing by NK cells (demonstrating specific lysis rates proportional to the concentration of NK cells in culture), the percentage of tumour cell kill by NK cells was not increased following 3x4Gy or 1x20Gy irradiation (*Figure 4.10a*). Next, primary cancer-associated fibroblasts (CAFs), which form a major component of the tumour stroma (Kalluri, 2016), were isolated *ex vivo* from unirradiated AT3-OVA tumours as representative stromal cells. The CAFs were irradiated and subjected to a similar ^{51}Cr release killing assay. Radiation also did not alter the susceptibility of CAFs to NK cell killing (*Figure 4.10b*).

It is possible that high BED regimens, by causing greater cell kill and release of larger amounts of tumour-associated antigens, could lead to increased production of tumour cell-reactive antibodies by humoral immune responses, which upon binding to tumour cells increased their vulnerability to NK cell killing by ADCC. To test this hypothesis, serum was collected from AT3-OVA tumour-bearing mice at day 0 (just prior to RT) and day 13 post 1x20Gy irradiation and titrated onto cultured AT3-OVA tumour cells *in vitro*. A fluorescently-labelled antibody, reactive to mouse IgG, was used to confirm the presence of tumour cell-reactive antibodies. The proportion of cells with positive staining was quantified by flow cytometry across a range of serum dilutions, which showed an expected concentration-dependent response (*Figure 4.11a*). Compared to non-tumour bearing mice (normal mouse serum, NMS), tumour-bearing mice (day 0 mouse serum) developed tumour cell-reactive antibodies with a titre increase of about 33-fold, consistent with the highly immunogenic status of the AT3-OVA tumour cell line (*Figure 4.11b*). Between days 0 and 13 post RT, there was only an approximately 2-fold increase in antibody titre (*Figure 4.11b*), suggesting that tumour irradiation had not significantly generated further tumour cell-reactive antibodies during this interval. This small increase was unlikely to have mediated a biologically-significant ADCC effect. To confirm this, tumour-bearing mice were treated with anti-Fc receptor (FcR) blocking antibodies from day 10 post 1x20Gy irradiation to disrupt the ADCC process. No effect of FcR blockade on tumour control following RT was detected (*Figure 4.11c*), indicating that ADCC was likely not a critical player in the supporting radiation BED-dependent NK cell responses.

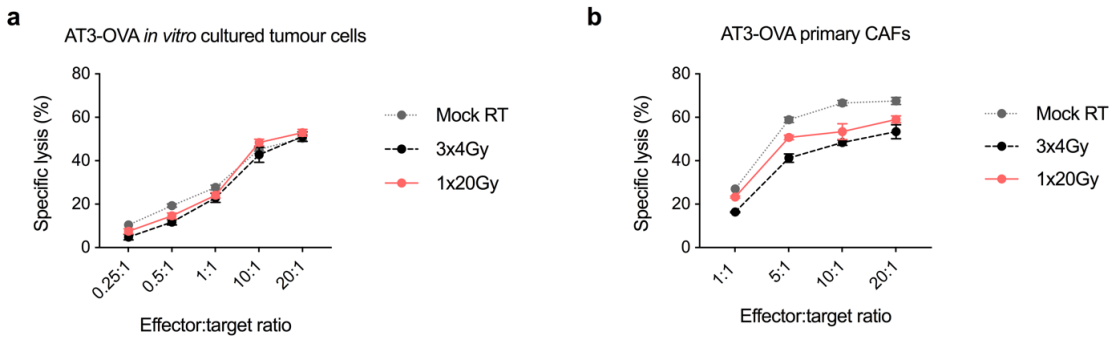

Figure 4.10. Tumour and stromal cells are not sensitised by irradiation for NK cell-mediated killing. **a & b,** Specific killing of *in vitro* irradiated (**a**) AT3-OVA tumour cells and (**b**) primary AT3-OVA cancer-associated fibroblasts (CAFs) by IL-2 activated NK cells, as determined by a 24-hour 51-chromium (^{51}Cr) release assay. AT3-OVA CAFs were isolated from *ex vivo* unirradiated AT3-OVA tumours. Both cell types were co-cultured with NK cells 48 hours after completion of irradiation. (**a**) *n*=11-22 replicates per group combined from 3-4 independent experiments, (**b**) n=3 replicates per group, representative of 1 experiment. Data points represent mean ± SEM.

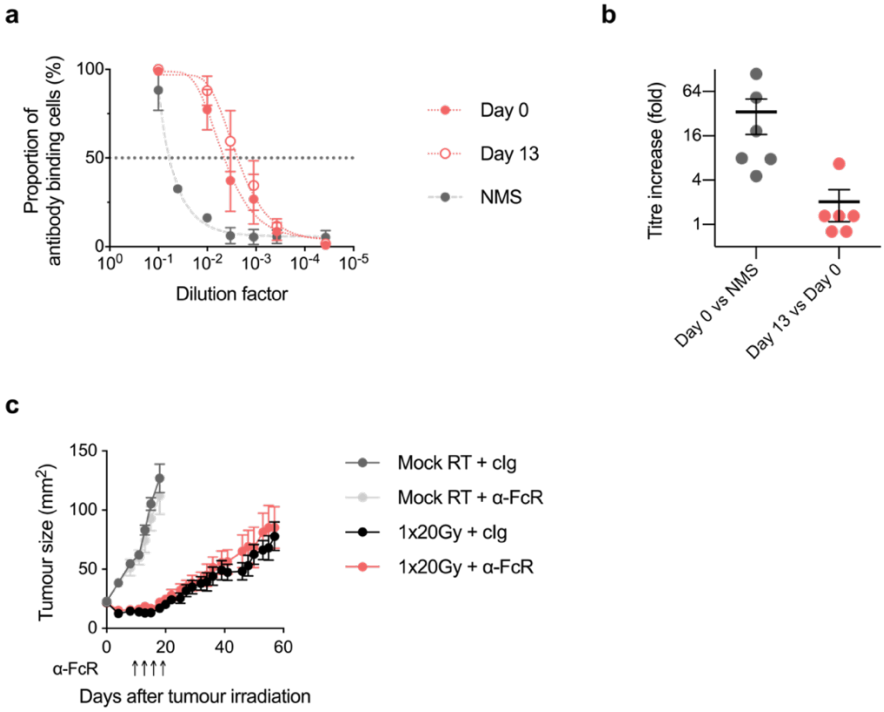

Figure 4.11. ADCC does not contribute to the immune-mediated control of irradiated AT3-OVA tumours. a & b, (**a**) Flow cytometric detection of AT3-OVA tumour cell-reactive antibodies in the serum of mice. Serum was bled from tumour-bearing mice on the day of (day 0) and on day 13 post 1x20Gy irradiation. Serum from non-tumour bearing mice (normal mouse serum, NMS) was used as a control. Collected serum samples were serially diluted onto cultured AT3-OVA tumour cells *in vitro*. A fluorescently-labelled antibody reactive against mouse IgG was used to detect levels of cell-bound mouse antibody. The serum dilution at which 50% of tumour cells were coated with mouse antibodies was used a comparative measure of antibody titre between groups. *n*=6 mice per group, each sample was run in replicate. Data is presented as mean proportion of antibody-bound tumour cells per serum dilution factor ± SEM. (**b**) Re-representation of data in (**a**) showing fold change in serum antibody levels in response to AT3-OVA tumour inoculation (Day 0 vs NMS samples) and 1x20Gy irradiation (Day 13 vs Day 0 samples). **c,** AT3-OVA tumour growth post 1x20Gy irradiation in mice treated with anti-Fc receptor (FcR) blocking or isotype control antibodies Fc receptor. Anti-FcR and control antibodies (200µg/mouse for the first injection, 150 µg/mouse thereafter) were administered every 3 days from day 10 post RT, for a total of 4 injections. Data is presented as mean ± SEM.

6. Radiation dose-fractionation effects on the expression of NK cell-activating and inhibitory ligands *in vivo*

The effects of high and low BED irradiation on the expression of NK cell-activating and inhibitory ligands in AT3-OVA tumours grown in mice were next examined as a possible factor underpinning the differential NK cell responses generated. For this analysis, attempts were made to use the GFP expression of AT3-OVA tumour cells to differentiate between tumour and stromal cells in *ex vivo* tumours. However, the GFP marker proved unreliable due to variable loss of GFP expression in developing AT3-OVA tumours *in vivo* over time, even without RT (*Appendix Figure 4*). Thus, while GFP^+ cells were certainly AT3-OVA tumour cells, GFP^- cells were likely a composite of tumour and stromal cells. To avoid introducing biases, all non-lymphocytes regardless of GFP expression status ($CD45^-GFP^{\pm}$) were analysed as a group, referred hereon as tumour/stromal cells.

At day 2 post RT, increased surface expression of the NK cell-activating ligands RAE1 and CD155 relative to mock-irradiated controls were most pronounced on tumour/stromal cells in 1x20Gy-irradiated tumours (*Figure 4.12a*), which may reflect a greater DNA damage response in these tumours (Gasser *et al.*, 2005; Martinet and Smyth, 2015). However, by day 13, expression of these ligands in 1x20Gy-irradiated tumours dropped below that of the mock-irradiated group (*Figure 4.12b*). To determine if the reduction in expression was a result of preferential killing of RAE1-high and CD155-high cells by NK cells, irradiated tumours from mice that had been depleted of NK cells were examined *ex vivo*. Consistent with RAE1-high cells being targets of NK cell recognition and killing, cells expressing this ligand were modestly restored in the absence of NK cells (*Figure 4.12b*). However, CD155 expression levels remained unchanged. Curiously, H2-K^b and H2-D^b-expression was also rescued with NK cell depletion, which may reflect a "NK cell-helper" effect on $CD8^+$ T cell activity against MHC-I expressing cells. Alternatively, NK cell responses following 1x20Gy irradiation could have collaterally depleted targets of $CD8^+$ T cells, which may in part explain the restricted contribution of $CD8^+$ T cells to the anti-tumour efficacy of the 1x20Gy regimen. Examination of the other NK cell-activating ligands CD112, MULT1, H60 and Qa1 revealed either no staining or no significant modulation following 1x20Gy irradiation, irrespective of NK cell depletion. Therefore, among the NK cell-modulating ligands examined, only RAE1 emerged as a putative ligand involved in supporting radiation BED-dependent NK cell responses.

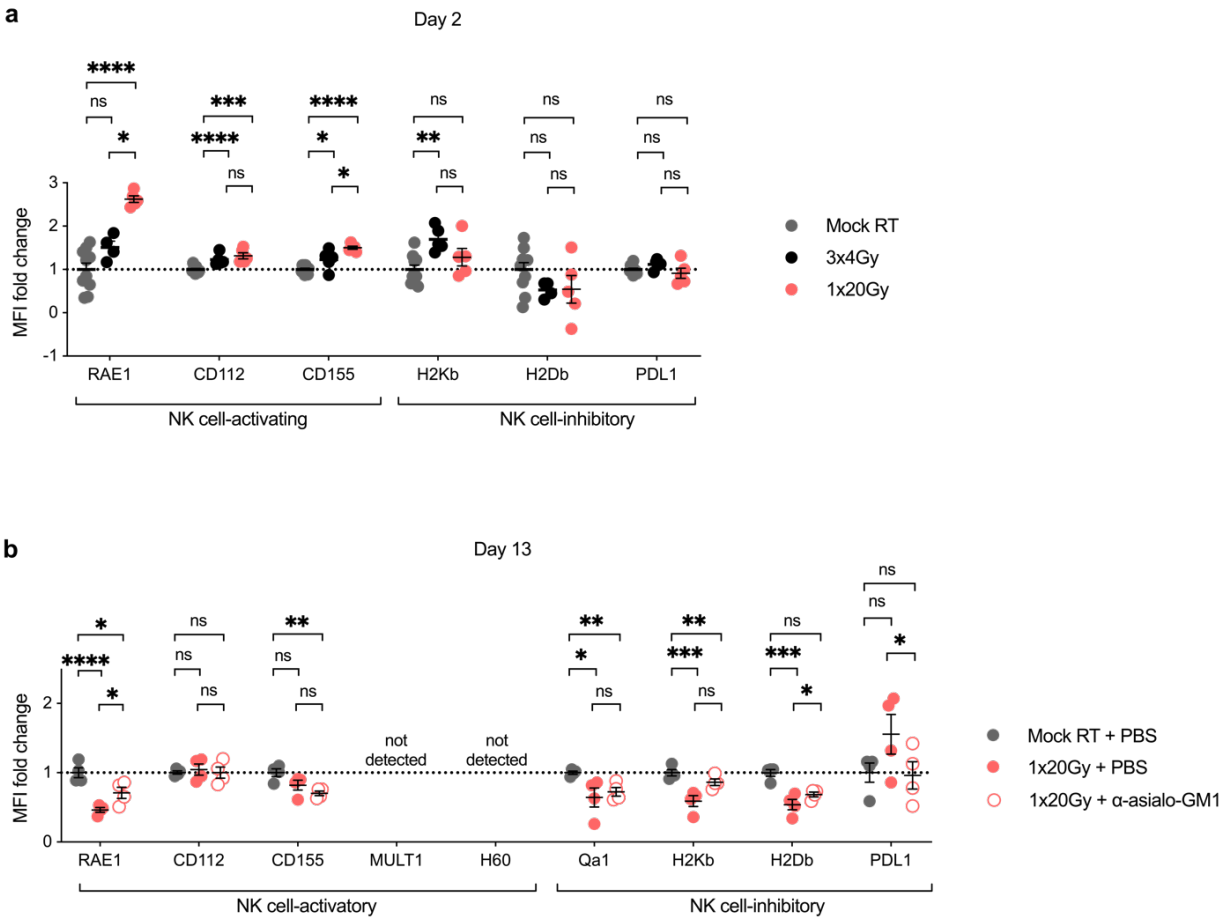

Figure 4.12. Radiation-induced modulation of NK cell-activating and inhibitory ligands *in vivo*. AT3-OVA tumours were irradiated at 25-35mm^2 and harvested at time points that were aligned to post completion of RT for flow cytometric analysis. **a,** Expression of RAE1, CD112, CD155, H2-K^b, H2-D^b and PD-L1 on tumour/stromal cells (CD45$^-$GFP$^\pm$) in tumours at day 2 post RT. Data is combined from 2 independent experiments. **b,** Expression of RAE1, CD112, CD155, MULT1, H60, Qa1, H2-K^b, H2-D^b and PD-L1 on tumour/stromal cells (CD45$^-$GFP$^\pm$) in tumours at day 13 post RT, harvested from mice treated with anti-asialoGM-1 or PBS, administered every 3 days from start of RT to end of experiment. Data is representative of 1 experiment. *ns: non-significant, * p<0.05, ** p<0.01, *** p<0.001, **** p<0.0001*

7. Transcriptional changes in tumour/stromal cells after radiation exposure

To investigate other biological processes that may drive sustained NK cell responses following high BED radiation, gene expression changes in the tumour/stromal compartment of AT3-OVA tumours grown in mice at day 5 and 13 post RT were examined by RNAseq. Although $CD45^-GFP^+$ and $CD45^-GFP^-$ cells were sorted apart from the tumours, extraction and sequencing of RNA from those samples were performed on the same days. Therefore, transcript counts could be concatenated to form a composite tumour/stromal cell group for analysis without being affected by batch effect issues. Since 3x4Gy-irradiated tumours were demonstrating escape from immune-mediated control and were entering an exponential growth phase at day 13 (*Figure 4.1c)*, sequencing of tumour/stromal cell RNA from that group was not performed.

Differential gene expression analysis of the tumour/stromal compartment of irradiated tumours revealed distinct transcriptional profiles compared to mock-irradiated tumours at day 5 and 13 (*Figure 4.13a*). Supporting the flow-based findings, there was no significant modulation in gene expression of NK cell-activating and NK cell-inhibitory ligands (*Figure 4.13b*). Examination of cytokine transcripts revealed that expression of *Csf1*, *Cxcl1*, *Cxcl2*, *Cxcl17* and *Il23a*, which encode for inflammatory cytokines that attract a range of immune subsets, were consistently upregulated in both irradiated groups at days 5 and 13 (*Figure 4.13c*). A small but statistically significant upregulation of *Il15* and *Il18* expression was seen at day 13 post 1x20Gy irradiation. Their gene products, IL-15 and IL-18, are notably important for the proliferation and function of NK cells (Guillerey *et al.*, 2016).

Gene set testing by GSEA revealed that enriched signatures were dominated by those relating to developmental processes (*Figure 4.14a*). The abundance of glandular and epithelial cell-related processes may reflect the mammary gland and epithelial origin of the AT3-OVA tumour cell line. These signatures, although interesting, likely bore little relevance to NK cell activity. Because GSEA is a sensitive test designed to detect potentially small but coordinated changes in a set of related genes, the abundance of overlapping significant hits was an impediment for hypothesis discovery. To narrow down the terms returned, only dominant differentially expressed genes that met a specific threshold (adjusted p value of < 0.05 and $\log_2$-fold change of > 1) were tested for over-represented Gene Ontology-Biological Processes (GO-BP) terms. As expected, many of the same terms relating to developmental processes remained significant, but other terms of interest could now be appreciated on this stricter analysis (*Figure 4.14b*). In particular, response to type I IFN (IFN-α and β), cellular senescence, cell cycle checkpoint, regulation of IL-1β production, and leukocyte chemotaxis signatures were over-represented. These terms were potentially inter-

related and therefore hypothesis-generating, since type I IFN responses following genotoxic stress have been reported to promote senescence and the senescence-associated secretory phenotype (SASP) (Yu *et al.*, 2015), which could involve the release of IL-1β and CXCL1 (Lasry and Ben-Neriah, 2015) as well as increased NK cell surveillance and infiltration (Krizhanovsky *et al.*, 2008; Soriani *et al.*, 2009; Iannello *et al.*, 2013).

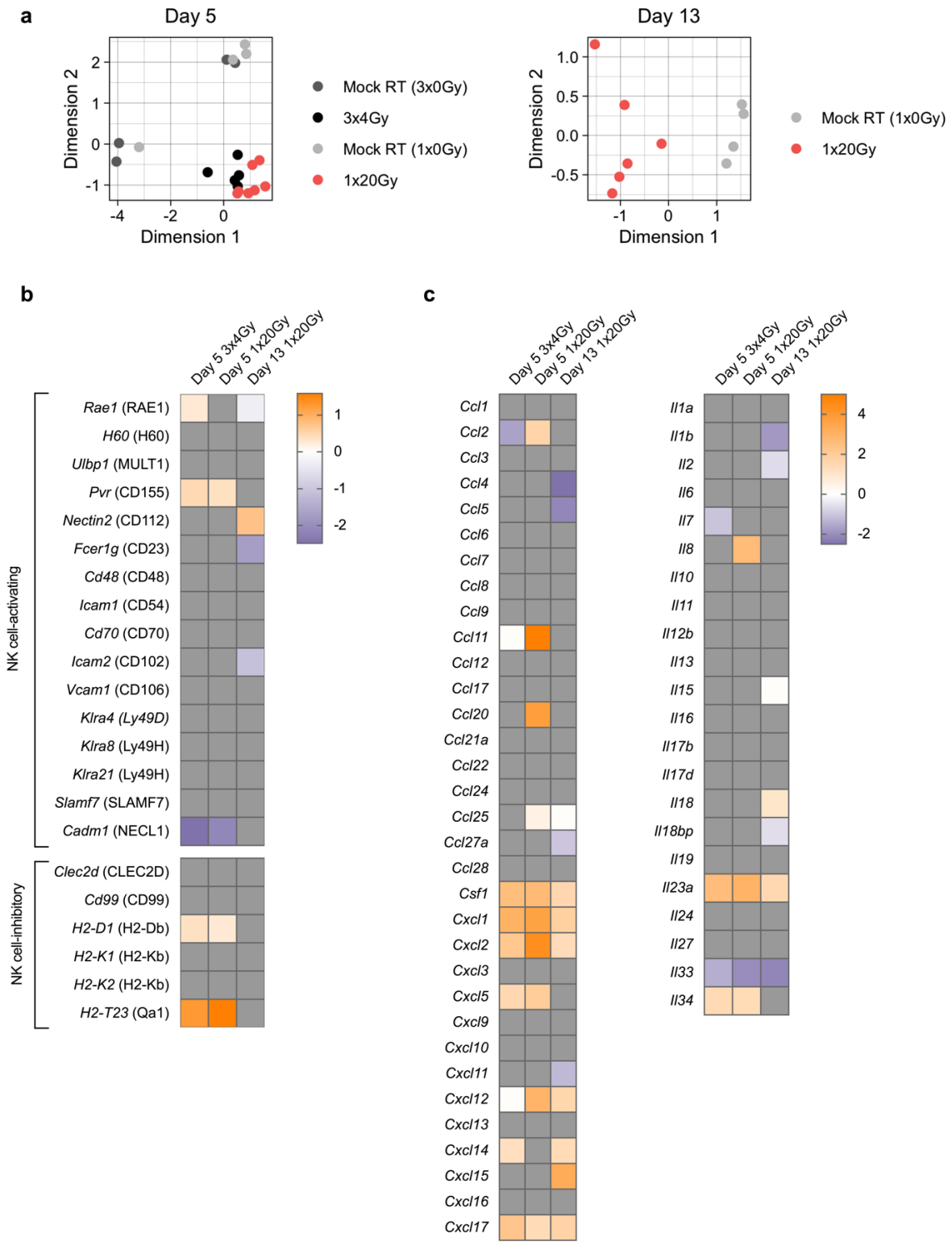
a
Day 5
Dimension 2
Dimension 1
Mock RT (3x0Gy)
3x4Gy
Mock RT (1x0Gy)
1x20Gy
Day 13
Dimension 2
Dimension 1
Mock RT (1x0Gy)
1x20Gy
b
Day 5 3x4Gy
Day 5 1x20Gy
Day 13 1x20Gy
NK cell-activating
Rae1 (RAE1)
H60 (H60)
Ulbp1 (MULT1)
Pvr (CD155)
Nectin2 (CD112)
Fcer1g (CD23)
Cd48 (CD48)
Icam1 (CD54)
Cd70 (CD70)
Icam2 (CD102)
Vcam1 (CD106)
Klra4 (Ly49D)
Klra8 (Ly49H)
Klra21 (Ly49H)
Slamf7 (SLAMF7)
Cadm1 (NECL1)
NK cell-inhibitory
Clec2d (CLEC2D)
Cd99 (CD99)
H2-D1 (H2-Db)
H2-K1 (H2-Kb)
H2-K2 (H2-Kb)
H2-T23 (Qa1)
c
Day 5 3x4Gy
Day 5 1x20Gy
Day 13 1x20Gy
Ccl1
Ccl2
Ccl3
Ccl4
Ccl5
Ccl6
Ccl7
Ccl8
Ccl9
Ccl11
Ccl12
Ccl17
Ccl20
Ccl21a
Ccl22
Ccl24
Ccl25
Ccl27a
Ccl28
Csf1
Cxcl1
Cxcl2
Cxcl3
Cxcl5
Cxcl9
Cxcl10
Cxcl11
Cxcl12
Cxcl13
Cxcl14
Cxcl15
Cxcl16
Cxcl17
Day 5 3x4Gy
Day 5 1x20Gy
Day 13 1x20Gy
Il1a
Il1b
Il2
Il6
Il7
Il8
Il10
Il11
Il12b
Il13
Il15
Il16
Il17b
Il17d
Il18
Il18bp
Il19
Il23a
Il24
Il27
Il33
Il34

Figure 4.13. Expression of NK cell-relevant ligand and cytokine transcripts in the tumour/stromal compartment of AT3-OVA tumours post RT. a, MDS plot of mock-irradiated (3x0Gy and 1x0Gy) and irradiated (3x4Gy and 1x20Gy) tumour/stromal RNAseq samples at days 5 and 13 post completion of RT. Samples were processed for RNAseq as described in *Figure 3.10a*. Essentially, AT3-OVA tumours were irradiated and harvested at time points that were aligned to post completion of RT. Tumour/stromal cells ($CD45^{-}GFP^{\pm}$ cells) were flow-sorted from single cell AT3-OVA tumour suspensions and processed for RNAseq analysis. n=4-6 tumours per group. **b & c,** Heat map of differentially expressed genes for (**b**) NK cell-activating and inhibitory ligands (parentheses denote corresponding protein name) and (**c**) chemokines and interleukins in the tumour/stromal compartment of 3x4Gy and 1x20Gy-irradiated AT3-OVA tumours, compared to their respective mock-irradiated controls. Log_2-fold change in expression with adjusted p<0.1 is expressed. Grey squares represent non-significant modulation.

a

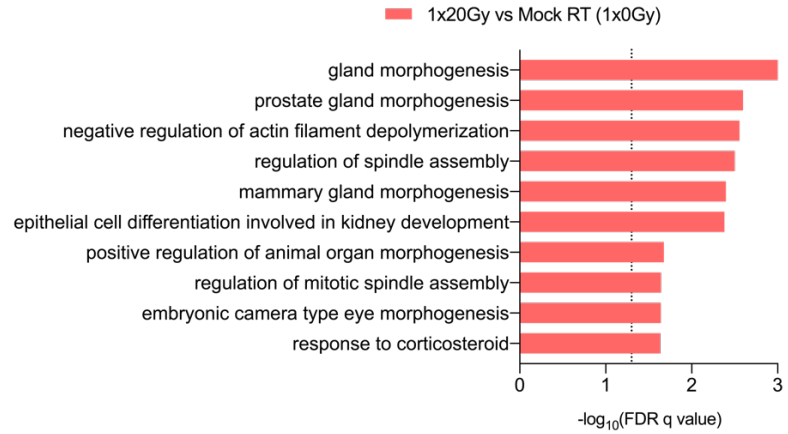
1x20Gy vs Mock RT (1x0Gy)
gland morphogenesis
prostate gland morphogenesis
negative regulation of actin filament depolymerization
regulation of spindle assembly
mammary gland morphogenesis
epithelial cell differentiation involved in kidney development
positive regulation of animal organ morphogenesis
regulation of mitotic spindle assembly
embryonic camera type eye morphogenesis
response to corticosteroid
0
1
2
3
-log10(FDR q value)

b

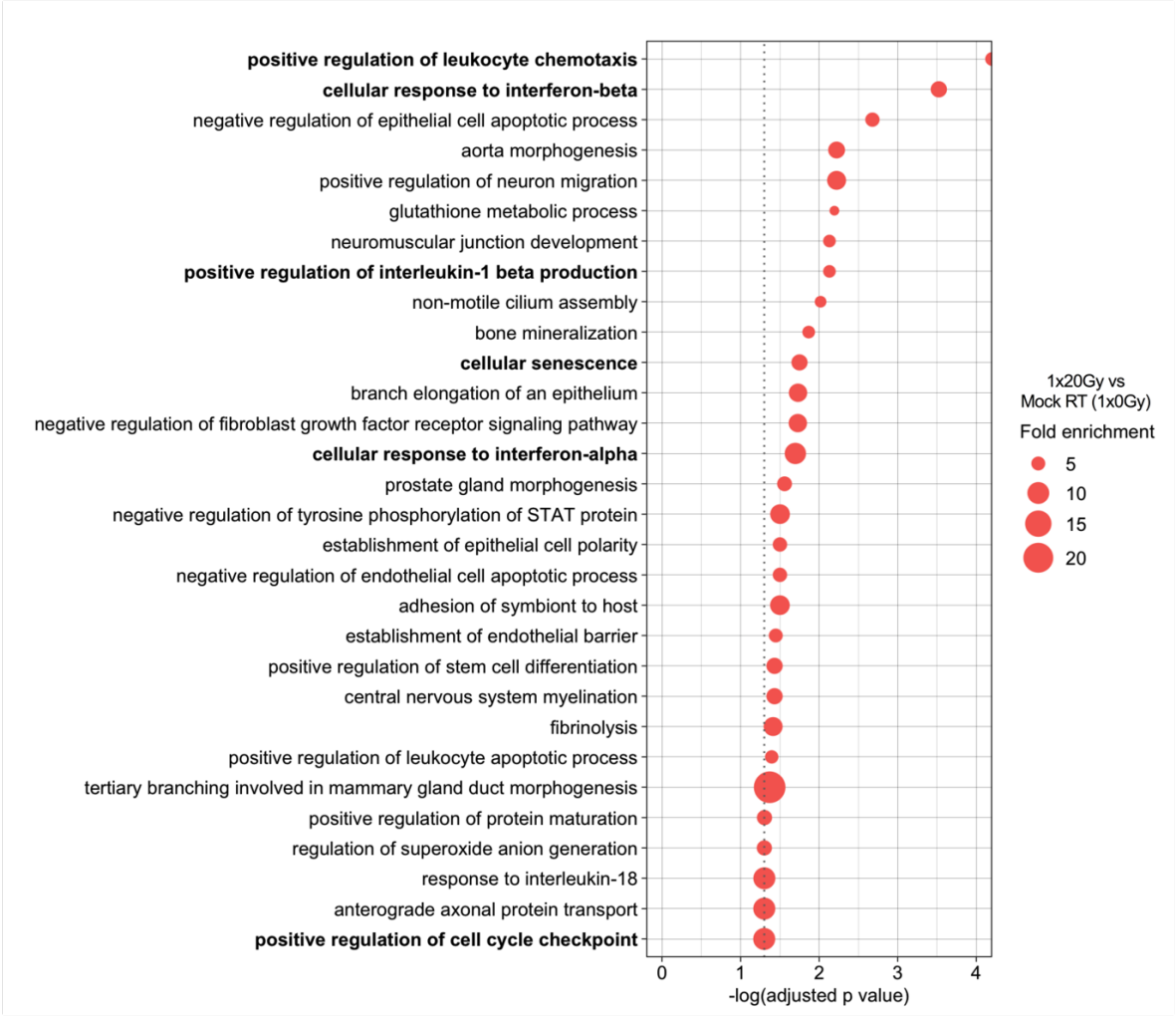
positive regulation of leukocyte chemotaxis
cellular response to interferon-beta
negative regulation of epithelial cell apoptotic process
aorta morphogenesis
positive regulation of neuron migration
glutathione metabolic process
neuromuscular junction development
positive regulation of interleukin-1 beta production
non-motile cilium assembly
bone mineralization
cellular senescence
branch elongation of an epithelium
negative regulation of fibroblast growth factor receptor signaling pathway
cellular response to interferon-alpha
prostate gland morphogenesis
negative regulation of tyrosine phosphorylation of STAT protein
establishment of epithelial cell polarity
negative regulation of endothelial cell apoptotic process
adhesion of symbiont to host
establishment of endothelial barrier
positive regulation of stem cell differentiation
central nervous system myelination
fibrinolysis
positive regulation of leukocyte apoptotic process
tertiary branching involved in mammary gland duct morphogenesis
positive regulation of protein maturation
regulation of superoxide anion generation
response to interleukin-18
anterograde axonal protein transport
positive regulation of cell cycle checkpoint
0
1
2
3
4
-log(adjusted p value)
1x20Gy vs Mock RT (1x0Gy)
Fold enrichment
5
10
15
20

Figure 4.14. Gene signatures in the tumour/stromal compartment of AT3-OVA tumours post RT. Tumour/stromal cells ($CD45^{-}GFP^{\pm}$ cells) were flow-sorted from single cell AT3-OVA tumour suspensions at day 13 post mock or 1x20Gy irradiation and processed for RNAseq analysis. **a & b,** Top GO-BP terms enriched in the tumour/stromal compartment of 1x20Gy-irradiated AT3-OVA tumours at day 13 post RT, compared to its respective mock-irradiated control, (**a**) by GSEA and by (**b**) PANTHER, when restricted to differentially expressed genes with an adjusted *p* value < 0.05 and $\log_2$-fold change > 1. Redundant terms in the PANTHER analysis were filtered out by the in-built hierarchical sorting. Bold terms highlight a putative link between type I IFN production, cellular senescence, and NK cell infiltration.

8. Investigating the link between radiation-induced cellular senescence and NK cell responses following high BED irradiation

To investigate the putative link between radiation-induced senescence and NK cell responses, the capacity of radiation to evoke a senescence state in AT3-OVA tumour cells was first determined. Morphologically, a proportion of AT3-OVA tumour cells developed a flat, enlarged "pancake appearance" following irradiation *in vitro*, consistent with that classically described for senescent cells (*Figure 4.15a*). Furthermore, these cells showed staining for X-gal, a histochemical marker of senescence-associated β-galactosidase (SA-β-gal), in a manner that was proportional to radiation dose (*Figure 4.15b*). 9H-(1,3-dichloro-9,9-dimethylacridin-2-one-7-yl) beta-d-galactopyranoside (DDAOG), which is cleaved by SA-β-gal into a molecule that emits a far-red fluorescent signal upon excitation, was also used for flow-based detection of SA-β-gal (Debacq-Chainiaux *et al.*, 2009; Gong *et al.*, 2009; Flor *et al.*, 2016). In line with above findings, a dose-dependent increase in the proportion of $DDAOG^+$ cells was detected in AT3-OVA cells after radiation exposure (*Figure 4.15c*).

In AT3-OVA tumours harvested from mice, the proportion of $DDAOG^+$ tumour/stromal cells at days 5 and 13 post 1x20Gy irradiation was increased relative to mock-irradiated controls (*Figure 4.16a*). However, by day 21, such increases were no longer detectable (*Figure 4.16a*), which may reflect the outgrowth of non-senescent ($DDAOG^-$) cells when tumours entered into an exponential growth phase. Due to technical difficulties, X-gal staining in AT3-OVA tumour sections to confirm these observations was not possible. However, tumour/stromal cells in irradiated tumours were transcriptionally enriched for senescence gene signatures (*Figure 4.14b*, *Figure 4.16b*), including upregulated transcripts for the cell cycle proteins p53 and p21 (the *Trp53* and *Cdkn1a* genes, respectively) (*Figure 4.16c*). The independent and varying roles of the p53/p21 and p16/pRB pathways in senescence, with the latter being more associated with epigenetically-induced rather than DNA damage-induced senescence (Herbig *et al.*, 2004; Petrova *et al.*, 2016), may explain the lack of differential regulation for p16 transcripts (the *Cdkn2a* gene) (*Fig 4.16c*).

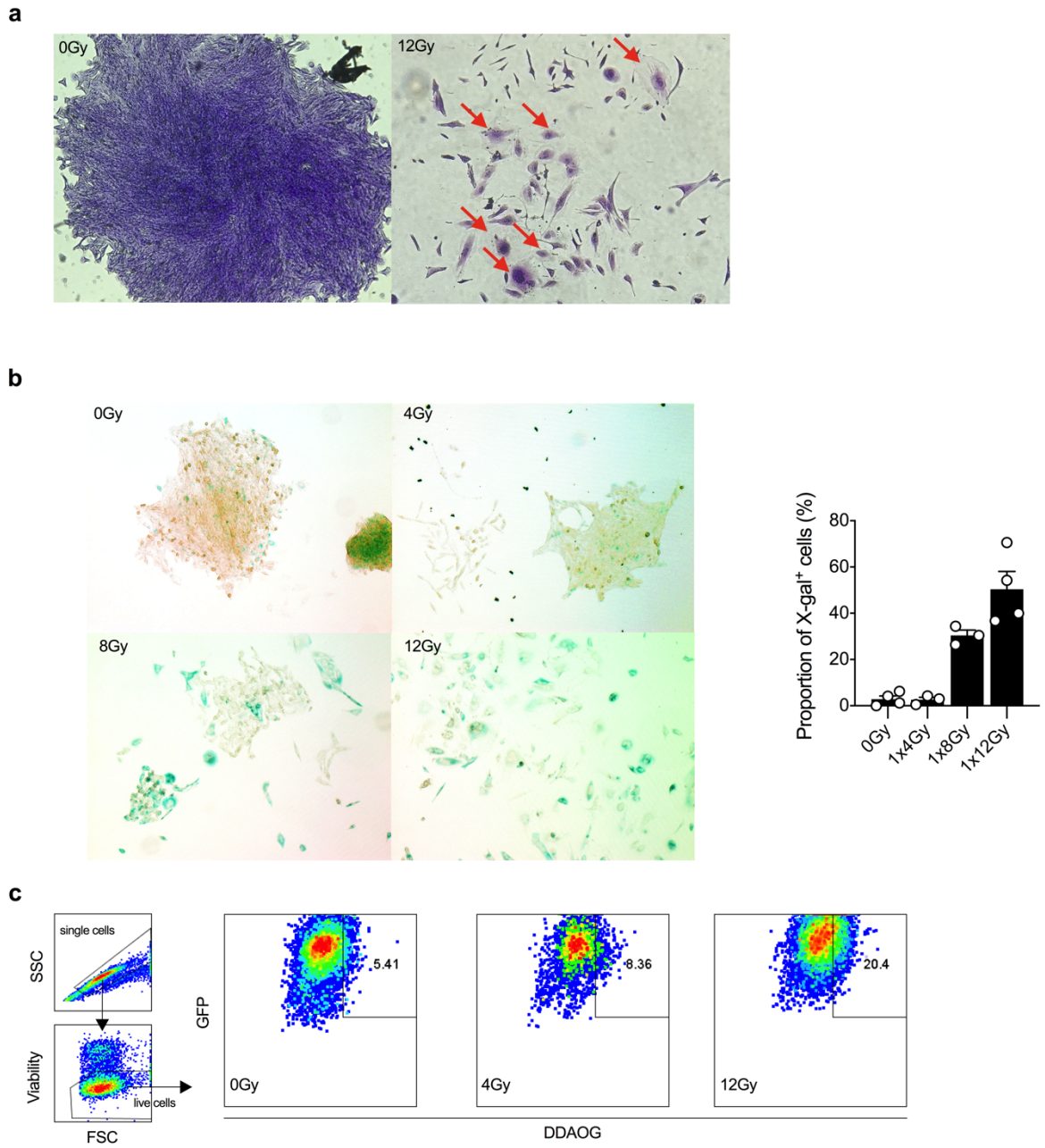

Figure 4.15. ***In vitro*** **evidence of radiation-induced cellular senescence in AT3-OVA tumour cells. a,** Low power field (LPF) (4x) images of crystal violet-stained AT3-OVA tumour cells at day 9 post mock and 1x12Gy irradiation *in vitro*. Red arrows indicate senescent cells with flat, enlarged morphology. These experiments were performed as part of the clonogenic assays presented in *Figure 3.1a*. Data is representative of 2 independent experiments. **b,** LPF images of cytoplasmic X-gal staining of AT3-OVA cells at day 6 post *in vitro* irradiation, quantified on the right, as the average percentage of X-gal$^+$ cells among all cells in 3 randomly selected LPFs per sample. Data is representative of 1 experiment. **c,** Flow cytometry gating strategy and proportion of DDAOG$^+$ cells among cultured AT3-OVA tumour cells at day 3 post *in vitro* irradiation. Data is representative of 1 experiment.

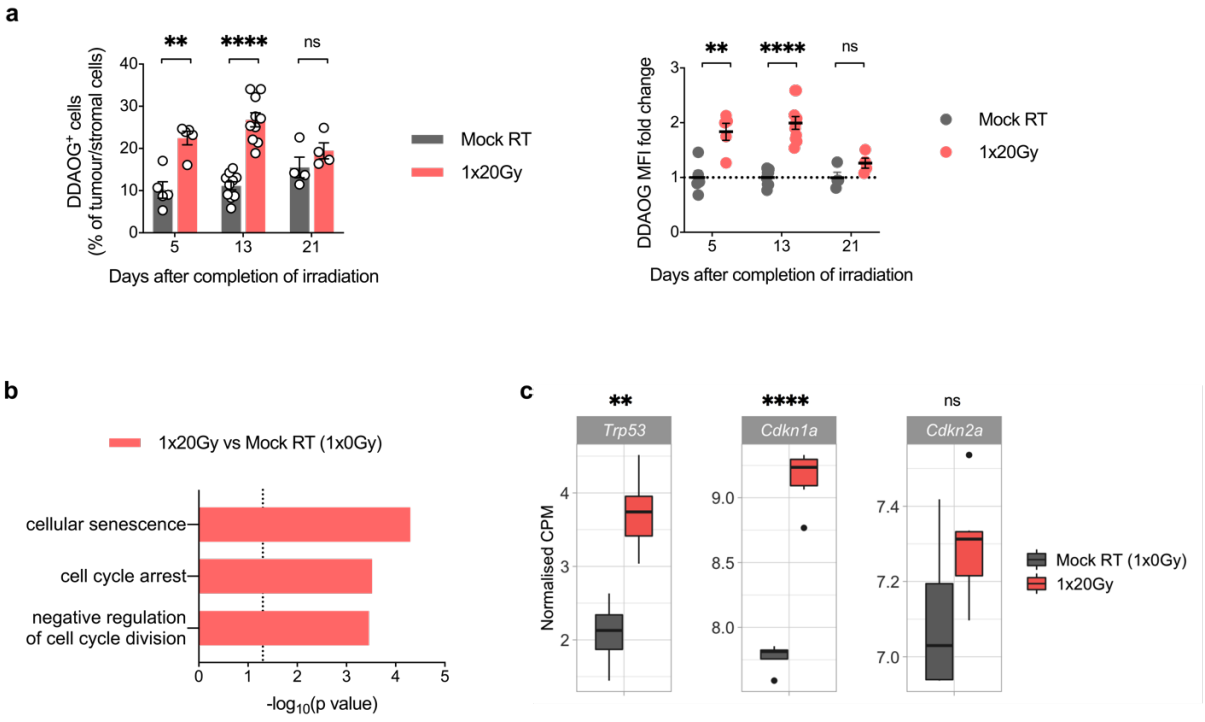

Figure 4.16. *In vivo* evidence of radiation-induced cellular senescence in AT3-OVA tumours. a, Mock and 1x20Gy-irradiated AT3-OVA tumours were harvested at day 13 post RT and processed for DDAOG analysis by flow cytometry. *Left*: Proportion of DDAOG^{+} cells, gated on tumour/stromal cells (CD45^{-} GFP$^{\pm}$). *Right*: DDAOG signal in tumour/stromal cells presented as fold change in MFI relative to mock-irradiated controls (dotted line). Data is combined from 2 independent experiments. **b,** Enrichment of GO-BP senescence-related terms in the tumour/stromal compartment of 1x20Gy-irradiated AT3-OVA tumours at day 13 post RT, compared to its respective mock-irradiated control. Samples were processed as described in *Figure 1.13*. Analysis was performed using ROAST. **c,** Transcript counts of *Trp53*, *Cdkn1a* and *Cdkn2a* (encoding for p53, p21, and p16, respectively) in the tumour/stromal compartment of mock and 1x20Gy-irradiated AT3-OVA tumours at day 13 post RT. Statistical comparisons represent adjusted *p* values. *CPM: counts per million, ns: non-significant, ** p<0.01, **** p<0.0001*

To determine if these changes could also be detected in human cancers, the human rectal adenocarcinoma transcriptomic dataset (GSE15781) described earlier (*Figure 4.4a*) was examined for radiation-induced senescence signatures. Indeed, tumours that received chemoRT prior to surgery were enriched for a cellular senescence signature compared to tumours that received surgery alone (*Figure 4.17a*). Moreover, when analysis was restricted to only tumours that received chemoRT prior to surgery, tumours with higher gene enrichment scores for cellular senescence also had higher scores for NK cell-mediated cytotoxicity (*Figure 4.17b*). Collectively, these data established grounds to further explore the potential impact of radiation-induced senescence on NK cell responses.

Since the type I IFN response pathway was enriched in gene set analysis of AT3-OVA tumour/stromal cells (*Figure 4.14b*) and has been implicated in mediating cellular senescence via both autocrine and paracrine processes in response to genotoxic stressors, such as irradiation (Yu *et al.*, 2015; Ruiz de Galarreta and Lujambio, 2017), the link between the two processes was next examined. Type I IFN signalling in AT3-OVA cell cultures and in AT3-OVA tumour-bearing wildtype mice were blocked using an antibody against the IFN-α/β receptor subunit 1 (IFNAR1), and the DDAOG signal following irradiation was determined. In both irradiated AT3-OVA cell cultures and *ex vivo* irradiated AT3-OVA tumours, a decrease in DDAOG signal was detected with IFNAR1 blockade, indicating less cells entering senescence following irradiation when type I IFN signalling was eliminated (*Figure 4.18a*, *Appendix Figure 5*). This decrease in senescent cells was not observed in mock-irradiated controls, corroborating the close link between type I IFN signalling and DNA damage-induced senescence. Having established that IFNAR1 blockade reduced the proportion of senescent cells in AT3-OVA tumours, the impact of IFNAR1 blockade on tumour-associated NK cell numbers was next examined. At day 13 post RT, 1x20Gy-irradiated tumours treated with anti-IFNAR1 antibodies were found to have reduced NK cell numbers compared to 1x20Gy-irradiated tumours that remained responsive to type I IFN signalling (*Figure 4.18b*). The impact of IFNAR1 blockade on tumour-associated immune cell numbers appeared to be selective for NK cells, as T cell numbers were not affected.

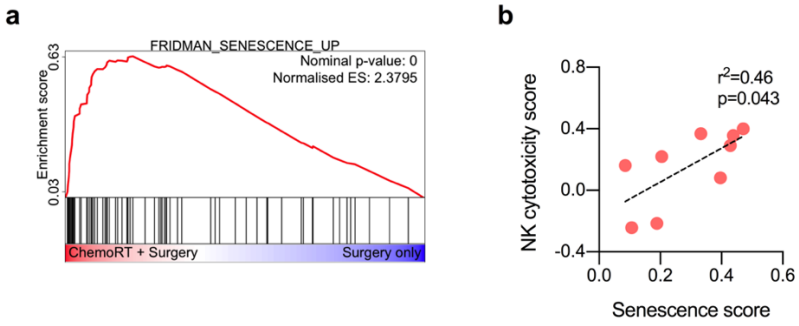

Figure 4.17. Radiation-induced cellular senescence signatures can be detected in human rectal adenocarcinomas. a, GSEA plot of the Fridman senescence (from the C2 collection in the MSigDB database), using the GSE15781 dataset described in *Figure 4.4a*. Tumours that received chemoRT and surgery (the chemoRT + S group) were compared to tumours that received surgery only (the S group). **b,** Correlation of the NK cell-mediated cytotoxicity (KEGG) and Fridman senescence gene set enrichment scores in individual tumours from the chemoRT + S group, from the GSE15781 dataset. Each point represents a tumour. Gene set enrichment scores of individual tumours were calculated using Gene Set Variation Analysis (GSVA).

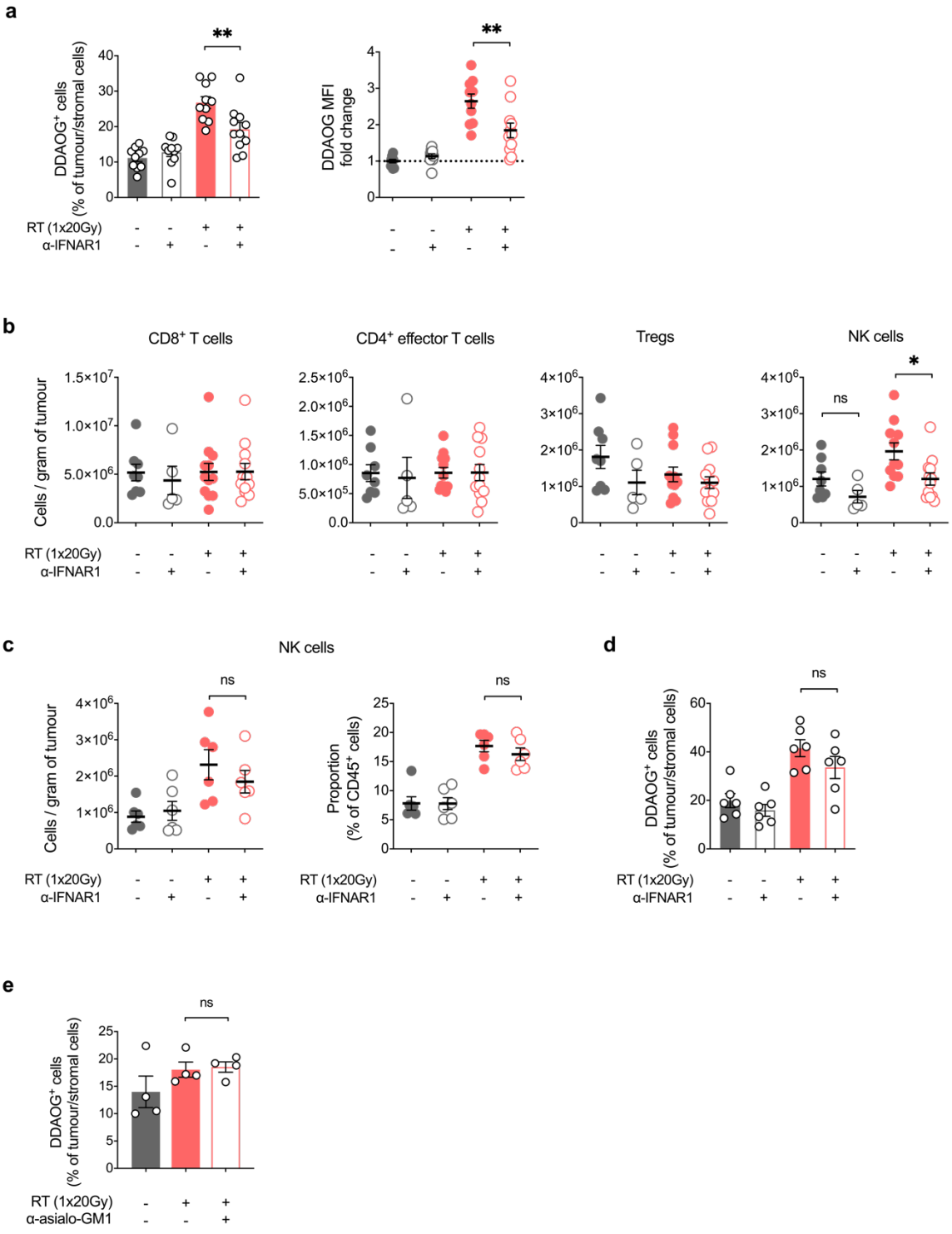

Figure 4.18. Testing the putative link between type I IFN axis, cellular senescence, and NK cell infiltration. a & b, Mock and 1x20Gy-irradiated AT3-OVA tumours were harvested from wildtype mice at day 13 post RT for flow cytometric analysis. Mice were treated with anti-IFNAR1 blocking or isotype control antibody (300μg/mouse for the first injection, 150μg/mouse thereafter), administered every 3 days from start of RT to end of experiment. (**a**) Proportion of DDAOG$^+$ cells (left) and DDAOG signal presented

as fold change MFI relative to mock-irradiated controls (dotted line) (right), gated on tumour/stromal ($CD45^{-}GFP^{\pm}$) cells in mock and 1x20Gy-irradiated AT3-OVA tumours at day 13 post RT. Data is combined from 2 independent experiments. (**b**) Absolute numbers of $CD8^{+}$, $CD4^{+}$ effector T cells, Tregs and NK cells. Data is combined from 2 independent experiments. **c & d,** Mock and 1x20Gy-irradiated AT3-OVA tumours were harvested from *Ifnar1*$^{-/-}$ mice at day 13 post RT for flow cytometric analysis. Mice were treated with anti-IFNAR1 blocking or isotype control antibody, administered every 3 days from start of RT to end of experiment. (**c**) Absolute numbers of NK cells. (**d**) Proportion of $DDAOG^{+}$ cells, gated on tumour/stromal ($CD45^{-}GFP^{\pm}$) cells. Data represents 1 experiment. **e**, Flow cytometric analysis of proportion of $DDAOG^{+}$ cells, gated on tumour/stromal ($CD45^{-}GFP^{\pm}$) cells in mock and 1x20Gy-irradiated AT3-OVA tumours at day 13 post RT, harvested from wildtype mice treated with anti-asialoGM1 or PBS. Anti-asialoGM1 or PBS were administered every 3 days from start of RT to end of experiment. Data is representative of 1 experiment. *ns: non-significant, * $p<0.05$, ** $p<0.01$*

Because these experiments were performed on wildtype mice, a direct effect of IFNAR1 blockade on NK cells could not be ruled out. To investigate the tumour cell-intrinsic role of the type I IFN pathway *in vivo*, AT3-OVA tumour-bearing *Ifnar1*$^{-/-}$ mice were used, in which only the implanted tumour cells expressed IFNAR1 and were responsive to type I IFN. Surprisingly, in this setting, tumour-associated NK cell numbers were not significantly impacted by the addition of anti-IFNAR1 antibody treatment to selectively abrogate tumour cell-intrinsic type I IFN responsiveness (*Figure 4.18c*). This suggests that the reduction in NK cell numbers observed earlier in tumours from wildtype mice treated with RT and anti-IFNAR1 antibodies (*Figure 4.18b*) was at least in part due to loss of host-intrinsic type I IFN signalling within NK cells. Complicating interpretation of this data nonetheless was the observation that anti-IFNAR1 antibody treatment of *Ifnar1*$^{-/-}$ mice did not significantly reduce the proportion of DDAOG^{+} cells in AT3-OVA tumours relative to mice treated with control isotype antibodies (*Figure 4.18d*), as opposed to what was observed earlier in wildtype mice (*Figure 4.18a*). A possible explanation for this discrepancy is that in wildtype mice, both tumour and host stromal cells when stimulated by type I IFN could have secreted factors that further induced senescence of neighbouring cells (Ruiz de Galarreta and Lujambio, 2017), whereas this contribution from host cells to the paracrine type I IFN-senescence axis was lost in *Ifnar1*$^{-/-}$ mice. Because the change in proportion of senescent cells was not significant in *Ifnar1*$^{-/-}$ mice, interpretation of the effect on NK cell frequency is obscured. However, since the type I IFN pathway was not found to be critical for tumour control following 1x20Gy irradiation in AT3-OVA tumours (*Figure 3.3c*), the significance of this avenue of investigation on overall anti-tumour responses is questionable.

Given that senescent cells have been linked with NK cell surveillance (Krizhanovsky *et al.*, 2008; Soriani *et al.*, 2009; Iannello *et al.*, 2013), senescent cells could also have been preferential targets for NK cell killing and thus contributed to sustained NK cell responses in AT3-OVA tumours. To examine this, the impact of NK cell depletion on the proportion of DDAOG^{+} cells in 1x20Gy-irradiated tumours was compared. No difference in the proportion of DDAOG^{+} cells was detected at day 13 post RT between NK cell-depleted and non-depleted groups, suggesting that senescent cells were not a major target for elimination by NK cells (*Figure 4.18e*).

Altogether, these data demonstrated that in addition to apoptosis and necrosis (described in Chapter 3), irradiation of AT3-OVA tumour cells also induced senescence as a cellular endpoint, which was at least in part mediated by type I IFN. Nonetheless, the connection between senescent cells and NK cell infiltration was unable to be established within the timeframe of this PhD project.

Discussion

Given the importance of NK cells in the evolution and control of cancer, their role in supporting the anti-tumour effects of RT is under-investigated. The current state of knowledge regarding the interaction between RT and NK cells is largely derived from *in vitro* reports of radiation-induced tumour cell-intrinsic changes in surface ligand and chemokine expression (Gasser *et al.*, 2005; Kim *et al.*, 2006; Yoon *et al.*, 2016), and *in vivo* studies that have used immunodeficient models with NK cell adoptive transfer (Canter *et al.*, 2017; Kim *et al.*, 2019). In light of this, the aim of this chapter was to clarify the anti-tumour role of host NK cells in the context of RT in a more physiologically-relevant immunocompetent setting, and the impact of radiation dose-fractionation on the kinetics and regulation of radiation-induced NK cell responses. Results herein demonstrated that RT can induce NK cell responses that contributed to tumour control, independent of immunotherapy. Across two mouse models of cancer and two human cancers, radiation-induced NK cell responses appeared to be contingent on a sufficient radiation BED, rather than DPF. In AT3-OVA tumours, the requirement of a sufficiently high radiation BED parameter was a function of the effector-suppressor dynamics between NK cells and Tregs over the early (days 0-13) and late (days 14-21) post irradiation phases. In the early post irradiation phase, NK cell numbers increased in AT3-OVA tumours regardless of the radiation dose-fractionation employed, but the anti-tumour activity of these NK cells was constrained by the concurrent accumulation of radiation-induced Tregs. High BED radiation regimens, however, generated longer-lasting NK cell responses that outlasted the transient radiation-induced Treg responses. Conversely, depletion of Tregs in AT3-OVA tumours unleashed early-phase NK cell responses, resulting in highly effective in control of tumour growth, irrespective of the radiation dose-fractionation employed.

The biphasic nature of radiation-induced NK cell responses in AT3-OVA tumours raises the question of whether early and late-phase NK cell responses might be driven by different processes. The kinetics of the accumulation of early-phase NK cells in AT3-OVA tumours was almost identical to that of T cells, which suggests a general inflammatory response caused by tissue damage from radiation. This is supported by higher gene expression levels of inflammatory cytokines and their receptors in the early post irradiation time points (*Figure 4.8, Figure 4.13c, Appendix Tables 1-4*, also discussed in Chapter 3). Late-phase NK cell responses, however, required a sufficiently high radiation BED for their induction. Because BED is essentially a measure of cumulative radiation-induced DNA damage, it is reasonable to deduce that the late-phase modulation of NK cells in AT3-OVA tumours was a reflection of the overall genotoxic stress inflicted by the direct effects of radiation on tumour/stromal cells.

A well-recognised consequence of radiation-induced genotoxic stress is entry into cellular senescence. Although in permanent cell cycle block, senescent cells remain metabolically active, and over time develop SASP. The secretion profile of SASP include immunomodulatory cytokines, growth factors, and matrix metalloproteinases, which exert a myriad of pro- and anti-tumour effects (Lasry and Ben-Neriah, 2015). Among these secondary effects are increased NK cell infiltration and surveillance (Krizhanovsky *et al.*, 2008; Soriani *et al.*, 2009; Iannello *et al.*, 2013). Based on detection of X-gal and DDAOG as reporters of SA-β-gal and on gene expression profile analysis, irradiation of AT3-OVA tumours was found to induce cellular senescence, which was likely partly dependent on a type I IFN-mediated paracrine pathway. However, the link between radiation-induced cellular senescence and sustained late-phase NK cell responses could not be conclusively determined within the timeframe of this PhD project. Senescent cells did not appear to be the primary target of NK cell killing, consistent with a recent report describing expression of the non-classical MHC-I molecule HLA-E on senescent cells (the orthologous molecule in mice being Qa1), which inhibited NK cell killing through binding with the NKG2A receptor (Pereira *et al.*, 2019). This however did not exclude the possibility that senescent cells were a source of chemoattractants for NK cells via induction of SASP. RNAseq analysis of tumour/stromal cells in 1x20Gy-irradiated tumours at day 13 post RT revealed upregulation of some SASP genes such as *Cxcl1*, *Il15*, *Igf1*, and *Mmp3* (*Figure 4.13c*, *Appendix Table 6*, some data not shown), but because the samples were not enriched for senescent cells, the presence of SASP could not be accurately determined. To address this, enrichment of senescent cells from *ex vivo* tumours by flow-sorting based on DDAOG signal and detection of SASP factors in those samples with quantitative reverse transcription PCR (RT-qPCR) or Western blotting analysis should be done. A complementary method of investigation could involve using senolytics to selectively eliminate senescent cells and assessing the resultant impact on NK cell responses. Newer BH3-mimetics such as ABT-263 have demonstrated preferential killing of senescent cells both *in vitro* and *in vivo* through targeting the anti-apoptotic proteins BCL-2, BCL-W and BCL-XL, which are upregulated in senescent cells (Chang *et al.*, 2016; Wang *et al.*, 2017). A pilot experiment towards the end of my PhD candidature demonstrated that ABT-263 did indeed have senolytic activity against AT3-OVA tumour cells that had entered into radiation-induced senescence (*Appendix Figure 6*). ABT-263 could therefore be a viable method to selectively target senescent cells for future mechanistic study of NK cell responses to RT. Another aspect to address in future work is to determine the level of cellular senescence within tumours *in vivo* at a late time point after irradiation with a low BED regimen, such as with the 3x4Gy regimen. Presumably, if cellular senescence was to be the distinguishing factor for high BED regimens in evoking longer-

lasting NK cell responses, a difference in cellular senescence levels *in vivo* would be detectable between radiation regimens with different BEDs.

To further investigate if the presence of a specific cytokine milieu could have favoured the selective persistence of NK cells over T cell subsets in the late post irradiation phase, the IFN-γ-inducible CXCR3 pathway was examined as a putative candidate for the recruitment of NK cells into irradiated AT3-OVA tumours following high BED irradiation. However, although blockade of CXCR3 potently abrogated NK cell numbers within the tumours, it also affected all other T cell subsets in similar proportions, ultimately leaving the immune equilibrium preserved. While $CXCR3^+$ T and NK cells have been described in tumour settings (Wendel *et al.*, 2008; Chow *et al.*, 2019), it is unclear whether the widespread loss of tumour T and NK cell infiltration in AT3-OVA tumours was a direct effect of CXCR3 blockade, or an indirect effect secondary to changes in other immune subsets. Detection of CXCR3 surface expression levels on T and NK cells by flow analysis was attempted, but required further optimisation which was not carried out due to the lack of separation in the tumour growth curves with CXCR3 blockade. IL-18 and IL-23 are two other cytokines that might have played a role in supporting NK cell responses in AT3-OVA tumours in the late post irradiation phase. IL-18 is a pro-inflammatory cytokine expressed by both haemopoietic and non-haemopoietic cells, including fibroblasts and endothelial cells, that activates and potently induces IFN-γ production by NK cells (Dinarello *et al.*, 2013; Yasuda *et al.*, 2019). IL-23 in combination with IL-18 has been reported to stimulate NK cells and reduce $CD8^+$ T cell infiltration into tumours (Langowski *et al.*, 2006; Ziblat *et al.*, 2017). Transcripts for IL-18 and the IL-18 receptor complex (consisting of α and β chains encoded by *Il18r1* and *Il18rap* respectively) were upregulated in tumour/stromal and immune cells in a cognate fashion at day 13 post 1x20Gy irradiation (*Figure 4.8, Figure 4.13c*), accompanied by the enrichment of the gene signature for response to IL-18 in tumour/stromal cells at the same time point (*Figure 4.14b*). Transcripts for IL-23 were also upregulated at day 13 (*Figure 4.13c*). As another putative candidate, *Cxcr6* was found to be upregulated in the immune compartment of AT3-OVA tumours at day 13 post 1x20Gy irradiation, in keeping with the aforementioned *in vitro* study implicating the CXCL16-CXCR6 axis in NK cell migration following irradiation (Yoon *et al.*, 2016), but no differential expression of *Cxcl16* was detected (*Figure 4.8, Figure 4.13c*). To address the complexity of investigating a list of candidate factors, T and NK cells could be separately isolated from tumours at a point when they show differential regulation by radiation BED (such as at day 13 post RT), and examined by RNAseq for contrasting patterns of cytokine-related pathways between the cellular subsets. This may help narrow down candidate factors for investigation.

The potential significance of radiation-induced NK cell responses lies not only in their ability to directly kill tumour cells, but also in their capacity to support adaptive immune responses. NK cells have been shown to be instrumental for the recruitment of cDC1s into tumours, which in turn are critical for anti-tumour $CD8^+$ T cell responses (Bottcher *et al.*, 2018). In the same study, the NK cell-chemokine-cDC1 axis could be correlated with survival in cancer patients. Additionally, NK cell-derived IFN-γ promotes DC maturation and Th1 polarisation of $CD4^+$ T cells, further supporting $CD8^+$ T cell function (Martin-Fontecha *et al.*, 2004; Pallmer and Oxenius, 2016). Therefore, NK cells can mediate a "helper-effect" that extends beyond its cytotoxic function. Several aspects of the data thus far point to the importance of the NK cell-T cell crosstalk in AT3-OVA tumours following RT. Firstly, the DC activation gene signature was found to be induced at day 13 post 1x20Gy irradiation when NK cells produced high amounts of IFN-γ, but not earlier at day 5 when the IFN-γ production signature was not enriched in the tumour immune microenvironment (*Figure 4.7b, d, and Appendix Figure 7*). Secondly, depletion of NK cells in the context of high BED irradiation resulted in recovery of MHC-I-expressing tumour/stromal cells (*Figure 4.7b*), suggesting a component of NK cell-mediated engagement of tumour/stromal cells by T cells. As another pointer to their co-dependent rather than independent anti-tumour contributions, therapeutic synergy between RT and Treg depletion by 9H10 anti-CTLA-4 antibodies was fully, rather than partially, abrogated when either $CD8^+$ T or NK cells were depleted (*Figure 3.15a, Figure 4.6a*). These circumferential observations of a positive interplay between NK and T cells need to be verified. Changes in DC and T cell numbers or function with either depletion or amplification of NK cell responses would help elucidate this.

Because radiation-induced NK cell responses have not been nearly as extensively investigated and reported as radiation-induced T cell responses, it was important that pre-clinical observations in this study could be corroborated in human cancers. In fact, in the two human cancer transcriptomic datasets analysed, T cell responses were not uniformly observed after RT, yet NK cell responses were. Although it was not possible to separate the contribution of chemotherapy from that of RT in the rectal cancer dataset, it is widely accepted that RT is the primary treatment modality in the neoadjuvant setting for locally advanced rectal adenocarcinomas, whereas fluorouracil-based chemotherapy is added as a radiosensitiser (Colorectal Cancer Collaborative, 2001). Moreover, results from the PDAC dataset suggest that RT, rather than chemotherapy, was more capable of evoking NK cell responses. Interestingly, results from the PDAC dataset also corroborate findings from AT3-OVA tumours that the radiation BED parameter, rather than DPF, was the principal determinant of effective NK cell responses following RT. In AT3-OVA tumours, transient radiation-induced Treg responses were central to this dependency on radiation BED. It is possible that PDACs, which have a fibroinflammatory stroma and Treg-rich immune

microenvironment (Jang *et al.*, 2017), also exhibited radiation-induced Treg responses similar to AT3-OVA tumours. Indeed, cell type profiling revealed that the abundance of tumour-associated Tregs in PDAC tumours, based on *FOXP3* expression, was reduced following neoadjuvant FOLFORINOX chemotherapy compared to tumours that did not receive neoadjuvant therapy, but this was significantly restored with the combination of neoadjuvant FOLFORINOX chemotherapy and RT (*Appendix Figure 8*). Thus, it is likely that tumour-associated Treg responses were induced by RT in PDAC tumours. Outcome data was not available in the rectal cancer and PDAC datasets to correlate radiation-induced NK cell responses with oncological endpoints. However, having established that NK cell responses were generated following RT, it follows that these responses could potentially be leveraged by immunotherapy for greater therapeutic benefit. This hypothesis is examined in Chapter 5.

Given the observation in AT3-OVA tumours that late-phase NK cells were a primary source of IFN-γ in the post irradiation tumour microenvironment, IFN-γ gene signatures were also tested on the two human cancer datasets as an exploratory analysis. ChemoRT enriched for an IFN-γ signature in the rectal cancer dataset, but not in the PDAC dataset (*Appendix Figure 9a-b*). While this may reflect differences in the tumour microenvironment or in the time points of tissue collection, the use of the Nanostring platform in the PDAC dataset necessitated testing of a different IFN-γ gene set, which was curated for predicting responsiveness to anti-PD-1 checkpoint blockade (Ayers *et al.*, 2017). This is likely to have contributed to the discrepancy. Intriguingly, although type I IFN signalling, particularly that of IFN-β, has been the subject of focus as a crucial pathway for mediating radiation abscopal responses (Formenti *et al.*, 2018), analysis of pre- and post-SABR tumour biopsies from a phase I trial of SABR with pembrolizumab (an anti-PD-1 antibody) revealed that expression of a pre-determined panel of IFN-γ-related genes correlated with abscopal tumour responses (Luke *et al.*, 2018). While further transcriptional analyses are still to come out from this study, these preliminary findings suggest that the IFN-γ axis could also play an important role alongside type I IFNs as therapeutically-desirable pathways induced by RT.

Altogether, this chapter represents the first body of work to thoroughly examine the mechanisms of radiation-induced NK cell responses in a physiologically-relevant *in vivo* context, independent of immunotherapy. Importantly, results herein illustrate that the impact of radiation dose-fractionation on anti-tumour immune responses is dictated by a highly dynamic interaction between effector and suppressor subsets within the tumour immune microenvironment.

Chapter 5: The impact of radiation dose-fractionation on the anti-tumour activity of immune checkpoint blockade

Abstract

Durable responses to immune checkpoint blockade that translate to increased long-term survival in metastatic patients illustrate the significant potential of harnessing host immune responses against cancer. However, such remarkable responses are currently restricted to a subset of patients and a limited number of cancer types. As a strategy to overcome therapeutic resistance and improve response rates, radiation therapy (RT) is increasingly being trialled in combination with cancer immunotherapy. Nonetheless, the impact of radiation dose-fractionation on such combination approaches is poorly understood. This chapter examined how the differential effects of radiation dose-fractionation on anti-tumour immune responses affected their suitability for partnering with immune checkpoint blockade therapy. In AT3-OVA mammary carcinoma tumours, which were refractory to immune checkpoint inhibitors when given as monotherapy, combinatorial efficacy between RT and $CD8^+$ T cell-directed immunotherapies was found to be contingent on radiation dose-fractionation regimens that evoked $CD8^+$ T cell responses, but the selection of radiation regimen was not critical for pairing with regulatory T cell (Treg)-depleting anti-CTLA-4 antibodies. Furthermore, radiation-induced natural killer (NK) cell responses could be leveraged with immune checkpoint blockade, but required consideration of the effector-suppressor dynamics post RT for timing of immunotherapy. Interestingly, anti-PD-1 and anti-PD-L1 therapy exhibited differential interactions with RT, suggesting non-identical mechanisms of action. Altogether, RT and immune checkpoint blockade combination strategies do not universally synergise, but require selection of radiation regimens and checkpoint targets that are predicated on biological rationale. This highlights the importance of ongoing fundamental mechanistic studies to inform the optimal use of RT as a partner to combat resistance to cancer immunotherapy.

Introduction

Cancer immunotherapy, particularly antibody-based immune checkpoint inhibitors, has dramatically redefined our paradigm on strategies for treating solid cancers. Leveraging the immune system to control and eliminate cancer represents a strategy that is fundamentally distinct to the other major cancer treatment modalities which directly target tumour cells. The observation that cancer immunotherapy can achieve long-term responses in patients with metastatic disease reflects the unique advantage of this approach. However, not all cancer patients respond to immunotherapy, and for those who demonstrate an initial response, some will develop resistance to treatment (Sharma *et al.*, 2017).

A growing body of work attests that radiation therapy (RT) and immune checkpoint blockade can act via non-overlapping and complementary mechanisms to overcome therapeutic resistance and promote tumour immunity. For example, Twyman-Saint Victor *et al.* elegantly demonstrated using mouse models of melanoma and patient tumour and blood samples that while blockade of cytotoxic T-lymphocyte-associated protein 4 (CTLA-4) antagonised regulatory T cell (Treg) suppression and promoted expansion of $CD8^+$ T cells, RT shaped the T cell receptor (TCR) repertoire of the expanded T cell clones for efficient tumour cell recognition, and blockade of programmed death-ligand 1 (PD-L1) reinvigorated exhausted T cells (Twyman-Saint Victor *et al.*, 2015). In recognition of the potential therapeutic synergy between RT and immune checkpoint blockade, there has been a rapid proliferation of clinical trials testing this combination strategy, some of which have started to mature and report outcomes (Kang *et al.*, 2016). Most compellingly, the PACIFIC and PEMBRO-RT randomised trials demonstrated findings in favour of superior outcomes in patients with non-small cell lung cancer who received RT and immune checkpoint blockade, compared to either modality alone (Antonia *et al.*, 2018; Theelen *et al.*, 2019). Notably, the PACIFIC trial employed a conventionally fractionated radiation regimen with PD-L1 blockade, while the PEMBRO-RT trial used a stereotactic ablative radiotherapy (SABR) regimen in conjunction with blockade of programmed cell death protein 1 (PD-1). However, because few studies have taken into consideration the differential effects of radiation dose-fractionation on anti-tumour responses when combining with immunotherapy, the degree to which the observed therapeutic interactions were dependent on the radiation dose-fractionation employed is poorly defined.

In this chapter, insights gained from Chapters 3 and 4 on the impact of radiation dose-fractionation on anti-tumour $CD8^+$ T cell and natural killer (NK) cell responses were tested in combination with immune checkpoint inhibitors that target the adaptive and innate arms of the immune system.

These include blocking antibodies against CTLA-4, PD-1, PD-L1, T cell immunoreceptor with Ig and ITIM domains (TIGIT), CD96, T-cell immunoglobulin and mucin domain-3 (TIM-3), Ly49C/I and NKG2A. Antibodies against CTLA-4, PD-1 and PD-L1 were designed to enhance $CD8^+$ T cell responses and are currently in clinical use for a range of cancer types (Wei *et al.*, 2018). TIGIT, CD96 and TIM-3 comprise a next wave of checkpoint receptors in the translational pipeline, being expressed not only expressed on T cells, but also on innate immune cells, including NK cells in particular (Anderson *et al.*, 2016; Dougall *et al.*, 2017; Zhang *et al.*, 2018). Ly49C and Ly49I are NK cell-inhibitory receptors that recognise the major histocompatibility complex class I (MHC-I) H2-D^d haplotype. They belong to the Ly49 family of receptors on NK cells in mice, which is orthologous to the killer cell immunoglobulin-like receptors (KIRs) in humans, yet have evolved independently to the human counterparts as a remarkable example of convergent evolution (Guethlein *et al.*, 2015). NKG2A is another NK cell-inhibitory receptor, which heterodimerises with CD94 on the cell surface and recognises the non-classical MHC-I molecule HLA-E in humans and Qa1 in mice (Andre *et al.*, 2018). In addition to NK cells, the NKG2A-CD94 complex is also expressed on a subset of $CD8^+$ T cells and NK-T cells. Importantly, results herein demonstrated that radiation dose-fractionation regimens are not equivalent in their ability to support the anti-tumour effects of immune checkpoint blockade. Thus, a deeper understanding of the underlying processes is important to guide the selection of the radiation regimen and also the checkpoint for inhibition for optimal therapeutic synergy.

Results

1. Combining RT with anti-CTLA-4, anti-PD-1 or anti-PD-L1 therapy

The combination of RT and anti-CTLA-4 therapy was tested earlier in Chapter 3 (*Figures 3.13-3.15*). Briefly, treatment with anti-CTLA-4 antibodies engineered to block the CTLA-4 checkpoint but not deplete Tregs only showed combinatorial effects with radiation regimens that could independently prime $CD8^+$ T cell responses (*Figure 3.14d*), suggesting that the regulation of $CD8^+$ T cell responses by radiation dose per fraction (DPF) also dictated therapeutic synergy with CTLA-4 blockade in AT3-OVA tumours. By contrast, because Tregs were enriched in AT3-OVA tumours following RT irrespective of the radiation dose-fractionation used, treatment with anti-CTLA-4 antibodies that were capable of depleting Tregs via antibody-dependent cellular cytotoxicity (ADCC) demonstrated marked therapeutic synergy with all radiation regimens tested, by potentiating the anti-tumour activity of both $CD8^+$ T and NK cell responses (*Figure 3.13c, Figure 3.15a, Figure 4.6a*).

Similar to non-Treg-depleting blockade of CTLA-4, anti-PD-1 therapy (RMP1-14 clone, rat IgG2a isotype, Bio X Cell), which had no single agent activity in AT3-OVA tumours, improved control of tumours when given with 3x4Gy and 9x4Gy irradiation but not with 1x20Gy irradiation (*Figure 5.1a*). Confirming the requirement of $CD8^+$ T cell responses for these combinatorial effects, the ability of anti-PD-1 therapy to improve tumour control and mouse survival following 3x4Gy irradiation was abrogated with concurrent depletion of $CD8^+$ T cells (*Figure 5.1b*). Mice treated with $CD8^+$ T cell depleting antibodies alone were not included in this experiment since AT3-OVA tumours had been shown in Chapter 3 to be unaffected by this treatment (*Figure 3.2a*).

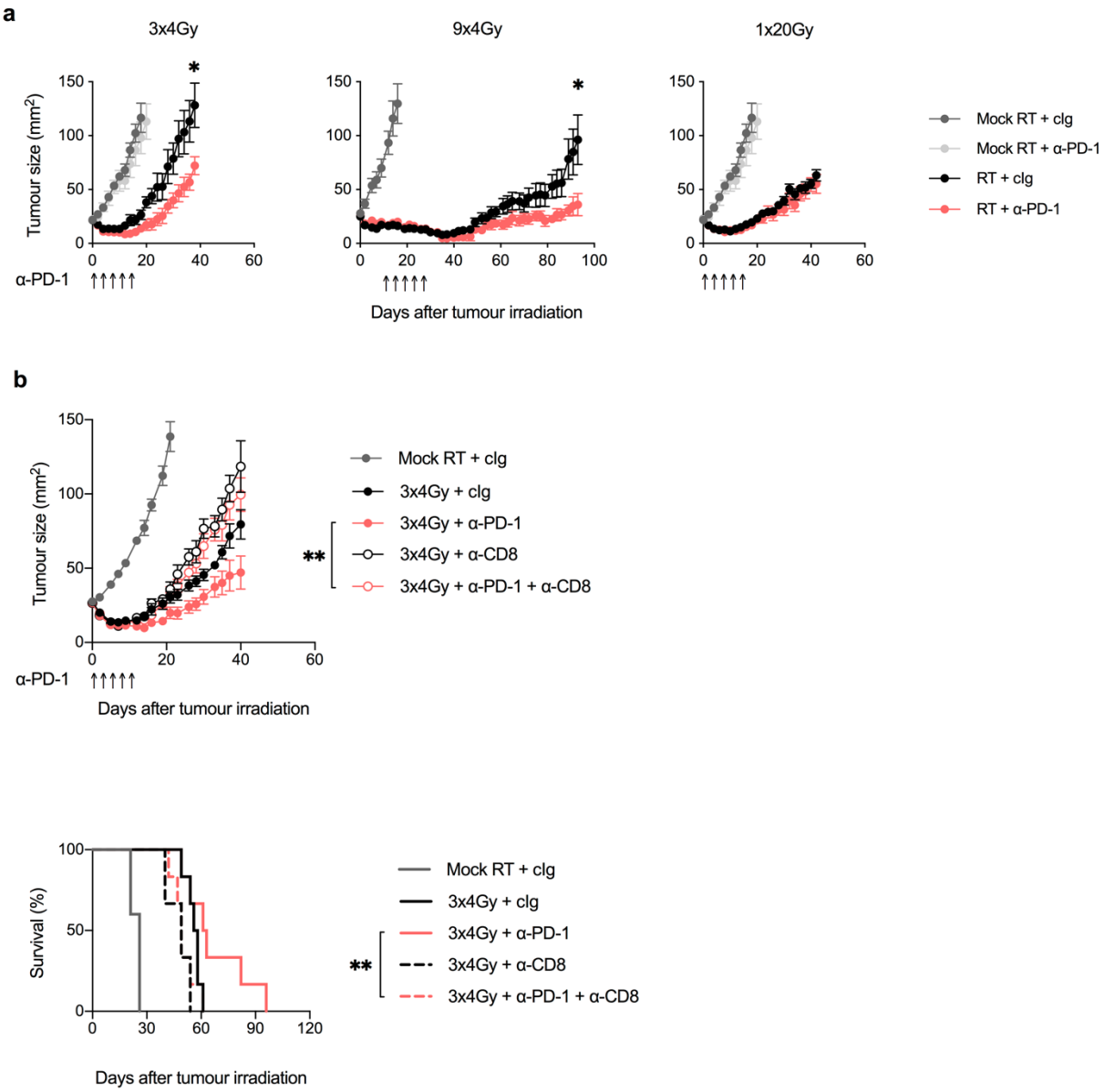

Figure 5.1. Radiation regimens with low-to-moderate DPFs can enhance the anti-tumour activity of anti-PD-1 therapy in a CD8$^+$ T cell-dependent manner. AT3-OVA tumour cells were injected into the mammary fat pads (m.f.p.) of C57BL/6 wildtype mice (1.5x10^6 cells/mouse) to allow orthotopic tumours to form. Tumours were irradiated when they reached 25-35mm^2. RT was given daily, 5 fractions per week. Mice were culled when tumours reached 100-150mm^2. Survival of remaining mice were monitored until at least day 60 post initiation of treatment. **a,** AT3-OVA tumour growth after RT in mice treated with anti-PD-1 or isotype control antibodies. Anti-PD-1 or isotype control antibodies (150μg/mouse for the first injection, 100μg/mouse thereafter) were administered every 4 days from start of RT, for a total of 4 injections. Arrows indicate the time of antibody treatment. Statistical comparisons were made between the RT + anti-PD-1 and RT + cIg groups. *n*=5-6 mice per group, representative of 2 independent experiments.

b, AT3-OVA tumour growth (first panel) and mouse survival (second panel) post RT in mice treated with anti-PD-1 and $CD8^+$ T cell depleting antibodies, or with their respective isotype control antibodies. Anti-PD-1 or isotype control antibodies were administered every 4 days from start of RT, for a total of 4 injections. $CD8^+$ T cell depleting or control isotype antibodies were administered every 3 days from start of RT to end of experiment. Arrows indicate the time of anti-PD-1 antibody treatment. *n*=5-6 mice per group, representative of 1 experiment. Tumour growth data presented as mean ± SEM, * $p<0.05$, ** $p<0.01$

To complement the findings of anti-PD-1 therapy, similar experiments to that described above were performed with anti-PD-L1 antibodies (clone 6E11, mouse IgG1 isotype, kindly provided by Roche Pharmaceuticals). Surprisingly, anti-PD-L1 therapy, which had no single agent activity in AT3-OVA tumours, improved tumour control and mouse survival following both 3x4Gy and 1x20Gy irradiation, compared to RT alone (*Figure 5.2a*). To confirm that the discrepancy in the ability of anti-PD-1 and anti-PD-L1 therapies to promote the anti-tumour effects of the 1x20Gy regimen was not influenced by species and/or isotype-related differences in the antibodies, a commercially available rat IgG2b anti-PD-L1 antibody (10F.9G2 clone, Bio X Cell) was tested with the 1x20Gy regimen. Treatment with the 10F.9G2 antibody demonstrated similar improvements in tumour control and mouse survival following 1x20Gy irradiation to those observed with the 6E11 antibody (*Figure 5.2b*), suggesting that the ability of RT to promote the anti-tumour activity of anti-PD-L1 therapy was not regulated by radiation DPF. Concurrent depletion of either $CD8^+$ T cells or NK cells resulted in abrogation of combinatorial therapeutic efficacy between 1x20Gy irradiation and 10F.9G2 antibody treatment (*Figure 5.3a-b*). Notably, the loss of tumour control with NK cell depletion was more pronounced and occurred earlier than that with $CD8^+$ T cell depletion (approximately day 10 *vs.* day 20, respectively). These observations suggest that PD-L1 blockade potentiated both $CD8^+$ T and NK cell responses against AT3-OVA tumours following RT, but amplification of NK cell responses appeared to be the more dominant mechanism of interaction.

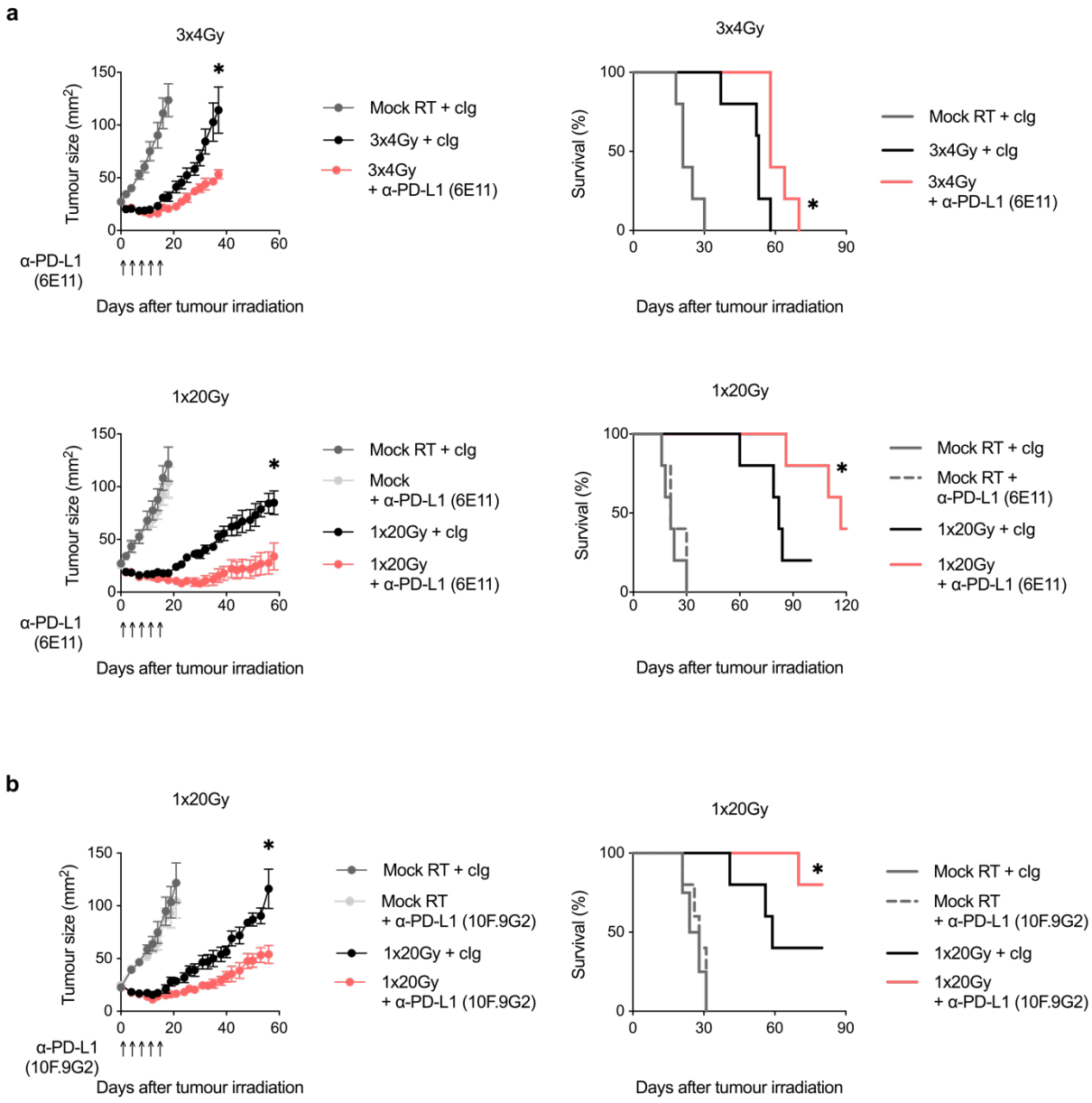

Figure 5.2. RT can enhance the anti-tumour activity of anti-PD-L1 therapy regardless of radiation DPF. a-b, AT3-OVA tumour growth (left) and mouse survival (right) after RT in mice treated with (**a**) 6E11 anti-PD-L1 or isotype control antibodies, or (**b**) 10F.9G2 anti-PD-L1 or isotype control antibodies. The experimental set up was similar to that described in *Figure 5.1*. 6E11 and 10F.9G2 anti-PD-L1 or their respective isotype control antibodies (150μg/mouse for the first injection, 100μg/mouse thereafter) were administered every 4 days from start of RT, for a total of 5 injections. Arrows indicate the time of antibody treatment. Statistical comparisons were made between the RT + anti-PDL-1 and RT + cIg groups. *n*=5-6 mice per group, representative of (**a**) 1 experiment, and (**b**) 2 independent experiments. Tumour growth data is presented as mean ± SEM, * $p<0.05$, *** $p<0.001$

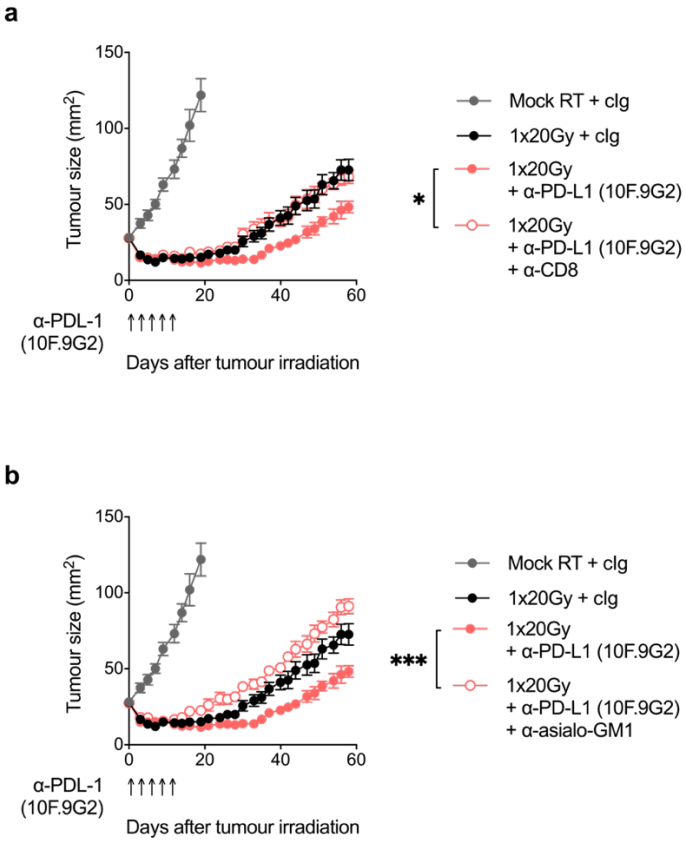

Figure 5.3. The combinatorial effect between 1x20Gy irradiation and anti-PD-L1 therapy is mediated by both CD8$^+$ T and NK cells. a-b, AT3-OVA tumour growth post RT in mice treated with 10F.9G2 anti-PD-L1 antibodies or isotype control antibodies, in combination with (**a**) CD8$^+$ T cell depleting or (**b**) anti-asialo-GM1 antibodies. 10F.9G2 anti-PD-L1 or isotype control antibodies were administered every 4 days from start of RT, for a total of 4 injections. CD8$^+$ T cell depleting (or isotype control antibodies) and anti-asialo-GM1 antibodies (or PBS) were administered every 3 days from start of RT to end of experiment. Arrows indicate the time of anti-PD-L1 antibody treatment. *n*=5-6 mice per group, representative of 1 experiment. Data is presented as mean ± SEM, * $p<0.05$, *** $p<0.001$

2. Combining RT with anti-Ly49C/I therapy or anti-NKG2A therapy

To investigate if anti-tumour NK cell responses evoked by radiation could be supported with immune checkpoint inhibitors, mouse antibodies with dual specificity for the NK cell-inhibitory Ly49C and Ly49I receptors (kindly provided by Bristol-Myers Squibb (BMS)) were tested. Upregulation of transcripts for Ly49C (*Klra3* gene) in the immune compartment of irradiated AT3-OVA tumours at day 13 post 1x20Gy irradiation (*Appendix Figure 10*) provided rationale for testing this antibody following irradiation with regimens of high biological effective dose (BED). At the time when these experiments were performed, an interim report from a phase I/II clinical trial testing lirilumab (an anti-KIR2DL1/2/3 antibody) with nivolumab (anti-PD-1 therapy) in head and neck squamous cell carcinomas suggested combinatorial efficacy between the two checkpoint inhibitors (Althammer *et al.*, 2016). Based on this, 1x20Gy irradiation was tested in AT3-OVA tumours in combination with anti-Ly49C/I therapy, and in combination with doublet anti-Ly49C/I and anti-PD-1 therapy. Surprisingly, anti-Ly49C/I therapy appeared to have a deleterious effect on the anti-tumour activity of 1x20Gy irradiation, which could be overcome when paired with anti-PD-1 therapy (*Figure 5.4a-b*). Due to a lack of anti-Ly49C/I antibody availability and the fact that lirilumab failed to demonstrate therapeutic benefit in two subsequent expanded clinical trials (Innate Pharma, 2017; Vey *et al.*, 2017), no further work on this pathway was pursued.

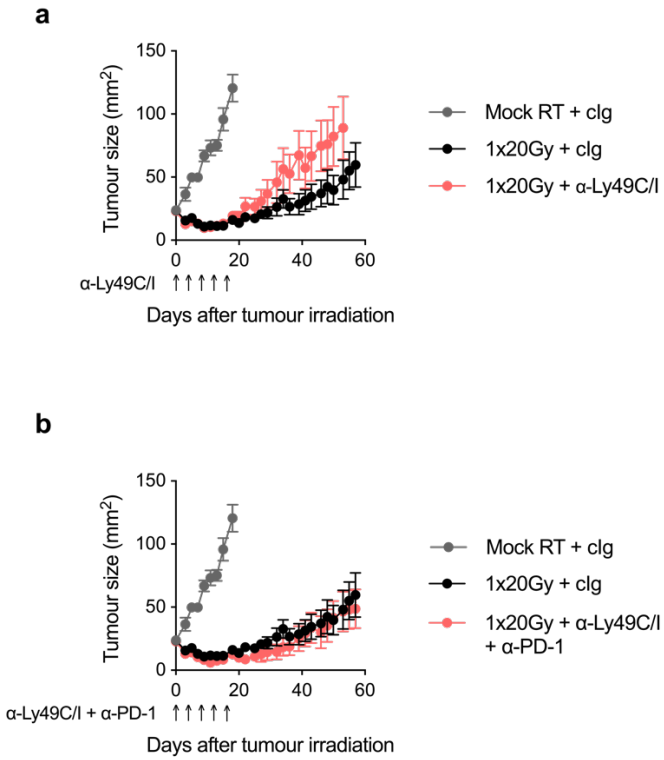

Figure 5.4. 1x20Gy irradiation does not enhance the anti-tumour activity of anti-Ly49C/I therapy. a-b, AT3-OVA tumour growth after RT in mice treated with (**a**) anti-Ly49C/I or isotype control antibodies, (**b**) and in combination with anti-PD-1 antibodies. The experimental set up was similar to that described in *Figure 5.1*. Anti-Ly49C/I or isotype control antibodies (200µg/mouse for the first injection, 150µg/mouse thereafter) were administered every 4 days from start of RT, for a total of 5 injections. Anti-PD-1 antibodies (150µg/mouse for the first injection, 100µg/mouse thereafter) were administered in a similar schedule. Arrows indicate the time of antibody treatment. *n*=5-6 mice per group, representative of 1 experiment. Data is presented as mean ± SEM.

The inhibitory receptor NKG2A was examined as an alternate target to promote radiation-induced NK cell responses. Elevated expression of NKG2A was detected on the surface of tumour-associated NK cells at day 13 post irradiation with both 3x4Gy and 1x20Gy regimens compared to the mock-irradiated controls, although the upregulation was most pronounced with the 1x20Gy regimen (*Figure 4.7b*). To test if blockade of this receptor could potentiate radiation-induced NK cell responses, mouse anti-NKG2A antibodies (kindly provided by BMS) were administered concurrently with 3x4Gy and 1x20Gy irradiation of AT3-OVA tumours. Treatment with the anti-NKG2A antibody did not demonstrate single agent activity, but significantly improved tumour control following 3x4Gy irradiation compared to RT alone (*Figure 5.5a*). By contrast, only a trend towards improved tumour control was observed with 1x20Gy irradiation and anti-NKG2A therapy compared to RT alone (*Figure 5.5a*). The significant combinatorial effect between anti-NKG2A therapy and the 3x4Gy regimen occurred within a timeframe that was consistent with the induction of $CD8^+$ T cell responses by radiation, raising the possibility that $CD8^+$ T cells were the principal target of NKG2A blockade in this setting.

In Chapter 4, it was determined that the anti-tumour function of tumour-associated NK cells was restricted by radiation-induced Tregs during the early post irradiation phase (days 0-13 post completion of RT), but high BED radiation evoked sustained NK cell responses that persisted into the late post irradiation phase when the radiation-induced Treg response had resolved (days 14-21 post completion of RT) (*Figure 4.5a, Figure 4.7a*). To selectively target these late-phase NK cell responses, initiation of anti-NKG2A therapy was delayed until day 10 post 1x20Gy irradiation (administered between days 10-26 post RT, as opposed to days 0-16 when anti-NKG2A therapy was given concurrently with 1x20Gy irradiation). Delayed anti-NKG2A therapy following 1x20Gy irradiation significantly improved tumour control compared to RT alone (*Figure 5.5b*). Further work will need to determine the contribution of $CD8^+$ T and NK cells to this combinatorial effect.

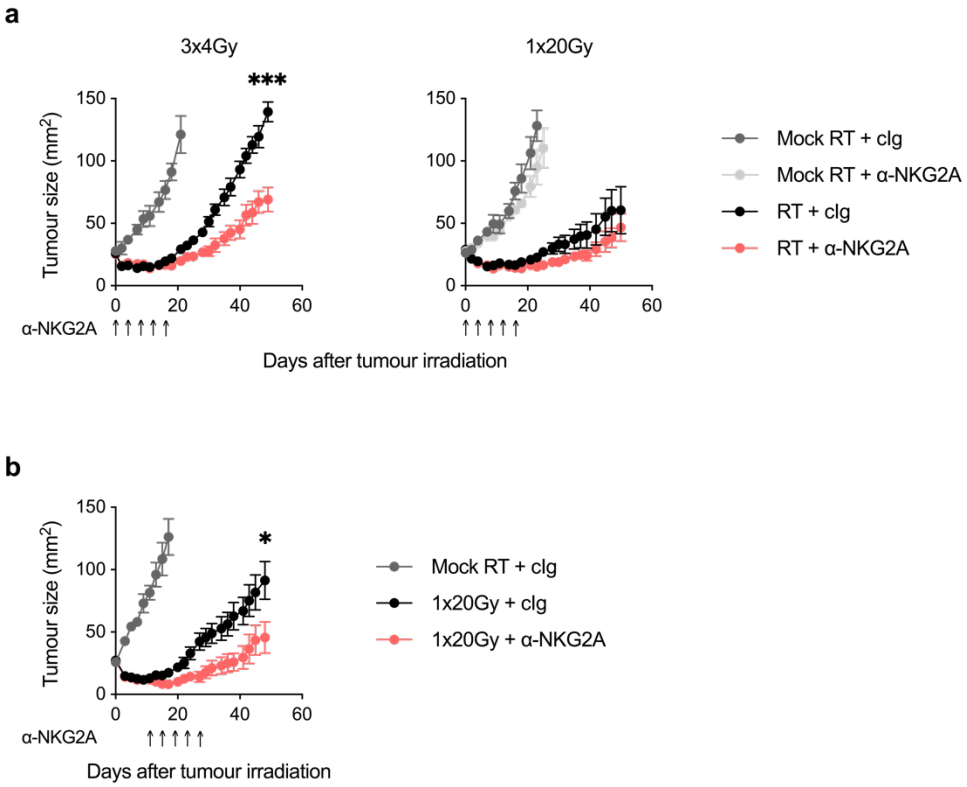

Figure 5.5. The timing of anti-NKG2A therapy may influence its therapeutic synergy with 1x20Gy irradiation. a, AT3-OVA tumour growth after RT in mice treated with (**a**) concurrent and (**b**) delayed anti-NKG2A or control isotype antibodies. Anti-NKG2A or isotype control antibodies (200µg/mouse for the first injection, 150µg/mouse thereafter) were administered every 4 days (**a**) from start of RT, for a total of 5 injections (days 0, 4, 8, 12, and 16 post RT), or (**b**) from day 10 post RT, for a total of 5 injections (days 10, 14, 18, 22, 26 post RT. Arrows indicate the time of antibody treatment. Statistical comparisons were made between the RT + anti-NKG2A and RT + cIg groups. *n*=5-6 mice per group, representative of 2 independent experiments. Data is presented as mean ± SEM. * $p<0.05$, *** $p<0.001$

3. Combining RT with anti-TIGIT/CD96 or anti-TIM-3 therapy

Blockade of TIGIT, CD96 or TIM-3 could present an opportunity to target both adaptive and innate arms of the immune response to RT. RNAseq analysis of the immune compartment of AT3-OVA tumours revealed that *Tigit* gene expression was upregulated at day 5 post irradiation with the 1x20Gy regimen but not with the 3x4Gy regimen (*Figure 3.11f*). To examine the biological significance of this observation, anti-TIGIT and anti-CD96 antibodies (both kindly provided by BMS) were tested. Anti-TIGIT, anti-CD96 and dual anti-TIGIT/CD96 therapy did not demonstrate either activity against AT3-OVA tumours either by themselves or in combination with 1x20Gy irradiation (*Figure 5.6a-c*). Anti-TIM-3 antibodies (kindly provided by BMS) also did not demonstrate single agent activity or therapeutic synergy with either 3x4Gy or 1x20Gy irradiation (*Figure 5.6d*). These data suggest that TIGIT, CD96 and TIM-3 were not dominant immune regulatory pathways induced by RT in AT3-OVA tumours.

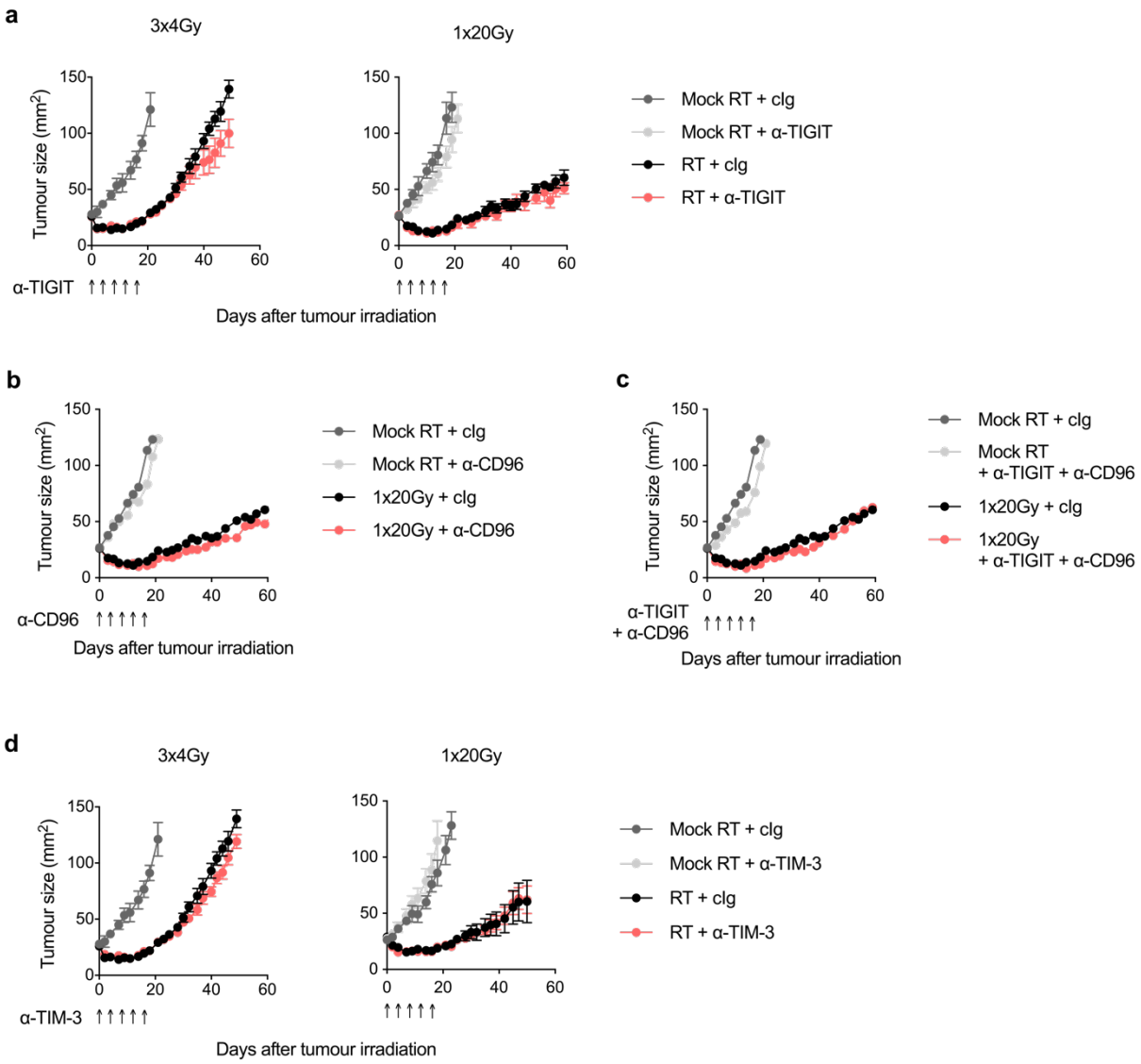

Figure 5.6. RT does not enhance the anti-tumour activity of anti-TIGIT, anti-CD96, or anti-TIM-3 therapy. a-d, AT3-OVA tumour growth after RT in mice treated with (**a**) anti-TIGIT, (**b**) anti-CD96, (**c**) doublet anti-TIGIT and anti-CD96, (**d**) anti-TIM-3, or their respective isotype control antibodies. The experimental set up was similar to that described in *Figure 5.1*. All antibodies (200μg/mouse for the first injection, 150μg/mouse thereafter) were administered every 4 days from start of RT, for a total of 5 injections. Arrows indicate the time of antibody treatment. *n*=5-6 mice per group, representative of 1 experiment. Data is presented as mean ± SEM.

Discussion

The focus of this chapter was to determine if insights gained from Chapter 3 and 4 could help guide the rational application of RT with immune checkpoint blockade. A range of immune checkpoint inhibitors was tested with radiation dose-fractionation regimens of known capacities to evoke anti-tumour $CD8^+$ T and NK cell responses. Some of these experiments were performed as part of an ongoing collaboration between the Peter MacCallum Cancer Centre and pharmaceutical industry-supported immuno-oncology collaborative networks, namely the Immunotherapy Centres of Research Excellence (imCORE) with Roche Phamarceuticals and the International Immuno-Oncology Network (IION) with BMS. Importantly, because AT3-OVA tumours were refractory to all tested immune checkpoint inhibitors when given as monotherapy, except for the 9D9 IgG2a anti-CTLA-4 antibody (*Figure 3.14a*), any combinatorial advantage was indicative of favourable alterations in the tumour immune microenvironment triggered by radiation. Findings from this chapter demonstrated that the selection of radiation dose-fractionation can potentially influence combinatorial efficacy with immune checkpoint inhibitors, particularly those directed at rescuing the anti-tumour function of $CD8^+$ T cells.

Chapter 3 demonstrated that radiation regimens with low-to-moderate DPFs were more effective at priming $CD8^+$ T cell responses in AT3-OVA tumours than regimens with high DPFs. In line with this, it was confirmed in this chapter that $CD8^+$ T cell-targeted checkpoint inhibitors such as anti-PD-1, non-depleting anti-CTLA-4 and even anti-NKG2A antibodies only synergised therapeutically with the 3x4Gy regimen (as well as the 9x4Gy regimen which was also tested in conjunction anti-PD-1 antibodies), but not with the 1x20Gy regimen. Intriguingly, a non-equivalence between anti-PD-1 and anti-PD-L1 therapy was observed, with the latter also demonstrating combinatorial efficacy with the 1x20Gy regimen. While PD-L1 blockade is thought to act largely through the same axis as PD-1 blockade, it is increasingly recognised that anti-PD-L1 therapy could engage additional effector pathways that are independent of PD-1. For example, a recent report by Dong *et al.* demonstrated that NK cells upregulated PD-L1 expression upon encountering tumour cells, and anti-PD-L1 antibody engagement with $PD\text{-}L1^+$ NK cells surprisingly triggered a positive regulatory event that promoted the anti-tumour function of NK cells both *in vitro* and *in vivo* (Dong *et al.*, 2019). The 10F.9G2 anti-PD-L1 antibody has also been reported to exert anti-tumour activity via ADCC-mediated clearance of tumour-associated myeloid-derived suppressor cells (Dahan *et al.*, 2015), although whether this also applied to the 6E1 anti-PD-L1 antibody is unknown. Whether these mechanisms underpinned how anti-PD-L1 therapy promoted the anti-tumour activity of NK cells in AT3-OVA tumours following 1x20Gy irradiation will need to be clarified. Interestingly, the therapeutic synergy between the 1x20Gy

regimen and anti-PD-L1 therapy was also in part mediated by $CD8^+$ T cells, even though neither modality was able to independently evoke $CD8^+$ T cell responses. Of note, $CD8^+$ T cell-mediated tumour control following 1x20Gy irradiation and anti-PD-L1 therapy was evident 20-25 days post RT, which was significantly later than what was observed with primary radiation-induced $CD8^+$ T cell responses in the context of low-to-moderate DPF regimens when given without immunotherapy (days 10-15 post completion of RT) (*Figure 3.2a*). Furthermore, NK cell-mediated tumour control was more pronounced and occurred around 10 days earlier than $CD8^+$ T cell-mediated tumour control in the context of concurrent anti-PD-L1 therapy. Given that NK cells can promote the tumour infiltration and maturation of DCs (Pallmer and Oxenius, 2016; Bottcher *et al.*, 2018), these observations raise the possibility that secondary $CD8^+$ T cell responses were being supported by the amplified NK cell responses following co-treatment with 1x20Gy irradiation and anti-PD-L1 therapy (*Figs. 5.3c-d*). Importantly, these differences in anti-PD-1 and anti-PD-L1 therapy suggest that despite the close relationship between this receptor-ligand pair, anti-PD-1 therapy is potentially more restrictive than anti-PD-L1 therapy in its therapeutic synergy with RT.

It was also demonstrated in Chapter 3 that RT enriched for Tregs in AT3-OVA tumours irrespective of the dose-fractionation employed, resulting in significantly suppressed anti-tumour function of $CD8^+$ T and NK cells. Correspondingly, short-term depletion of Tregs rationally-timed to coincide with radiation-induced Treg responses greatly improved immune-mediated control of AT3-OVA tumours, resulting in tumour cures. Therefore, for tumour types that exhibit radiation-induced Treg responses, the potential synergy between RT and Treg-directed interventions could be independent of radiation dose-fractionation. This PhD project has illustrated that a potential strategy for targeting tumour-associated Tregs in conjunction with RT is by using anti-CTLA-4 antibodies capable of inducing ADCC. However, the capacity for the human anti-CTLA-4 antibodies ipilimumab (of the IgG1 isotype) and tremelimumab (of the IgG2 isotype) to induce Treg depletion in human cancers is unclear. Studies examining this question have yielded conflicting results thus far, which is in part due to complexities surrounding the need for patient-paired pre- and post-therapy tumour samples, the variations in normalising cell counts, and the non-Treg expression of Foxp3 in humans (Romano *et al.*, 2015; Arce Vargas *et al.*, 2018; Wei *et al.*, 2018; Sharma *et al.*, 2019). An altered version of ipilimumab with a non-fucosylated Fc domain has nonetheless been designed for enhanced depleting function and is being investigated in a clinical trial (NCT03110307). Although not examined in this study, glucocorticoid-induced tumour necrosis factor receptor (GITR) is another promising target for the functional manipulation and/or antibody-based Treg depletion. GITR is a co-stimulatory molecule constitutively expressed at high levels by Tregs, which upon stimulation inhibits the

suppressive function of Tregs (Shimizu *et al.*, 2002). A recent first-in-human phase I trial reported a good safety profile for the anti-GITR antibody TRX518 and demonstrated that the antibody could reduce circulating and tumour-associated Tregs (Zappasodi *et al.*, 2019). Interestingly, in the RNAseq analyses performed for this PhD project, transcripts for GITR (*Tnfrsf18* gene) were found to be highly upregulated in the immune compartment of 1x20Gy-irradiated AT3-OVA tumours (*Figure 3.11f*), which may provide rationale to further examine this receptor as an avenue for Treg-directed therapy in combination with RT. Altogether, results from this study suggest that interventions directed at circumventing the transient immunosuppressive microenvironment generated by radiation, tailored to the tumour type, may create a highly favourable therapeutic window by harnessing both anti-tumour $CD8^+$ T cell and NK cell responses.

Beyond targeting T cells, NK cell-directed immunotherapies are increasingly investigated as a strategy to circumvent tumour resistance to $CD8^+$ T cell-directed approaches (Guillerey *et al.*, 2016). As discussed above, NK cell responses in AT3-OVA tumours evoked by RT could be potentiated with Treg-depleting anti-CTLA-4 therapy or with anti-PD-L1 therapy. Intriguingly, anti-Ly49C/I therapy appeared to exert a negative impact on the control of AT3-OVA tumours following 1x20Gy irradiation, but co-treatment with doublet anti-Ly49C/I and anti-PD-1 therapy did not. The reasons for these surprising results are unknown. Although pro-tumour effects of NK cells have been described and could have been promoted by blockade of Ly49C/I (Bruno *et al.*, 2014), this seemed unlikely given the significant anti-tumour role of NK cells observed in AT3-OVA tumours in all other conditions. Due to a lack of further Ly49C/I antibodies for investigation, these experiments were not replicated to confirm the findings, and additional work on this pathway was not undertaken. The NKG2A checkpoint receptor was another target investigated in this study as a strategy to harness radiation-induced NK cell responses, given that expression of this receptor was particularly elevated on tumour-associated NK cells following high BED irradiation. Importantly, the ability of anti-NKG2A therapy to promote the anti-tumour activity of 1x20Gy irradiation was influenced by the timing of the two modalities relative to each other, since only delayed (days 10-26 post RT), but not early (days 0-16 post RT), application of NKG2A blockade with the 1x20Gy regimen achieved synergistic control of AT3-OVA tumours. While the role of NK cells in mediating this combinatorial effect needs to be confirmed, the importance of a temporal gap between completion of RT and initiation of NKG2A blockade could reflect the kinetics of Treg responses within the tumours post RT, whereby radiation-induced Tregs exerted potent suppression of NK cell function in the early post irradiation phase but had subsided by day 13 post completion of RT. In contrast, tumour-associated NK cell responses induced by high BED radiation were sustained up to day 21 post RT, thus creating a window to intervene with NKG2A blockade. Significantly, in addition to radiation dose-fractionation,

immunotherapeutic agent, and tumour type, these findings highlight the importance of timing as a fourth factor in considering the optimal combination strategy between RT and immune checkpoint blockade.

Overall, this chapter demonstrated that radiation dose-fractionation regimens are not equivalent in their ability to therapeutically synergise with immune checkpoint blockade. Ongoing work to more comprehensively understand the impact of RT on the composition, functional status, and dynamics of the tumour-associated immune cell contexture across different tumour types is therefore crucial for the development of combination strategies that are predicated on biological rationale. At present, biomarkers that may assist in guiding RT and cancer immunotherapy combination strategies are undefined. Testing of any putative biomarkers in models of tumour metastasis to examine if they translate to the regulation of radiation abscopal effects will also be of value. Altogether, such insights will help ensure the optimal use of RT not only as a powerful cytotoxic modality, but also as an important adjunct to cancer immunotherapy in re-establishing immune control of cancer.

Chapter 6: Conclusions and Future Directions

Selecting the radiation dose-fractionation most appropriate for the patient is one of the most important tasks of a radiation oncologist. This decision is intricately linked to a multitude of factors, not least of which include medical evidence, clinical judgment, patient preference, availability of radiation therapy (RT) technologies, and departmental policies. Progress in radiobiology has greatly advanced the understanding of how dose-fractionation parameters such as total dose, dose per fraction (DPF), dose rate, and overall treatment time affect DNA damage and repair, cell death and proliferation, and ultimately tumour control and normal tissue complications. These insights enable the radiation oncologist to safely tailor radiation regimens in extraordinary clinical situations, as well as allow the development and testing of newer dose-fractionation regimens optimised for the treatment of different tumour types. For example, altered fractionation schedules that shorten the overall treatment time for rapidly proliferating cancers such as head and neck squamous cell carcinomas and small cell lung cancers have shown superiority in oncological outcomes compared to conventionally fractionated regimens, while hypofractionated regimens using DPFs larger than 2Gy have become standard of care for the treatment of tumours with low α/β ratios such as breast and prostate cancers (Ang, 1998; Turrisi *et al.*, 1999; Bentzen *et al.*, 2008; Dearnaley *et al.*, 2016).

Beyond direct cell kill by induction of irreparable DNA damage, there remains little doubt now that RT also exerts pleiotropic "non-target" effects on the tumour immune microenvironment, which can overcome points of failure in the cancer-immunity cycle and help (re-)establish immune control of the tumour. The therapeutic potential of leveraging such effects in combination with cancer immunotherapy is substantiated by a robust body of pre-clinical work and early clinical trial outcomes. Nonetheless, the promise of this strategy has brought to focus several major gaps in knowledge that hamper the optimal use of RT to evoke beneficial immunological responses. For the radiation oncologist, a major deficiency in the translation of this concept into clinical practice is the lack of mechanistic understanding to guide the selection of radiation dose-fractionation regimens. This formed the research focus of this PhD project. Three overarching conclusions can be drawn from the collective work presented in this thesis, which can also serve as general principles for approaching further study on this topic:

1. Radiation dose-fractionation regimens are not equivalent in their capacity to evoke anti-tumour immune responses. Chapter 3 presented data suggesting that radiation-induced $CD8^+$ T cell responses in AT3-OVA tumours were regulated by high radiation DPF, rather than total dose, as represented by biological effective dose (BED). By contrast, results in Chapter 4 suggest that radiation-induced NK cell responses in the same tumours were independent of radiation DPF but required a sufficient BED. Given these immune

response characteristics, it can be inferred that radiation regimens of low-to-moderate DPF but high BED can evoke both $CD8^+$ T and NK cell responses to control AT3-OVA tumours when given as monotherapy. Indeed, irradiation of AT3-OVA tumours with the 3x8Gy (BED_{16} 36Gy) and 9x4Gy (BED_{16} 45Gy) regimens controlled tumours for longer than with the 1x20Gy (BED_{16} 45Gy) regimen, even though their BEDs, which are only a measure of cell kill by DNA damage, were lower than or the same as that of 1x20Gy (*Figure 3.3a, Figure 4.1c*). Furthermore, because radiation dose-fractionation regimens have different capacities to evoke anti-tumour immune responses, it follows that synergy with a specific immunotherapeutic agent will in part depend on the radiation dose-fractionation regimen employed, as demonstrated in Chapter 5. These findings illustrate the potential of optimising radiation dose-fractionation regimens, with and without immunotherapy, to maximally harness innate and adaptive immune responses for controlling tumours, beyond classical radiobiological considerations of DNA damage and repair.

2. Radiation-induced anti-tumour immune responses are not simply a function of the radiation dose-fractionation's capacity to induce effector responses, but are also defined by the immune-regulatory microenvironment generated. Chapters 3 and 4 established that radiation DPF-dependent regulatory T cell (Treg) enrichment within AT3-OVA tumours played a central role in determining the ability of $CD8^+$ T and NK cell responses to exert tumour control. This regulatory mechanism was tumour type-dependent, as similar Treg responses were not observed in MC38 tumours following irradiation. Significantly, in AT3-OVA tumours, the radiosensitisation effect achieved by short-term, rationally-timed Treg depletion was more profound than strategies to release effector cell-intrinsic immune checkpoints, such as with PD-1, PD-L1 or NKG2A blockade (Chapters 3 and 5). Thus, interventions directed against radiation-induced immunosuppressive microenvironments, tailored to the tumour type, can synergise with RT by simultaneously promoting the anti-tumour activity of multiple effector arms. These findings complement landmark work by the Demaria and Formenti group, which raised the importance of considering tumour cell-intrinsic regulation of immunogenicity across different radiation dose-fractionation regimens (Vanpouille-Box *et al.*, 2017). Herein, the equal importance of understanding tumour cell-extrinsic regulation on immune responses is demonstrated.

3. A deeper understanding of the dynamics of radiation-induced immune responses, beyond static observations, is vital and can reveal opportunities to target anti-tumour immune responses otherwise missed. Work in this thesis demonstrated that the frequency and

function of various immune subsets within tumours changed over time following irradiation. Across all dose-fractionation regimens tested, the abundance of Tregs within tumours exhibited a characteristic pattern of modulation, synchronised to the completion of irradiation, that was very similar regardless of the total dose or overall treatment time of the dose-fractionation regimen used. Appreciation of such dynamics informed the rationally-timed depletion of radiation-induced Tregs in this PhD project (Chapter 3). Furthermore, observation of the biphasic nature of radiation-induced NK cell responses guided the successful timing of NKG2A blockade following tumour irradiation, at a phase when the enrichment of radiation-induced Tregs had resolved but NK cell responses were maintained (Chapters 4 and 5). Conversely, examination at a single time point, for example at day 3 when tumour-associated Tregs were transiently scant, could have falsely represented the post irradiation immune contexture. Studying longitudinal changes in the tumour microenvironment over time requires meticulous planning and is not practicable in human cancers, but observations made from this PhD project attest to its importance and to the value of using pre-clinical models to define new paradigms.

Moving forward, the refashioning of RT as a modality to shape immune responses will undoubtedly require rethinking of conventional radiation oncology practices. Conceptually, RT is uniquely positioned to be partnered with cancer immunotherapy from two angles: priming and debulking. The two approaches are not necessarily mutually exclusive. One of the biggest barriers to the successful application of immune checkpoint blockade is a "cold" tumour microenvironment, in which there is little or no pre-existing T cell infiltration to manipulate for therapeutic gain. Although the exact factors driving such phenotypes are not yet fully understood, RT is often proposed as a promising candidate to overcome this conundrum, given its ability to promote the antigenicity and adjuvanticity of tumour cells upon cell kill to instigate T cell priming. Importantly, RT is geographically precise and is able to target poorly perfused and deep tumours, which may be challenging to access for other priming strategies such as systemic chemotherapy and intra-tumoural injection of innate immune agonists. Illustrating this potential, Zheng *et al.* developed a "cold" pancreatic tumour model that was poorly infiltrated with $CD8^+$ T cells and showed that RT promoted T cell infiltration and efficacy of immunotherapy in those tumours (Zheng *et al.*, 2016). Evidence for the conversion of a "cold" to "hot" tumour by radiation in the clinical setting however is still to be conclusively demonstrated. Concurrently, molecular imaging of PD-1/PD-L1 using positron-emission tomography (PET) is emerging as a tool to non-invasively determine the immune contexture of tumours at baseline and post treatment, potentially serving as a powerful biomarker to select patients for treatment with PD-1/PD-L1 blockade (Bensch *et al.*, 2018; Verhoeff *et al.*, 2020). It is easy to envisage that RT could be heavily utilised

in conjunction with such functional imaging techniques to selectively treat tumours with low PD-L1 tracer uptake (suggesting low baseline inflammation) for example, as an adjuvant modality to induce a favourable tumour immune microenvironment for cancer immunotherapy.

The priming of T cell responses and breaking down of immunosuppressive barriers may require radiation dose-fractionation regimens and volumes that are significantly different to those used in conventional "treat to tolerance" approaches aimed to maximise direct tumour cell kill. Pre-clinically, low radiation doses between 0.5Gy to 2Gy were sufficient to repolarise immunosuppressive M2 macrophages into the pro-inflammatory M1 phenotype, leading to T cell recruitment into the tumour (Klug *et al.*, 2013). High doses and/or repeated fractions of radiation, especially to volumes that include normal vasculature and lymphoid organs, could also subject a greater proportion of naïve lymphocytes to radiation cell kill (Yovino *et al.*, 2013; Tang *et al.*, 2014). Indeed, radiation-induced lymphopaenia is increasingly found to be a negative prognostic factor across various solid cancers (Grossman *et al.*, 2011; Campian *et al.*, 2013; Tang *et al.*, 2014; Wild *et al.*, 2015; Davuluri *et al.*, 2017). Perhaps more provocatively, recent pre-clinical and clinical data have raised the possibility that partial irradiation of tumours may in fact be adequate to elicit robust immune responses that can control the entire tumour and even distant tumours (Luke *et al.*, 2018; Markovsky *et al.*, 2019). Radiation dose de-escalation and volume minimisation, including subtotal tumour volumes, are markedly counterintuitive to conventional dogma in radiation oncology, and will undoubtedly require cautious and judicious testing to confirm their safety and validity. However, these novel ideas should not be dismissed, especially in light of the momentous paradigm shifts that have taken place in the immuno-oncology era.

RT is also well-suited as a debulking strategy in combination with cancer immunotherapy, both in metastatic and localised disease contexts to reduce the overall tumour load. Underpinning this line of thought is the observation that patients with a more limited burden of disease respond better to cancer immunotherapy (Huang *et al.*, 2017; Joseph *et al.*, 2018; Robert *et al.*, 2018). The interaction between disease burden and outcomes is also seen in combined treatments of RT and cancer immunotherapy (discussed in Chapter 1, Section 3.3). Therefore, it is possible that in appropriately selected patients with metastatic disease, irradiation of all sites of known disease (a "debulking approach") could synergise more effectively with cancer immunotherapy than single-site irradiation (an "abscopal approach"), which conventionally has involved irradiation of a lesion that is most symptomatic or imminently so (Brooks and Chang, 2019). There are additional reasons to favour multi-site irradiation over single-site irradiation. Primarily, irradiation of all sites of known disease increases the likelihood of exposing a wider repertoire of tumour-associated antigens for T cell priming, which may address the significant mutational

heterogeneity commonly found between metastatic lesions (Jiménez-Sánchez *et al.*, 2017; Angelova *et al.*, 2018). Irradiation of all sites of known disease could also promote immune cell access to lesions that would otherwise be poorly immune-infiltrated, as well as destroy subclonal populations resistant to immune-mediated elimination. While abscopal approaches in the clinic have produced higher proportions of systemic responses when combined with cancer immunotherapy, the response rates are still low at 10-30% (Golden *et al.*, 2015; Twyman-Saint Victor *et al.*, 2015; Formenti *et al.*, 2018). At the same time, recent studies examining complete metastatic ablation and radiation debulking of the primary tumour in patients with metastatic disease, independent of immunotherapy, have reported surprising improvements in survival that likely extend beyond local control of irradiated tumours (Parker *et al.*, 2018; Palma *et al.*, 2019; Phillips *et al.*, 2020). Taken together, leveraging the unique ability of RT to aggressively and effectively reduce the overall disease burden may be a rational strategy to test in partnership with cancer immunotherapy. Indeed, it is worth noting that the most remarkable therapeutic synergy observed between the two modalities thus far was demonstrated by the PACIFIC trial, in which patients with Stage III non-small cell lung cancer had only overt locoregional disease (Antonia *et al.*, 2018). In this study, curative-intent radiation was employed to essentially achieve maximum tumour debulking, facilitating in principle more efficient eradication of residual microscopic disease by subsequent PD-L1 blockade. The safety profile of multi-site irradiation, especially in combination with cancer immunotherapy, must however be a paramount consideration. A recent study testing this strategy using stereotactic ablative radiotherapy (SABR) and PD-1 blockade has reported acceptable toxicity (Luke *et al.*, 2018).

Importantly, clinical investigations must be accompanied by careful translational work to reveal the underlying biology. Although pre-RT tumour tissue from patients (usually biopsy specimens) are often collected, post RT tumour specimens are currently lacking, yet are an invaluable asset for validating mechanistic findings from pre-clinical studies. Serial blood samples are useful but may not reflect important local biological processes occurring within irradiated lesions. Of all the entries screened in the Gene Expression Omnibus (GEO) during this PhD project, only two datasets were found to contain pre- and post RT tumour specimens, which were analysed and reported in Chapter 4. Longitudinal collection of tissue specimens has yielded significant mechanistic insights in chemotherapy and immunotherapy settings (Kim *et al.*, 2018; Gide *et al.*, 2019; Yost *et al.*, 2019). As the value of studying the immunological effects of radiation is increasingly recognised, efforts to collect pre- and post RT tumour specimens are intensifying internationally. For example, the aforementioned study of multi-site SABR with PD-1 blockade also reported early immune analysis on paired pre- and post-SABR tumour specimens (Luke *et al.*, 2018), and a clinical trial is being set up in the UK that involves serial tissue biopsies in

patients undergoing RT for various cancer types (private communication). Acknowledging that not all patients may consent to sequential invasive biopsies, a strategy of less resistance is to consider cancers for which neoadjuvant RT forms a component of standard care. For such cancers, which include gastro-oesophageal, rectal, pancreas, bladder cancers and sarcomas, post RT tissue specimens could be obtained from planned surgical resections and compared to pre-RT biopsies without subjecting patients to additional invasive procedures. Advances in high dimensional and highly multi-parametric assays such as mass cytometry, multiplexed immunohistochemistry, and next generation sequencing have at the same time opened up new possibilities in the analyses of such samples. Correlating radiation-induced changes in tumours with clinical outcomes could both corroborate pre-clinical findings and reveal clues to feed back into further pre-clinical study using mouse models. Setting up such programmes of tissue collection will require substantive logistical effort and research funding, but may in the long-term yield invaluable translational data.

To continue empowering advances on the clinical front, enlarging the groundwork in fundamental pre-clinical research is crucial. In the laboratory, mechanistic studies thus far have focused on studying immunomodulatory changes in tumour cells. Much less is known about how the non-immune stromal compartment, composed primarily of the tumour vasculature and cancer-associated fibroblasts (CAFs), influences immune responses following irradiation. Evidence is mounting that these stromal tissues are not innocent bystanders, but play an under-appreciated role in shaping the tumour immune contexture (Joyce and Fearon, 2015; Turley *et al.*, 2015). Importantly, vascular endothelial tissues and fibroblasts have different radiation response characteristics to tumour cells (Arnold *et al.*, 2018). Alongside the growing clinical uptake of SABR, radiobiology research on high DPF regimens has led to the proposition that indirect, hypoxic tumour cell death via vascular endothelial damage could be a predominant mechanism of tumour control with such radiation regimens, as opposed to larger proportions of direct tumour cell death with conventionally fractionated regimens (Song *et al.*, 2019). Mechanistically, tumour vascular endothelial cells have been reported to be more prone to apoptosis via the ceramide pathway following irradiation with high DPF regimens (Garcia-Barros *et al.*, 2003; Truman *et al.*, 2010). Fibroblasts, being late-responding mesenchymal cells, have low α/β ratios and therefore demonstrate increased sensitivity to damage by large radiation DPFs, as opposed to tumour cells which commonly have higher α/β ratios (Joiner and Kogel, 2018). The effects of radiation on CAFs are pleiotropic, including induction of an altered secretion profile, increased deposition of ECM, and entry into senescence (Arnold *et al.*, 2018; Wang *et al.*, 2019). Therefore, it is possible that the differential radiation response characteristics between stromal and tumour cells may underpin the differential immune responses observed between radiation dose-

fractionation regimens. These under-investigated tissue components warrant more research focus to better understand the regulation of immune responses following RT.

Dissecting the impact of tumour type, tissue compartments, tissue niche, and volume of irradiation on the immunological effects of RT will require investment into suitable pre-clinical models and irradiation platforms. Because tumour location can dictate tissue-specific recruitment of immune cells into tumours (Lehmann *et al.*, 2017), it is possible that different tissue niches can influence the induction of immune responses by radiation even for the same tumour type, such as in the case of metastatic lesions in different organ sites. Little data currently exist to verify this, which represents a significant gap in knowledge, considering cancer metastases are a significant epidemiological burden and constitute the predominant cause of cancer-related death (Budczies *et al.*, 2015). Moreover, subcutaneous tumour models, which are often used as a surrogate when the tumour cell line's organ of origin is difficult to access for orthotopic implantation, may not accurately represent the immune contexture of their normal organ site (Zhao *et al.*, 2017). Therefore, studying the immunomodulatory effects of radiation in physiologically relevant tissue niches will require use of a range of mouse models, which may include a combination of transplantable and autochthonous models of tumourigenesis, as well as experimental and spontaneous models of metastases. Specialised transgenic mice would also greatly facilitate examination of complex tissue compartments, such as the tumour stroma, by expression of reporter molecules or depletion of specific cellular subsets. Equally important are irradiation platforms that are capable of safely delivering radiation to different anatomical sites in mice. *In vivo* radiation research work has traditionally used single beam radiation set-ups that are limited to irradiation of peripheral lesions (such as subcutaneous or mammary fat pad tumours) due to the inability to shape the radiation volume. Creative solutions in collaboration with medical physicists involving 3D-printing of customised immobilisation jigs, optimisation of radiation dosimetry, and even utilisation of clinical radiation machines could potentially circumvent some of the constraints. More advanced small animal irradiators with rotating gantries, variable collimators and on-board computerised tomography (CT) allow the freedom to target deep structures while minimising collateral irradiation of neighbouring structures, which enable investigation of primary and metastatic tumours in different organ sites. Altogether, moving forward to tackle the more complex questions of radiation and immuno-oncology research in the laboratory will require appropriate mouse models and infrastructure, as well as close collaboration between clinical, radiobiology, medical physics and immunology research teams.

The refashioning of RT to leverage synergistic interactions with cancer immunotherapy holds promise in the war against cancer, but is unquestionably still in its nascence. Rapid progress has

been made in our knowledge of the mechanisms, efficacy, and safety of this combination strategy. Even in recent years, landmark findings in both pre-clinical and clinical spaces have been reported, which have both shed much-needed insight into the underlying immunological processes evoked by radiation and solidified the clinical potential of this combination treatment approach. Nonetheless, significant further investigative work is required to address the outstanding gaps as outlined throughout this thesis, some of which will require innovative strategies to tackle. Results presented in this PhD thesis contribute towards a clearer understanding of the impact of radiation dose-fractionation on the immunomodulatory effects of radiation, but more broadly also illustrate general principles in studying this question. Perhaps more importantly, this PhD project has been foundational on a personal front in developing the skills and frameworks for thinking to critically and creatively approach scientific research in oncology.

Appendices

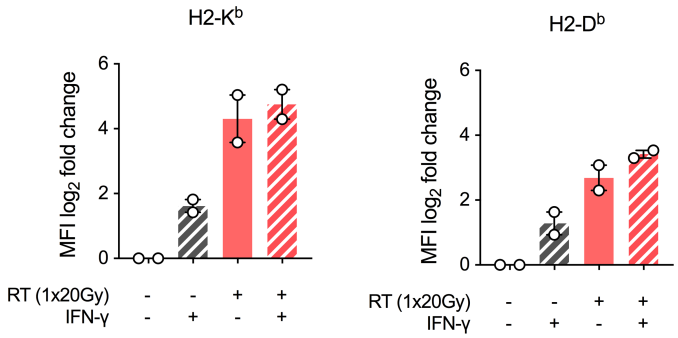

Appendix Figure 1. **Modulation of MHC-I surface expression on cultured AT3-OVA tumour cells by RT and IFN-γ.** AT3-OVA tumour cells were plated and irradiated in a similar experimental set up to *Figure 3.4*. IFN-γ (1ng/mL) was added into the culture medium 24 hours prior to 1x20Gy irradiation. Cells were harvested 24 hours after radiation exposure and processed for flow cytometry. Data presented as $\log_2$ fold change in MFI over mock controls (mock-irradiated and non-IFN-γ-treated).

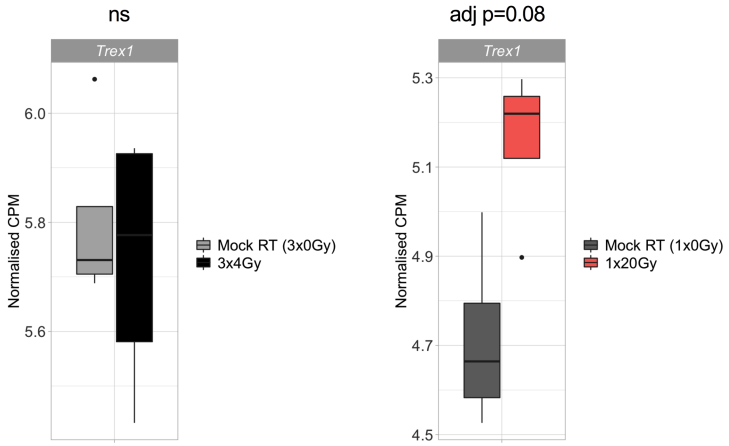

Appendix Figure 2. Modulation of *Trex1* transcript levels in tumour/stromal cells by RT *in vivo*. Normalised *Trex1* transcript counts by RNAseq in tumour/stromal (CD45-) cells flow-sorted from *ex vivo* AT3-OVA tumours at day 1 (16-20 hours) after completion of RT. Samples were compared to their respective mock-irradiated controls. Refer *Figure 3.10* for experimental schema. *CPM: counts per million*

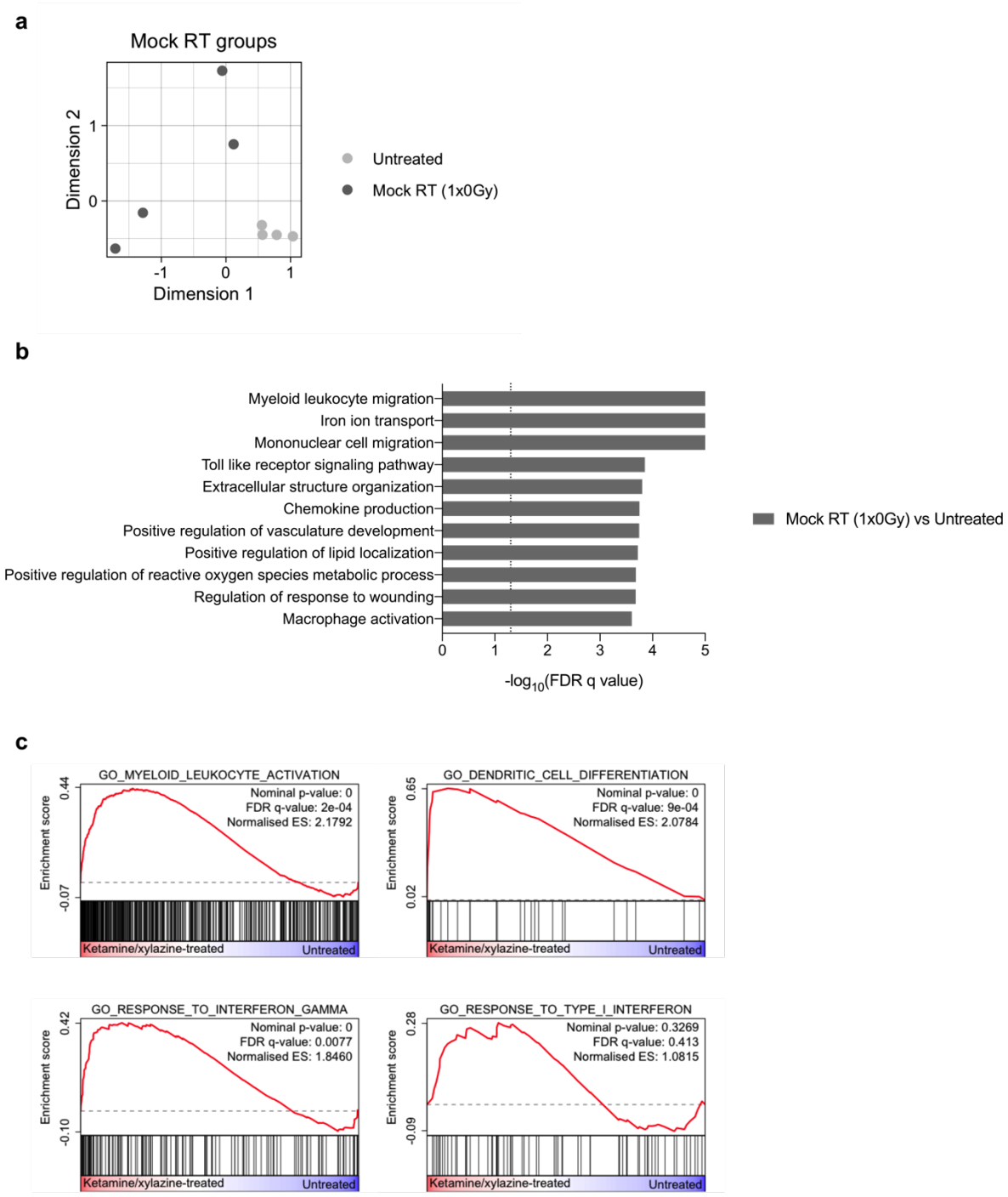

Appendix Figure 3. Ketamine/xylazine has immunomodulatory effects in AT3-OVA tumours. AT3-OVA tumour-bearing mice were treated with 1 injection of ketamine/xylazine and the tumours were harvested the following day (16-20 hours) as 1x0Gy tumours. AT3-OVA tumours were also harvested from mice that had not received any treatment. Immune ($CD45^+$) cells were flow-sorted from single cell tumour suspensions and processed for RNAseq. **a,** MDS plot of 1x0Gy (unirradiated, ketamine/xylazine-treated) and untreated (unirradiated, non-ketamine/xylazine treated) tumours. **b-c,** (**b**) GO-BP terms and (**c**) GSEA plots of selected GO-BP terms enriched by ketamine/xylazine treatment in the immune compartment of

AT3-OVA tumours. Analysis was performed using GSEA, comparing 1x0Gy tumours with untreated tumours.

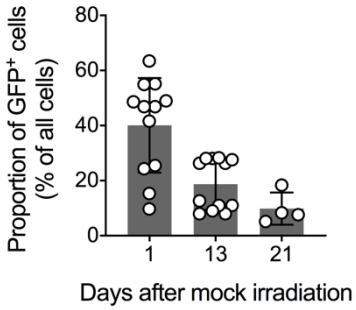

Appendix Figure 4. Proportion of GFP$^+$ CD45$^-$ cells in mock-irradiated AT3-OVA tumours over time. AT3-OVA tumours were irradiated at 25-35mm^2 and harvested at time points that were aligned to post completion of RT for flow cytometric analysis. Mock-irradiated tumours were analysed for the frequency of GFP$^+$ CD45$^-$ cells, presented as proportion of all live cells. Data is combined from 3 independent experiments.

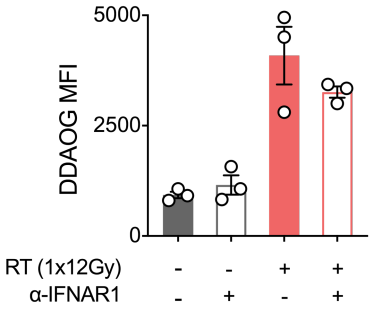

Appendix Figure 5. Effect of IFNAR1 blockade on radiation-induced cellular senescence of AT3-OVA tumour cells *in vitro*. DDAOG MFI on cultured AT3-OVA tumour cells at day 6 post 1x12Gy irradiation in combination with anti-IFNAR1 antibody treatment. Anti-IFNAR1 antibodies (1µg/mL) were added into the culture medium 24 hours prior to radiation exposure. *MFI: mean fluorescence intensity*

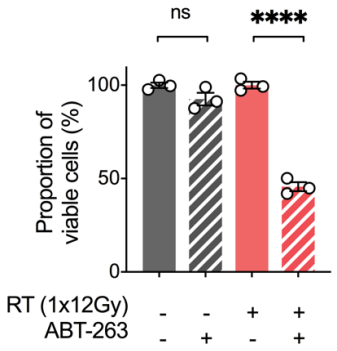

Appendix Figure 6. Selective killing of radiation-induced senescent AT3-OVA tumour cells by ABT-263 *in vitro*. Proportion of viable AT3-OVA tumour cells (defined as PI^-) following co-treatment with RT and ABT-263. Cultured AT3-OVA tumour cells were irradiated with 1x12Gy and left for 6 days for cells to enter senescence before ABT-263 was added into the culture medium at 1.25μM final concentration. Cells were harvested 48 hours later for flow cytometric analysis. *** *p<0.001*

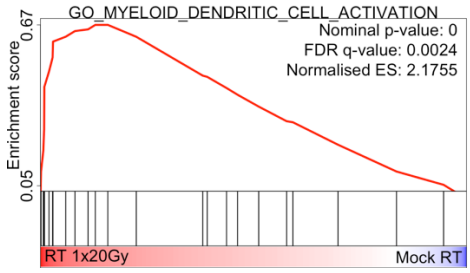

Appendix Figure 7. DCs are activated in AT3-OVA tumours in the late post irradiation phase. GSEA plot of the myeloid DC activation gene set (GO-BP) in the immune compartment of 1x20Gy-irradiated AT3-OVA tumours at day 13 post RT. Comparison was made to its mock-irradiated control (1x0Gy). An accompanying IFN-γ production gene signature was also enriched at this time point (*Figure 4.7d*).

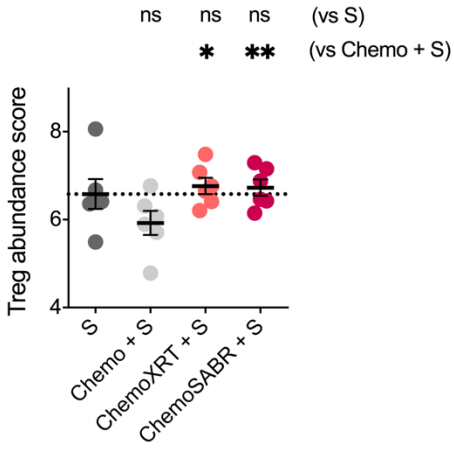

Appendix Figure 8. Treg abundance in human pancreatic ductal adenocarcinoma post irradiation. Abundance scores were calculated using the Cell Type Profiling Module of the nSolver Advanced Analysis package, which quantifies cell populations using marker genes representative of given cell types. Data is taken from the GSE129492 dataset described in *Figure 4.3*.

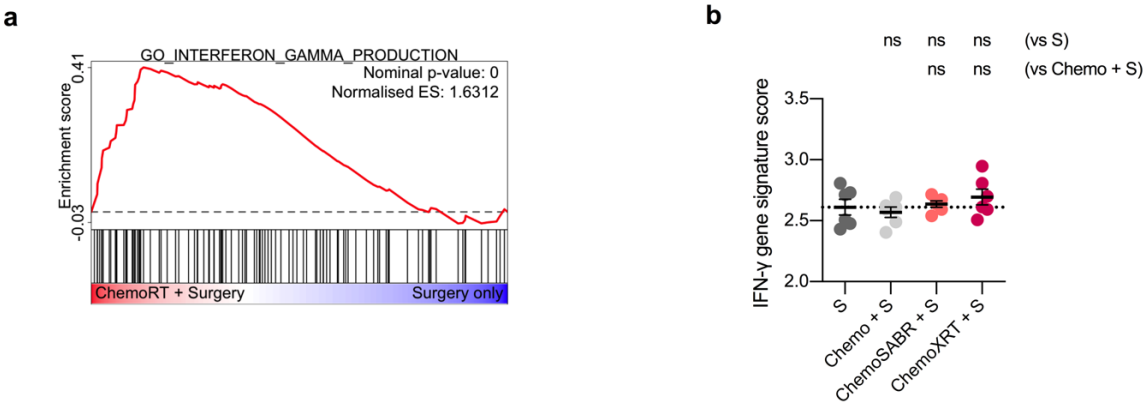

Appendix Figure 9. IFN-γ gene signature in human rectal adenocarcinoma and pancreatic ductal adenocarcinomas post irradiation. a, GSEA plot of IFN-γ production gene set (GO-BP) in human rectal adenocarcinomas, using the GSE129492 dataset, as described in *Figure 4.4a*. **b,** IFN-γ signature scores in human pancreatic ductal adenocarcinomas, using the GSE129492 dataset, as described in *Figure 4.3a*. A 6-gene IFN-γ signature (*IDO1*, *CXCL10*, *CXCL9*, *HLA-DRA*, *STAT1*, and *IFNG*) as developed and calculated by Ayers *et al.* (Ayers *et al.*, 2017) was used.

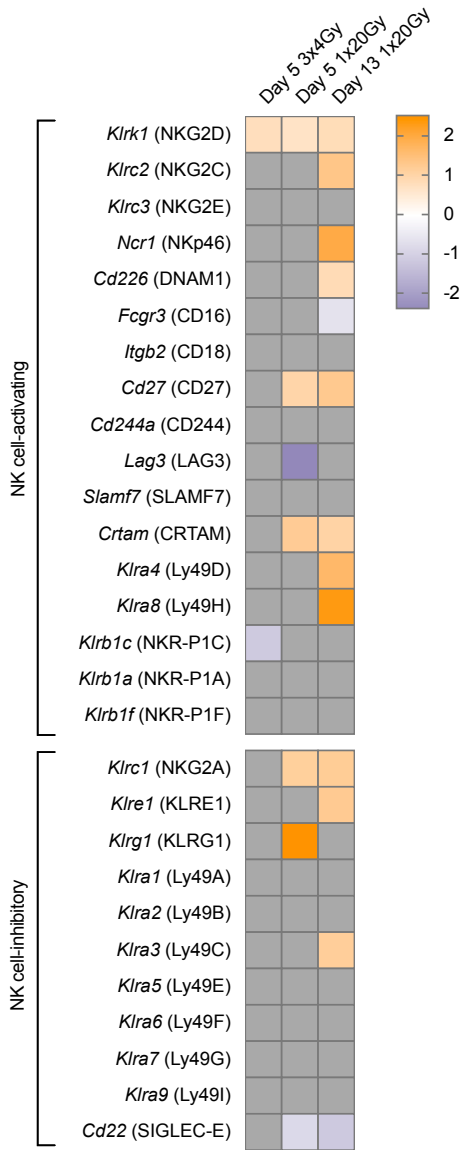

Appendix Figure 10. Expression of NK cell-activating and inhibitory receptors in the immune compartment of AT3-OVA tumours post RT. Heat map of differentially expressed genes for NK cell-activating and inhibitory receptors (parentheses denote corresponding protein name) in the immune compartment of 3x4Gy and 1x20Gy-irradiated AT3-OVA tumours, compared to their respective mock-irradiated controls. Log_2-fold change in expression with adjusted $p<0.1$ is expressed. Grey squares represent non-significant modulation.

Differential gene expression analysis (3x4Gy *vs.* 3x0Gy, day 5, immune cells)

Gene	logFC	AveExpr	t	P.Value	adj.P.Val	B
Inhba	3.274	2.788	4.596	4.89E-04	1.59E-02	0.042
Ly6i	3.073	1.936	3.807	2.15E-03	3.84E-02	-1.292
F10	2.999	4.218	6.651	1.51E-05	2.72E-03	3.304
Chac1	2.942	1.937	5.867	5.32E-05	4.95E-03	2.207
Dnahc2	2.513	1.406	4.538	5.44E-04	1.71E-02	0.024
Ermn	2.391	1.658	3.604	3.16E-03	4.88E-02	-1.683
Mcpt8	2.319	1.048	3.635	2.98E-03	4.72E-02	-1.549
Neb	2.146	3.420	4.347	7.74E-04	2.10E-02	-0.614
Gbp2b	2.119	3.556	4.247	9.34E-04	2.33E-02	-0.818
Gm24289	2.048	1.487	3.771	2.30E-03	4.04E-02	-1.373
Htr7	2.014	3.423	6.336	2.48E-05	3.45E-03	2.836
Mmp19	2.013	5.844	6.507	1.89E-05	3.00E-03	2.863
Il23a	1.993	1.283	4.193	1.03E-03	2.48E-02	-0.591
B3gnt5	1.913	2.676	4.394	7.10E-04	2.00E-02	-0.424
Olr1	1.904	2.800	5.682	7.25E-05	5.49E-03	1.827
Ptgs2	1.849	5.122	5.336	1.31E-04	7.58E-03	0.933
Gpr126	1.792	1.968	4.185	1.05E-03	2.50E-02	-0.691
Klhl41	1.777	0.536	3.773	2.29E-03	4.03E-02	-1.286
Clec4e	1.761	6.005	7.505	4.22E-06	1.48E-03	4.394
Tnfsf15	1.759	2.407	3.907	1.77E-03	3.44E-02	-1.274
Flrt3	1.729	4.990	8.039	1.99E-06	1.05E-03	5.229
Klf4	1.722	8.907	4.960	2.54E-04	1.13E-02	0.143
Samd11	1.717	1.852	3.683	2.72E-03	4.47E-02	-1.614
Cacnb4	1.668	2.002	4.909	2.78E-04	1.20E-02	0.591
Fpr2	1.666	3.616	4.247	9.33E-04	2.33E-02	-0.873
Kmo	1.660	4.257	6.073	3.79E-05	4.20E-03	2.286
Hdc	1.624	5.094	5.169	1.75E-04	9.09E-03	0.619
Arg2	1.621	3.598	5.552	9.03E-05	6.15E-03	1.486
Slc4a11	1.618	3.561	4.961	2.53E-04	1.13E-02	0.450
Rora	1.579	6.197	3.798	2.18E-03	3.88E-02	-2.033
P2rx5	1.554	2.800	6.792	1.22E-05	2.41E-03	3.587
Rab11fip1	1.534	5.791	11.750	2.44E-08	9.71E-05	9.663
Ramp3	1.511	6.894	5.774	6.22E-05	5.30E-03	1.584
Mefv	1.510	5.489	5.805	5.90E-05	5.23E-03	1.695
Slc7a11	1.505	6.438	5.368	1.24E-04	7.32E-03	0.884
Gm15987	1.493	1.083	4.657	4.38E-04	1.51E-02	0.221
Cdkn1a	1.472	9.125	6.800	1.20E-05	2.41E-03	3.291

AC123702.2	1.455	2.821	3.859	1.94E-03	3.59E-02	-1.461
Amn	1.430	1.655	3.661	2.83E-03	4.60E-02	-1.630
Upp1	1.426	3.356	3.843	2.00E-03	3.66E-02	-1.604
Rgag4	1.408	3.286	5.153	1.80E-04	9.21E-03	0.820
Ctla4	1.380	6.346	3.909	1.77E-03	3.44E-02	-1.831
Pira2	1.375	4.106	4.496	5.88E-04	1.79E-02	-0.506
Ffar2	1.373	2.997	5.332	1.32E-04	7.59E-03	1.176
Rnf149	1.371	6.684	3.800	2.17E-03	3.87E-02	-2.051
Ikzf2	1.370	5.940	4.091	1.25E-03	2.78E-02	-1.463
Bcl2l14	1.367	3.123	5.091	2.01E-04	9.63E-03	0.734
Cpm	1.343	2.552	3.646	2.92E-03	4.67E-02	-1.838
Atp2b4	1.335	5.646	3.604	3.16E-03	4.88E-02	-2.382
Slamf8	1.327	7.710	4.885	2.90E-04	1.22E-02	-0.007
Tnfrsf4	1.323	6.630	3.826	2.07E-03	3.73E-02	-2.001
Clec4a1	1.318	7.502	4.844	3.12E-04	1.25E-02	-0.083
1810033B17Rik	1.301	4.876	5.945	4.67E-05	4.56E-03	1.982
Pilrb1	1.295	3.814	3.709	2.58E-03	4.33E-02	-1.951
37865	1.270	2.954	4.847	3.10E-04	1.25E-02	0.325
Pecam1	1.268	5.859	6.349	2.43E-05	3.41E-03	2.581
Ccr2	1.233	6.642	4.212	9.97E-04	2.41E-02	-1.262
Myb	1.227	4.424	3.767	2.31E-03	4.05E-02	-1.945
Sdcbp2	1.222	4.820	4.322	8.12E-04	2.17E-02	-0.939
Slfn2	1.213	8.165	3.926	1.71E-03	3.36E-02	-1.813
Agpat4	1.205	5.853	7.926	2.33E-06	1.12E-03	5.000
Trem1	1.194	5.169	3.879	1.87E-03	3.53E-02	-1.821
Lin54	1.191	5.859	5.768	6.28E-05	5.32E-03	1.601
Bax	1.186	4.501	4.709	3.98E-04	1.44E-02	-0.171
Nufip1	1.184	5.094	4.298	8.48E-04	2.24E-02	-1.010
Il4i1	1.179	2.716	4.965	2.52E-04	1.13E-02	0.562
Gbp5	1.178	5.707	3.717	2.55E-03	4.30E-02	-2.175
Zfp667	1.169	4.100	5.918	4.89E-05	4.64E-03	2.019
Siglecg	1.169	2.945	4.072	1.30E-03	2.83E-02	-1.119
Il2ra	1.160	6.258	4.992	2.40E-04	1.08E-02	0.205
C3	1.154	7.806	3.796	2.19E-03	3.89E-02	-2.067
Braf	1.140	5.334	3.900	1.79E-03	3.46E-02	-1.793
Zeb2	1.140	7.114	3.623	3.05E-03	4.78E-02	-2.401
Il1r2	1.138	8.052	5.365	1.25E-04	7.33E-03	0.864
Adora2a	1.123	5.479	4.431	6.62E-04	1.93E-02	-0.796
Naaa	1.122	7.058	4.924	2.70E-04	1.18E-02	0.064
Il7r	1.117	6.131	3.618	3.08E-03	4.81E-02	-2.390

Adora2b	1.084	3.758	3.932	1.69E-03	3.34E-02	-1.538
Inf2	1.083	4.572	4.608	4.79E-04	1.57E-02	-0.379
Fcgr4	1.076	8.144	4.341	7.83E-04	2.11E-02	-1.020
Zbtb1	1.076	5.438	4.395	7.09E-04	2.00E-02	-0.863
Fam46a	1.071	7.843	5.194	1.68E-04	8.82E-03	0.557
Smchd1	1.069	7.454	3.919	1.73E-03	3.39E-02	-1.832
Cd5	1.068	5.500	3.805	2.15E-03	3.85E-02	-1.997
Cd274	1.059	5.817	3.602	3.18E-03	4.90E-02	-2.406
Csf2rb	1.057	8.419	6.225	2.97E-05	3.81E-03	2.348
Etv3	1.057	6.715	5.789	6.06E-05	5.27E-03	1.609
Fut7	1.055	3.361	3.765	2.32E-03	4.06E-02	-1.789
Cwc25	1.053	6.543	7.091	7.74E-06	1.93E-03	3.737
Rnf157	1.052	5.201	3.964	1.59E-03	3.22E-02	-1.664
Mxd1	1.051	8.225	7.321	5.51E-06	1.69E-03	4.086
Sesn2	1.045	4.577	3.996	1.50E-03	3.10E-02	-1.535
Ttc39c	1.043	4.381	4.886	2.89E-04	1.22E-02	0.160
Cmtm7	1.043	5.136	4.752	3.68E-04	1.40E-02	-0.171
Malt1	1.041	6.412	5.505	9.79E-05	6.37E-03	1.119
Rapgef2	1.035	6.208	3.859	1.94E-03	3.59E-02	-1.929
Procr	1.035	6.576	3.588	3.26E-03	4.99E-02	-2.463
Gnb4	1.033	4.587	4.044	1.37E-03	2.92E-02	-1.443
Dnaaf3	1.031	3.472	3.680	2.74E-03	4.49E-02	-1.967
Cd300ld	1.026	4.788	4.119	1.19E-03	2.68E-02	-1.325

Appendix Table 1. Top 100 upregulated genes in immune (CD45$^+$) cells from AT3-OVA tumours at day 5 post 3x4Gy-irradiation. Differentially expressed genes filtered by logFC > 0, adjusted p value < 0.05 are listed and ranked by logFC. *logFC: log fold-change, AveExpr: average expression, P.Value: nominal p value, adj.P.Val: adjusted p value.*

Differential gene expression analysis (3x4Gy *vs.* 3x0Gy, day 5, tumour/stromal cells)

Gene	logFC	AveExpr	t	P.Value	adj.P.Val	B
Clca3	5.409	2.437	4.254	4.01E-04	6.41E-03	0.176
Car8	5.360	0.251	4.889	9.26E-05	2.30E-03	0.691
Msc	5.235	2.345	3.699	1.45E-03	1.52E-02	-0.964
Entpd3	4.899	-0.033	4.456	2.51E-04	4.63E-03	-0.026
Ido1	4.855	2.201	3.439	2.64E-03	2.26E-02	-1.479
Ltf	4.412	5.435	15.458	1.80E-12	7.67E-09	18.241
Tox3	4.292	-0.845	5.329	3.41E-05	1.14E-03	1.244
Wnt5a	4.271	2.430	3.213	4.43E-03	3.25E-02	-1.951
Fer1l4	4.268	1.517	3.240	4.16E-03	3.10E-02	-1.862
Muc13	4.252	2.231	3.368	3.11E-03	2.53E-02	-1.648
Atg9b	4.235	0.953	4.871	9.65E-05	2.34E-03	0.902
Scnn1b	4.210	-0.463	5.132	5.32E-05	1.55E-03	0.964
Sncg	4.160	3.315	8.021	1.25E-07	1.93E-05	7.388
Clca2	4.112	4.094	6.545	2.41E-06	1.61E-04	4.967
Fgb	4.092	4.827	5.925	9.10E-06	4.42E-04	3.607
Msx2	4.074	-1.125	3.776	1.21E-03	1.34E-02	-1.197
Clca1	3.951	0.444	3.921	8.67E-04	1.07E-02	-0.661
Krt4	3.942	0.321	3.887	9.38E-04	1.13E-02	-0.743
Adra1a	3.916	-0.991	3.241	4.16E-03	3.09E-02	-2.016
Agxt2	3.909	-1.084	4.057	6.33E-04	8.78E-03	-0.727
Alox12e	3.907	-0.667	4.268	3.87E-04	6.22E-03	-0.369
Prom1	3.896	3.370	3.826	1.08E-03	1.25E-02	-0.772
BC030870	3.879	-0.357	3.731	1.35E-03	1.44E-02	-1.098
Cldn4	3.863	7.571	12.010	1.63E-10	1.52E-07	14.321
Gipc2	3.845	4.164	4.312	3.50E-04	5.84E-03	0.154
Piezo2	3.727	2.946	3.018	6.89E-03	4.39E-02	-2.410
Kcnh1	3.702	2.038	4.066	6.19E-04	8.65E-03	-0.205
Ovol1	3.673	4.665	12.259	1.14E-10	1.42E-07	14.222
Sptlc3	3.645	0.063	3.833	1.06E-03	1.24E-02	-0.858
Krt19	3.642	6.347	5.498	2.34E-05	8.67E-04	2.561
Fzd10	3.638	-0.229	3.808	1.13E-03	1.29E-02	-1.094
Pls1	3.611	1.073	3.975	7.64E-04	9.87E-03	-0.469
Atp6v0e2	3.591	1.268	5.000	7.18E-05	1.90E-03	1.524
Cep112	3.584	0.751	3.380	3.03E-03	2.49E-02	-1.615
Fam83g	3.522	0.410	3.426	2.72E-03	2.30E-02	-1.555
Cthrc1	3.504	-1.167	4.511	2.21E-04	4.21E-03	-0.074
Ly6g6c	3.498	0.031	5.016	6.93E-05	1.84E-03	0.957
Ubd	3.460	6.302	8.838	2.76E-08	6.22E-06	9.274
Tmprss2	3.459	5.004	5.726	1.41E-05	5.93E-04	3.192

Slc44a4	3.446	0.061	3.214	4.42E-03	3.24E-02	-2.005
Gm14137	3.422	-0.334	4.589	1.84E-04	3.73E-03	0.341
9530053A07Rik	3.417	-1.492	3.561	1.99E-03	1.88E-02	-1.547
Grb14	3.401	2.605	3.591	1.86E-03	1.79E-02	-1.250
Gfpt2	3.389	2.768	4.870	9.66E-05	2.34E-03	1.486
Proc	3.388	0.103	4.227	4.26E-04	6.62E-03	-0.121
Nfe2l3	3.388	-0.145	3.388	2.97E-03	2.45E-02	-1.647
Lrrc8e	3.382	0.542	3.557	2.01E-03	1.89E-02	-1.298
Hoxb3os	3.372	0.222	3.897	9.17E-04	1.12E-02	-0.724
Map1b	3.361	2.708	3.050	6.40E-03	4.17E-02	-2.335
Stc2	3.340	3.975	3.086	5.91E-03	3.96E-02	-2.474
Upk3a	3.339	3.299	4.197	4.56E-04	6.93E-03	-0.112
Bend7	3.287	0.334	3.375	3.06E-03	2.50E-02	-1.639
Cldn10	3.278	2.149	4.022	6.86E-04	9.22E-03	-0.296
S100a14	3.274	4.437	5.138	5.25E-05	1.54E-03	1.931
Tacstd2	3.265	5.469	6.649	1.94E-06	1.43E-04	5.091
Dnaic1	3.239	-0.659	2.950	8.01E-03	4.84E-02	-2.496
Samd5	3.235	-1.396	3.745	1.31E-03	1.42E-02	-1.285
Thsd4	3.218	2.723	5.521	2.22E-05	8.36E-04	2.796
Hoxb2	3.214	-0.600	3.066	6.17E-03	4.07E-02	-2.279
Klk10	3.210	-0.304	3.138	5.24E-03	3.65E-02	-2.119
Fam174b	3.173	2.032	4.246	4.07E-04	6.47E-03	0.171
Rassf6	3.167	0.663	3.171	4.87E-03	3.46E-02	-2.020
Upk2	3.159	-0.254	3.731	1.35E-03	1.44E-02	-1.123
Cdo1	3.127	4.279	4.590	1.84E-04	3.73E-03	0.761
Wnt7b	3.099	4.713	6.653	1.92E-06	1.42E-04	5.157
Tspan1	3.095	3.967	5.758	1.31E-05	5.65E-04	3.326
S100g	3.093	1.538	6.809	1.39E-06	1.11E-04	4.654
Pllp	3.090	1.342	4.456	2.51E-04	4.63E-03	0.527
Ccdc162	3.090	1.232	3.205	4.51E-03	3.28E-02	-1.929
Scnn1a	3.088	1.339	3.828	1.08E-03	1.25E-02	-0.719
Has2	3.083	1.271	3.505	2.27E-03	2.04E-02	-1.347
Clu	3.080	6.059	5.203	4.53E-05	1.39E-03	1.881
Apod	3.077	8.150	11.985	1.69E-10	1.52E-07	14.293
Syt7	3.074	2.808	4.837	1.04E-04	2.46E-03	1.408
Slc1a1	3.071	-0.651	3.905	8.99E-04	1.10E-02	-0.919
Tmem56	3.042	5.124	4.643	1.63E-04	3.38E-03	0.742
Cxcl1	3.036	9.156	10.681	1.23E-09	6.83E-07	12.341
Phlda3	3.010	6.676	17.941	1.15E-13	1.47E-09	21.132
Capn5	2.996	2.634	3.985	7.47E-04	9.74E-03	-0.419
Atp2c2	2.989	1.159	3.887	9.38E-04	1.13E-02	-0.615
2010001M06Rik	2.953	3.088	7.193	6.35E-07	6.12E-05	6.148

Rundc3a	2.946	0.423	3.039	6.57E-03	4.25E-02	-2.262
Prkaa2	2.923	-1.060	4.058	6.31E-04	8.78E-03	-0.741
Celf5	2.917	-0.692	4.237	4.17E-04	6.53E-03	-0.441
Nxf7	2.908	-1.474	3.133	5.31E-03	3.68E-02	-2.248
Agtr1a	2.907	2.750	4.517	2.18E-04	4.18E-03	0.738
Fam212b	2.887	2.811	12.322	1.04E-10	1.42E-07	13.365
Cdc42ep5	2.877	0.343	4.308	3.53E-04	5.85E-03	0.046
Fgg	2.860	4.203	4.196	4.58E-04	6.94E-03	-0.173
Krt7	2.847	5.963	8.065	1.15E-07	1.84E-05	7.860
Mgmt	2.829	0.366	3.441	2.63E-03	2.26E-02	-1.493
Tmem30b	2.816	2.825	4.755	1.26E-04	2.82E-03	1.244
Rps4y2	2.814	2.718	3.181	4.77E-03	3.41E-02	-2.157
Tuba8	2.812	2.854	4.781	1.19E-04	2.70E-03	1.293
Edn1	2.800	2.383	4.687	1.47E-04	3.14E-03	1.099
Cox6b2	2.782	-1.140	3.470	2.46E-03	2.16E-02	-1.652
Grhl3	2.776	-0.778	3.405	2.86E-03	2.39E-02	-1.756
Sftpd	2.775	0.706	3.218	4.38E-03	3.22E-02	-1.904
Slc5a8	2.768	1.246	4.100	5.73E-04	8.20E-03	-0.195
Pak6	2.766	0.376	2.987	7.38E-03	4.61E-02	-2.340

Appendix Table 2. Top 100 upregulated genes in tumour/stromal ($CD45^{-}GFP^{\pm}$) cells from AT3-OVA tumours at day 5 post 3x4Gy-irradiation. Differentially expressed genes filtered by logFC > 0, adjusted p value < 0.05 are listed and ranked by logFC. *logFC: log fold-change, AveExpr: average expression, P.Value: nominal p value, adj.P.Val: adjusted p value.*

Differential gene expression analysis (1x20Gy *vs.* 1x0Gy, day 5, immune cells)

Gene	logFC	AveExpr	t	P.Value	adj.P.Val	B
Chac1	3.819	2.211	6.293	1.53E-05	1.22E-03	3.297
Traj12	3.474	-0.773	4.262	7.02E-04	1.33E-02	-0.428
Gm21738	3.446	0.924	3.308	4.86E-03	4.25E-02	-1.960
Cxcl3	3.391	0.017	3.721	2.09E-03	2.52E-02	-1.230
Ptprr	3.381	-0.766	3.703	2.17E-03	2.58E-02	-1.315
Krt222	3.323	-0.841	4.546	3.99E-04	9.26E-03	0.001
Gm14861	3.238	-1.321	4.428	5.04E-04	1.07E-02	-0.204
Gm10801	3.218	1.440	3.344	4.51E-03	4.08E-02	-1.949
Gm11225	2.900	-0.745	3.386	4.14E-03	3.84E-02	-1.827
Inhba	2.885	2.972	6.547	9.87E-06	9.49E-04	3.739
Slc17a1	2.756	-1.214	3.490	3.35E-03	3.35E-02	-1.675
Mcpt4	2.746	1.705	6.481	1.11E-05	1.02E-03	3.594
Il23a	2.743	0.620	5.882	3.18E-05	1.92E-03	2.456
Pou6f2	2.636	-0.556	3.535	3.05E-03	3.17E-02	-1.560
Map6	2.615	0.532	3.634	2.49E-03	2.82E-02	-1.366
Nos1	2.614	0.313	5.182	1.16E-04	4.30E-03	1.296
Podnl1	2.578	2.172	4.830	2.29E-04	6.59E-03	0.746
Ctla4	2.556	6.428	6.343	1.41E-05	1.18E-03	2.932
Rps10-ps3	2.538	-0.388	3.617	2.58E-03	2.87E-02	-1.407
Fam122c	2.518	-0.854	3.465	3.53E-03	3.46E-02	-1.695
Tarm1	2.518	1.191	3.312	4.81E-03	4.22E-02	-2.026
Cpm	2.517	2.165	6.538	1.00E-05	9.55E-04	3.734
Klrg1	2.507	3.945	6.686	7.79E-06	8.89E-04	3.851
Gm26016	2.500	-0.272	3.562	2.89E-03	3.08E-02	-1.497
Cma1	2.473	3.752	6.561	9.63E-06	9.49E-04	3.657
Snora31	2.450	-0.525	3.794	1.80E-03	2.32E-02	-1.121
F10	2.427	4.349	6.487	1.09E-05	1.01E-03	3.437
Foxp3	2.426	3.234	5.400	7.72E-05	3.40E-03	1.655
RP23-159J2.2	2.347	2.210	5.601	5.32E-05	2.61E-03	2.138
Folr4	2.314	2.919	5.375	8.09E-05	3.51E-03	1.645
Mcpt8	2.284	0.662	3.465	3.52E-03	3.46E-02	-1.692
Ly6i	2.242	1.719	3.982	1.23E-03	1.84E-02	-0.830
Ermn	2.160	1.623	3.464	3.53E-03	3.46E-02	-1.820
Cpa3	2.148	3.576	5.856	3.34E-05	1.98E-03	2.415
Hdc	2.096	5.066	7.352	2.60E-06	4.84E-04	4.787
Samd11	2.051	1.657	5.563	5.69E-05	2.72E-03	2.088
Gm22748	2.012	3.007	6.048	2.36E-05	1.57E-03	2.839
Neb	1.995	3.168	4.741	2.72E-04	7.30E-03	0.379
Gata2	1.970	1.502	4.742	2.71E-04	7.30E-03	0.616

1500009L16Rik	1.940	1.375	3.352	4.44E-03	4.04E-02	-2.008
Gm8213	1.926	4.989	5.328	8.84E-05	3.71E-03	1.179
Traj18	1.878	3.715	4.698	2.96E-04	7.72E-03	0.177
F7	1.877	2.435	3.185	6.23E-03	4.97E-02	-2.564
Olr1	1.869	2.701	5.109	1.34E-04	4.70E-03	1.152
RP24-286J21.4	1.851	0.367	3.246	5.51E-03	4.59E-02	-2.083
AC137156.1	1.819	-0.302	3.220	5.81E-03	4.76E-02	-2.090
Sv2c	1.815	2.634	3.270	5.25E-03	4.44E-02	-2.438
Tnfrsf4	1.813	6.193	5.264	9.97E-05	3.96E-03	0.908
Clec4e	1.800	6.032	8.476	4.63E-07	1.97E-04	6.454
Dusp4	1.782	3.376	4.002	1.18E-03	1.80E-02	-1.144
Gm4707	1.780	3.621	5.644	4.90E-05	2.48E-03	1.998
Olfml2a	1.773	-0.409	3.281	5.13E-03	4.39E-02	-1.983
Fam83g	1.769	0.284	3.754	1.95E-03	2.41E-02	-1.152
A630023P12Rik	1.738	-0.313	3.186	6.23E-03	4.97E-02	-2.150
Gstt1	1.735	0.169	3.407	3.96E-03	3.72E-02	-1.778
AC153562.1	1.724	1.157	3.767	1.91E-03	2.38E-02	-1.193
B3gnt5	1.723	2.536	5.086	1.40E-04	4.77E-03	1.128
Ccno	1.713	1.208	3.466	3.52E-03	3.46E-02	-1.781
Gm22767	1.705	0.765	3.701	2.18E-03	2.58E-02	-1.277
Myl4	1.698	0.255	3.569	2.85E-03	3.06E-02	-1.488
Ttn	1.692	1.136	3.212	5.91E-03	4.82E-02	-2.241
Mcpt2	1.689	5.770	9.560	1.01E-07	8.36E-05	8.034
Fam212b	1.684	-0.320	3.502	3.27E-03	3.32E-02	-1.597
Fpr2	1.678	3.608	4.565	3.84E-04	9.05E-03	-0.089
Lrrc32	1.656	2.817	5.398	7.74E-05	3.40E-03	1.662
Cd5	1.645	5.170	4.643	3.29E-04	8.15E-03	-0.208
Icos	1.619	7.723	4.374	5.61E-04	1.14E-02	-0.930
Gm11772	1.615	0.827	3.721	2.09E-03	2.52E-02	-1.252
Myb	1.611	4.241	4.261	7.03E-04	1.33E-02	-0.823
Scarna9	1.604	1.913	3.307	4.86E-03	4.25E-02	-2.212
Xlr4a	1.580	0.181	3.200	6.05E-03	4.87E-02	-2.155
Alpk2	1.560	1.928	4.746	2.70E-04	7.30E-03	0.563
Cxcl2	1.559	9.538	7.356	2.58E-06	4.84E-04	4.588
Cxcl1	1.547	6.081	6.525	1.03E-05	9.61E-04	3.246
Rasgef1a	1.542	1.196	3.684	2.25E-03	2.64E-02	-1.364
Gm6977	1.530	0.766	3.717	2.11E-03	2.54E-02	-1.256
Edn1	1.527	1.312	3.340	4.54E-03	4.09E-02	-2.048
Etnk2	1.524	-0.044	3.214	5.88E-03	4.81E-02	-2.115
Ffar2	1.492	3.002	5.746	4.07E-05	2.19E-03	2.265
Map9	1.491	2.370	5.601	5.31E-05	2.61E-03	2.093
Bcat1	1.483	1.146	3.205	5.98E-03	4.85E-02	-2.277

Stx11	1.478	5.539	6.388	1.30E-05	1.12E-03	3.047
Zfp831	1.472	1.445	3.292	5.01E-03	4.34E-02	-2.159
Ccdc88c	1.470	1.592	3.290	5.03E-03	4.34E-02	-2.188
Atp2b4	1.465	5.432	4.223	7.58E-04	1.39E-02	-1.096
Cass4	1.462	2.567	4.222	7.60E-04	1.39E-02	-0.567
Cd28	1.459	5.489	3.876	1.53E-03	2.10E-02	-1.808
Tnfrsf18	1.450	6.685	4.983	1.70E-04	5.42E-03	0.319
Cd2	1.449	5.871	4.658	3.20E-04	8.06E-03	-0.271
Ddit4	1.445	6.679	7.216	3.23E-06	5.34E-04	4.402
Gimap7	1.435	2.338	3.497	3.30E-03	3.33E-02	-1.954
Arnt2	1.425	2.349	4.290	6.63E-04	1.28E-02	-0.391
4930579G24Rik	1.419	1.216	3.540	3.03E-03	3.16E-02	-1.651
Rora	1.419	6.268	4.678	3.08E-04	7.91E-03	-0.263
Gm5150	1.418	0.107	3.239	5.58E-03	4.64E-02	-2.083
Eomes	1.412	2.984	3.268	5.26E-03	4.45E-02	-2.558
Htr7	1.406	3.722	6.787	6.56E-06	8.41E-04	3.990
Siglecg	1.403	3.170	5.191	1.14E-04	4.25E-03	1.197
Rgs16	1.396	6.073	3.344	4.51E-03	4.08E-02	-2.952
Rnf149	1.394	7.129	5.221	1.08E-04	4.09E-03	0.766

Appendix Table 3. Top 100 upregulated genes in immune (CD45$^+$) cells from AT3-OVA tumours at day 5 post 1x20Gy-irradiation. Differentially expressed genes filtered by logFC > 0, adjusted p value < 0.05 are listed and ranked by logFC. *logFC: log fold-change, AveExpr: average expression, P.Value: nominal p value, adj.P.Val: adjusted p value.*

Differential gene expression analysis (1x20Gy *vs.* 1x0Gy, day 5, tumour/stromal cells)

Gene	logFC	AveExpr	t	P.Value	adj.P.Val	B
Defb1	5.575	0.860	2.858	9.83E-03	3.62E-02	-2.569
Ido1	5.474	2.201	4.119	5.48E-04	4.30E-03	-0.130
AC131780.1	5.244	0.105	5.557	2.05E-05	4.01E-04	1.917
AA474408	5.026	5.174	3.568	1.96E-03	1.09E-02	-1.550
Ccl11	5.021	-0.850	4.224	4.29E-04	3.62E-03	-0.386
Msx2	4.844	-1.125	4.711	1.39E-04	1.63E-03	0.344
Efemp1	4.821	0.461	4.414	2.76E-04	2.67E-03	0.345
Has1	4.792	1.661	4.069	6.15E-04	4.69E-03	-0.207
Dpep1	4.529	0.022	4.148	5.12E-04	4.10E-03	-0.309
Alox12e	4.518	-0.667	5.047	6.46E-05	9.39E-04	0.865
Clec3b	4.504	2.145	4.552	2.01E-04	2.14E-03	0.807
Ces2g	4.463	-1.407	4.312	3.50E-04	3.14E-03	-0.287
Gm15987	4.425	-0.464	5.274	3.86E-05	6.38E-04	1.212
Entpd3	4.418	-0.033	4.441	2.60E-04	2.56E-03	0.114
Cxcl2	4.407	7.073	5.606	1.84E-05	3.69E-04	2.741
Ltf	4.370	5.435	16.546	5.15E-13	1.59E-09	19.487
Fzd10	4.302	-0.229	4.870	9.66E-05	1.23E-03	0.744
Mfap5	4.250	1.404	4.316	3.47E-04	3.12E-03	0.253
Aebp1	4.228	1.060	4.196	4.58E-04	3.79E-03	-0.003
Gabra3	4.207	-1.279	4.485	2.35E-04	2.40E-03	-0.018
Gpx3	4.187	3.478	3.385	2.99E-03	1.48E-02	-1.879
Gpc3	4.176	0.561	3.746	1.30E-03	8.02E-03	-0.909
Muc16	4.159	-0.652	3.539	2.10E-03	1.14E-02	-1.527
Gdf15	4.144	2.906	5.367	3.13E-05	5.42E-04	2.524
Sncg	4.093	3.315	10.343	2.11E-09	5.76E-07	11.380
Ankrd1	4.052	-0.811	4.400	2.85E-04	2.73E-03	-0.170
Mycl1	3.978	1.513	2.898	8.99E-03	3.37E-02	-2.518
Ogn	3.959	0.274	4.132	5.32E-04	4.22E-03	-0.209
Cox6b2	3.955	-1.140	4.874	9.58E-05	1.23E-03	0.521
Tox3	3.932	-0.845	4.893	9.16E-05	1.20E-03	0.596
9530053A07Rik	3.917	-1.492	4.131	5.33E-04	4.23E-03	-0.642
Dpt	3.909	2.260	4.266	3.89E-04	3.38E-03	0.203
Tmprss2	3.881	5.004	6.973	9.92E-07	4.57E-05	5.776
Msc	3.855	2.345	3.405	2.85E-03	1.43E-02	-1.578
Clca3	3.851	2.437	3.132	5.32E-03	2.29E-02	-2.110
Ccl20	3.809	0.411	3.757	1.27E-03	7.91E-03	-0.978
Pi16	3.783	1.043	3.676	1.53E-03	9.06E-03	-1.009
Car8	3.764	0.251	3.986	7.45E-04	5.34E-03	-0.585
Pcolce2	3.763	0.650	3.627	1.72E-03	9.89E-03	-1.132

Sfrp2	3.756	1.106	3.780	1.20E-03	7.62E-03	-0.800
Shc2	3.734	-0.657	3.806	1.13E-03	7.26E-03	-1.003
Hoxb3os	3.702	0.222	4.134	5.29E-04	4.21E-03	-0.344
Pamr1	3.698	-0.052	3.223	4.33E-03	1.95E-02	-1.921
Tox2	3.681	4.291	4.198	4.56E-04	3.79E-03	-0.179
Adam23	3.677	-0.563	2.965	7.74E-03	3.02E-02	-2.454
Gm22641	3.670	-1.004	3.517	2.21E-03	1.18E-02	-1.589
Cxcl1	3.669	9.156	13.845	1.32E-11	1.41E-08	16.801
Rarres2	3.662	-0.178	3.144	5.18E-03	2.24E-02	-2.071
Ms4a4d	3.654	0.302	4.763	1.24E-04	1.49E-03	0.822
n-R5s33	3.639	-1.226	4.215	4.38E-04	3.68E-03	-0.472
Cd34	3.621	1.952	5.943	8.75E-06	2.17E-04	3.643
Mansc1	3.593	1.360	5.482	2.42E-05	4.51E-04	2.460
Mcam	3.561	5.732	7.727	2.20E-07	1.64E-05	7.193
Serping1	3.553	3.391	4.569	1.93E-04	2.08E-03	0.728
Hoxb2	3.551	-0.600	3.309	3.56E-03	1.69E-02	-1.904
Mgmt	3.549	0.366	3.779	1.21E-03	7.63E-03	-0.942
Celf5	3.519	-0.692	5.487	2.39E-05	4.49E-04	1.614
Lif	3.509	8.570	12.291	1.09E-10	7.36E-08	14.729
Dgki	3.508	0.554	4.123	5.42E-04	4.27E-03	-0.226
Plat	3.496	1.161	3.753	1.28E-03	7.94E-03	-0.853
Svep1	3.487	0.217	4.188	4.67E-04	3.84E-03	-0.060
Cdh11	3.476	-1.187	3.317	3.49E-03	1.67E-02	-1.903
Figf	3.474	0.148	3.502	2.28E-03	1.21E-02	-1.382
Scnn1b	3.470	-0.463	4.752	1.27E-04	1.52E-03	0.624
Col1a2	3.462	5.007	5.371	3.10E-05	5.40E-04	2.290
Fam212b	3.461	2.811	16.219	7.44E-13	1.59E-09	17.363
Grhl3	3.452	-0.778	4.320	3.44E-04	3.10E-03	-0.262
Ovol1	3.432	4.665	15.205	2.43E-12	3.75E-09	18.135
Cldn10	3.431	2.149	4.418	2.74E-04	2.65E-03	0.531
Fam83g	3.414	0.410	3.351	3.23E-03	1.57E-02	-1.691
Podn	3.408	0.661	7.252	5.63E-07	3.14E-05	5.291
Aqp3	3.407	-0.720	3.144	5.18E-03	2.24E-02	-2.096
Sptlc3	3.393	0.063	3.437	2.65E-03	1.36E-02	-1.589
Thbd	3.386	0.045	3.406	2.85E-03	1.43E-02	-1.606
Atg9b	3.370	0.953	5.510	2.27E-05	4.29E-04	2.572
Spef2	3.368	0.376	2.667	1.49E-02	4.93E-02	-2.899
Tacstd2	3.338	5.469	7.435	3.91E-07	2.44E-05	6.645
Clca5	3.336	1.956	6.809	1.39E-06	5.83E-05	5.193
1700007K13Rik	3.330	1.584	7.778	2.00E-07	1.54E-05	6.620
Cldn4	3.315	7.571	11.430	3.85E-10	1.67E-07	13.482
Prss23	3.304	2.544	9.423	9.83E-09	1.73E-06	9.835
Col14a1	3.292	2.673	4.147	5.13E-04	4.10E-03	-0.111

Cd248	3.291	1.370	4.360	3.13E-04	2.90E-03	0.408
Greb1	3.283	-0.206	3.140	5.22E-03	2.25E-02	-2.063
Zbtb16	3.245	-0.638	3.107	5.63E-03	2.38E-02	-2.202
Tgm1	3.239	-0.117	4.546	2.04E-04	2.15E-03	0.336
Mgam	3.238	-0.906	4.068	6.17E-04	4.70E-03	-0.715
Ctsf	3.227	0.079	4.621	1.71E-04	1.91E-03	0.623
Proc	3.226	0.103	3.793	1.17E-03	7.43E-03	-0.957
Fam174b	3.226	2.032	3.983	7.52E-04	5.37E-03	-0.377
Lum	3.225	1.972	4.904	8.93E-05	1.18E-03	1.560
Fgfr2	3.216	4.435	6.105	6.16E-06	1.72E-04	4.000
Prom2	3.214	3.019	3.998	7.26E-04	5.24E-03	-0.510
Rps4y2	3.193	2.718	3.496	2.32E-03	1.23E-02	-1.470
Abca8a	3.192	0.582	5.093	5.81E-05	8.67E-04	1.728
Mmrn2	3.190	1.412	6.690	1.78E-06	6.97E-05	4.902
Slc44a4	3.181	0.061	3.552	2.04E-03	1.11E-02	-1.314
Adrb1	3.179	1.078	3.491	2.34E-03	1.24E-02	-1.376
Snhg11	3.176	2.383	3.463	2.50E-03	1.30E-02	-1.571
Flnc	3.174	-0.813	4.407	2.81E-04	2.70E-03	-0.028

Appendix Table 4. Top 100 upregulated genes in tumour/stromal ($CD45^{-}GFP^{\pm}$) cells from AT3-OVA tumours at day 5 post 1x20Gy-irradiation. Differentially expressed genes filtered by logFC > 0, adjusted p value < 0.05 are listed and ranked by logFC. *logFC: log fold-change, AveExpr: average expression, P.Value: nominal p value, adj.P.Val: adjusted p value.*

Differential gene expression analysis (1x20Gy *vs.* 1x0Gy, day 13, immune cells)

Feature	logFC	AveExpr	T	P.Value	adj.P.Val	B
Gm23935	4.110	1.288	3.356	3.59E-03	4.91E-02	-1.831
AA474408	3.672	6.262	5.222	6.14E-05	4.34E-03	1.798
Gm22641	3.470	0.287	4.408	3.55E-04	1.21E-02	-0.425
Il1f9	3.054	0.818	4.228	5.26E-04	1.56E-02	-0.450
Muc16	2.877	-0.576	3.632	1.96E-03	3.41E-02	-1.706
Gm22513	2.874	0.315	3.669	1.81E-03	3.26E-02	-1.406
Gm15564	2.694	0.586	3.536	2.42E-03	3.88E-02	-1.540
Snord55	2.680	1.346	5.376	4.44E-05	3.62E-03	1.677
Grb14	2.638	1.994	3.795	1.37E-03	2.75E-02	-0.899
Ly6g6c	2.612	-0.622	3.451	2.92E-03	4.36E-02	-1.950
Mmp9	2.448	2.403	5.936	1.40E-05	1.84E-03	3.080
mt-Tc	2.436	2.371	5.721	2.17E-05	2.45E-03	2.712
Gm8054	2.404	-1.045	3.402	3.25E-03	4.61E-02	-2.066
Gm20692	2.352	-0.359	3.349	3.65E-03	4.95E-02	-2.023
Klra8	2.332	1.839	3.546	2.37E-03	3.84E-02	-1.362
38231	2.329	-0.739	3.343	3.70E-03	4.98E-02	-2.103
Scnn1b	2.282	-0.095	3.487	2.70E-03	4.21E-02	-1.754
Gm26191	2.233	1.850	3.680	1.76E-03	3.22E-02	-1.107
Clca1	2.215	-0.198	3.511	2.56E-03	4.05E-02	-1.726
Adamts14	2.206	2.460	4.547	2.62E-04	1.00E-02	0.589
Msc	2.198	2.121	3.914	1.05E-03	2.36E-02	-0.655
Upk3a	2.169	2.761	3.635	1.95E-03	3.41E-02	-1.212
Gm10056	2.039	1.402	4.611	2.28E-04	9.26E-03	0.541
Styk1	1.991	2.638	3.757	1.49E-03	2.91E-02	-0.972
Ncr1	1.958	3.442	4.157	6.16E-04	1.71E-02	-0.222
Wnt5a	1.937	3.110	4.046	7.86E-04	2.00E-02	-0.421
Ovol1	1.937	1.353	3.894	1.10E-03	2.42E-02	-0.751
Dntt	1.906	0.870	4.179	5.87E-04	1.65E-02	-0.330
Prom1	1.897	3.252	3.796	1.36E-03	2.75E-02	-0.946
Klra13-ps	1.858	2.709	4.588	2.40E-04	9.57E-03	0.687
RP23-81C12.3	1.857	17.161	4.722	1.79E-04	8.04E-03	0.359
Snora30	1.848	2.568	4.726	1.77E-04	8.00E-03	0.955
Sgms2	1.830	3.202	4.968	1.05E-04	5.71E-03	1.444
G0s2	1.821	2.753	3.568	2.25E-03	3.73E-02	-1.362
Hic1	1.802	1.713	3.554	2.33E-03	3.81E-02	-1.347
Nrxn2	1.795	1.148	3.827	1.27E-03	2.64E-02	-0.887
Gm24924	1.781	1.221	3.607	2.07E-03	3.54E-02	-1.274
S100a9	1.771	4.979	4.925	1.16E-04	6.10E-03	1.213
Rsph9	1.727	0.035	3.429	3.07E-03	4.48E-02	-1.749

Clca2	1.700	2.610	5.867	1.61E-05	2.04E-03	3.114
Gm26225	1.693	2.689	4.431	3.37E-04	1.17E-02	0.375
Hdc	1.686	5.571	6.643	3.44E-06	1.00E-03	4.627
Klra4	1.650	3.576	4.745	1.70E-04	7.84E-03	0.968
Prr7	1.645	3.079	3.695	1.70E-03	3.17E-02	-1.152
Fer1l4	1.639	1.528	3.635	1.94E-03	3.41E-02	-1.196
S100a14	1.625	4.928	5.507	3.37E-05	3.09E-03	2.418
Dtx1	1.621	2.370	3.341	3.72E-03	4.99E-02	-1.791
Gimap8	1.612	4.992	6.406	5.46E-06	1.29E-03	4.201
Tmprss2	1.593	3.947	3.555	2.32E-03	3.80E-02	-1.568
Cyb5d1	1.580	0.462	3.359	3.57E-03	4.89E-02	-1.786
Gem	1.571	3.746	5.441	3.87E-05	3.34E-03	2.368
Smim5	1.569	2.039	4.292	4.58E-04	1.41E-02	0.085
Spib	1.567	4.102	5.704	2.24E-05	2.47E-03	2.875
Siglech	1.562	4.360	5.896	1.51E-05	1.96E-03	3.240
AC102739.1	1.528	1.516	3.771	1.44E-03	2.85E-02	-0.939
Slc45a3	1.507	2.166	4.222	5.34E-04	1.57E-02	-0.044
Tuba8	1.490	2.704	3.512	2.55E-03	4.04E-02	-1.485
Ltb	1.490	5.416	4.249	5.02E-04	1.51E-02	-0.295
Cldn3	1.489	5.473	4.536	2.68E-04	1.02E-02	0.319
Eomes	1.484	4.423	6.204	8.14E-06	1.55E-03	3.838
Samd3	1.456	3.423	4.015	8.41E-04	2.07E-02	-0.541
Tbx21	1.442	7.901	5.609	2.73E-05	2.69E-03	2.453
Gfpt2	1.438	2.187	3.571	2.24E-03	3.72E-02	-1.323
Myh14	1.430	3.274	3.833	1.26E-03	2.63E-02	-0.900
Zfp831	1.429	3.165	4.549	2.61E-04	1.00E-02	0.588
Nr2f2	1.425	1.731	3.340	3.72E-03	4.99E-02	-1.752
Vps37b	1.410	9.168	4.887	1.25E-04	6.32E-03	0.889
Fam65b	1.393	5.322	6.304	6.68E-06	1.48E-03	3.976
Itgb3	1.388	3.038	5.194	6.52E-05	4.38E-03	1.892
Ccr9	1.382	4.930	4.991	1.00E-04	5.53E-03	1.333
Arhgap32	1.368	3.283	4.920	1.17E-04	6.12E-03	1.337
Tmem56	1.368	4.369	5.607	2.74E-05	2.69E-03	2.657
AC123702.2	1.363	2.099	3.626	1.98E-03	3.44E-02	-1.214
Klrc2	1.346	4.723	5.616	2.69E-05	2.67E-03	2.647
Cldn4	1.344	6.227	4.038	7.99E-04	2.01E-02	-0.827
mt-Ta	1.339	2.459	3.687	1.74E-03	3.18E-02	-1.121
Gm4707	1.328	4.074	7.132	1.36E-06	7.47E-04	5.567
Gm11722	1.324	3.765	4.354	3.99E-04	1.29E-02	0.120
Lax1	1.322	3.180	4.695	1.90E-04	8.35E-03	0.882
AC123702.1	1.310	3.088	5.270	5.55E-05	4.07E-03	2.042
Gm20069	1.308	1.926	3.691	1.72E-03	3.17E-02	-1.084
Abcb9	1.301	5.975	5.512	3.34E-05	3.09E-03	2.336

S100a8	1.298	6.051	4.273	4.76E-04	1.45E-02	-0.306
Lars2	1.295	4.810	4.002	8.66E-04	2.08E-02	-0.769
Setbp1	1.283	3.770	4.388	3.71E-04	1.23E-02	0.191
Krt7	1.280	4.426	3.845	1.22E-03	2.59E-02	-1.045
Satb1	1.279	5.878	4.620	2.23E-04	9.17E-03	0.455
Rgs16	1.277	6.748	5.704	2.25E-05	2.47E-03	2.690
Homer2	1.276	3.904	5.194	6.51E-05	4.38E-03	1.854
Cd27	1.267	6.415	6.009	1.21E-05	1.75E-03	3.326
Rnf125	1.262	5.857	5.301	5.19E-05	3.96E-03	1.902
Cdo1	1.254	3.676	4.677	1.97E-04	8.45E-03	0.806
Klre1	1.247	4.968	4.783	1.57E-04	7.42E-03	0.886
Camk2n1	1.247	5.798	5.995	1.24E-05	1.76E-03	3.330
2010001M06Rik	1.240	2.499	3.697	1.70E-03	3.16E-02	-1.104
Il18r1	1.235	6.417	5.510	3.35E-05	3.09E-03	2.305
Garnl3	1.229	1.795	3.704	1.67E-03	3.14E-02	-1.055
Ccl5	1.228	8.482	4.703	1.86E-04	8.24E-03	0.511
Gm14044	1.222	2.895	3.581	2.19E-03	3.66E-02	-1.385
Sytl2	1.222	4.265	4.941	1.12E-04	5.94E-03	1.293

Appendix Table 5. Top 100 upregulated genes in immune ($CD45^+$) cells from AT3-OVA tumours at day 13 post 1x20Gy-irradiation. Differentially expressed genes filtered by logFC > 0, adjusted p value < 0.05 are listed and ranked by logFC. *logFC: log fold-change, AveExpr: average expression, P.Value: nominal p value, adj.P.Val: adjusted p value.*

Differential gene expression analysis (1x20Gy *vs.* 1x0Gy, day 13, tumour/stromal cells)

Feature	logFC	AveExpr	t	P.Value	adj.P.Val	B
Kcnh1	4.261	2.695	5.231	1.16E-04	1.14E-03	1.351
Areg	3.989	4.657	6.365	1.53E-05	3.39E-04	3.347
Map1b	3.765	3.963	5.563	6.28E-05	8.00E-04	2.007
Wnt5a	3.719	4.095	7.667	1.86E-06	1.11E-04	5.316
Ptpn13	3.702	2.069	4.723	3.02E-04	2.11E-03	0.473
Clca3a2	3.645	4.979	12.460	4.11E-09	4.11E-06	11.039
Gipc2	3.632	4.682	7.391	2.85E-06	1.47E-04	4.960
Muc13	3.613	2.960	4.546	4.25E-04	2.65E-03	0.229
Pllp	3.612	2.679	7.059	4.84E-06	1.93E-04	4.149
Itih5	3.599	4.009	5.987	2.94E-05	5.09E-04	2.725
Sytl2	3.598	3.501	4.414	5.50E-04	3.19E-03	-0.031
Atg9b	3.498	1.891	6.088	2.47E-05	4.64E-04	2.546
Fer1l4	3.435	2.362	4.456	5.07E-04	3.01E-03	0.059
Snhg11	3.433	3.421	5.042	1.65E-04	1.43E-03	1.104
Tmprss2	3.432	5.082	7.267	3.47E-06	1.63E-04	4.769
Upk3a	3.427	5.165	7.275	3.43E-06	1.63E-04	4.779
Adrb1	3.410	2.524	6.210	1.99E-05	4.08E-04	2.921
Edn1	3.375	2.469	4.780	2.71E-04	1.96E-03	0.626
Mum1l1	3.371	4.161	4.888	2.20E-04	1.73E-03	0.779
1810010D01Rik	3.365	2.254	6.345	1.58E-05	3.47E-04	3.060
Cxcl15	3.269	3.070	4.860	2.33E-04	1.78E-03	0.784
Mgmt	3.255	1.673	5.861	3.67E-05	5.76E-04	2.191
Msc	3.255	3.991	6.609	1.01E-05	2.78E-04	3.739
Gm44250	3.210	1.377	4.924	2.06E-04	1.66E-03	0.717
Ffar4	3.185	3.678	7.142	4.23E-06	1.81E-04	4.538
Prom2	3.172	3.770	6.782	7.60E-06	2.43E-04	4.002
Prom1	3.169	5.073	8.344	6.78E-07	7.05E-05	6.354
Gm4617	3.165	3.265	7.989	1.14E-06	9.01E-05	5.638
Col8a1	3.138	3.380	4.676	3.31E-04	2.24E-03	0.443
Samd5	3.134	1.932	4.308	6.77E-04	3.70E-03	-0.211
Tacstd2	3.103	5.801	8.681	4.19E-07	5.21E-05	6.824
Spef2	3.081	1.856	3.688	2.33E-03	9.08E-03	-1.296
Trpc6	3.071	2.439	5.546	6.47E-05	8.15E-04	1.913
Ahnak2	3.053	4.004	11.369	1.37E-08	7.60E-06	9.748
Igsf9	3.046	4.104	6.833	6.99E-06	2.33E-04	4.097

Piezo2	3.044	3.845	6.494	1.23E-05	3.07E-04	3.555
Agtr1a	3.025	3.641	5.619	5.67E-05	7.55E-04	2.103
Rbm20	3.017	1.404	4.185	8.64E-04	4.43E-03	-0.457
Ptn	3.011	4.584	8.162	8.85E-07	8.14E-05	6.086
Cgn	2.994	4.121	6.062	2.58E-05	4.76E-04	2.842
Krt19	2.990	7.681	11.146	1.78E-08	8.55E-06	9.921
Mboat1	2.973	5.408	8.715	4.00E-07	5.11E-05	6.872
Nid1	2.972	2.429	5.390	8.62E-05	9.68E-04	1.659
Ltf	2.971	6.674	8.989	2.73E-07	4.13E-05	7.234
Scnn1b	2.969	1.802	6.566	1.09E-05	2.87E-04	3.269
Rgl3	2.965	2.259	5.887	3.51E-05	5.67E-04	2.424
Vtcn1	2.954	2.257	6.596	1.03E-05	2.82E-04	3.472
Fam174b	2.950	3.931	7.223	3.72E-06	1.67E-04	4.689
Btc	2.949	1.829	3.617	2.69E-03	1.01E-02	-1.421
Grb14	2.917	3.644	4.718	3.05E-04	2.12E-03	0.490
Gm42418	2.909	16.157	8.332	6.91E-07	7.12E-05	6.328
Ctse	2.901	1.833	5.607	5.79E-05	7.67E-04	1.902
Cdo1	2.885	5.376	6.942	5.85E-06	2.17E-04	4.230
Col17a1	2.853	2.691	5.978	2.99E-05	5.11E-04	2.647
Bik	2.852	3.391	8.481	5.57E-07	6.24E-05	6.351
S100a14	2.837	6.593	10.540	3.66E-08	1.47E-05	9.211
Capn5	2.814	4.253	7.306	3.26E-06	1.60E-04	4.830
Cldn10	2.795	2.622	5.893	3.47E-05	5.62E-04	2.507
Cd55	2.792	1.640	5.665	5.22E-05	7.21E-04	1.950
Fgb	2.782	6.168	6.098	2.42E-05	4.63E-04	2.756
Fgg	2.778	5.478	6.450	1.32E-05	3.16E-04	3.408
Fgfr2	2.772	4.999	7.069	4.76E-06	1.90E-04	4.449
Ubd	2.768	6.525	8.388	6.37E-07	6.73E-05	6.392
Gfpt2	2.763	3.733	6.754	7.95E-06	2.48E-04	3.967
Ston2	2.756	3.135	5.650	5.36E-05	7.31E-04	2.154
Ppfibp2	2.735	4.386	7.398	2.82E-06	1.46E-04	4.972
Prss23	2.731	1.760	6.474	1.27E-05	3.13E-04	3.155
Prlr	2.724	8.260	10.341	4.67E-08	1.60E-05	8.973
BC030870	2.724	1.732	4.758	2.82E-04	2.03E-03	0.546
Ovol1	2.719	4.471	14.029	8.39E-10	3.16E-06	12.387
Cldn4	2.716	8.438	12.808	2.84E-09	3.70E-06	11.694
Hoxb4	2.709	2.036	4.271	7.28E-04	3.91E-03	-0.263
Kif5c	2.708	3.091	6.575	1.07E-05	2.86E-04	3.641

Pgr	2.696	3.841	5.421	8.13E-05	9.40E-04	1.739
Hs3st6	2.693	1.497	6.604	1.02E-05	2.79E-04	3.246
Gm45266	2.688	1.935	5.199	1.23E-04	1.18E-03	1.296
Rps4l	2.674	4.409	6.804	7.32E-06	2.38E-04	4.049
Tmprss4	2.670	1.851	6.126	2.31E-05	4.49E-04	2.707
Fam213b	2.665	2.251	6.003	2.86E-05	5.00E-04	2.623
Cep112	2.665	1.894	4.614	3.73E-04	2.42E-03	0.324
Hlf	2.664	2.840	8.958	2.85E-07	4.25E-05	6.764
Papln	2.647	1.792	8.606	4.66E-07	5.41E-05	5.762
Basp1	2.642	6.511	8.916	3.02E-07	4.41E-05	7.134
Ppl	2.635	3.410	5.316	9.88E-05	1.04E-03	1.576
Esr1	2.623	2.582	5.562	6.28E-05	8.00E-04	1.977
Tox2	2.614	4.432	5.034	1.67E-04	1.45E-03	0.977
Stc2	2.613	5.858	7.776	1.58E-06	1.01E-04	5.505
Gm15459	2.610	1.245	4.466	4.97E-04	2.96E-03	0.007
Tmem30b	2.606	3.191	6.582	1.06E-05	2.84E-04	3.666
Map1a	2.600	0.621	3.211	6.09E-03	1.86E-02	-2.125
Gstk1	2.598	2.319	5.377	8.82E-05	9.77E-04	1.647
Tuba8	2.589	4.283	7.808	1.50E-06	1.00E-04	5.577
Slc12a2	2.587	9.791	8.755	3.78E-07	5.04E-05	6.899
Sec14l4	2.584	3.094	5.970	3.03E-05	5.13E-04	2.686
Fam71a	2.582	2.148	5.252	1.11E-04	1.11E-03	1.422
Mroh2a	2.578	1.440	2.703	1.68E-02	4.05E-02	-3.005
Nckap5	2.577	2.857	3.988	1.28E-03	5.83E-03	-0.808
Egflam	2.571	2.349	4.600	3.83E-04	2.46E-03	0.323
Pon3	2.553	2.409	5.866	3.64E-05	5.74E-04	2.448
Slc5a5	2.538	3.216	4.198	8.42E-04	4.34E-03	-0.461

Appendix Table 6. Top 100 upregulated genes in tumour/stromal ($CD45^{-}GFP^{\pm}$) cells from AT3-OVA tumours at day 13 post 1x20Gy-irradiation. Differentially expressed genes filtered by logFC > 0, adjusted p value < 0.05 are listed and ranked by logFC. *logFC: log fold-change, AveExpr: average expression, P.Value: nominal p value, adj.P.Val: adjusted p value.*

Bibliography

Aaes, T.L., Kaczmarek, A., Delvaeye, T., De Craene, B., De Koker, S., Heyndrickx, L., et al. (2016). Vaccination with Necroptotic Cancer Cells Induces Efficient Anti-tumor Immunity. *Cell Rep* 15(2)**,** 274-287. doi: 10.1016/j.celrep.2016.03.037.

Abdel-Rahman, O. (2016). Correlation between PD-L1 expression and outcome of NSCLC patients treated with anti-PD-1/PD-L1 agents: A meta-analysis. *Crit Rev Oncol Hematol* 101**,** 75-85. doi: 10.1016/j.critrevonc.2016.03.007.

Ahn, G.O., and Brown, J.M. (2008). Matrix metalloproteinase-9 is required for tumor vasculogenesis but not for angiogenesis: role of bone marrow-derived myelomonocytic cells. *Cancer Cell* 13(3)**,** 193-205. doi: 10.1016/j.ccr.2007.11.032.

Althammer, S., Steele, K., Rebelatto, M., Tan, T.H., Wiestler, T., Schmidt, G., et al. (2016). 31st Annual Meeting and Associated Programs of the Society for Immunotherapy of Cancer (SITC 2016): late breaking abstracts. *Journal for ImmunoTherapy of Cancer* 4(2)**,** 91. doi: 10.1186/s40425-016-0191-4.

Anders, S., Pyl, P.T., and Huber, W. (2015). HTSeq--a Python framework to work with high-throughput sequencing data. *Bioinformatics* 31(2)**,** 166-169. doi: 10.1093/bioinformatics/btu638.

Anderson, A.C., Joller, N., and Kuchroo, V.K. (2016). Lag-3, Tim-3, and TIGIT: Co-inhibitory Receptors with Specialized Functions in Immune Regulation. *Immunity* 44(5)**,** 989-1004. doi: 10.1016/j.immuni.2016.05.001.

Anderson, S.L., Duke-Novakovski, T., and Singh, B. (2014). The immune response to anesthesia: part 2 sedatives, opioids, and injectable anesthetic agents. *Vet Anaesth Analg* 41(6)**,** 553-566. doi: 10.1111/vaa.12191.

Andre, P., Denis, C., Soulas, C., Bourbon-Caillet, C., Lopez, J., Arnoux, T., et al. (2018). Anti-NKG2A mAb Is a Checkpoint Inhibitor that Promotes Anti-tumor Immunity by Unleashing Both T and NK Cells. *Cell* 175(7)**,** 1731-1743 e1713. doi: 10.1016/j.cell.2018.10.014.

Ang, K.K. (1998). Altered fractionation trials in head and neck cancer. *Semin Radiat Oncol* 8(4)**,** 230-236. doi: 10.1016/s1053-4296(98)80020-9.

Angelova, M., Mlecnik, B., Vasaturo, A., Bindea, G., Fredriksen, T., Lafontaine, L., et al. (2018). Evolution of Metastases in Space and Time under Immune Selection. *Cell* 175(3)**,** 751-765.e716. doi: 10.1016/j.cell.2018.09.018.

Antonia, S.J., Villegas, A., Daniel, D., Vicente, D., Murakami, S., Hui, R., et al. (2018). Overall Survival with Durvalumab after Chemoradiotherapy in Stage III NSCLC. *N Engl J Med* 379(24)**,** 2342-2350. doi: 10.1056/NEJMoa1809697.

Antonia, S.J., Villegas, A., Daniel, D., Vicente, D., Murakami, S., Hui, R., et al. (2017). Durvalumab after Chemoradiotherapy in Stage III Non-Small-Cell Lung Cancer. *N Engl J Med* 377(20)**,** 1919-1929. doi: 10.1056/NEJMoa1709937.

Apetoh, L., Ghiringhelli, F., Tesniere, A., Obeid, M., Ortiz, C., Criollo, A., et al. (2007). Toll-like receptor 4-dependent contribution of the immune system to anticancer chemotherapy and radiotherapy. *Nat Med* 13(9)**,** 1050-1059. doi: 10.1038/nm1622.

Arce Vargas, F., Furness, A.J.S., Litchfield, K., Joshi, K., Rosenthal, R., Ghorani, E., et al. (2018). Fc Effector Function Contributes to the Activity of Human Anti-CTLA-4 Antibodies. *Cancer Cell* 33(4)**,** 649-663 e644. doi: 10.1016/j.ccell.2018.02.010.

Arina, A., Beckett, M., Fernandez, C., Zheng, W., Pitroda, S., Chmura, S.J., et al. (2019). Tumor-reprogrammed resident T cells resist radiation to control tumors. *Nat Commun* 10(1)**,** 3959. doi: 10.1038/s41467-019-11906-2.

Arnold, K.M., Flynn, N.J., Raben, A., Romak, L., Yu, Y., Dicker, A.P., et al. (2018). The Impact of Radiation on the Tumor Microenvironment: Effect of Dose and Fractionation Schedules. *Cancer Growth Metastasis* 11**,** 1179064418761639. doi: 10.1177/1179064418761639.

Ayers, M., Lunceford, J., Nebozhyn, M., Murphy, E., Loboda, A., Kaufman, D.R., et al. (2017). IFN-gamma-related mRNA profile predicts clinical response to PD-1 blockade. *J Clin Invest* 127(8)**,** 2930-2940. doi: 10.1172/JCI91190.

Ball, D., Mai, G.T., Vinod, S., Babington, S., Ruben, J., Kron, T., et al. (2019). Stereotactic ablative radiotherapy versus standard radiotherapy in stage 1 non-small-cell lung cancer (TROG 09.02 CHISEL): a phase 3, open-label, randomised controlled trial. *Lancet Oncol* 20(4)**,** 494-503. doi: 10.1016/S1470-2045(18)30896-9.

Balogh, A., Persa, E., Bogdandi, E.N., Benedek, A., Hegyesi, H., Safrany, G., et al. (2013). The effect of ionizing radiation on the homeostasis and functional integrity of murine splenic regulatory T cells. *Inflamm Res* 62(2)**,** 201-212. doi: 10.1007/s00011-012-0567-y.

Barcellos-Hoff, M.H. (1993). Radiation-induced transforming growth factor beta and subsequent extracellular matrix reorganization in murine mammary gland. *Cancer Res* 53(17)**,** 3880-3886.

Barry, K.C., Hsu, J., Broz, M.L., Cueto, F.J., Binnewies, M., Combes, A.J., et al. (2018). A natural killer-dendritic cell axis defines checkpoint therapy-responsive tumor microenvironments. *Nat Med* 24(8)**,** 1178-1191. doi: 10.1038/s41591-018-0085-8.

Basu, S., Binder, R.J., Ramalingam, T., and Srivastava, P.K. (2001). CD91 is a common receptor for heat shock proteins gp96, hsp90, hsp70, and calreticulin. *Immunity* 14(3)**,** 303-313. doi: 10.1016/s1074-7613(01)00111-x.

Benci, J.L., Johnson, L.R., Choa, R., Xu, Y., Qiu, J., Zhou, Z., et al. (2019). Opposing Functions of Interferon Coordinate Adaptive and Innate Immune Responses to Cancer Immune Checkpoint Blockade. *Cell* 178(4)**,** 933-948 e914. doi: 10.1016/j.cell.2019.07.019.

Bensch, F., van der Veen, E.L., Lub-de Hooge, M.N., Jorritsma-Smit, A., Boellaard, R., Kok, I.C., et al. (2018). (89)Zr-atezolizumab imaging as a non-invasive approach to assess clinical response to PD-L1 blockade in cancer. *Nat Med* 24(12)**,** 1852-1858. doi: 10.1038/s41591-018-0255-8.

Bentzen, S.M., Agrawal, R.K., Aird, E.G., Barrett, J.M., Barrett-Lee, P.J., Bliss, J.M., et al. (2008). The UK Standardisation of Breast Radiotherapy (START) Trial A of radiotherapy hypofractionation for treatment of early breast cancer: a randomised trial. *Lancet Oncol* 9(4)**,** 331-341. doi: 10.1016/s1470-2045(08)70077-9.

Bernier, J., Hall, E.J., and Giaccia, A. (2004). Radiation oncology: a century of achievements. *Nat Rev Cancer* 4(9)**,** 737-747. doi: 10.1038/nrc1451.

Bolger, A.M., Lohse, M., and Usadel, B. (2014). Trimmomatic: a flexible trimmer for Illumina sequence data. *Bioinformatics* 30(15)**,** 2114-2120. doi: 10.1093/bioinformatics/btu170.

Bos, P.D., Plitas, G., Rudra, D., Lee, S.Y., and Rudensky, A.Y. (2013). Transient regulatory T cell ablation deters oncogene-driven breast cancer and enhances radiotherapy. *J Exp Med* 210(11)**,** 2435-2466. doi: 10.1084/jem.20130762.

Bottcher, J.P., Bonavita, E., Chakravarty, P., Blees, H., Cabeza-Cabrerizo, M., Sammicheli, S., et al. (2018). NK Cells Stimulate Recruitment of cDC1 into the Tumor Microenvironment Promoting Cancer Immune Control. *Cell* 172(5)**,** 1022-1037 e1014. doi: 10.1016/j.cell.2018.01.004.

Bottcher, J.P., and Reis, E.S.C. (2018). The Role of Type 1 Conventional Dendritic Cells in Cancer Immunity. *Trends Cancer* 4(11)**,** 784-792. doi: 10.1016/j.trecan.2018.09.001.

Bouquet, F., Pal, A., Pilones, K.A., Demaria, S., Hann, B., Akhurst, R.J., et al. (2011). TGFbeta1 inhibition increases the radiosensitivity of breast cancer cells in vitro and promotes tumor control by radiation in vivo. *Clin Cancer Res* 17(21)**,** 6754-6765. doi: 10.1158/1078-0432.CCR-11-0544.

Brach, M.A., Hass, R., Sherman, M.L., Gunji, H., Weichselbaum, R., and Kufe, D. (1991). Ionizing radiation induces expression and binding activity of the nuclear factor kappa B. *J Clin Invest* 88(2)**,** 691-695. doi: 10.1172/JCI115354.

Brady, J., Carotta, S., Thong, R.P., Chan, C.J., Hayakawa, Y., Smyth, M.J., et al. (2010). The interactions of multiple cytokines control NK cell maturation. *J Immunol* 185(11)**,** 6679-6688. doi: 10.4049/jimmunol.0903354.

Brooks, E.D., and Chang, J.Y. (2019). Time to abandon single-site irradiation for inducing abscopal effects. *Nat Rev Clin Oncol* 16(2)**,** 123-135. doi: 10.1038/s41571-018-0119-7.

Broz, M.L., Binnewies, M., Boldajipour, B., Nelson, A.E., Pollack, J.L., Erle, D.J., et al. (2014). Dissecting the tumor myeloid compartment reveals rare activating antigen-presenting cells critical for T cell immunity. *Cancer Cell* 26(5)**,** 638-652. doi: 10.1016/j.ccell.2014.09.007.

Bruno, A., Ferlazzo, G., Albini, A., and Noonan, D.M. (2014). A think tank of TINK/TANKs: tumor-infiltrating/tumor-associated natural killer cells in tumor progression and angiogenesis. *J Natl Cancer Inst* 106(8)**,** dju200. doi: 10.1093/jnci/dju200.

Budczies, J., von Winterfeld, M., Klauschen, F., Bockmayr, M., Lennerz, J.K., Denkert, C., et al. (2015). The landscape of metastatic progression patterns across major human cancers. *Oncotarget* 6(1)**,** 570-583. doi: 10.18632/oncotarget.2677.

Bulliard, Y., Jolicoeur, R., Windman, M., Rue, S.M., Ettenberg, S., Knee, D.A., et al. (2013). Activating Fc gamma receptors contribute to the antitumor activities of immunoregulatory receptor-targeting antibodies. *J Exp Med* 210(9)**,** 1685-1693. doi: 10.1084/jem.20130573.

Burnette, B.C., Liang, H., Lee, Y., Chlewicki, L., Khodarev, N.N., Weichselbaum, R.R., et al. (2011). The efficacy of radiotherapy relies upon induction of type i interferon-dependent innate and adaptive immunity. *Cancer Res* 71(7)**,** 2488-2496. doi: 10.1158/0008-5472.CAN-10-2820.

Burr, M.L., Sparbier, C.E., Chan, K.L., Chan, Y.C., Kersbergen, A., Lam, E.Y.N., et al. (2019). An Evolutionarily Conserved Function of Polycomb Silences the MHC Class I Antigen Presentation Pathway and Enables Immune Evasion in Cancer. *Cancer Cell* 36(4)**,** 385-401 e388. doi: 10.1016/j.ccell.2019.08.008.

Campian, J.L., Ye, X., Brock, M., and Grossman, S.A. (2013). Treatment-related lymphopenia in patients with stage III non-small-cell lung cancer. *Cancer Invest* 31(3)**,** 183-188. doi: 10.3109/07357907.2013.767342.

Canter, R.J., Grossenbacher, S.K., Foltz, J.A., Sturgill, I.R., Park, J.S., Luna, J.I., et al. (2017). Radiotherapy enhances natural killer cell cytotoxicity and localization in pre-clinical canine sarcomas and first-in-dog clinical trial. *J Immunother Cancer* 5(1)**,** 98. doi: 10.1186/s40425-017-0305-7.

Casares, N., Pequignot, M.O., Tesniere, A., Ghiringhelli, F., Roux, S., Chaput, N., et al. (2005). Caspase-dependent immunogenicity of doxorubicin-induced tumor cell death. *J Exp Med* 202(12)**,** 1691-1701. doi: 10.1084/jem.20050915.

Cha, E., Klinger, M., Hou, Y., Cummings, C., Ribas, A., Faham, M., et al. (2014). Improved survival with T cell clonotype stability after anti-CTLA-4 treatment in cancer patients. *Sci Transl Med* 6(238)**,** 238ra270. doi: 10.1126/scitranslmed.3008211.

Chakraborty, M., Abrams, S.I., Camphausen, K., Liu, K., Scott, T., Coleman, C.N., et al. (2003). Irradiation of tumor cells up-regulates Fas and enhances CTL lytic activity and CTL adoptive immunotherapy. *J Immunol* 170(12)**,** 6338-6347. doi: 10.4049/jimmunol.170.12.6338.

Chakraborty, M., Abrams, S.I., Coleman, C.N., Camphausen, K., Schlom, J., and Hodge, J.W. (2004). External beam radiation of tumors alters phenotype of tumor cells to render them susceptible to vaccine-mediated T-cell killing. *Cancer Res* 64(12)**,** 4328-4337. doi: 10.1158/0008-5472.CAN-04-0073.

Chandra, R.A., Wilhite, T.J., Balboni, T.A., Alexander, B.M., Spektor, A., Ott, P.A., et al. (2015). A systematic evaluation of abscopal responses following radiotherapy in patients with metastatic melanoma treated with ipilimumab. *Oncoimmunology* 4(11)**,** e1046028. doi: 10.1080/2162402X.2015.1046028.

Chang, J., Wang, Y., Shao, L., Laberge, R.M., Demaria, M., Campisi, J., et al. (2016). Clearance of senescent cells by ABT263 rejuvenates aged hematopoietic stem cells in mice. *Nat Med* 22(1)**,** 78-83. doi: 10.1038/nm.4010.

Chen, D.S., and Mellman, I. (2013). Oncology meets immunology: the cancer-immunity cycle. *Immunity* 39(1)**,** 1-10. doi: 10.1016/j.immuni.2013.07.012.

Chijioke, O., and Munz, C. (2013). Dendritic cell derived cytokines in human natural killer cell differentiation and activation. *Front Immunol* 4**,** 365. doi: 10.3389/fimmu.2013.00365.

Chow, M.T., Ozga, A.J., Servis, R.L., Frederick, D.T., Lo, J.A., Fisher, D.E., et al. (2019). Intratumoral Activity of the CXCR3 Chemokine System Is Required for the Efficacy of Anti-PD-1 Therapy. *Immunity* 50(6)**,** 1498-1512 e1495. doi: 10.1016/j.immuni.2019.04.010.

Christiaansen, A.F., Boggiatto, P.M., and Varga, S.M. (2014). Limitations of Foxp3(+) Treg depletion following viral infection in DEREG mice. *J Immunol Methods* 406**,** 58-65. doi: 10.1016/j.jim.2014.03.005.

Coates, P.J., Rundle, J.K., Lorimore, S.A., and Wright, E.G. (2008). Indirect macrophage responses to ionizing radiation: implications for genotype-dependent bystander signaling. *Cancer Res* 68(2)**,** 450-456. doi: 10.1158/0008-5472.CAN-07-3050.

Colorectal Cancer Collaborative, G. (2001). Adjuvant radiotherapy for rectal cancer: a systematic overview of 8,507 patients from 22 randomised trials. *Lancet* 358(9290)**,** 1291-1304. doi: 10.1016/S0140-6736(01)06409-1.

Coppe, J.P., Desprez, P.Y., Krtolica, A., and Campisi, J. (2010). The senescence-associated secretory phenotype: the dark side of tumor suppression. *Annu Rev Pathol* 5**,** 99-118. doi: 10.1146/annurev-pathol-121808-102144.

Coppola, A., Arriga, R., Lauro, D., Del Principe, M.I., Buccisano, F., Maurillo, L., et al. (2015). NK Cell Inflammation in the Clinical Outcome of Colorectal Carcinoma. *Front Med (Lausanne)* 2**,** 33. doi: 10.3389/fmed.2015.00033.

Couzin-Frankel, J. (2013). Breakthrough of the year 2013. Cancer immunotherapy. *Science* 342(6165)**,** 1432-1433. doi: 10.1126/science.342.6165.1432.

Crane, C.H. (2016). Hypofractionated ablative radiotherapy for locally advanced pancreatic cancer. *J Radiat Res* 57 Suppl 1**,** i53-i57. doi: 10.1093/jrr/rrw016.

Cursons, J., Souza-Fonseca-Guimaraes, F., Foroutan, M., Anderson, A., Hollande, F., Hediyeh-Zadeh, S., et al. (2019). A Gene Signature Predicting Natural Killer Cell Infiltration and Improved Survival in Melanoma Patients. *Cancer Immunol Res* 7(7)**,** 1162-1174. doi: 10.1158/2326-6066.CIR-18-0500.

Curtsinger, J.M., and Mescher, M.F. (2010). Inflammatory cytokines as a third signal for T cell activation. *Curr Opin Immunol* 22(3)**,** 333-340. doi: 10.1016/j.coi.2010.02.013.

Dahan, R., Sega, E., Engelhardt, J., Selby, M., Korman, A.J., and Ravetch, J.V. (2015). FcgammaRs Modulate the Anti-tumor Activity of Antibodies Targeting the PD-1/PD-L1 Axis. *Cancer Cell* 28(3)**,** 285-295. doi: 10.1016/j.ccell.2015.08.004.

Dart, A. (2018). Tumour microenvironment: Microbes matter. *Nat Rev Cancer* 18(1)**,** 1. doi: 10.1038/nrc.2017.120.

Davuluri, R., Jiang, W., Fang, P., Xu, C., Komaki, R., Gomez, D.R., et al. (2017). Lymphocyte Nadir and Esophageal Cancer Survival Outcomes After Chemoradiation Therapy. *Int J Radiat Oncol Biol Phys* 99(1)**,** 128-135. doi: 10.1016/j.ijrobp.2017.05.037.

Dearnaley, D., Syndikus, I., Mossop, H., Khoo, V., Birtle, A., Bloomfield, D., et al. (2016). Conventional versus hypofractionated high-dose intensity-modulated radiotherapy for prostate cancer: 5-year outcomes of the randomised, non-inferiority, phase 3 CHHiP trial. *Lancet Oncol* 17(8)**,** 1047-1060. doi: 10.1016/s1470-2045(16)30102-4.

Debacq-Chainiaux, F., Erusalimsky, J.D., Campisi, J., and Toussaint, O. (2009). Protocols to detect senescence-associated beta-galactosidase (SA-betagal) activity, a biomarker of senescent cells in culture and in vivo. *Nat Protoc* 4(12)**,** 1798-1806. doi: 10.1038/nprot.2009.191.

Delaney, G., Jacob, S., Featherstone, C., and Barton, M. (2005). The role of radiotherapy in cancer treatment: estimating optimal utilization from a review of evidence-based clinical guidelines. *Cancer* 104(6)**,** 1129-1137. doi: 10.1002/cncr.21324.

Delgoffe, G.M., Woo, S.R., Turnis, M.E., Gravano, D.M., Guy, C., Overacre, A.E., et al. (2013). Stability and function of regulatory T cells is maintained by a neuropilin-1-semaphorin-4a axis. *Nature* 501(7466)**,** 252-256. doi: 10.1038/nature12428.

Demaria, S., and Formenti, S.C. (2012). Radiation as an immunological adjuvant: current evidence on dose and fractionation. *Front Oncol* 2**,** 153. doi: 10.3389/fonc.2012.00153.

Demaria, S., Kawashima, N., Yang, A.M., Devitt, M.L., Babb, J.S., Allison, J.P., et al. (2005). Immune-mediated inhibition of metastases after treatment with local radiation and CTLA-4 blockade in a mouse model of breast cancer. *Clin Cancer Res* 11(2 Pt 1)**,** 728-734.

Demaria, S., Ng, B., Devitt, M.L., Babb, J.S., Kawashima, N., Liebes, L., et al. (2004). Ionizing radiation inhibition of distant untreated tumors (abscopal effect) is immune mediated. *Int J Radiat Oncol Biol Phys* 58(3)**,** 862-870. doi: 10.1016/j.ijrobp.2003.09.012.

Deng, L., Liang, H., Burnette, B., Beckett, M., Darga, T., Weichselbaum, R.R., et al. (2014a). Irradiation and anti-PD-L1 treatment synergistically promote antitumor immunity in mice. *J Clin Invest* 124(2)**,** 687-695. doi: 10.1172/JCI67313.

Deng, L., Liang, H., Xu, M., Yang, X., Burnette, B., Arina, A., et al. (2014b). STING-Dependent Cytosolic DNA Sensing Promotes Radiation-Induced Type I Interferon-Dependent Antitumor Immunity in Immunogenic Tumors. *Immunity* 41(5)**,** 843-852. doi: 10.1016/j.immuni.2014.10.019.

Dewan, M.Z., Galloway, A.E., Kawashima, N., Dewyngaert, J.K., Babb, J.S., Formenti, S.C., et al. (2009). Fractionated but not single-dose radiotherapy induces an immune-mediated abscopal effect when combined with anti-CTLA-4 antibody. *Clin Cancer Res* 15(17)**,** 5379-5388. doi: 10.1158/1078-0432.CCR-09-0265.

Diamond, J.M., Vanpouille-Box, C., Spada, S., Rudqvist, N.P., Chapman, J.R., Ueberheide, B.M., et al. (2018). Exosomes Shuttle TREX1-Sensitive IFN-Stimulatory dsDNA from Irradiated Cancer Cells to DCs. *Cancer Immunol Res* 6(8)**,** 910-920. doi: 10.1158/2326-6066.CIR-17-0581.

Diamond, M.S., Kinder, M., Matsushita, H., Mashayekhi, M., Dunn, G.P., Archambault, J.M., et al. (2011). Type I interferon is selectively required by dendritic cells for immune rejection of tumors. *J Exp Med* 208(10)**,** 1989-2003. doi: 10.1084/jem.20101158.

Dieu-Nosjean, M.C., Antoine, M., Danel, C., Heudes, D., Wislez, M., Poulot, V., et al. (2008). Long-term survival for patients with non-small-cell lung cancer with intratumoral lymphoid structures. *J Clin Oncol* 26(27)**,** 4410-4417. doi: 10.1200/JCO.2007.15.0284.

Dinarello, C.A., Novick, D., Kim, S., and Kaplanski, G. (2013). Interleukin-18 and IL-18 binding protein. *Front Immunol* 4**,** 289. doi: 10.3389/fimmu.2013.00289.

Diskin, B., Adam, S., Cassini, M.F., Sanchez, G., Liria, M., Aykut, B., et al. (2020). PD-L1 engagement on T cells promotes self-tolerance and suppression of neighboring macrophages and effector T cells in cancer. *Nat Immunol*. doi: 10.1038/s41590-020-0620-x.

Dong, W., Wu, X., Ma, S., Wang, Y., Nalin, A.P., Zhu, Z., et al. (2019). The Mechanism of Anti-PD-L1 Antibody Efficacy against PD-L1-Negative Tumors Identifies NK Cells Expressing PD-L1 as a Cytolytic Effector. *Cancer Discov* 9(10)**,** 1422-1437. doi: 10.1158/2159-8290.cd-18-1259.

Donskov, F., and von der Maase, H. (2006). Impact of immune parameters on long-term survival in metastatic renal cell carcinoma. *J Clin Oncol* 24(13)**,** 1997-2005. doi: 10.1200/JCO.2005.03.9594.

Dou, Z., Ghosh, K., Vizioli, M.G., Zhu, J., Sen, P., Wangensteen, K.J., et al. (2017). Cytoplasmic chromatin triggers inflammation in senescence and cancer. *Nature* 550(7676)**,** 402-406. doi: 10.1038/nature24050.

Dougall, W.C., Kurtulus, S., Smyth, M.J., and Anderson, A.C. (2017). TIGIT and CD96: new checkpoint receptor targets for cancer immunotherapy. *Immunol Rev* 276(1)**,** 112-120. doi: 10.1111/imr.12518.

Dovedi, S.J., Adlard, A.L., Lipowska-Bhalla, G., McKenna, C., Jones, S., Cheadle, E.J., et al. (2014). Acquired resistance to fractionated radiotherapy can be overcome by concurrent PD-L1 blockade. *Cancer Res* 74(19)**,** 5458-5468. doi: 10.1158/0008-5472.CAN-14-1258.

Drake, C.G., Jaffee, E., and Pardoll, D.M. (2006). Mechanisms of immune evasion by tumors. *Adv Immunol* 90**,** 51-81. doi: 10.1016/S0065-2776(06)90002-9.

Dunn, G.P., Bruce, A.T., Ikeda, H., Old, L.J., and Schreiber, R.D. (2002). Cancer immunoediting: from immunosurveillance to tumor escape. *Nat Immunol* 3(11)**,** 991-998. doi: 10.1038/ni1102-991.

Dunn, P.L., and North, R.J. (1991). Selective radiation resistance of immunologically induced T cells as the basis for irradiation-induced T-cell-mediated regression of immunogenic tumor. *J Leukoc Biol* 49(4)**,** 388-396. doi: 10.1002/jlb.49.4.388.

Engelhard, V.H., Rodriguez, A.B., Mauldin, I.S., Woods, A.N., Peske, J.D., and Slingluff, C.L., Jr. (2018). Immune Cell Infiltration and Tertiary Lymphoid Structures as Determinants of Antitumor Immunity. *J Immunol* 200(2)**,** 432-442. doi: 10.4049/jimmunol.1701269.

Eriksson, D., and Stigbrand, T. (2010). Radiation-induced cell death mechanisms. *Tumour Biol* 31(4)**,** 363-372. doi: 10.1007/s13277-010-0042-8.

Fares, C.M., Van Allen, E.M., Drake, C.G., Allison, J.P., and Hu-Lieskovan, S. (2019). Mechanisms of Resistance to Immune Checkpoint Blockade: Why Does Checkpoint Inhibitor Immunotherapy Not Work for All Patients? *Am Soc Clin Oncol Educ Book* 39**,** 147-164. doi: 10.1200/EDBK_240837.

Farren, M.R., Sayegh, L., Ware, M.B., Chen, H.R., Gong, J., Liang, Y., et al. (2020). Immunologic alterations in the pancreatic cancer microenvironment of patients treated with neoadjuvant chemotherapy and radiotherapy. *JCI Insight* 5(1). doi: 10.1172/jci.insight.130362.

Ferrari de Andrade, L., Tay, R.E., Pan, D., Luoma, A.M., Ito, Y., Badrinath, S., et al. (2018). Antibody-mediated inhibition of MICA and MICB shedding promotes NK cell-driven tumor immunity. *Science* 359(6383)**,** 1537-1542. doi: 10.1126/science.aao0505.

Ferris, R.L., Lenz, H.J., Trotta, A.M., Garcia-Foncillas, J., Schulten, J., Audhuy, F., et al. (2018). Rationale for combination of therapeutic antibodies targeting tumor cells and immune checkpoint receptors: Harnessing innate and adaptive immunity through IgG1 isotype immune effector stimulation. *Cancer Treat Rev* 63**,** 48-60. doi: 10.1016/j.ctrv.2017.11.008.

Filatenkov, A., Baker, J., Mueller, A.M., Kenkel, J., Ahn, G.O., Dutt, S., et al. (2015). Ablative Tumor Radiation Can Change the Tumor Immune Cell Microenvironment to Induce Durable Complete Remissions. *Clin Cancer Res* 21(16)**,** 3727-3739. doi: 10.1158/1078-0432.CCR-14-2824.

Flor, A.C., Doshi, A.P., and Kron, S.J. (2016). Modulation of therapy-induced senescence by reactive lipid aldehydes. *Cell Death Discov* 2. doi: 10.1038/cddiscovery.2016.45.

Formenti, S.C., and Demaria, S. (2009). Systemic effects of local radiotherapy. *Lancet Oncol* 10(7)**,** 718-726. doi: 10.1016/S1470-2045(09)70082-8.

Formenti, S.C., and Demaria, S. (2012). Radiation therapy to convert the tumor into an in situ vaccine. *Int J Radiat Oncol Biol Phys* 84(4)**,** 879-880. doi: 10.1016/j.ijrobp.2012.06.020.

Formenti, S.C., Rudqvist, N.P., Golden, E., Cooper, B., Wennerberg, E., Lhuillier, C., et al. (2018). Radiotherapy induces responses of lung cancer to CTLA-4 blockade. *Nat Med* 24(12)**,** 1845-1851. doi: 10.1038/s41591-018-0232-2.

Fowler, J.F. (1989). The linear-quadratic formula and progress in fractionated radiotherapy. *Br J Radiol* 62(740)**,** 679-694. doi: 10.1259/0007-1285-62-740-679.

Fowler, J.F. (2010). 21 years of biologically effective dose. *Br J Radiol* 83(991)**,** 554-568. doi: 10.1259/bjr/31372149.

Freeman, A.J., Vervoort, S.J., Ramsbottom, K.M., Kelly, M.J., Michie, J., Pijpers, L., et al. (2019). Natural Killer Cells Suppress T Cell-Associated Tumor Immune Evasion. *Cell Rep* 28(11)**,** 2784-2794 e2785. doi: 10.1016/j.celrep.2019.08.017.

Fuertes, M.B., Kacha, A.K., Kline, J., Woo, S.R., Kranz, D.M., Murphy, K.M., et al. (2011). Host type I IFN signals are required for antitumor CD8+ T cell responses through CD8{alpha}+ dendritic cells. *J Exp Med* 208(10)**,** 2005-2016. doi: 10.1084/jem.20101159.

Galluzzi, L., Buque, A., Kepp, O., Zitvogel, L., and Kroemer, G. (2017). Immunogenic cell death in cancer and infectious disease. *Nat Rev Immunol* 17(2)**,** 97-111. doi: 10.1038/nri.2016.107.

Galluzzi, L., Vitale, I., Aaronson, S.A., Abrams, J.M., Adam, D., Agostinis, P., et al. (2018). Molecular mechanisms of cell death: recommendations of the Nomenclature Committee on Cell Death 2018. *Cell Death Differ* 25(3)**,** 486-541. doi: 10.1038/s41418-017-0012-4.

Galon, J., and Bruni, D. (2019). Approaches to treat immune hot, altered and cold tumours with combination immunotherapies. *Nat Rev Drug Discov* 18(3)**,** 197-218. doi: 10.1038/s41573-018-0007-y.

Galon, J., and Bruni, D. (2020). Tumor Immunology and Tumor Evolution: Intertwined Histories. *Immunity* 52(1)**,** 55-81. doi: 10.1016/j.immuni.2019.12.018.

Gameiro, S.R., Jammeh, M.L., Wattenberg, M.M., Tsang, K.Y., Ferrone, S., and Hodge, J.W. (2014). Radiation-induced immunogenic modulation of tumor enhances antigen processing and calreticulin exposure, resulting in enhanced T-cell killing. *Oncotarget* 5(2)**,** 403-416. doi: 10.18632/oncotarget.1719.

Gannon, P.O., Poisson, A.O., Delvoye, N., Lapointe, R., Mes-Masson, A.M., and Saad, F. (2009). Characterization of the intra-prostatic immune cell infiltration in androgen-deprived prostate cancer patients. *J Immunol Methods* 348(1-2)**,** 9-17. doi: 10.1016/j.jim.2009.06.004.

Ganss, R., Ryschich, E., Klar, E., Arnold, B., and Hammerling, G.J. (2002). Combination of T-cell therapy and trigger of inflammation induces remodeling of the vasculature and tumor eradication. *Cancer Res* 62(5)**,** 1462-1470.

Garcia-Barros, M., Paris, F., Cordon-Cardo, C., Lyden, D., Rafii, S., Haimovitz-Friedman, A., et al. (2003). Tumor response to radiotherapy regulated by endothelial cell apoptosis. *Science* 300(5622)**,** 1155-1159. doi: 10.1126/science.1082504.

Garnett, C.T., Palena, C., Chakraborty, M., Tsang, K.Y., Schlom, J., and Hodge, J.W. (2004). Sublethal irradiation of human tumor cells modulates phenotype resulting in enhanced killing by cytotoxic T lymphocytes. *Cancer Res* 64(21)**,** 7985-7994. doi: 10.1158/0008-5472.CAN-04-1525.

Gascoigne, K.E., and Taylor, S.S. (2008). Cancer cells display profound intra- and interline variation following prolonged exposure to antimitotic drugs. *Cancer Cell* 14(2)**,** 111-122. doi: 10.1016/j.ccr.2008.07.002.

Gasser, S., Orsulic, S., Brown, E.J., and Raulet, D.H. (2005). The DNA damage pathway regulates innate immune system ligands of the NKG2D receptor. *Nature* 436(7054)**,** 1186-1190. doi: 10.1038/nature03884.

Gehrke, N., Mertens, C., Zillinger, T., Wenzel, J., Bald, T., Zahn, S., et al. (2013). Oxidative damage of DNA confers resistance to cytosolic nuclease TREX1 degradation and potentiates STING-dependent immune sensing. *Immunity* 39(3)**,** 482-495. doi: 10.1016/j.immuni.2013.08.004.

Gide, T.N., Quek, C., Menzies, A.M., Tasker, A.T., Shang, P., Holst, J., et al. (2019). Distinct Immune Cell Populations Define Response to Anti-PD-1 Monotherapy and Anti-PD-1/Anti-CTLA-4 Combined Therapy. *Cancer Cell* 35(2)**,** 238-255 e236. doi: 10.1016/j.ccell.2019.01.003.

Gluck, S., Guey, B., Gulen, M.F., Wolter, K., Kang, T.W., Schmacke, N.A., et al. (2017). Innate immune sensing of cytosolic chromatin fragments through cGAS promotes senescence. *Nat Cell Biol* 19(9)**,** 1061-1070. doi: 10.1038/ncb3586.

Golden, E.B., Chhabra, A., Chachoua, A., Adams, S., Donach, M., Fenton-Kerimian, M., et al. (2015). Local radiotherapy and granulocyte-macrophage colony-stimulating factor to generate abscopal responses in patients with metastatic solid tumours: a proof-of-principle trial. *Lancet Oncol* 16(7)**,** 795-803. doi: 10.1016/S1470-2045(15)00054-6.

Golden, E.B., Demaria, S., Schiff, P.B., Chachoua, A., and Formenti, S.C. (2013). An abscopal response to radiation and ipilimumab in a patient with metastatic non-small cell lung cancer. *Cancer Immunol Res* 1(6)**,** 365-372. doi: 10.1158/2326-6066.CIR-13-0115.

Golden, E.B., Frances, D., Pellicciotta, I., Demaria, S., Helen Barcellos-Hoff, M., and Formenti, S.C. (2014). Radiation fosters dose-dependent and chemotherapy-induced immunogenic cell death. *Oncoimmunology* 3**,** e28518. doi: 10.4161/onci.28518.

Golden, E.B., Pellicciotta, I., Demaria, S., Barcellos-Hoff, M.H., and Formenti, S.C. (2012). The convergence of radiation and immunogenic cell death signaling pathways. *Front Oncol* 2**,** 88. doi: 10.3389/fonc.2012.00088.

Goldszmid, R.S., Idoyaga, J., Bravo, A.I., Steinman, R., Mordoh, J., and Wainstok, R. (2003). Dendritic cells charged with apoptotic tumor cells induce long-lived protective CD4+ and CD8+ T cell immunity against B16 melanoma. *J Immunol* 171(11)**,** 5940-5947. doi: 10.4049/jimmunol.171.11.5940.

Gong, H., Zhang, B., Little, G., Kovar, J., Chen, H., Xie, W., et al. (2009). beta-Galactosidase activity assay using far-red-shifted fluorescent substrate DDAOG. *Anal Biochem* 386(1)**,** 59-64. doi: 10.1016/j.ab.2008.11.031.

Gong, Y., Fan, Z., Luo, G., Yang, C., Huang, Q., Fan, K., et al. (2019). The role of necroptosis in cancer biology and therapy. *Mol Cancer* 18(1)**,** 100. doi: 10.1186/s12943-019-1029-8.

Gorin, J.B., Menager, J., Gouard, S., Maurel, C., Guilloux, Y., Faivre-Chauvet, A., et al. (2014). Antitumor immunity induced after alpha irradiation. *Neoplasia* 16(4)**,** 319-328. doi: 10.1016/j.neo.2014.04.002.

Gough, M.J., Young, K., and Crittenden, M. (2013). The impact of the myeloid response to radiation therapy. *Clin Dev Immunol* 2013**,** 281958. doi: 10.1155/2013/281958.

Grayson, J.M., Harrington, L.E., Lanier, J.G., Wherry, E.J., and Ahmed, R. (2002). Differential sensitivity of naive and memory CD8+ T cells to apoptosis in vivo. *J Immunol* 169(7)**,** 3760-3770. doi: 10.4049/jimmunol.169.7.3760.

Green, D.R., Ferguson, T., Zitvogel, L., and Kroemer, G. (2009). Immunogenic and tolerogenic cell death. *Nat Rev Immunol* 9(5)**,** 353-363. doi: 10.1038/nri2545.

Grossman, S.A., Ye, X., Lesser, G., Sloan, A., Carraway, H., Desideri, S., et al. (2011). Immunosuppression in patients with high-grade gliomas treated with radiation and temozolomide. *Clin Cancer Res* 17(16)**,** 5473-5480. doi: 10.1158/1078-0432.ccr-11-0774.

Guethlein, L.A., Norman, P.J., Hilton, H.G., and Parham, P. (2015). Co-evolution of MHC class I and variable NK cell receptors in placental mammals. *Immunol Rev* 267(1)**,** 259-282. doi: 10.1111/imr.12326.

Guillerey, C., Huntington, N.D., and Smyth, M.J. (2016). Targeting natural killer cells in cancer immunotherapy. *Nat Immunol* 17(9)**,** 1025-1036. doi: 10.1038/ni.3518.

Gupta, A., Probst, H.C., Vuong, V., Landshammer, A., Muth, S., Yagita, H., et al. (2012). Radiotherapy promotes tumor-specific effector CD8+ T cells via dendritic cell activation. *J Immunol* 189(2)**,** 558-566. doi: 10.4049/jimmunol.1200563.

Hanahan, D., and Weinberg, R.A. (2011). Hallmarks of cancer: the next generation. *Cell* 144(5)**,** 646-674. doi: 10.1016/j.cell.2011.02.013.

Harding, S.M., Benci, J.L., Irianto, J., Discher, D.E., Minn, A.J., and Greenberg, R.A. (2017). Mitotic progression following DNA damage enables pattern recognition within micronuclei. *Nature* 548(7668)**,** 466-470. doi: 10.1038/nature23470.

Hartley, G.P., Chow, L., Ammons, D.T., Wheat, W.H., and Dow, S.W. (2018). Programmed Cell Death Ligand 1 (PD-L1) Signaling Regulates Macrophage Proliferation and Activation. *Cancer Immunol Res* 6(10)**,** 1260-1273. doi: 10.1158/2326-6066.CIR-17-0537.

Heckmann, M., Douwes, K., Peter, R., and Degitz, K. (1998). Vascular activation of adhesion molecule mRNA and cell surface expression by ionizing radiation. *Exp Cell Res* 238(1)**,** 148-154. doi: 10.1006/excr.1997.3826.

Herberman, R.B., Nunn, M.E., Holden, H.T., and Lavrin, D.H. (1975). Natural cytotoxic reactivity of mouse lymphoid cells against syngeneic and allogeneic tumors. II. Characterization of effector cells. *Int J Cancer* 16(2)**,** 230-239. doi: 10.1002/ijc.2910160205.

Herbig, U., Jobling, W.A., Chen, B.P., Chen, D.J., and Sedivy, J.M. (2004). Telomere shortening triggers senescence of human cells through a pathway involving ATM, p53, and p21(CIP1), but not p16(INK4a). *Mol Cell* 14(4)**,** 501-513. doi: 10.1016/s1097-2765(04)00256-4.

Heylmann, D., Rodel, F., Kindler, T., and Kaina, B. (2014). Radiation sensitivity of human and murine peripheral blood lymphocytes, stem and progenitor cells. *Biochim Biophys Acta* 1846(1)**,** 121-129. doi: 10.1016/j.bbcan.2014.04.009.

Hiniker, S.M., Chen, D.S., Reddy, S., Chang, D.T., Jones, J.C., Mollick, J.A., et al. (2012). A systemic complete response of metastatic melanoma to local radiation and immunotherapy. *Transl Oncol* 5(6)**,** 404-407. doi: 10.1593/tlo.12280.

Huang, A.C., Postow, M.A., Orlowski, R.J., Mick, R., Bengsch, B., Manne, S., et al. (2017). T-cell invigoration to tumour burden ratio associated with anti-PD-1 response. *Nature* 545(7652)**,** 60-65. doi: 10.1038/nature22079.

Hui, E., Cheung, J., Zhu, J., Su, X., Taylor, M.J., Wallweber, H.A., et al. (2017). T cell costimulatory receptor CD28 is a primary target for PD-1-mediated inhibition. *Science* 355(6332)**,** 1428-1433. doi: 10.1126/science.aaf1292.

Huynh, M.L., Fadok, V.A., and Henson, P.M. (2002). Phosphatidylserine-dependent ingestion of apoptotic cells promotes TGF-beta1 secretion and the resolution of inflammation. *J Clin Invest* 109(1)**,** 41-50. doi: 10.1172/JCI11638.

Iannello, A., Thompson, T.W., Ardolino, M., Lowe, S.W., and Raulet, D.H. (2013). p53-dependent chemokine production by senescent tumor cells supports NKG2D-dependent tumor elimination by natural killer cells. *J Exp Med* 210(10)**,** 2057-2069. doi: 10.1084/jem.20130783.

Im, S.J., Hashimoto, M., Gerner, M.Y., Lee, J., Kissick, H.T., Burger, M.C., et al. (2016). Defining CD8+ T cells that provide the proliferative burst after PD-1 therapy. *Nature* 537(7620)**,** 417-421. doi: 10.1038/nature19330.

Innate Pharma (2017). *Innate Pharma provides an update on Lirilumab* [Online]. Available: https://www.innate-pharma.com/en/news-events/press-releases/innate-pharma-provides-update-lirilumab [Accessed 27 March 2020].

Ishigami, S., Natsugoe, S., Tokuda, K., Nakajo, A., Che, X., Iwashige, H., et al. (2000). Prognostic value of intratumoral natural killer cells in gastric carcinoma. *Cancer* 88(3)**,** 577-583.

Jang, J.E., Hajdu, C.H., Liot, C., Miller, G., Dustin, M.L., and Bar-Sagi, D. (2017). Crosstalk between Regulatory T Cells and Tumor-Associated Dendritic Cells Negates Anti-tumor Immunity in Pancreatic Cancer. *Cell Rep* 20(3)**,** 558-571. doi: 10.1016/j.celrep.2017.06.062.

Jiménez-Sánchez, A., Memon, D., Pourpe, S., Veeraraghavan, H., Li, Y., Vargas, H.A., et al. (2017). Heterogeneous Tumor-Immune Microenvironments among Differentially Growing Metastases in an Ovarian Cancer Patient. *Cell* 170(5)**,** 927-938.e920. doi: 10.1016/j.cell.2017.07.025.

Jobling, M.F., Mott, J.D., Finnegan, M.T., Jurukovski, V., Erickson, A.C., Walian, P.J., et al. (2006). Isoform-specific activation of latent transforming growth factor beta (LTGF-beta) by reactive oxygen species. *Radiat Res* 166(6)**,** 839-848. doi: 10.1667/RR0695.1.

Joiner, M., and Kogel, A.v.d. (2018). *Basic clinical radiobiology.* Boca Raton, FL: CRC Press/Taylor & Francis Group.

Joseph, R.W., Elassaiss-Schaap, J., Kefford, R., Hwu, W.J., Wolchok, J.D., Joshua, A.M., et al. (2018). Baseline Tumor Size Is an Independent Prognostic Factor for Overall Survival in Patients with Melanoma Treated with Pembrolizumab. *Clin Cancer Res* 24(20)**,** 4960-4967. doi: 10.1158/1078-0432.ccr-17-2386.

Joyce, J.A., and Fearon, D.T. (2015). T cell exclusion, immune privilege, and the tumor microenvironment. *Science* 348(6230)**,** 74-80. doi: 10.1126/science.aaa6204.

Kachikwu, E.L., Iwamoto, K.S., Liao, Y.P., DeMarco, J.J., Agazaryan, N., Economou, J.S., et al. (2011). Radiation enhances regulatory T cell representation. *Int J Radiat Oncol Biol Phys* 81(4)**,** 1128-1135. doi: 10.1016/j.ijrobp.2010.09.034.

Kalluri, R. (2016). The biology and function of fibroblasts in cancer. *Nat Rev Cancer* 16(9)**,** 582-598. doi: 10.1038/nrc.2016.73.

Kamphorst, A.O., Wieland, A., Nasti, T., Yang, S., Zhang, R., Barber, D.L., et al. (2017). Rescue of exhausted CD8 T cells by PD-1-targeted therapies is CD28-dependent. *Science* 355(6332)**,** 1423-1427. doi: 10.1126/science.aaf0683.

Kang, J., Demaria, S., and Formenti, S. (2016). Current clinical trials testing the combination of immunotherapy with radiotherapy. *J Immunother Cancer* 4**,** 51. doi: 10.1186/s40425-016-0156-7.

Kiessling, R., Klein, E., Pross, H., and Wigzell, H. (1975). "Natural" killer cells in the mouse. II. Cytotoxic cells with specificity for mouse Moloney leukemia cells. Characteristics of the killer cell. *Eur J Immunol* 5(2)**,** 117-121. doi: 10.1002/eji.1830050209.

Kim, C., Gao, R., Sei, E., Brandt, R., Hartman, J., Hatschek, T., et al. (2018). Chemoresistance Evolution in Triple-Negative Breast Cancer Delineated by Single-Cell Sequencing. *Cell* 173(4)**,** 879-893.e813. doi: 10.1016/j.cell.2018.03.041.

Kim, D., Langmead, B., and Salzberg, S.L. (2015). HISAT: a fast spliced aligner with low memory requirements. *Nat Methods* 12(4)**,** 357-360. doi: 10.1038/nmeth.3317.

Kim, J.Y., Son, Y.O., Park, S.W., Bae, J.H., Chung, J.S., Kim, H.H., et al. (2006). Increase of NKG2D ligands and sensitivity to NK cell-mediated cytotoxicity of tumor cells by heat shock and ionizing radiation. *Exp Mol Med* 38(5)**,** 474-484. doi: 10.1038/emm.2006.56.

Kim, K.W., Jeong, J.U., Lee, K.H., Uong, T.N.T., Rhee, J.H., Ahn, S.J., et al. (2019). Combined NK Cell Therapy and Radiation Therapy Exhibit Long-Term Therapeutic and Antimetastatic Effects in a Human Triple Negative Breast Cancer Model. *Int J Radiat Oncol Biol Phys*. doi: 10.1016/j.ijrobp.2019.09.041.

Kleffel, S., Posch, C., Barthel, S.R., Mueller, H., Schlapbach, C., Guenova, E., et al. (2015). Melanoma Cell-Intrinsic PD-1 Receptor Functions Promote Tumor Growth. *Cell* 162(6)**,** 1242-1256. doi: 10.1016/j.cell.2015.08.052.

Klug, F., Prakash, H., Huber, P.E., Seibel, T., Bender, N., Halama, N., et al. (2013). Low-dose irradiation programs macrophage differentiation to an iNOS(+)/M1 phenotype that orchestrates effective T cell immunotherapy. *Cancer Cell* 24(5)**,** 589-602. doi: 10.1016/j.ccr.2013.09.014.

Ko, A., Kanehisa, A., Martins, I., Senovilla, L., Chargari, C., Dugue, D., et al. (2014). Autophagy inhibition radiosensitizes in vitro, yet reduces radioresponses in vivo due to deficient immunogenic signalling. *Cell Death Differ* 21(1)**,** 92-99. doi: 10.1038/cdd.2013.124.

Kolesnick, R., and Fuks, Z. (2003). Radiation and ceramide-induced apoptosis. *Oncogene* 22(37)**,** 5897-5906. doi: 10.1038/sj.onc.1206702.

Krasnova, Y., Putz, E.M., Smyth, M.J., and Souza-Fonseca-Guimaraes, F. (2017). Bench to bedside: NK cells and control of metastasis. *Clin Immunol* 177**,** 50-59. doi: 10.1016/j.clim.2015.10.001.

Krizhanovsky, V., Yon, M., Dickins, R.A., Hearn, S., Simon, J., Miething, C., et al. (2008). Senescence of activated stellate cells limits liver fibrosis. *Cell* 134(4)**,** 657-667. doi: 10.1016/j.cell.2008.06.049.

Kroemer, G., Galluzzi, L., Vandenabeele, P., Abrams, J., Alnemri, E.S., Baehrecke, E.H., et al. (2009). Classification of cell death: recommendations of the Nomenclature Committee on Cell Death 2009. *Cell Death Differ* 16(1)**,** 3-11. doi: 10.1038/cdd.2008.150.

Kroemer, G., and Levine, B. (2008). Autophagic cell death: the story of a misnomer. *Nat Rev Mol Cell Biol* 9(12)**,** 1004-1010. doi: 10.1038/nrm2529.

Krysko, D.V., Garg, A.D., Kaczmarek, A., Krysko, O., Agostinis, P., and Vandenabeele, P. (2012). Immunogenic cell death and DAMPs in cancer therapy. *Nat Rev Cancer* 12(12)**,** 860-875. doi: 10.1038/nrc3380.

Kurokawa, T., Oelke, M., and Mackensen, A. (2001). Induction and clonal expansion of tumor-specific cytotoxic T lymphocytes from renal cell carcinoma patients after stimulation with autologous dendritic cells loaded with tumor cells. *Int J Cancer* 91(6)**,** 749-756. doi: 10.1002/1097-0215(200002)9999:9999<::aid-ijc1141>3.0.co;2-x.

Kwon, E.D., Drake, C.G., Scher, H.I., Fizazi, K., Bossi, A., van den Eertwegh, A.J., et al. (2014). Ipilimumab versus placebo after radiotherapy in patients with metastatic castration-resistant prostate cancer that had progressed after docetaxel chemotherapy (CA184-043): a multicentre, randomised, double-blind, phase 3 trial. *Lancet Oncol* 15(7)**,** 700-712. doi: 10.1016/S1470-2045(14)70189-5.

Kwon, J., and Bakhoum, S.F. (2020). The Cytosolic DNA-Sensing cGAS-STING Pathway in Cancer. *Cancer Discov* 10(1)**,** 26-39. doi: 10.1158/2159-8290.CD-19-0761.

Lacotte, S., Brun, S., Muller, S., and Dumortier, H. (2009). CXCR3, inflammation, and autoimmune diseases. *Ann N Y Acad Sci* 1173**,** 310-317. doi: 10.1111/j.1749-6632.2009.04813.x.

Lahl, K., and Sparwasser, T. (2011). In vivo depletion of FoxP3+ Tregs using the DEREG mouse model. *Methods Mol Biol* 707**,** 157-172. doi: 10.1007/978-1-61737-979-6_10.

Lang, X., Green, M.D., Wang, W., Yu, J., Choi, J.E., Jiang, L., et al. (2019). Radiotherapy and immunotherapy promote tumoral lipid oxidation and ferroptosis via synergistic repression of SLC7A11. *Cancer Discov*. doi: 10.1158/2159-8290.CD-19-0338.

Langowski, J.L., Zhang, X., Wu, L., Mattson, J.D., Chen, T., Smith, K., et al. (2006). IL-23 promotes tumour incidence and growth. *Nature* 442(7101)**,** 461-465. doi: 10.1038/nature04808.

Larkin, J., Chiarion-Sileni, V., Gonzalez, R., Grob, J.J., Cowey, C.L., Lao, C.D., et al. (2015). Combined Nivolumab and Ipilimumab or Monotherapy in Untreated Melanoma. *N Engl J Med* 373(1)**,** 23-34. doi: 10.1056/NEJMoa1504030.

Lasry, A., and Ben-Neriah, Y. (2015). Senescence-associated inflammatory responses: aging and cancer perspectives. *Trends Immunol* 36(4)**,** 217-228. doi: 10.1016/j.it.2015.02.009.

Law, C.W., Chen, Y., Shi, W., and Smyth, G.K. (2014). voom: Precision weights unlock linear model analysis tools for RNA-seq read counts. *Genome Biol* 15(2)**,** R29. doi: 10.1186/gb-2014-15-2-r29.

Lee, Y., Auh, S.L., Wang, Y., Burnette, B., Wang, Y., Meng, Y., et al. (2009). Therapeutic effects of ablative radiation on local tumor require CD8+ T cells: changing strategies for cancer treatment. *Blood* 114(3)**,** 589-595. doi: 10.1182/blood-2009-02-206870.

Lehmann, B., Biburger, M., Brückner, C., Ipsen-Escobedo, A., Gordan, S., Lehmann, C., et al. (2017). Tumor location determines tissue-specific recruitment of tumor-associated macrophages and antibody-dependent immunotherapy response. *Sci Immunol* 2(7). doi: 10.1126/sciimmunol.aah6413.

Lei, P., Bai, T., and Sun, Y. (2019). Mechanisms of Ferroptosis and Relations With Regulated Cell Death: A Review. *Front Physiol* 10**,** 139. doi: 10.3389/fphys.2019.00139.

Li, J., Byrne, K.T., Yan, F., Yamazoe, T., Chen, Z., Baslan, T., et al. (2018a). Tumor Cell-Intrinsic Factors Underlie Heterogeneity of Immune Cell Infiltration and Response to Immunotherapy. *Immunity* 49(1)**,** 178-193 e177. doi: 10.1016/j.immuni.2018.06.006.

Li, M., You, L., Xue, J., and Lu, Y. (2018b). Ionizing Radiation-Induced Cellular Senescence in Normal, Non-transformed Cells and the Involved DNA Damage Response: A Mini Review. *Front Pharmacol* 9**,** 522. doi: 10.3389/fphar.2018.00522.

Liang, H., Deng, L., Hou, Y., Meng, X., Huang, X., Rao, E., et al. (2017). Host STING-dependent MDSC mobilization drives extrinsic radiation resistance. *Nat Commun* 8(1)**,** 1736. doi: 10.1038/s41467-017-01566-5.

Lim, J.Y., Gerber, S.A., Murphy, S.P., and Lord, E.M. (2014). Type I interferons induced by radiation therapy mediate recruitment and effector function of CD8(+) T cells. *Cancer Immunol Immunother* 63(3)**,** 259-271. doi: 10.1007/s00262-013-1506-7.

Lob, S., Konigsrainer, A., Rammensee, H.G., Opelz, G., and Terness, P. (2009). Inhibitors of indoleamine-2,3-dioxygenase for cancer therapy: can we see the wood for the trees? *Nat Rev Cancer* 9(6)**,** 445-452. doi: 10.1038/nrc2639.

Loblaw, A., Cheung, P., D'Alimonte, L., Deabreu, A., Mamedov, A., Zhang, L., et al. (2013). Prostate stereotactic ablative body radiotherapy using a standard linear accelerator: toxicity, biochemical, and pathological outcomes. *Radiother Oncol* 107(2)**,** 153-158. doi: 10.1016/j.radonc.2013.03.022.

Lopez-Castejon, G., and Brough, D. (2011). Understanding the mechanism of IL-1β secretion. *Cytokine Growth Factor Rev* 22(4)**,** 189-195. doi: 10.1016/j.cytogfr.2011.10.001.

Lopez-Soto, A., Gonzalez, S., Smyth, M.J., and Galluzzi, L. (2017). Control of Metastasis by NK Cells. *Cancer Cell* 32(2)**,** 135-154. doi: 10.1016/j.ccell.2017.06.009.

Lotze, M.T., and Tracey, K.J. (2005). High-mobility group box 1 protein (HMGB1): nuclear weapon in the immune arsenal. *Nat Rev Immunol* 5(4)**,** 331-342. doi: 10.1038/nri1594.

Lu, D., Ni, Z., Liu, X., Feng, S., Dong, X., Shi, X., et al. (2019). Beyond T Cells: Understanding the Role of PD-1/PD-L1 in Tumor-Associated Macrophages. *J Immunol Res* 2019**,** 1919082. doi: 10.1155/2019/1919082.

Lu, L., Barbi, J., and Pan, F. (2017). The regulation of immune tolerance by FOXP3. *Nat Rev Immunol* 17(11)**,** 703-717. doi: 10.1038/nri.2017.75.

Lugade, A.A., Moran, J.P., Gerber, S.A., Rose, R.C., Frelinger, J.G., and Lord, E.M. (2005). Local radiation therapy of B16 melanoma tumors increases the generation of tumor antigen-specific effector cells that traffic to the tumor. *J Immunol* 174(12)**,** 7516-7523. doi: 10.4049/jimmunol.174.12.7516.

Lugade, A.A., Sorensen, E.W., Gerber, S.A., Moran, J.P., Frelinger, J.G., and Lord, E.M. (2008). Radiation-induced IFN-gamma production within the tumor microenvironment influences antitumor immunity. *J Immunol* 180(5)**,** 3132-3139. doi: 10.4049/jimmunol.180.5.3132.

Luke, J.J., Lemons, J.M., Karrison, T.G., Pitroda, S.P., Melotek, J.M., Zha, Y., et al. (2018). Safety and Clinical Activity of Pembrolizumab and Multisite Stereotactic Body Radiotherapy in Patients With Advanced Solid Tumors. *J Clin Oncol* 36(16)**,** 1611-1618. doi: 10.1200/JCO.2017.76.2229.

Ma, Y., Kepp, O., Ghiringhelli, F., Apetoh, L., Aymeric, L., Locher, C., et al. (2010). Chemotherapy and radiotherapy: cryptic anticancer vaccines. *Semin Immunol* 22(3)**,** 113-124. doi: 10.1016/j.smim.2010.03.001.

Marcu, L.G. (2010). Altered fractionation in radiotherapy: from radiobiological rationale to therapeutic gain. *Cancer Treat Rev* 36(8)**,** 606-614. doi: 10.1016/j.ctrv.2010.04.004.

Marcus, A., Mao, A.J., Lensink-Vasan, M., Wang, L., Vance, R.E., and Raulet, D.H. (2018). Tumor-Derived cGAMP Triggers a STING-Mediated Interferon Response in Non-tumor Cells to Activate the NK Cell Response. *Immunity* 49(4)**,** 754-763 e754. doi: 10.1016/j.immuni.2018.09.016.

Markovsky, E., Budhu, S., Samstein, R.M., Li, H., Russell, J., Zhang, Z., et al. (2019). An Antitumor Immune Response Is Evoked by Partial-Volume Single-Dose Radiation in 2 Murine Models. *Int J Radiat Oncol Biol Phys* 103(3)**,** 697-708. doi: 10.1016/j.ijrobp.2018.10.009.

Martin, M., Lefaix, J., and Delanian, S. (2000). TGF-beta1 and radiation fibrosis: a master switch and a specific therapeutic target? *Int J Radiat Oncol Biol Phys* 47(2)**,** 277-290. doi: 10.1016/s0360-3016(00)00435-1.

Martin-Fontecha, A., Thomsen, L.L., Brett, S., Gerard, C., Lipp, M., Lanzavecchia, A., et al. (2004). Induced recruitment of NK cells to lymph nodes provides IFN-gamma for T(H)1 priming. *Nat Immunol* 5(12)**,** 1260-1265. doi: 10.1038/ni1138.

Martinet, L., and Smyth, M.J. (2015). Balancing natural killer cell activation through paired receptors. *Nat Rev Immunol* 15(4)**,** 243-254. doi: 10.1038/nri3799.

Maruhashi, T., Okazaki, I.M., Sugiura, D., Takahashi, S., Maeda, T.K., Shimizu, K., et al. (2018). LAG-3 inhibits the activation of CD4(+) T cells that recognize stable pMHCII through its conformation-dependent recognition of pMHCII. *Nat Immunol* 19(12)**,** 1415-1426. doi: 10.1038/s41590-018-0217-9.

Matsumura, S., Wang, B., Kawashima, N., Braunstein, S., Badura, M., Cameron, T.O., et al. (2008). Radiation-induced CXCL16 release by breast cancer cells attracts effector T cells. *J Immunol* 181(5)**,** 3099-3107. doi: 10.4049/jimmunol.181.5.3099.

Mattarollo, S.R., Loi, S., Duret, H., Ma, Y., Zitvogel, L., and Smyth, M.J. (2011). Pivotal role of innate and adaptive immunity in anthracycline chemotherapy of established tumors. *Cancer Res* 71(14)**,** 4809-4820. doi: 10.1158/0008-5472.CAN-11-0753.

McMahon, S.J. (2018). The linear quadratic model: usage, interpretation and challenges. *Phys Med Biol* 64(1)**,** 01TR01. doi: 10.1088/1361-6560/aaf26a.

Mi, H., Muruganujan, A., Ebert, D., Huang, X., and Thomas, P.D. (2019). PANTHER version 14: more genomes, a new PANTHER GO-slim and improvements in enrichment analysis tools. *Nucleic Acids Res* 47(D1)**,** D419-D426. doi: 10.1093/nar/gky1038.

Michaud, M., Martins, I., Sukkurwala, A.Q., Adjemian, S., Ma, Y., Pellegatti, P., et al. (2011). Autophagy-dependent anticancer immune responses induced by chemotherapeutic agents in mice. *Science* 334(6062)**,** 1573-1577. doi: 10.1126/science.1208347.

Morel, S., Levy, F., Burlet-Schiltz, O., Brasseur, F., Probst-Kepper, M., Peitrequin, A.L., et al. (2000). Processing of some antigens by the standard proteasome but not by the immunoproteasome results in poor presentation by dendritic cells. *Immunity* 12(1)**,** 107-117. doi: 10.1016/s1074-7613(00)80163-6.

Moses, A.G., Maingay, J., Sangster, K., Fearon, K.C., and Ross, J.A. (2009). Pro-inflammatory cytokine release by peripheral blood mononuclear cells from patients with advanced pancreatic cancer: relationship to acute phase response and survival. *Oncol Rep* 21(4)**,** 1091-1095. doi: 10.3892/or_00000328.

Muroyama, Y., Nirschl, T.R., Kochel, C.M., Lopez-Bujanda, Z., Theodros, D., Mao, W., et al. (2017). Stereotactic Radiotherapy Increases Functionally Suppressive Regulatory T Cells in the Tumor Microenvironment. *Cancer Immunol Res* 5(11)**,** 992-1004. doi: 10.1158/2326-6066.CIR-17-0040.

Nishimura, H., Nose, M., Hiai, H., Minato, N., and Honjo, T. (1999). Development of lupus-like autoimmune diseases by disruption of the PD-1 gene encoding an ITIM motif-carrying immunoreceptor. *Immunity* 11(2)**,** 141-151. doi: 10.1016/s1074-7613(00)80089-8.

Obeid, M., Panaretakis, T., Joza, N., Tufi, R., Tesniere, A., van Endert, P., et al. (2007). Calreticulin exposure is required for the immunogenicity of gamma-irradiation and UVC light-induced apoptosis. *Cell Death Differ* 14(10)**,** 1848-1850. doi: 10.1038/sj.cdd.4402201.

Oh, D.Y., Cham, J., Zhang, L., Fong, G., Kwek, S.S., Klinger, M., et al. (2017). Immune Toxicities Elicted by CTLA-4 Blockade in Cancer Patients Are Associated with Early Diversification of the T-cell Repertoire. *Cancer Res* 77(6)**,** 1322-1330. doi: 10.1158/0008-5472.CAN-16-2324.

Ohshima, Y., Tsukimoto, M., Takenouchi, T., Harada, H., Suzuki, A., Sato, M., et al. (2010). gamma-Irradiation induces P2X(7) receptor-dependent ATP release from B16 melanoma cells. *Biochim Biophys Acta* 1800(1)**,** 40-46. doi: 10.1016/j.bbagen.2009.10.008.

Ovcinnikovs, V., Ross, E.M., Petersone, L., Edner, N.M., Heuts, F., Ntavli, E., et al. (2019). CTLA-4-mediated transendocytosis of costimulatory molecules primarily targets migratory dendritic cells. *Sci Immunol* 4(35). doi: 10.1126/sciimmunol.aaw0902.

Overgaard, J. (2011). Hypoxic modification of radiotherapy in squamous cell carcinoma of the head and neck--a systematic review and meta-analysis. *Radiother Oncol* 100(1)**,** 22-32. doi: 10.1016/j.radonc.2011.03.004.

Pallmer, K., and Oxenius, A. (2016). Recognition and Regulation of T Cells by NK Cells. *Front Immunol* 7**,** 251. doi: 10.3389/fimmu.2016.00251.

Palma, D.A., Olson, R., Harrow, S., Gaede, S., Louie, A.V., Haasbeek, C., et al. (2019). Stereotactic ablative radiotherapy versus standard of care palliative treatment in patients with oligometastatic cancers (SABR-COMET): a randomised, phase 2, open-label trial. *Lancet* 393(10185)**,** 2051-2058. doi: 10.1016/S0140-6736(18)32487-5.

Pan, H., Simpson, D.R., Mell, L.K., Mundt, A.J., and Lawson, J.D. (2011). A survey of stereotactic body radiotherapy use in the United States. *Cancer* 117(19)**,** 4566-4572. doi: 10.1002/cncr.26067.

Park, S.S., Dong, H., Liu, X., Harrington, S.M., Krco, C.J., Grams, M.P., et al. (2015). PD-1 Restrains Radiotherapy-Induced Abscopal Effect. *Cancer Immunol Res* 3(6)**,** 610-619. doi: 10.1158/2326-6066.CIR-14-0138.

Parker, B.S., Rautela, J., and Hertzog, P.J. (2016). Antitumour actions of interferons: implications for cancer therapy. *Nat Rev Cancer* 16(3)**,** 131-144. doi: 10.1038/nrc.2016.14.

Parker, C.C., James, N.D., Brawley, C.D., Clarke, N.W., Hoyle, A.P., Ali, A., et al. (2018). Radiotherapy to the primary tumour for newly diagnosed, metastatic prostate cancer (STAMPEDE): a randomised controlled phase 3 trial. *Lancet* 392(10162)**,** 2353-2366. doi: 10.1016/s0140-6736(18)32486-3.

Pauken, K.E., Sammons, M.A., Odorizzi, P.M., Manne, S., Godec, J., Khan, O., et al. (2016). Epigenetic stability of exhausted T cells limits durability of reinvigoration by PD-1 blockade. *Science* 354(6316)**,** 1160-1165. doi: 10.1126/science.aaf2807.

Paul, W.E. (2013). *Fundamental immunology.* Philadelphia: Wolters Kluwer Health/Lippincott Williams & Wilkins.

Pereira, B.I., Devine, O.P., Vukmanovic-Stejic, M., Chambers, E.S., Subramanian, P., Patel, N., et al. (2019). Senescent cells evade immune clearance via HLA-E-mediated NK and CD8(+) T cell inhibition. *Nat Commun* 10(1)**,** 2387. doi: 10.1038/s41467-019-10335-5.

Persa, E., Balogh, A., Safrany, G., and Lumniczky, K. (2015). The effect of ionizing radiation on regulatory T cells in health and disease. *Cancer Lett* 368(2)**,** 252-261. doi: 10.1016/j.canlet.2015.03.003.

Petrova, N.V., Velichko, A.K., Razin, S.V., and Kantidze, O.L. (2016). Small molecule compounds that induce cellular senescence. *Aging Cell* 15(6)**,** 999-1017. doi: 10.1111/acel.12518.

Pettus, B.J., Chalfant, C.E., and Hannun, Y.A. (2002). Ceramide in apoptosis: an overview and current perspectives. *Biochim Biophys Acta* 1585(2-3)**,** 114-125. doi: 10.1016/s1388-1981(02)00331-1.

Philip, M., Fairchild, L., Sun, L., Horste, E.L., Camara, S., Shakiba, M., et al. (2017). Chromatin states define tumour-specific T cell dysfunction and reprogramming. *Nature* 545(7655)**,** 452-456. doi: 10.1038/nature22367.

Phillips, R., Shi, W.Y., Deek, M., Radwan, N., Lim, S.J., Antonarakis, E.S., et al. (2020). Outcomes of Observation vs Stereotactic Ablative Radiation for Oligometastatic Prostate Cancer: The ORIOLE Phase 2 Randomized Clinical Trial. *JAMA Oncol*. doi: 10.1001/jamaoncol.2020.0147.

Piret, B., Schoonbroodt, S., and Piette, J. (1999). The ATM protein is required for sustained activation of NF-kappaB following DNA damage. *Oncogene* 18(13)**,** 2261-2271. doi: 10.1038/sj.onc.1202541.

Postow, M.A., Callahan, M.K., Barker, C.A., Yamada, Y., Yuan, J., Kitano, S., et al. (2012). Immunologic correlates of the abscopal effect in a patient with melanoma. *N Engl J Med* 366(10)**,** 925-931. doi: 10.1056/NEJMoa1112824.

Price, J.G., Idoyaga, J., Salmon, H., Hogstad, B., Bigarella, C.L., Ghaffari, S., et al. (2015). CDKN1A regulates Langerhans cell survival and promotes Treg cell generation upon exposure to ionizing irradiation. *Nat Immunol* 16(10)**,** 1060-1068. doi: 10.1038/ni.3270.

Prise, K.M., Schettino, G., Folkard, M., and Held, K.D. (2005). New insights on cell death from radiation exposure. *Lancet Oncol* 6(7)**,** 520-528. doi: 10.1016/S1470-2045(05)70246-1.

Qu, Y., Jin, S., Zhang, A., Zhang, B., Shi, X., Wang, J., et al. (2010). Gamma-ray resistance of regulatory CD4+CD25+Foxp3+ T cells in mice. *Radiat Res* 173(2)**,** 148-157. doi: 10.1667/RR0978.1.

Quarmby, S., Hunter, R.D., and Kumar, S. (2000). Irradiation induced expression of CD31, ICAM-1 and VCAM-1 in human microvascular endothelial cells. *Anticancer Res* 20(5B)**,** 3375-3381.

Qureshi, O.S., Zheng, Y., Nakamura, K., Attridge, K., Manzotti, C., Schmidt, E.M., et al. (2011). Trans-endocytosis of CD80 and CD86: a molecular basis for the cell-extrinsic function of CTLA-4. *Science* 332(6029)**,** 600-603. doi: 10.1126/science.1202947.

Reits, E.A., Hodge, J.W., Herberts, C.A., Groothuis, T.A., Chakraborty, M., Wansley, E.K., et al. (2006). Radiation modulates the peptide repertoire, enhances MHC class I expression, and induces successful antitumor immunotherapy. *J Exp Med* 203(5)**,** 1259-1271. doi: 10.1084/jem.20052494.

Reynders, K., Illidge, T., Siva, S., Chang, J.Y., and De Ruysscher, D. (2015). The abscopal effect of local radiotherapy: using immunotherapy to make a rare event clinically relevant. *Cancer Treat Rev* 41(6)**,** 503-510. doi: 10.1016/j.ctrv.2015.03.011.

Ribas, A., and Wolchok, J.D. (2018). Cancer immunotherapy using checkpoint blockade. *Science* 359(6382)**,** 1350-1355. doi: 10.1126/science.aar4060.

Ringborg, U., Bergqvist, D., Brorsson, B., Cavallin-Stahl, E., Ceberg, J., Einhorn, N., et al. (2003). The Swedish Council on Technology Assessment in Health Care (SBU) systematic overview of radiotherapy for cancer including a prospective survey of radiotherapy practice in Sweden 2001--summary and conclusions. *Acta Oncol* 42(5-6)**,** 357-365. doi: 10.1080/02841860310010826.

Robert, C., Ribas, A., Hamid, O., Daud, A., Wolchok, J.D., Joshua, A.M., et al. (2018). Durable Complete Response After Discontinuation of Pembrolizumab in Patients With Metastatic Melanoma. *J Clin Oncol* 36(17)**,** 1668-1674. doi: 10.1200/jco.2017.75.6270.

Robert, L., Tsoi, J., Wang, X., Emerson, R., Homet, B., Chodon, T., et al. (2014). CTLA4 blockade broadens the peripheral T-cell receptor repertoire. *Clin Cancer Res* 20(9)**,** 2424-2432. doi: 10.1158/1078-0432.ccr-13-2648.

Rodriguez, P.C., Quiceno, D.G., Zabaleta, J., Ortiz, B., Zea, A.H., Piazuelo, M.B., et al. (2004). Arginase I production in the tumor microenvironment by mature myeloid cells inhibits T-cell receptor expression and antigen-specific T-cell responses. *Cancer Res* 64(16)**,** 5839-5849. doi: 10.1158/0008-5472.CAN-04-0465.

Rodriguez-Ruiz, M.E., Rodriguez, I., Garasa, S., Barbes, B., Solorzano, J.L., Perez-Gracia, J.L., et al. (2016). Abscopal Effects of Radiotherapy Are Enhanced by Combined Immunostimulatory mAbs and Are Dependent on CD8 T Cells and Crosspriming. *Cancer Res* 76(20)**,** 5994-6005. doi: 10.1158/0008-5472.CAN-16-0549.

Romano, E., Kusio-Kobialka, M., Foukas, P.G., Baumgaertner, P., Meyer, C., Ballabeni, P., et al. (2015). Ipilimumab-dependent cell-mediated cytotoxicity of regulatory T cells ex vivo by nonclassical monocytes in melanoma patients. *Proc Natl Acad Sci U S A* 112(19)**,** 6140-6145. doi: 10.1073/pnas.1417320112.

Rubner, Y., Muth, C., Strnad, A., Derer, A., Sieber, R., Buslei, R., et al. (2014). Fractionated radiotherapy is the main stimulus for the induction of cell death and of Hsp70 release of p53 mutated glioblastoma cell lines. *Radiat Oncol* 9(1)**,** 89. doi: 10.1186/1748-717X-9-89.

Rudqvist, N.P., Pilones, K.A., Lhuillier, C., Wennerberg, E., Sidhom, J.W., Emerson, R.O., et al. (2018). Radiotherapy and CTLA-4 Blockade Shape the TCR Repertoire of Tumor-Infiltrating T Cells. *Cancer Immunol Res* 6(2)**,** 139-150. doi: 10.1158/2326-6066.CIR-17-0134.

Ruiz de Galarreta, M., and Lujambio, A. (2017). DNA sensing in senescence. *Nat Cell Biol* 19(9)**,** 1008-1009. doi: 10.1038/ncb3603.

Sabin, R.J., and Anderson, R.M. (2011). Cellular Senescence - its role in cancer and the response to ionizing radiation. *Genome Integr* 2(1)**,** 7. doi: 10.1186/2041-9414-2-7.

Sakaguchi, S., Yamaguchi, T., Nomura, T., and Ono, M. (2008). Regulatory T cells and immune tolerance. *Cell* 133(5)**,** 775-787. doi: 10.1016/j.cell.2008.05.009.

Sakuishi, K., Apetoh, L., Sullivan, J.M., Blazar, B.R., Kuchroo, V.K., and Anderson, A.C. (2010). Targeting Tim-3 and PD-1 pathways to reverse T cell exhaustion and restore anti-tumor immunity. *J Exp Med* 207(10)**,** 2187-2194. doi: 10.1084/jem.20100643.

Santin, A.D., Hermonat, P.L., Hiserodt, J.C., Chiriva-Internati, M., Woodliff, J., Theus, J.W., et al. (1997). Effects of irradiation on the expression of major histocompatibility complex class I antigen and adhesion costimulation molecules ICAM-1 in human cervical cancer. *Int J Radiat Oncol Biol Phys* 39(3)**,** 737-742. doi: 10.1016/s0360-3016(97)00372-6.

Schadendorf, D., Hodi, F.S., Robert, C., Weber, J.S., Margolin, K., Hamid, O., et al. (2015). Pooled Analysis of Long-Term Survival Data From Phase II and Phase III Trials of Ipilimumab in Unresectable or Metastatic Melanoma. *J Clin Oncol* 33(17)**,** 1889-1894. doi: 10.1200/JCO.2014.56.2736.

Schadt, L., Sparano, C., Schweiger, N.A., Silina, K., Cecconi, V., Lucchiari, G., et al. (2019). Cancer-Cell-Intrinsic cGAS Expression Mediates Tumor Immunogenicity. *Cell Rep* 29(5)**,** 1236-1248 e1237. doi: 10.1016/j.celrep.2019.09.065.

Schaue, D., Ratikan, J.A., Iwamoto, K.S., and McBride, W.H. (2012). Maximizing tumor immunity with fractionated radiation. *Int J Radiat Oncol Biol Phys* 83(4)**,** 1306-1310. doi: 10.1016/j.ijrobp.2011.09.049.

Schreiber, R.D., Old, L.J., and Smyth, M.J. (2011). Cancer immunoediting: integrating immunity's roles in cancer suppression and promotion. *Science* 331(6024)**,** 1565-1570. doi: 10.1126/science.1203486.

Schumacher, T.N., and Schreiber, R.D. (2015). Neoantigens in cancer immunotherapy. *Science* 348(6230)**,** 69-74. doi: 10.1126/science.aaa4971.

Seifert, L., Werba, G., Tiwari, S., Giao Ly, N.N., Nguy, S., Alothman, S., et al. (2016). Radiation Therapy Induces Macrophages to Suppress T-Cell Responses Against Pancreatic Tumors in Mice. *Gastroenterology* 150(7)**,** 1659-1672 e1655. doi: 10.1053/j.gastro.2016.02.070.

Selby, M.J., Engelhardt, J.J., Quigley, M., Henning, K.A., Chen, T., Srinivasan, M., et al. (2013). Anti-CTLA-4 antibodies of IgG2a isotype enhance antitumor activity through reduction of intratumoral regulatory T cells. *Cancer Immunol Res* 1(1)**,** 32-42. doi: 10.1158/2326-6066.cir-13-0013.

Sharabi, A.B., Lim, M., DeWeese, T.L., and Drake, C.G. (2015a). Radiation and checkpoint blockade immunotherapy: radiosensitisation and potential mechanisms of synergy. *Lancet Oncol* 16(13)**,** e498-509. doi: 10.1016/S1470-2045(15)00007-8.

Sharabi, A.B., Nirschl, C.J., Kochel, C.M., Nirschl, T.R., Francica, B.J., Velarde, E., et al. (2015b). Stereotactic Radiation Therapy Augments Antigen-Specific PD-1-Mediated Antitumor Immune Responses via Cross-Presentation of Tumor Antigen. *Cancer Immunol Res* 3(4)**,** 345-355. doi: 10.1158/2326-6066.CIR-14-0196.

Sharma, A., Bode, B., Wenger, R.H., Lehmann, K., Sartori, A.A., Moch, H., et al. (2011). gamma-Radiation promotes immunological recognition of cancer cells through increased expression of cancer-testis antigens in vitro and in vivo. *PLoS One* 6(11)**,** e28217. doi: 10.1371/journal.pone.0028217.

Sharma, A., Subudhi, S.K., Blando, J., Scutti, J., Vence, L., Wargo, J., et al. (2019). Anti-CTLA-4 Immunotherapy Does Not Deplete FOXP3(+) Regulatory T Cells (Tregs) in Human Cancers. *Clin Cancer Res* 25(4)**,** 1233-1238. doi: 10.1158/1078-0432.CCR-18-0762.

Sharma, P., Hu-Lieskovan, S., Wargo, J.A., and Ribas, A. (2017). Primary, Adaptive, and Acquired Resistance to Cancer Immunotherapy. *Cell* 168(4)**,** 707-723. doi: 10.1016/j.cell.2017.01.017.

Sheard, M.A., Uldrijan, S., and Vojtesek, B. (2003). Role of p53 in regulating constitutive and X-radiation-inducible CD95 expression and function in carcinoma cells. *Cancer Res* 63(21)**,** 7176-7184.

Shevach, E.M. (2018). Foxp3(+) T Regulatory Cells: Still Many Unanswered Questions-A Perspective After 20 Years of Study. *Front Immunol* 9**,** 1048. doi: 10.3389/fimmu.2018.01048.

Shevach, E.M., and Thornton, A.M. (2014). tTregs, pTregs, and iTregs: similarities and differences. *Immunol Rev* 259(1)**,** 88-102. doi: 10.1111/imr.12160.

Shi, W., and Siemann, D.W. (2006). Augmented antitumor effects of radiation therapy by 4-1BB antibody (BMS-469492) treatment. *Anticancer Res* 26(5A)**,** 3445-3453.

Shiao, S.L., Ruffell, B., DeNardo, D.G., Faddegon, B.A., Park, C.C., and Coussens, L.M. (2015). TH2-Polarized CD4(+) T Cells and Macrophages Limit Efficacy of Radiotherapy. *Cancer Immunol Res* 3(5)**,** 518-525. doi: 10.1158/2326-6066.CIR-14-0232.

Shimizu, J., Yamazaki, S., Takahashi, T., Ishida, Y., and Sakaguchi, S. (2002). Stimulation of CD25(+)CD4(+) regulatory T cells through GITR breaks immunological self-tolerance. *Nat Immunol* 3(2)**,** 135-142. doi: 10.1038/ni759.

Siddiqui, I., Schaeuble, K., Chennupati, V., Fuertes Marraco, S.A., Calderon-Copete, S., Pais Ferreira, D., et al. (2019). Intratumoral Tcf1(+)PD-1(+)CD8(+) T Cells with Stem-like Properties Promote Tumor Control in Response to Vaccination and Checkpoint Blockade Immunotherapy. *Immunity* 50(1)**,** 195-211.e110. doi: 10.1016/j.immuni.2018.12.021.

Simpson, T.R., Li, F., Montalvo-Ortiz, W., Sepulveda, M.A., Bergerhoff, K., Arce, F., et al. (2013). Fc-dependent depletion of tumor-infiltrating regulatory T cells co-defines the efficacy of anti-CTLA-4 therapy against melanoma. *J Exp Med* 210(9)**,** 1695-1710. doi: 10.1084/jem.20130579.

Siva, S., Callahan, J., MacManus, M.P., Martin, O., Hicks, R.J., and Ball, D.L. (2013). Abscopal [corrected] effects after conventional and stereotactic lung irradiation of non-small-cell lung cancer. *J Thorac Oncol* 8(8)**,** e71-72. doi: 10.1097/JTO.0b013e318292c55a.

Snipstad, K., Fenton, C.G., Kjaeve, J., Cui, G., Anderssen, E., and Paulssen, R.H. (2010). New specific molecular targets for radio-chemotherapy of rectal cancer. *Mol Oncol* 4(1)**,** 52-64. doi: 10.1016/j.molonc.2009.11.002.

Song, C.W., Glatstein, E., Marks, L.B., Emami, B., Grimm, J., Sperduto, P.W., et al. (2019). Biological Principles of Stereotactic Body Radiation Therapy (SBRT) and Stereotactic Radiation Surgery (SRS): Indirect Cell Death. *Int J Radiat Oncol Biol Phys*. doi: 10.1016/j.ijrobp.2019.02.047.

Soo, R.A., Chen, Z., Yan Teng, R.S., Tan, H.L., Iacopetta, B., Tai, B.C., et al. (2018). Prognostic significance of immune cells in non-small cell lung cancer: meta-analysis. *Oncotarget* 9(37)**,** 24801-24820. doi: 10.18632/oncotarget.24835.

Soriani, A., Zingoni, A., Cerboni, C., Iannitto, M.L., Ricciardi, M.R., Di Gialleonardo, V., et al. (2009). ATM-ATR-dependent up-regulation of DNAM-1 and NKG2D ligands on multiple myeloma cells by therapeutic agents results in enhanced NK-cell susceptibility and is associated with a senescent phenotype. *Blood* 113(15)**,** 3503-3511. doi: 10.1182/blood-2008-08-173914.

Stamell, E.F., Wolchok, J.D., Gnjatic, S., Lee, N.Y., and Brownell, I. (2013). The abscopal effect associated with a systemic anti-melanoma immune response. *Int J Radiat Oncol Biol Phys* 85(2)**,** 293-295. doi: 10.1016/j.ijrobp.2012.03.017.

Stewart, T.J., and Abrams, S.I. (2007). Altered immune function during long-term host-tumor interactions can be modulated to retard autochthonous neoplastic growth. *J Immunol* 179(5)**,** 2851-2859. doi: 10.4049/jimmunol.179.5.2851.

Stone, H.B., Peters, L.J., and Milas, L. (1979). Effect of host immune capability on radiocurability and subsequent transplantability of a murine fibrosarcoma. *J Natl Cancer Inst* 63(5)**,** 1229-1235.

Strauss, L., Mahmoud, M.A.A., Weaver, J.D., Tijaro-Ovalle, N.M., Christofides, A., Wang, Q., et al. (2020). Targeted deletion of PD-1 in myeloid cells induces antitumor immunity. *Sci Immunol* 5(43). doi: 10.1126/sciimmunol.aay1863.

Strome, S.E., Voss, S., Wilcox, R., Wakefield, T.L., Tamada, K., Flies, D., et al. (2002). Strategies for antigen loading of dendritic cells to enhance the antitumor immune response. *Cancer Res* 62(6)**,** 1884-1889.

Subramanian, A., Tamayo, P., Mootha, V.K., Mukherjee, S., Ebert, B.L., Gillette, M.A., et al. (2005). Gene set enrichment analysis: a knowledge-based approach for interpreting genome-wide expression profiles. *Proc Natl Acad Sci U S A* 102(43)**,** 15545-15550. doi: 10.1073/pnas.0506580102.

Tam, S.Y., Wu, V.W., and Law, H.K. (2017). Influence of autophagy on the efficacy of radiotherapy. *Radiat Oncol* 12(1)**,** 57. doi: 10.1186/s13014-017-0795-y.

Tang, C., Liao, Z., Gomez, D., Levy, L., Zhuang, Y., Gebremichael, R.A., et al. (2014). Lymphopenia association with gross tumor volume and lung V5 and its effects on non-small cell lung cancer patient outcomes. *Int J Radiat Oncol Biol Phys* 89(5)**,** 1084-1091. doi: 10.1016/j.ijrobp.2014.04.025.

Theelen, W., Peulen, H.M.U., Lalezari, F., van der Noort, V., de Vries, J.F., Aerts, J., et al. (2019). Effect of Pembrolizumab After Stereotactic Body Radiotherapy vs Pembrolizumab Alone on Tumor Response in Patients With Advanced Non-Small Cell Lung Cancer: Results of the PEMBRO-RT Phase 2 Randomized Clinical Trial. *JAMA Oncol*. doi: 10.1001/jamaoncol.2019.1478.

Tibbs, M.K. (1997). Wound healing following radiation therapy: a review. *Radiother Oncol* 42(2)**,** 99-106. doi: 10.1016/s0167-8140(96)01880-4.

Trowell, O.A. (1952). The sensitivity of lymphocytes to ionising radiation. *J Pathol Bacteriol* 64(4)**,** 687-704. doi: 10.1002/path.1700640403.

Truman, J.P., García-Barros, M., Kaag, M., Hambardzumyan, D., Stancevic, B., Chan, M., et al. (2010). Endothelial membrane remodeling is obligate for anti-angiogenic radiosensitization during tumor radiosurgery. *PLoS One* 5(9). doi: 10.1371/annotation/6e222ad5-b175-4a00-9d04-4d120568a897.

Turley, S.J., Cremasco, V., and Astarita, J.L. (2015). Immunological hallmarks of stromal cells in the tumour microenvironment. *Nat Rev Immunol* 15(11)**,** 669-682. doi: 10.1038/nri3902.

Turrisi, A.T., 3rd, Kim, K., Blum, R., Sause, W.T., Livingston, R.B., Komaki, R., et al. (1999). Twice-daily compared with once-daily thoracic radiotherapy in limited small-cell lung cancer treated concurrently with cisplatin and etoposide. *N Engl J Med* 340(4)**,** 265-271. doi: 10.1056/nejm199901283400403.

Twyman-Saint Victor, C., Rech, A.J., Maity, A., Rengan, R., Pauken, K.E., Stelekati, E., et al. (2015). Radiation and dual checkpoint blockade activate non-redundant immune mechanisms in cancer. *Nature* 520(7547)**,** 373-377. doi: 10.1038/nature14292.

Vakifahmetoglu, H., Olsson, M., and Zhivotovsky, B. (2008). Death through a tragedy: mitotic catastrophe. *Cell Death Differ* 15(7)**,** 1153-1162. doi: 10.1038/cdd.2008.47.

Vanpouille-Box, C., Diamond, J.M., Pilones, K.A., Zavadil, J., Babb, J.S., Formenti, S.C., et al. (2015). TGFbeta Is a Master Regulator of Radiation Therapy-Induced Antitumor Immunity. *Cancer Res* 75(11)**,** 2232-2242. doi: 10.1158/0008-5472.CAN-14-3511.

Vanpouille-Box, C., Formenti, S.C., and Demaria, S. (2017). TREX1 dictates the immune fate of irradiated cancer cells. *Oncoimmunology* 6(9)**,** e1339857. doi: 10.1080/2162402X.2017.1339857.

Vatner, R.E., and Formenti, S.C. (2015). Myeloid-derived cells in tumors: effects of radiation. *Semin Radiat Oncol* 25(1)**,** 18-27. doi: 10.1016/j.semradonc.2014.07.008.

Verbrugge, I., Hagekyriakou, J., Sharp, L.L., Galli, M., West, A., McLaughlin, N.M., et al. (2012). Radiotherapy increases the permissiveness of established mammary tumors to rejection by immunomodulatory antibodies. *Cancer Res* 72(13)**,** 3163-3174. doi: 10.1158/0008-5472.CAN-12-0210.

Verhoeff, S.R., van den Heuvel, M.M., van Herpen, C.M.L., Piet, B., Aarntzen, E., and Heskamp, S. (2020). Programmed Cell Death-1/Ligand-1 PET Imaging: A Novel Tool to Optimize Immunotherapy? *PET Clin* 15(1)**,** 35-43. doi: 10.1016/j.cpet.2019.08.008.

Vesely, M.D., Kershaw, M.H., Schreiber, R.D., and Smyth, M.J. (2011). Natural innate and adaptive immunity to cancer. *Annu Rev Immunol* 29**,** 235-271. doi: 10.1146/annurev-immunol-031210-101324.

Vey, N., Dumas, P.-Y., Recher, C., Gastaud, L., Lioure, B., Bulabois, C.-E., et al. (2017). Randomized Phase 2 Trial of Lirilumab (anti-KIR monoclonal antibody, mAb) As Maintenance Treatment in Elderly Patients (pts) with Acute Myeloid Leukemia (AML): Results of the Effikir Trial. *Blood* 130(Supplement 1)**,** 889-889. doi: 10.1182/blood.V130.Suppl_1.889.889.

von Boehmer, H. (2005). Mechanisms of suppression by suppressor T cells. *Nat Immunol* 6(4)**,** 338-344. doi: 10.1038/ni1180.

Voorwerk, L., Slagter, M., Horlings, H.M., Sikorska, K., van de Vijver, K.K., de Maaker, M., et al. (2019). Immune induction strategies in metastatic triple-negative breast cancer to enhance the sensitivity to PD-1 blockade: the TONIC trial. *Nat Med* 25(6)**,** 920-928. doi: 10.1038/s41591-019-0432-4.

Wang, L., Leite de Oliveira, R., Wang, C., Fernandes Neto, J.M., Mainardi, S., Evers, B., et al. (2017). High-Throughput Functional Genetic and Compound Screens Identify Targets for Senescence Induction in Cancer. *Cell Rep* 21(3)**,** 773-783. doi: 10.1016/j.celrep.2017.09.085.

Wang, T., Niu, G., Kortylewski, M., Burdelya, L., Shain, K., Zhang, S., et al. (2004). Regulation of the innate and adaptive immune responses by Stat-3 signaling in tumor cells. *Nat Med* 10(1)**,** 48-54. doi: 10.1038/nm976.

Wang, Z., Tang, Y., Tan, Y., Wei, Q., and Yu, W. (2019). Cancer-associated fibroblasts in radiotherapy: challenges and new opportunities. *Cell Commun Signal* 17(1)**,** 47. doi: 10.1186/s12964-019-0362-2.

Watanabe, T., Gaedicke, S., Guffart, E., Firat, E., and Niedermann, G. (2019). Adding Indoximod to Hypofractionated Radiotherapy with Anti-PD-1 Checkpoint Blockade Enhances Early NK and CD8(+) T-Cell-Dependent Tumor Activity. *Clin Cancer Res*. doi: 10.1158/1078-0432.CCR-19-0476.

Waterhouse, P., Penninger, J.M., Timms, E., Wakeham, A., Shahinian, A., Lee, K.P., et al. (1995). Lymphoproliferative disorders with early lethality in mice deficient in Ctla-4. *Science* 270(5238)**,** 985-988. doi: 10.1126/science.270.5238.985.

Wei, S.C., Duffy, C.R., and Allison, J.P. (2018). Fundamental Mechanisms of Immune Checkpoint Blockade Therapy. *Cancer Discov* 8(9)**,** 1069-1086. doi: 10.1158/2159-8290.CD-18-0367.

Weiss, J.M., Bilate, A.M., Gobert, M., Ding, Y., Curotto de Lafaille, M.A., Parkhurst, C.N., et al. (2012). Neuropilin 1 is expressed on thymus-derived natural regulatory T cells, but not mucosa-generated induced Foxp3+ T reg cells. *J Exp Med* 209(10)**,** 1723-1742, S1721. doi: 10.1084/jem.20120914.

Wendel, M., Galani, I.E., Suri-Payer, E., and Cerwenka, A. (2008). Natural killer cell accumulation in tumors is dependent on IFN-gamma and CXCR3 ligands. *Cancer Res* 68(20)**,** 8437-8445. doi: 10.1158/0008-5472.CAN-08-1440.

Werthmoller, N., Frey, B., Wunderlich, R., Fietkau, R., and Gaipl, U.S. (2015). Modulation of radiochemoimmunotherapy-induced B16 melanoma cell death by the pan-caspase inhibitor zVAD-fmk induces anti-tumor immunity in a HMGB1-, nucleotide- and T-cell-dependent manner. *Cell Death Dis* 6**,** e1761. doi: 10.1038/cddis.2015.129.

Wild, A.T., Ye, X., Ellsworth, S.G., Smith, J.A., Narang, A.K., Garg, T., et al. (2015). The Association Between Chemoradiation-related Lymphopenia and Clinical Outcomes in Patients With Locally Advanced Pancreatic Adenocarcinoma. *Am J Clin Oncol* 38(3)**,** 259-265. doi: 10.1097/COC.0b013e3182940ff9.

Wlodkowic, D., Telford, W., Skommer, J., and Darzynkiewicz, Z. (2011). Apoptosis and beyond: cytometry in studies of programmed cell death. *Methods Cell Biol* 103**,** 55-98. doi: 10.1016/b978-0-12-385493-3.00004-8.

Woo, S.R., Fuertes, M.B., Corrales, L., Spranger, S., Furdyna, M.J., Leung, M.Y., et al. (2014). STING-dependent cytosolic DNA sensing mediates innate immune recognition of immunogenic tumors. *Immunity* 41(5)**,** 830-842. doi: 10.1016/j.immuni.2014.10.017.

Wrzesinski, S.H., Wan, Y.Y., and Flavell, R.A. (2007). Transforming growth factor-beta and the immune response: implications for anticancer therapy. *Clin Cancer Res* 13(18 Pt 1)**,** 5262-5270. doi: 10.1158/1078-0432.CCR-07-1157.

Wu, D., Lim, E., Vaillant, F., Asselin-Labat, M.L., Visvader, J.E., and Smyth, G.K. (2010). ROAST: rotation gene set tests for complex microarray experiments. *Bioinformatics* 26(17)**,** 2176-2182. doi: 10.1093/bioinformatics/btq401.

Wu, G.S., Burns, T.F., McDonald, E.R., 3rd, Jiang, W., Meng, R., Krantz, I.D., et al. (1997). KILLER/DR5 is a DNA damage-inducible p53-regulated death receptor gene. *Nat Genet* 17(2)**,** 141-143. doi: 10.1038/ng1097-141.

Xu, J., Escamilla, J., Mok, S., David, J., Priceman, S., West, B., et al. (2013). CSF1R signaling blockade stanches tumor-infiltrating myeloid cells and improves the efficacy of radiotherapy in prostate cancer. *Cancer Res* 73(9)**,** 2782-2794. doi: 10.1158/0008-5472.CAN-12-3981.

Xue, W., Zender, L., Miething, C., Dickins, R.A., Hernando, E., Krizhanovsky, V., et al. (2007). Senescence and tumour clearance is triggered by p53 restoration in murine liver carcinomas. *Nature* 445(7128)**,** 656-660. doi: 10.1038/nature05529.

Yadav, M., Louvet, C., Davini, D., Gardner, J.M., Martinez-Llordella, M., Bailey-Bucktrout, S., et al. (2012). Neuropilin-1 distinguishes natural and inducible regulatory T cells among regulatory T cell subsets in vivo. *J Exp Med* 209(10)**,** 1713-1722, S1711-1719. doi: 10.1084/jem.20120822.

Yasuda, K., Nakanishi, K., and Tsutsui, H. (2019). Interleukin-18 in Health and Disease. *Int J Mol Sci* 20(3). doi: 10.3390/ijms20030649.

Yokouchi, H., Yamazaki, K., Chamoto, K., Kikuchi, E., Shinagawa, N., Oizumi, S., et al. (2008). Anti-OX40 monoclonal antibody therapy in combination with radiotherapy results in therapeutic antitumor immunity to murine lung cancer. *Cancer Sci* 99(2)**,** 361-367. doi: 10.1111/j.1349-7006.2007.00664.x.

Yoon, M.S., Pham, C.T., Phan, M.T., Shin, D.J., Jang, Y.Y., Park, M.H., et al. (2016). Irradiation of breast cancer cells enhances CXCL16 ligand expression and induces the migration of natural killer cells expressing the CXCR6 receptor. *Cytotherapy* 18(12)**,** 1532-1542. doi: 10.1016/j.jcyt.2016.08.006.

Yost, K.E., Satpathy, A.T., Wells, D.K., Qi, Y., Wang, C., Kageyama, R., et al. (2019). Clonal replacement of tumor-specific T cells following PD-1 blockade. *Nat Med* 25(8)**,** 1251-1259. doi: 10.1038/s41591-019-0522-3.

Yovino, S., Kleinberg, L., Grossman, S.A., Narayanan, M., and Ford, E. (2013). The etiology of treatment-related lymphopenia in patients with malignant gliomas: modeling radiation dose to circulating lymphocytes explains clinical observations and suggests methods of modifying the impact of radiation on immune cells. *Cancer Invest* 31(2)**,** 140-144. doi: 10.3109/07357907.2012.762780.

Yu, Q., Katlinskaya, Y.V., Carbone, C.J., Zhao, B., Katlinski, K.V., Zheng, H., et al. (2015). DNA-damage-induced type I interferon promotes senescence and inhibits stem cell function. *Cell Rep* 11(5)**,** 785-797. doi: 10.1016/j.celrep.2015.03.069.

Zappasodi, R., Sirard, C., Li, Y., Budhu, S., Abu-Akeel, M., Liu, C., et al. (2019). Rational design of anti-GITR-based combination immunotherapy. *Nat Med* 25(5)**,** 759-766. doi: 10.1038/s41591-019-0420-8.

Zaretsky, J.M., Garcia-Diaz, A., Shin, D.S., Escuin-Ordinas, H., Hugo, W., Hu-Lieskovan, S., et al. (2016). Mutations Associated with Acquired Resistance to PD-1 Blockade in Melanoma. *N Engl J Med* 375(9)**,** 819-829. doi: 10.1056/NEJMoa1604958.

Zemmour, D., Zilionis, R., Kiner, E., Klein, A.M., Mathis, D., and Benoist, C. (2018). Single-cell gene expression reveals a landscape of regulatory T cell phenotypes shaped by the TCR. *Nat Immunol* 19(3)**,** 291-301. doi: 10.1038/s41590-018-0051-0.

Zeng, J., See, A.P., Phallen, J., Jackson, C.M., Belcaid, Z., Ruzevick, J., et al. (2013). Anti-PD-1 blockade and stereotactic radiation produce long-term survival in mice with intracranial gliomas. *Int J Radiat Oncol Biol Phys* 86(2)**,** 343-349. doi: 10.1016/j.ijrobp.2012.12.025.

Zhang, B., Bowerman, N.A., Salama, J.K., Schmidt, H., Spiotto, M.T., Schietinger, A., et al. (2007). Induced sensitization of tumor stroma leads to eradication of established cancer by T cells. *J Exp Med* 204(1)**,** 49-55. doi: 10.1084/jem.20062056.

Zhang, Q., Bi, J., Zheng, X., Chen, Y., Wang, H., Wu, W., et al. (2018). Blockade of the checkpoint receptor TIGIT prevents NK cell exhaustion and elicits potent anti-tumor immunity. *Nat Immunol* 19(7)**,** 723-732. doi: 10.1038/s41590-018-0132-0.

Zhao, X., Li, L., Starr, T.K., and Subramanian, S. (2017). Tumor location impacts immune response in mouse models of colon cancer. *Oncotarget* 8(33)**,** 54775-54787. doi: 10.18632/oncotarget.18423.

Zheng, W., Skowron, K.B., Namm, J.P., Burnette, B., Fernandez, C., Arina, A., et al. (2016). Combination of radiotherapy and vaccination overcomes checkpoint blockade resistance. *Oncotarget* 7(28)**,** 43039-43051. doi: 10.18632/oncotarget.9915.

Ziblat, A., Nunez, S.Y., Raffo Iraolagoitia, X.L., Spallanzani, R.G., Torres, N.I., Sierra, J.M., et al. (2017). Interleukin (IL)-23 Stimulates IFN-gamma Secretion by CD56(bright) Natural Killer Cells and Enhances IL-18-Driven Dendritic Cells Activation. *Front Immunol* 8**,** 1959. doi: 10.3389/fimmu.2017.01959.

Zingoni, A., Fionda, C., Borrelli, C., Cippitelli, M., Santoni, A., and Soriani, A. (2017). Natural Killer Cell Response to Chemotherapy-Stressed Cancer Cells: Role in Tumor Immunosurveillance. *Front Immunol* 8**,** 1194. doi: 10.3389/fimmu.2017.01194.